

Diss. ETH no. 16343

Electron Delocalization in Linearly π - Conjugated Compounds; a New Approach of Analysis

A dissertation submitted to the
SWISS FEDERAL INSTITUTE OF TECHNOLOGY ZÜRICH

For the degree of
Doctor of Natural Sciences

Presented by
Maurizio Bruschi
Dott. in Chimica Industriale, Università degli Studi di Milano (IT)

Born August 17, 1970

Citizen of Italy

Accepted on the recommendation of
PD Prof. Hans Peter Lüthi, examiner
Prof. Wilfred F. van Gunsteren, Prof. Jürg Hutter, co-examiners

Acknowledgements

I would like to thank Prof. Hans Peter Lüthi for the support he gave to facilitate this project. I am grateful for the opportunity to work with him which enabled me to enlarge my knowledge in the field of computational chemistry. I have greatly appreciated his advice and suggestions as well as the patience toward my bungling style and lack of organization.

I want to express my warmest gratitude to Prof. Wilfred van Gunsteren, not only for the opportunity - greatly appreciated - he provided me to finish this project, but also, for all I learned from him during the time I spent at IGC. The serene and friendly atmosphere he has set up in the IGC group together with the productive scientific research is an example of how a successful group should be managed and inspired.

I would like to thank all members of the IGC group (too many to be mentioned here more than three generations of PhD students) for the pleasant time in the group. My only regret is not having always been able to cultivate a deeper friendship with everybody except, perhaps, Dirk and Stefan. In particular, I would like to thank Maria Grazia for her excellent collaboration, her support when struggling with the interpretation of results, the preparation of manuscripts, and most importantly, her friendship in general. My thanks also go to Dirk, who was always an original and intelligent companion for scientific discussions and a friend inside and outside the lab.

I also would like to thank, with great gratitude, Prof. Piercarlo Fantucci since he first introduced me to the world of computational chemistry and has been in all these years a point of reference. Some development of the material of this thesis originated from his fruitful suggestions.

I am very grateful to Angelo and Fabio for their inestimable help and their endless hospitality. I spent with them a wonderful time in Zürich, and I learned a lot from our discussions about life in general.

I would like to thank Laura for many reasons, but here in particular, for the unconditionated support I received during the period of my thesis. I consider myself really lucky to share my life with her.

Last, I deeply thank my parents and my brother who have always been present in my life with their love and care. If I had any chance to continue my studies, it is only for the sacrifices of my parents and, in particular, my brother with whom I will be in debt forever. For this reason, I would like to dedicate this thesis to him.

Contents

Acknowledgements	ii
Contents	iv
Abbreviations	vii
Summary.....	ix
Riassunto.....	xii
Publications	xv
1 Introduction	1
1.1 Electron Delocalization in π -Conjugated Compounds	7
1.1.1 A Short Review of the History of Electron Delocalization in π - Conjugated Compounds.....	7
1.1.2 The Concept of Electron Delocalization and its Usefulness in Chemistry.....	11
1.2 An Overview of the Approaches for the Quantification of Electron Delocalization.....	14
1.2.1 Experimental Approaches.....	14
1.2.2 Theoretical Approaches	17
1.3 Acetylenic Carbon Rich Compounds as Example of Molecules with Extended π - Delocalization.....	21
1.4 Outline of the Thesis.....	26
1.5 References.....	28
2 A New Approach for the Investigation of Electron Delocalization	41
2.1 The Natural Bond Orbital (NBO) Approach	42
2.1.1 NAO Transformation; the Occupancy Weighted Symmetric Orthogonalization	43
2.1.2 NHO and NBO Transformation.....	46
2.2 A New Approach for the Analysis of Electron Delocalization Based on NBO Theory	49
2.2.1 Deletion Energies Protocol	49

2.2.2	Second-Order Orbital Interaction Energies Protocol.....	53
2.2.3	Other Electron Delocalization Indicators.....	57
2.2.4	Values and Drawbacks of the Approach.....	58
2.3	References.....	59
3	The Validation of the Approach	61
3.1	<i>1,3</i> -Butadiene: an Illustration of the Approach	61
3.1.1	Summary	61
3.1.2	Introduction.....	62
3.1.3	Computational Methods.....	63
3.1.4	Results and Discussion	64
3.1.5	Conclusions.....	69
3.2	<i>Through</i> versus <i>Cross</i> Electron Delocalization in Tetra- and Di- Ethyneethenes	70
3.2.1	Summary	70
3.2.2	Introduction.....	70
3.2.3	Computational Methods.....	72
3.2.4	Results and Discussion	77
3.2.5	Conclusions.....	96
3.3	References.....	97
4	Applications	104
4.1	Extended Systems: Electron Delocalization in Substituted Tetraethynylethene Model Compounds.....	105
4.1.1	Summary	105
4.1.2	Introduction.....	105
4.1.3	Computational Methods.....	107
4.1.4	Results and Discussion	107
4.1.5	Conclusions.....	121
4.2	Extended Systems: <i>Through</i> versus <i>Cross</i> Electron Delocalization in Polytriacylene Oligomers	122
4.2.1	Summary	122

4.2.2	Introduction.....	123
4.2.3	Computational Methods.....	126
4.2.4	Results and Discussion	127
4.2.5	Conclusions.....	150
4.3	Extended Systems: The Impact of Length and Type of Backbone on Electron Delocalization of Polyacetylene, Polydiacetylene, and Polytriacetylene.....	151
4.3.1	Summary	151
4.3.2	Introduction.....	152
4.3.3	Computational Methods.....	155
4.3.4	Results and Discussion	156
4.3.5	Conclusions.....	169
4.4	Extended Systems: the Impact of Donor and/or Acceptor Functional Groups on Electron Delocalization of Polytriacetylene and Perethynyl-Polytriacetylene Oligomers	170
4.4.1	Summary	170
4.4.2	Introduction.....	170
4.4.3	Computational Methods.....	172
4.4.4	Results and Discussion	173
4.4.5	Conclusions.....	190
4.5	References.....	191
5	Outlook.....	203
	<i>Curriculum Vitae</i>	206
	Complete List of Publications.....	207

Abbreviations

α	polarizability
B3LYP	Becke3 parameter exchange functional with Lee-Yang-Parr correlation functional
BLA	bond length alternation
DEE	1,2-diethynylethene; (E)-hex-3-ene-1,5-diyne
DFT	Density Functional Theory
DRE	Dewar resonance energy
CP	coupled perturbed
EA	electron affinity
ECL	effective conjugation length
E_{\max}	First allowed excitation energy
γ	second-order hyperpolarizability
HF	Hartree-Fock
HOMO	highest occupied molecular orbital
IP	ionization potential
λ_{\max}	maximum allowed absorption wavelength
LUMO	lowest unoccupied molecular orbital
<i>iso</i> -PDA	<i>iso</i> -polydiacetylene
<i>iso</i> -PTA	<i>iso</i> -polytriacetylene
MNDO	modified neglect of differential overlap
MO	molecular orbital
MPn	Møller-Plesset perturbation theory, where n is the order of correction
NAO	Natural Atomic Orbital
NBO	Natural Bond Orbital
NLMO	Natural Localized Molecular Orbital
NLO	nonlinear optics
PA	polyacetylene
PDA	polydiacetylene

pePTA	perethynyl-polytriacylene
PTA	polytriacylene
QSPR	quantitative structure-property relationship
SCF	self consistent field
SOIE	second-order orbital interaction energy
TDDFT	time-dependent density functional theory
TEE	tetraethynylethene, 3,4-diethynylhex-3-ene-1,5-diyne
THG	third harmonic generation
TRE	theoretical resonance energy
VB	valence bond
VRE	vertical resonance energy
ZINDO	Zerner's intermediate neglect of differential overlap

Summary

In the present thesis, an approach based on the Natural Bond Orbital (NBO) theory for the quantification of electron delocalization in extended π -conjugated organic compounds will be presented and discussed. The approach will be applied to the investigation of π -electron delocalization of a series of organic molecules characterized by the unique carbon-rich frameworks of diethynylethene (DEE) and tetraethynylethene (TEE). Molecular, electronic, and optical properties of these systems are also investigated and correlated to the extent of π -delocalization. By analyzing these relationships, the project aims to advance the fundamental knowledge of π -electron delocalization and how its modulation affects the different molecular and electronic observables.

In chapter 1 the concept of electron delocalization will be introduced, with a short overview on the historical development of the concept and the more recent theoretical and experimental methods for its evaluation. As general design guidelines, the main topological degrees of freedom that can be manipulated for the optimization of molecules to suit tailored properties will be also discussed. Chapter 1 concludes with an overview of a series of known DEE and TEE derivatives, which have been used as building blocks for the synthesis of functionalized compounds and carbon-rich nanometer-sized molecular systems.

The approach for the quantification of electron delocalization will be illustrated in Chapter 2. The chapter starts with an overview of the NBO theory and its applications for the analysis of wavefunctions. Then, our approach will be introduced and discussed. The general approach consists of an orbital deletion protocol and a second-order interaction energies protocol for the calculation of delocalization energies. In addition, other delocalization parameters such as the NBO occupancies are presented and discussed as useful tools for the analysis of electron delocalization. Finally, the values and the drawbacks of our approach in comparison to other theoretical methods will be critically discussed.

The Chapter 3 will be devoted to the validation of the approach on prototypical π -conjugated molecules such as *1,3*-butadiene and the parents DEE and TEE compounds. π -electron delocalization in *1,3*-butadiene renders the energy barrier for the rotation around the

central C-C bond significantly larger than that of the corresponding aliphatic molecule. The analysis of electron delocalization as a function of the torsional angle will show that the rotational barrier is totally ascribed to the change in delocalization energy. The application of the approach to the linearly π -conjugated DEE (t-DEE) and to the corresponding *cross*-conjugated isomer (g-DEE) reveals that the difference in stability is due to the difference in delocalization energy. The dissection of the delocalization energy into the vertical (π) and in-plane (σ) contributions shows that the difference in stability is essentially controlled by the vertical π -electron delocalization. However, σ -delocalization cannot be neglected and play a role to discriminate between *geminal* and *trans* conjugation. The importance of the σ -delocalization is also supported by the fact that the largest structural difference between *trans* and *geminal* isomers is not in the π bond lengths but rather in the σ bond lengths.

The application of our approach to the investigation of electron delocalization in extended π -conjugated compounds is the topic of Chapter 4. The chapter consists of four subchapters in which the effects of each topological degree of freedom on selected physical observables are investigated and discussed. Subchapter 4.1 will deal with the investigation of electron delocalization in two-dimensional substituted tetraethynylethene (TEE) model compounds in order to assess the efficiency of distinct π -conjugated paths, i.e. *geminal*, *cis*, and *trans*, as well as to predict the impact of substituents on a given backbone. The analysis of electron delocalization will show that the conjugation is strongly dependent on the nature of the substituent (donor vs. acceptor) rather than on the type of path considered (*through* vs. *cross*). Furthermore, the conjugation energy in a selected path is enhanced with increasing degree of substitution. In fact, the best *geminal* and *trans* paths are always those with donor or acceptor substituents, regardless of the neighborhood. This is due to a strong contribution of the substituents into the π^*_T orbitals of the backbone, which is in general much larger with the donors than with the acceptors. In subchapter 4.2 the *trans* versus *cross* modes of π -conjugation in polytriacetylene (PTA) and *iso*-polytriacetylene (*iso*-PTA) oligomers of increasing chain length will be investigated. The effective conjugation length (ECL) of the neutral species, as determined on the basis of the molecular structure and of delocalization energies is evaluated of about 24 conjugated bonds in PTA, and only 6 conjugated bonds in

iso-PTA. This means that in *iso*-PTA electron delocalization is switched off at the *cross*-conjugated carbon atoms. However, extended electron delocalization is observed for the positively and negatively charged *iso*-PTA oligomers; there the π -conjugation through *cross*-linked carbon atoms is *definitely* switched on. In subchapter 4.3 we will consider the impact of the insertion of ethynyl units into polyacetylene (PA) oligomers on π -electron delocalization, and correspondingly, on selected physical observables. The lateral addition of ethynyl units to PTA to give perethynyl-polytriacetylene (pePTA) is also studied in this subchapter. We will show that the incorporation of triple bonds in the PA chain, to give PDA and PTA, increases the total amount of π -delocalization, but, on the other hand, reduces the efficiency by which π -delocalization is promoted. The lateral addition of ethynyl groups to PTA also increases the π -delocalization, but does not improve the evolution of the molecular and electronic properties as a function of the chain size. Finally, the terminal functionalization of PTA and pePTA oligomers of increasing chain length with donor/acceptor groups is discussed in subchapter 4.4. All of the physical observables investigated appear to rapidly converge to the same saturation value of the parent oligomers, indicating that the effects of the donor/acceptor functionalization are significant only for short oligomers. The analysis of electron delocalization will show that the donor functional group promotes π -delocalization more efficiently than the acceptor one. Correspondingly, the donor-substituted derivatives show a faster convergence to a saturation value.

The thesis is concluded in Chapter 5 with a personal outlook on the future improvements of the approach for the evaluation of delocalization energies.

Riassunto

In questa tesi sarà presentato e discusso un nuovo approccio per la quantificazione della delocalizzazione elettronica in sistemi molecolari ad elevata coniugazione π . Questo approccio sarà applicato allo studio di una serie di molecole organiche caratterizzate dal dietinil-etene (DEE) e il tetraetnil-etene (TEE) come unità costitutive. L'estensione della delocalizzazione elettronica determinata con il nuovo approccio sarà correlata ad alcune proprietà molecolari ed elettroniche di questi sistemi. Questa analisi permetterà di raggiungere una migliore comprensione del concetto di delocalizzazione elettronica e del modo in cui questa influenza le diverse proprietà chimico-fisiche dei sistemi ad elevata coniugazione π .

Nel primo capitolo sarà discusso in dettaglio il significato di delocalizzazione elettronica partendo da una breve introduzione storica sulla sua origine e sui primi tentativi di quantificarla. Si procederà quindi a presentare i più recenti metodi teorici e sperimentali per la valutazione di questo parametro. Alcune regole guida per il progetto di nuovi composti si possono ottenere dall'analisi di alcune variabili topologiche la cui modifica permette l'ottimizzazione di molecole in modo da avere le proprietà desiderate. Le principali di queste variabili saranno introdotte nel primo capitolo e discusse in relazione a studi precedentemente svolti. Il primo capitolo terminerà con una breve descrizione dei derivati del dietinil- e tetraetniletene che saranno alla base dell'applicazione del nostro approccio.

L'approccio per la quantificazione della delocalizzazione elettronica sarà illustrato nel Capitolo 2. Il capitolo inizia con la descrizione della teoria NBO e delle sue applicazioni per l'analisi della funzione d'onda e prosegue con una discussione in dettaglio del nuovo approccio. Questo approccio è costituito da un protocollo basato sull'eliminazione di specifici orbitali NBO e da un protocollo basato sulle energie di interazione del secondo ordine. Inoltre, saranno introdotti alcuni parametri quali i numeri d'occupazione orbitalica che costituiscono degli utili mezzi per l'analisi della delocalizzazione elettronica e per la sua correlazione con le osservabili chimico-fisiche. Infine, nel Capitolo 2 saranno discussi i vantaggi e i limiti del nostro approccio rispetto ad altri metodi per l'analisi della delocalizzazione elettronica.

Il Capitolo 3 è dedicato alla validazione dell'approccio su semplici molecole con coniugazione π quali l'*1,3*-butadiene e il DEE non sostituito. La delocalizzazione π nell'*1,3*-butadiene rende la barriera energetica dovuta alla rotazione attorno al legame C–C più alta rispetto a quella del corrispondente composto alifatico. L'analisi della delocalizzazione elettronica in funzione della rotazione attorno a questo legame mostra che la barriera energetica è dovuta totalmente alla variazione dell'energia di delocalizzazione. L'applicazione dell'approccio al DEE caratterizzato da coniugazione lineare (t-DEE) e al corrispondente isomero caratterizzato da coniugazione geminale (g-DEE) rivela che la differenza in stabilità tra i due isomeri è dovuta esclusivamente alla differenza nell'energia di delocalizzazione. La scomposizione dei contributi energetici nelle componenti π e σ mostra che tale differenza è controllata dalla delocalizzazione π . Tuttavia, la delocalizzazione σ non può essere trascurata e ha un ruolo nel discriminare tra coniugazione geminale e lineare. L'importanza della delocalizzazione σ è supportata dal fatto che la maggiore differenza strutturale tra i due isomeri non è data dalle distanze dei legami π ma piuttosto dalla lunghezza del legame σ .

L'applicazione del nostro approccio allo studio della delocalizzazione elettronica in sistemi ad elevata coniugazione π , è l'argomento del Capitolo 4. Il capitolo consiste di quattro sottocapitoli nei quali vengono presi in considerazione gli effetti di ciascuna variabile topologica su alcune proprietà molecolari ed elettroniche. Il sottocapitolo 4.1 riguarda lo studio della delocalizzazione elettronica in composti modello costituiti da tetraetileni sostituiti con gruppi elettron-accettori e donatori. Sarà valutata l'efficienza dei diversi *pathway* di coniugazione π in modo da quantificare l'impatto del numero, della posizione e della natura dei sostituenti sull'estensione della delocalizzazione π . L'analisi mostrerà che la delocalizzazione è fortemente dipendente dalla natura del sostituito (donatore vs. accettore) piuttosto che dal modo di coniugazione considerato. Inoltre, l'energia di delocalizzazione associata ad un certo *pathway* è esaltata dall'aumento del grado di sostituzione. Questo è dovuto a un forte contributo dei sostituenti sull'orbitale π^*_T del tetraetilene, il quale è in genere più grande nel caso di gruppi donatori rispetto ai gruppi accettori. Nel sottocapitolo 4.2 sarà confrontata l'estensione della delocalizzazione π in oligomeri del polietilene

(PTA) e dell'*iso*-politriacetilene (*iso*-PTA) caratterizzati, rispettivamente, da un modo di coniugazione π lineare e geminale. La lunghezza della coniugazione effettiva delle specie neutre, determinata in base alle geometrie molecolari e alle energie di delocalizzazione, è pari a 24 legami coniugati per il PTA e solo 6 legami coniugati per l'*iso*-PTA indicando per quest'ultimo che la delocalizzazione π è interrotta all'atomo di carbonio con coniugazione geminale. Tuttavia, nel caso degli oligomeri di *iso*-PTA con carica positiva e negativa la delocalizzazione π si estende oltre l'atomo di carbonio geminale. Nel sottocapitolo 4.3 sarà considerato l'effetto sulla delocalizzazione π dovuto all'inserimento di unità etiniliche in oligomeri del poliacetilene (PA), e corrispondentemente, su alcune proprietà molecolari ed elettroniche. Inoltre, in questo sottocapitolo sarà studiata l'addizione laterale di unità etiniliche a oligomeri del PTA. I risultati ottenuti mostrano che l'inserimento di uno o due tripli legami nella catena del PA, aumentano l'estensione della delocalizzazione π ma diminuiscono l'efficienza con cui questa è promossa. L'addizione laterale di unità etiniliche ha anch'essa l'effetto di aumentare la delocalizzazione ma senza incrementare l'evoluzione delle proprietà elettroniche e molecolari in funzione della lunghezza della catena. Infine, nel sottocapitolo 4.4 sarà discusso l'effetto della sostituzione in posizione terminale di gruppi elettron-accettori e/o elettron-donatori sull'estensione della delocalizzazione π in funzione dell'aumento della lunghezza della catena di oligomeri del PTA e pePTA. In questo caso, tutte le proprietà investigate sembrano convergere allo stesso valore di saturazione osservato per gli oligomeri non sostituiti. Questo indica che l'effetto della sostituzione con i gruppi funzionali è significativa solo nel caso degli oligomeri più corti. L'analisi della delocalizzazione evidenzia che i gruppi elettron-donatori promuovono maggiormente la delocalizzazione elettronica rispetto ai gruppi elettron-accettori. Allo stesso tempo, i sistemi sostituiti con gruppi elettron-donatori mostrano una più rapida convergenza al valore di saturazione.

La tesi sarà conclusa con il Capito 5 in cui saranno esposte alcune considerazioni personali sugli sviluppi futuri dell'approccio per la valutazione dell'energia di delocalizzazione.

Publications

This thesis has lead to the following publications:

Subchapter 3.2

Maurizio Bruschi, Maria Grazia Giuffreda, Hans Peter Lüthi

Trans Versus Geminal Electron Delocalization in Tetra- and Diethynylethenes: A New Method of Analysis

Chemistry-a European Journal 8(18), **2002**, 4216-4227

Subchapter 4.1

Maria Grazia Giuffreda, Maurizio Bruschi, Hans Peter Lüthi

Electron Delocalization in Linearly π -conjugated Systems: A Concept for Quantitative Analysis

Chemistry-a European Journal 10(22), **2004**, 5671-5680

Subchapter 4.2

Maurizio Bruschi, Maria Grazia Giuffreda, Hans Peter Lüthi

Electron Delocalization in Extended Linearly π -conjugated Systems: Through Versus Cross Electron Delocalization in Polytriacetylene Oligomers

ChemPhysChem 6(3), **2005**, 511-519

Subchapter 4.3

Maurizio Bruschi, Maria Grazia Giuffreda, Hans Peter Lüthi

The impact of the Type and Strength of the Donor and/or Acceptor Functional Groups on the Electron Delocalization of Polytriacetylene and perethynyl-Polytriacetylene Oligomers

To be submitted to ChemPhysChem

Subchapter 4.4

Maurizio Bruschi, Maria Grazia Giuffreda, Hans Peter Lüthi

The Impact of Length and Type of the Backbone on the Electron Delocalization of Polyacetylenes, Polydiacetylenes, and Polytriacetylenes

To be submitted to ChemPhysChem

Related publications:

Maurizio Bruschi, Piercarlo Fantucci, Maddalena Pizzotti, Cristina Rovizzi

Tailoring Transition Metal Complexes for Nonlinear Optics Applications: A Theoretical Investigation of the Electronic Structure of $M(\text{CO})_x\text{ClyL}$ Complexes ($M = \text{Cr, W, Re, Ru, Os, Rh, Ir}$; $L = \text{Pyz, PyzBF}_3, \text{BPE, BPEBF}_3$)

Journal of Molecular Catalysis A **2003**, 204, 793-803

Maurizio Bruschi, Piercarlo Fantucci, Maddalena Pizzotti

Tailoring Transition Metal Complexes for Nonlinear Optics Applications. Part 2: A Theoretical Investigation of the Second Order Nonlinear Optical Properties of $M(\text{CO})_5\text{L}$ Complexes ($M=\text{Cr, W}$; $L=\text{Py, PyCHO, Pyz, PyzBF}_3, \text{BPE, BPEBF}_3$)

Journal of Physical Chemistry A **2005**, 109(42), 9637-9645

Maurizio Bruschi, Maria Grazia Giuffreda, Hans Peter Lüthi

'Measuring' Electron Delocalization in π -Conjugated Systems

Chimia **2005**, 59, 539-544

1 Introduction

The concept of electron delocalization is central to chemistry and is being broadly used to explain or to predict chemical phenomena or molecular and electronic observables. Properties such as dipole moments, polarizabilities, first and second-order hyperpolarizabilities, electron affinities, ionization potentials, and UV-vis absorption energies, are often discussed on the basis of electron delocalization. However, electron delocalization is not an observable of the molecular system: there is no operator \hat{I} such that electron delocalization can be expressed as an expectation value. Therefore, delocalization is a concept only, viewed differently and arbitrarily, both by theoretical and experimental chemists. Still, many attempts have been made to define theoretically or even to measure delocalization energies of π -conjugated systems. The dilemma to be afforded lies in the qualitative nature of the concept of electron delocalization, which renders any definition of delocalization parameters debatable since different values are possible with different definitions. On the other hand, the interest in π -conjugated compounds is not exclusively motivated by theory. Many of these compounds show very attractive chemical properties relevant to several areas of application, from biological chemistry to material science. For example, in the recent past, π -conjugated compounds have attracted considerable attention as materials for application in molecular electronics, with the vision to replace “silicon” by “organic materials”. In this respect, the

measure of electron delocalization of a π -conjugated molecular system may be very useful as a descriptor to assist the design of new compounds with tailored properties.

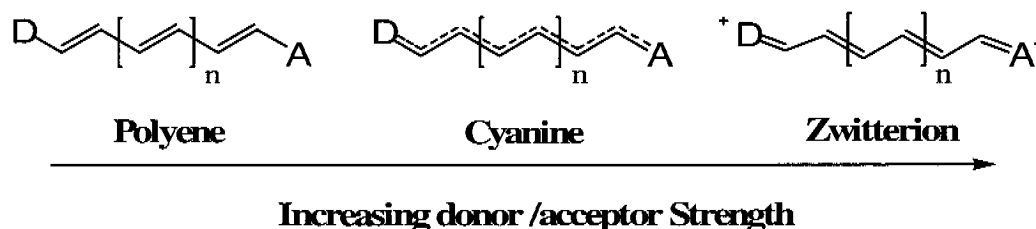


Figure 1.1: Schematic representation of a functionalized π -conjugated oligomer with various degrees of bond length alternation (BLA) induced by the length of the path and the substituents.

One important feature of π -conjugated molecular systems is their ability to change the electronic properties in response to external stimuli (substituents, optical excitation, etc.). The properties of the donor (D)/acceptor (A) functionalized polyacetylene (PA) shown in Figure 1.1, for example, can be “tuned” by the choice of functional groups. But also the length of the PA chain (the “backbone”), the use of spacers, i.e. units such as phenyl- or ethynyl-groups inserted into the oligomer chain, are additional options to be exploited for the optimization of molecular and electronic properties. Three important degrees of freedom that can be controlled in the design of molecules of this class with selected properties are:

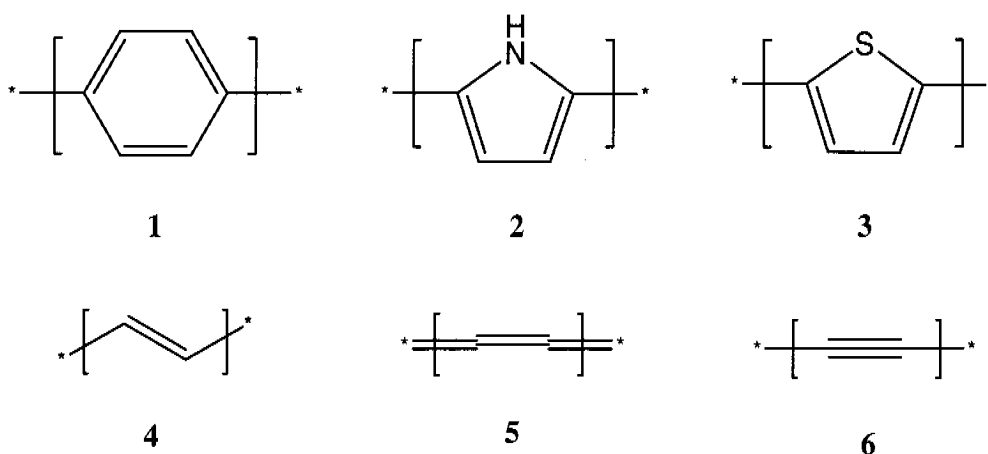
- Nature and length of the backbone (“bridge” between substituents)
- Type, strength, and position of the donor/acceptor functional groups
- Mode of the conjugation pathway (*trans*, *cis*, *geminal*; *through* or *cross*)

Nature and length of the backbone

π -electron delocalization is regulated by the type of the monomer unit used as a building block in the conjugated backbone. The strong influence of this moiety, bridging the donor

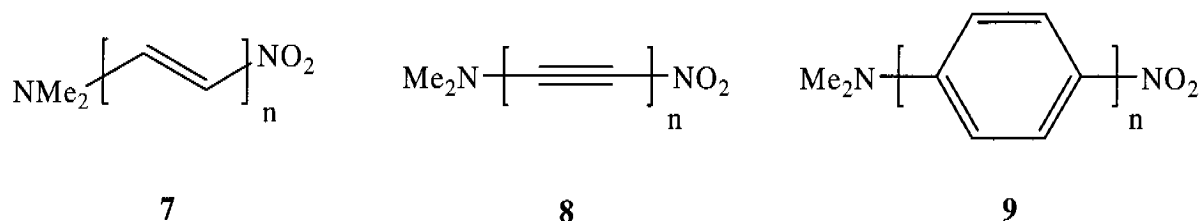
and/or acceptor functional groups, on the molecular and electronic properties of the material controls its application for a specific task.

The π -conjugated oligomers and polymers explored as materials for molecular electronics and photonics are based on aromatic rings, such as poly(para-phenylene) (PPP; **1**), polypyrrole (PPy; **2**) and polythiophene (PT; **3**), or nonaromatic π -conjugated chains such as polyene (**4**), cumulene (**5**) and polyyne (**6**).

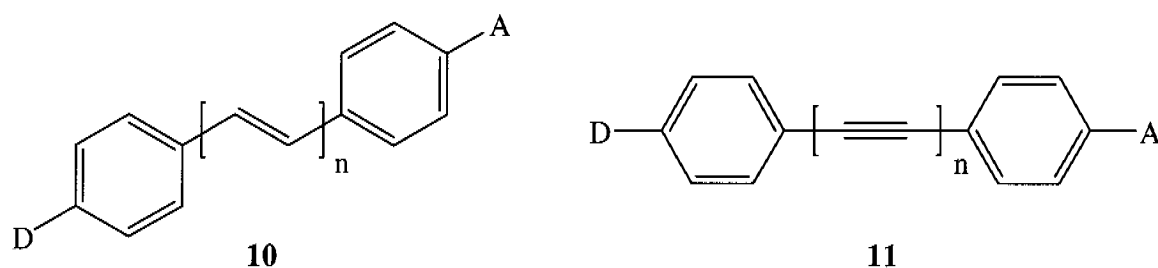


A number of experimental and theoretical investigations have suggested that these latter compounds exhibit much larger NLO response properties [1-9]. In fact, polyenes are often used as π -conjugated moieties in NLO active materials, as they provide the most effective pathway for an efficient charge transfer between the donor and the acceptor groups [1, 10]. Morley et al. [11, 12] using the correction vector approach on the basis of a Modified Complete Neglect of Differential Overlap (CNDO) method, including singly and doubly excited configurations (SDCI), predicted that the donor-acceptor polyenes (**7**) are significantly more efficient NLO materials than polyyenes (**8**), which, in turn, are more efficient than the corresponding polyphenylenes (**9**). In donor-acceptor substituted polyyenes and polyphenyls, the energetically favoured acetylenic form and the aromatic stabilization of the phenylene groups limit the extension of π -delocalization along the backbone. On the other hand, in the donor-acceptor substituted polyenes the neutral and charge separated forms

consisted of almost isoenergetic π -system with alternating double and single bonds, and, thus, allow more effective π -electron delocalization.



The calculation of first order hyperpolarizabilities β , using a Finite-Field (FF) approach with the semiempirical PM3 Hamiltonian, on donor-acceptor disubstituted α - ω -diphenylpolyenes (**10**) and the corresponding disubstituted α - ω -diphenylpolyyne (**11**), confirmed that polyyne gives lower NLO responses than polyenes [5, 6, 13].



An alternative explanation of the larger NLO values of polyenes with respect to polyyne can be formulated on the basis of the Sum-Over-State (SOS) approach for the calculation of the first and second-order hyperpolarizabilities [14]. Whereas only one major leading component of the SOS expansion (namely the HOMO \rightarrow LUMO transition) is present for the donor-acceptor functionalized polyenes, several transitions with large oscillator strength determine the hyperpolarizability values in the polyyne. These additional transitions involve p_y orbitals in the plane of the molecule, with transition moment vectors which oppose the direction of the charge transfer along the chain, and therefore, reduce the overall hyperpolarizability values [2, 15-17].

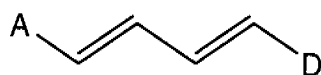
In π -conjugated compounds, the length of the conjugated chain (backbone) strongly affects the molecular and electronic properties, which can be tailored for a specific application of the material. An enhancement of the electronic and optical properties is expected with increasing length of the backbone until saturation of the property is reached. This limit is indicated as the effective conjugation length (ECL) of the backbone. Beyond this length, a further increase of the backbone size has no effect on the selected property. The evolution of the first and second hyperpolarizabilities β and γ with respect to the number of the monomer units (n) is usually given by the power law [13, 18, 19]:

$$\beta \text{ or } \gamma \propto n^z \quad (1.1)$$

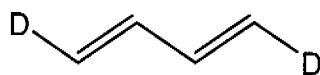
where z is a constant for any specific backbone. Brédas et al. [20] showed that the evolution of γ in polythiophene (PT) and polypyrrole (PPy) follows the power law for the shorter oligomers, with an exponent z equal to 3.9 and 4.9, respectively, whereas, from the oligomers of 6 and 7 monomer units for PT and PPy, respectively, the exponent starts to decrease indicating the incoming saturation effects.

Type, strength, and position of the donor/acceptor functional groups

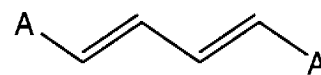
The nature, strength, position, and number of the donor/acceptor functionalities can affect dramatically the molecular and electronic properties of a π -conjugated compound. For example, Brédas et al. investigated the molecular and electronic structure of butadienes (**12-14**) functionalized with different donor ($-\text{NH}_2$, $-\text{NMe}_2$, $-\text{OH}$), and acceptor ($-\text{CHO}$, $-\text{CN}$, $-\text{NO}_2$) groups [21]. They performed Intermediate Neglect of Differential Overlap/Multi-Reference Determinant-Configuration Interaction (INDO/MRD-CI) calculations to determine the lowest singlet excited states. They showed that the largest bathochromic shift of the first transition energy was observed for the A/D derivatives (**12**) followed by the D/D (**13**), and finally, the A/A (**14**) substituted compounds. In addition, the transition energies of the A/D derivatives decreased with increasing π -donating and π -accepting strength of the substituents. This behaviour demonstrated a more effective charge transfer in the bis-nitro and bis-(dimethylamino) functionalized systems.



12



13

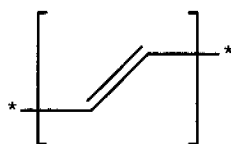


14

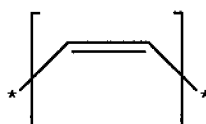
Morley et al. [11] in their investigation on the donor-acceptor functionalized polyenes, polyynes, and polyphenylenes showed that the maximum absorption wavelength (λ_{\max}) and the ground state dipole moment (μ_0) of polyphenylenes and polyynes tend to saturate at a smaller number of monomer units n compared to the corresponding functionalized polyenes.

Mode of the conjugation pathway

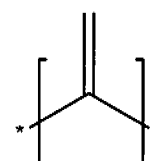
The third degree of freedom, which can be manipulated, to suit molecular systems with desired properties is the type of the conjugated pathway. Polyenes have been widely investigated in their *trans* conformation (**15**) since this conjugated pathway is expected to promote π -electron delocalization more efficiently along the molecular backbone. In fact, polyenes, in the *cis* (**16**) or *geminal* (**17**) configuration are not able to maintain planarity, due to the steric repulsion of hydrogen atoms, a characteristic that breaks down the π -electron delocalization.



15



16



17

The incorporation of acetylenic group into the polyene chain, as in the recently synthesized polytriacetylene (see section 1.3) provided fully planar molecular systems with a *cis* or

geminal π -conjugated pathway. In particular, the geminal (or cross) π -conjugation could provide an interesting device to modulate π -delocalization at the cross-linked carbon atom. However, this form of conjugation has sparsely been considered in material research and relatively little is known on the electronic communication via cross-conjugation in general.

It is a well-known fact that many of the thoughts leading to a breakthrough in chemistry were developed on the back of an envelope using simple concepts such as valence bonding (octet rule, resonance structures) and other qualitative concepts. To facilitate the communication between molecular modeling and physical organic chemistry, in this thesis we will introduce a method for the calculation of delocalization energies of π -conjugated compounds which helps to translate information obtained from first-principles theory (in particular electron densities) to qualitative concepts such as electron delocalization and π -conjugation. The method will be further applied to selected compounds with the aim of investigating the impact of the three topological variables discussed above on the molecular and electronic properties.

In the following subchapter we briefly review the historical evolution of the theory concerning electron delocalization, which provides a preface for the discussion of the concept of electron delocalization. Later we review more recent theoretical as well as computational approaches for the quantification of the electron delocalization.

1.1 Electron Delocalization in π -Conjugated Compounds

1.1.1 A Short Review of the History of Electron Delocalization in π -Conjugated Compounds

The description of electronic charge delocalized over multiple atoms as found in aromatic or in linearly π -conjugated compounds has been a fascinating topic since the discovery of benzene by Faraday [22] and the concept of its ‘partial valences’ of Kekulé [23] and Thiele [24] who postulated a structure virtually identical to that we know nowadays. The first

success of the theory of Kekulé and Thiele was obtained in the end of 1920's when the structure of hexamethylbenzene was solved by Lonsdale [25, 26] by means of X-ray diffraction, finding six identical carbon-carbon bond lengths.

However, the reason of the carbon-carbon bond equalization and of the special stability of benzene could not be explained until the development of quantum mechanics. In the early stage of quantum theory the Valence Bond (VB) method, developed by Slater and Pauling [27-34], and the Molecular Orbital (MO) method developed by Hund and Mulliken [35-38] gained a proper perspective with the recognition that electron waves are intrinsically delocalized.

In the context of his resonance theory, Pauling defined the resonance energy of a conjugated system as the energy change between the most stable resonance structure and the real system whose wavefunction is composed of all possible resonance structures [39, 40].

A fundamental step in the study of electron delocalization in π -conjugated molecules was done by Hückel, who first invoked that the π -type and σ -type orbitals were different for their symmetry with respect to the molecular plane. Based on this assumption, Hückel designed a method to tackle a many electron problem by considering the π -electron explicitly, while incorporating the rest in an effective monoelectronic Hamiltonian [41-44]. The expansion of π -MOs as a linear combination of p atomic orbitals

$$\phi_i = \sum_j c_{ij} \chi_j \quad (1.2)$$

leads to the equation:

$$\sum_i [(H_{ij}^{\text{eff}} - S_{ij} e_k) c_{ik}] = 0 \quad (1.3)$$

where the e_k 's are the roots of the secular equation:

$$\det(H_{ij}^{\text{eff}} - S_{ij} e_k) = 0 \quad (1.4)$$

The further assumption in the Hückel theory involves the integrals. The integral H_{ii} (labelled as α) was assumed to have the same value for every carbon atom in the molecule and it was called the Coulomb integral. Moreover, the integral H_{ij} (labelled as β) was assumed to have

the same value for any two carbon atoms bonded to each other and to vanish for all nonbonded carbon atoms. Finally, the integral S_{ij} was set equal to 1 if $i=j$ and equal to 0 for $i \neq j$.

The delocalization or resonance energy (RE) of a conjugated hydrocarbon X was defined by Hückel, taking ethylene (with a fully localized π -bond) as a reference system and using the equation:

$$RE(X) = E_{\pi}(X) - nE_{\pi}(\text{CH}_2=\text{CH}_2) \quad (1.5)$$

that is, as the difference between the π energy of X (E_{π}) and n times (where n is the number of unsaturated bonds) the π energy of ethylene. For example, the application of the Hückel method to benzene leads to the calculation of the π -electron ground state energy equal to:

$$E_{\pi} = 6\alpha + 8\beta. \quad (1.6)$$

In the case of ethylene (the reference system), the Hückel energy is $2\alpha + 2\beta$. Therefore, the RE of benzene was calculated as:

$$RE = E_{\text{benzene}} - 3E_{\text{ethylene}} = 2\beta \quad (1.7)$$

On the other hand, the resonance energy of 1,3-butadiene (with respect to two ethylene molecules as reference system) is equal to 0.472β , a value about four times lower than that obtained for benzene. This traditional method of calculating Hückel REs of π -conjugated hydrocarbons, by comparing the Hückel π -electron energy (E_{π}) of a molecule with n unsaturated bonds and $E_{\pi} = n(2\alpha + 2\beta)$ of n ethylene molecules has serious shortcomings. As mentioned above, in fact, the method predicts substantial resonance energy for linear polyenes, whereas experiment shows that the resonance stabilization in these molecules is rather small. Moreover, this method predicts significant resonance stabilization for certain cyclic polyenes that experiment reveals to be unstable, with no aromatic character. To produce more reliable results, it is important not only to improve the accuracy of the calculation but also to refer the resonance or delocalization energy to a proper reference system.

In 1951 Mulliken and Parr [45] calculated the resonance energy of benzene (and butadiene) with respect to a cyclic reference structure with three single (1.54 Å) and three

double (1.34 Å) localized bonds. On the other hand, Breslow [46] in 1963 suggested that the open chain analog might be the appropriate reference structure for the calculation of RE in cyclic π -conjugated compounds. That is, benzene should be compared to hexatriene instead of three isolated C=C bonds as in Hückel RE. The application of their method to several monocyclic ions gave results in better agreement with their expectation than Hückel results.

The problem was further addressed by Salem [47] who defined an empirical resonance energy of benzene as the difference between the absolute values of the observed heat of formation and the calculated heat of formation for a single Kekulé structure. This quantity then represents the additional stabilization in benzene due to the interaction between the conjugated double bonds not taken into account by one Kekulé structure.

Dewar and Chung in 1965 [48] investigated several annulenes using Hückel, Pariser-Parr-Pople (PPP) [49], and their own split p orbital (SPO) methods, with a Mulliken-Parr reference structure but with a single bond length of 1.48 Å. However, the results were not satisfactory since there was scarcely an improvement with respect to the Hückel results. In later works Dewar et al. [48, 50-52] investigated the delocalization in linear polyenes with the PPP method. They found that the energy in linear polyenes increases linearly as a function of the number of C-C and C=C bonds and that it can be represented accurately in terms of additive bond energies. Therefore, the calculated atomization energies could be written as:

$$\Delta H_a = n'E' + n''E'' + n_{CH}E_{CH} \quad (1.8)$$

where n' and n'' are respectively the numbers of formal C-C and formal C=C bonds in the polyene, $E' = 4.3499$ eV and $E'' = 5.5378$ eV are their energies, and n_{CH} and $E_{CH} = 4.4378$ eV are defined similarly for the C-H bonds. Dewar and de Llano [53, 54] then used the additivity of Equation 1.7 to define a polyene-like reference structure for the computation of RE of any conjugated hydrocarbon. For example, in the case of benzene the reference structure is given by a "cyclohexatriene" whose heat of atomization was calculated from Equation 1.9:

$$RE(\text{benzene}) = \Delta H_a(\text{benzene}) - \Delta H_a(\text{reference}) = \Delta H_a(\text{benzene}) - [3E' - 3E'' - 6E_{CH}]. \quad (1.9)$$

This RE has been named as Dewar resonance energy (DRE) and is accepted nowadays with some modification being determined routinely by using homodesmotic processes [55].

More recently, Hess and Schaad [56] used the Hückel approach and the Dewar and de Llano reference structure to calculate the RE of several acyclic and cyclic π -conjugated compounds. Since they did not obtain satisfactory RE for the acyclic systems with only two carbon-carbon bond types in the reference structure, they decided to introduce eight different types of carbon-carbon bond representatives of different σ frameworks. The RE of compound X is then defined as:

$$RE(X) = E_{\pi}(X) - E_{ref}(X) = E_{\pi}(X) - \sum_{ij} n_{ij} E_{ij} \quad (1.10)$$

where the sum in the equation goes over all defined bond types. The REs calculated with this method appear to predict with reasonable accuracy the aromatic and antiaromatic character of the molecular systems investigated. For example, in the case of benzene the energy of the reference structure is:

$$E_{\pi} = 3E_{HC=CH} + 3E_{HC-CH} = 7.61\beta \quad (1.11)$$

and therefore its Hückel RE is equal to

$$RE = E_{\pi}(\text{benzene}) - E_{\pi}(\text{reference}) = (7.61 - 8)\beta = -0.39\beta. \quad (1.12)$$

It should be noted that since the reference system is different with respect to the original work of Hückel, the RE differs significantly (-0.39β vs -2β). This resonance energy, normalized by the number of p electrons, was used as an aromaticity criterion.

Hess and Schaad [56] also pointed out that the accuracy of the calculated RE is more related to the choice of the reference structure than to the level of theory considered.

1.1.2 The Concept of Electron Delocalization and its Usefulness in Chemistry

The short overview concerning the early approaches to quantify delocalization energies presented above offers the opportunity for a discussion on the concept of electron delocalization and its applications in chemistry.

First, it is useful to give a clear definition of the terms conjugation, resonance, and delocalization, which are often used improperly. The term π -conjugation referred to unsaturated hydrocarbons was introduced to indicate a molecule with alternate saturated and unsaturated bonds. In the following, we will refer to this topological definition, and for example, the expression “extension of π -conjugation” will be only used to indicate an increasing number of alternating double (triple)/single bonds. The terms resonance and delocalization should be used in the framework of Valence Bond (VB) and Molecular Orbital (MO) theories, respectively. In fact, in Valence Bond theory the reference structure corresponds to the most stable resonance form, and resonance energies are calculated by taking into account the contributions of all other (less stable) resonance forms to the ‘exact’ wavefunction of the molecular system. On the other hand, in MO theory, the canonical wavefunction is composed by orbitals delocalized over the entire system, and delocalization energies are then calculated with respect to a reference system with completely localized orbitals. Clearly, in the limit of the resonance theory of Pauling, resonance and delocalization energies correspond to each other, at least, when they are defined as the energy difference between the actual (delocalized) wavefunction and the most stable (localized) resonance form.

It is important to note that electron delocalization is not an observable. This is clearly pointed out in the definition provided by IUPAC in 1994, which states “*a quantum mechanical concept most usually applied in organic chemistry to describe the pi bonding in a conjugated system. This bonding is not localized between two atoms: instead each link has a fractional double bond character or bond order*”. The experimental impossibility of measuring electron delocalization gave rise to many controversial discussions and issues around this milestone concept in chemistry. As outlined in the previous section, from a theoretical point of view, a critical point of discussion is not only the approach used for the calculation of delocalization (or resonance) energies but also (and mainly) the definition of the reference structure. In fact, quite different values have been reported for different definitions of the reference state (see section 1.1.1). This point has been clearly illustrated by Janoschek [57] who reviewed the different definitions of the resonance energy of benzene and found that the choice of a proper definition is only a matter of taste since different values

are possible with different definitions. Obviously, the key reason is that neither a molecular nor an electronic structure can be assumed for the fictitious reference molecules.

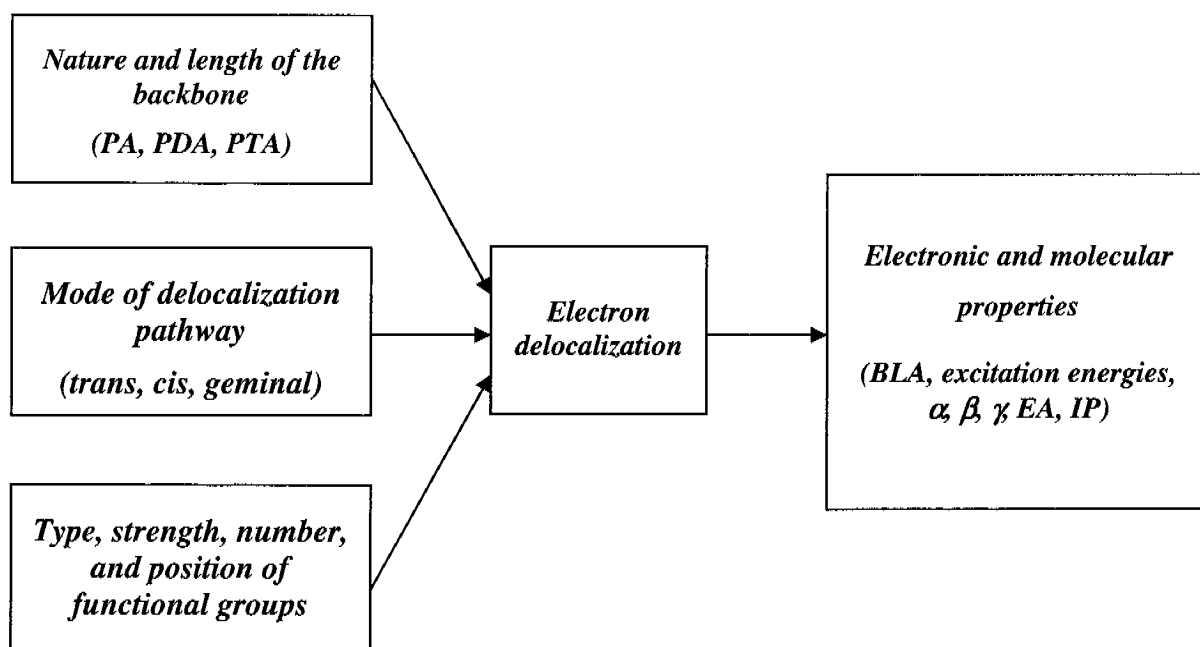


Figure 1.2: Chart illustrating the role of electron delocalization as a descriptor which correlates the molecular structure with physical observables.

In spite of the problems inherent to the definition and quantification of electron delocalization, this concept is useful to rationalize and understand the reactivity as well as the correlation between the molecular and electronic structure and the physical observables of many molecular systems. In this sense, the concept of electron delocalization is truly a milestone in chemistry. As illustrated by Heine et al. “the concept *per se* is a strong enough motivation that justifies the continuous effort of many researchers to develop in a more general way” [58]. According to these observations, methods aiming at the quantification of electron delocalization are highly valuable in the rationalization of chemical phenomena, provided that their physical meaning should not be overestimated. In this respect, delocalization parameters should properly be considered as *descriptors* in a quantitative structure-property relationship (QSPR) approach. This is clearly illustrated in Figure 1.2,

which explains the plan followed in this study. The manipulation of the topological degrees of freedom discussed at the very beginning of this section influences the molecular and electronic observables like the bond length alternation (BLA), the excitation energies, the nonlinear optical properties, the ionization potentials and the electron affinities. The electron delocalization is the descriptor which correlates (to different extents) with each of the above molecular observables.

Finally, it is helpful to define some terms concerning electron delocalization which will be widely used in the following. In this study, the extent of the electron delocalization in a π -conjugated molecular system will be quantified through the calculation of delocalization energies. A molecule in which the total amount of delocalization energy is larger with respect to a ‘comparable’ one is said to promote more electron delocalization. On the other hand, not only the total amount of delocalization energy is an important descriptor, but also, the rate at which it evolves as a function of the π -conjugated length. This will be referred to the term efficiency in promoting electron delocalization. For example, in the next chapters it will be shown that a certain conjugated pathway can promote more electron delocalization with respect to another one, but less efficiently.

1.2 An Overview of the Approaches for the Quantification of Electron Delocalization

1.2.1 Experimental Approaches

In the field of thermochemistry, resonance or delocalization energies of conjugated systems can be determined experimentally by means of the heats of formation and the heats of hydrogenation.

The heat of formation $(\Delta H^f)_{\text{obs}}$ of conjugated molecules can be measured by classical calorimetric experiments. $(\Delta H^f)_{\text{obs}}$, and in particular for aromatic systems, is much larger (in absolute value) than that evaluated by the sum of the so called bond energies, and indicated as *empirical heat of formation* $(\Delta H^f)_{\text{calc}}$. This quantity is therefore derived by assuming that

the bond energies are additive and roughly constant from substance to substance. For example, the heat of formation of CH_4 , $\text{CH}_3\text{-CH}_3$ and $\text{CH}_3\text{-CH=CH-CH}_3$ can be decomposed, under the assumption of bond energy additivity, as follows:

$$\Delta H_{\text{CH}_4}^f = 4E_{\text{C-H}} \quad (1.13)$$

$$\Delta H_{\text{CH}_3\text{-CH}_3}^f = E_{\text{C-C}} + 6E_{\text{C-H}} \quad (1.14)$$

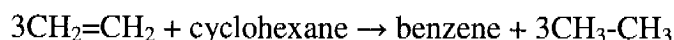
$$\Delta H_{\text{CH}_3\text{-CH=CH-CH}_3}^f = 2E_{\text{C-C}} + E_{\text{C=C}} + 8E_{\text{C-H}} \quad (1.15)$$

from which $E_{\text{C-H}}$, $E_{\text{C-C}}$ and $E_{\text{C=C}}$ are derived. $(\Delta H^f)_{\text{calc}}$ of benzene is then calculated as:

$$\Delta H_{\text{obs}}^f(\text{benzene}) = 6E_{\text{C-H}} + 3E_{\text{C-C}} + 3E_{\text{C=C}} \quad (1.16)$$

and compared to the corresponding $(\Delta H^f)_{\text{obs}}$. The interesting experimental fact concerning conjugated molecules is that they possess an observed heat of formation which is larger in absolute value (more negative) than the *empirical heat of formation* calculated from any single Kekulé formula. This difference is called the *empirical resonance energy*, and thus represents the additional stabilization of conjugated molecules due to interactions between the conjugated double bonds which are not taken into account by any Kekulé structure. For example, values of the *empirical resonance energy* calculated for benzene, naphthalene and azulene are equal to 36.0, 60.8 and 31.5 kcal mol⁻¹.

Resonance energies can also be evaluated from experimental heats of formation by designing proper isodesmic and homodesmotic reactions^a. However, the evaluation of resonance energies strongly depend on the compounds taken as references and many definitions have been suggested [59]. For example, the resonance energy of benzene according to the following isodesmic reactions:



differ by more than 15 kcal mol⁻¹, being equal to 64.2 and 48.9 kcal mol⁻¹, respectively [60].

^a An isodesmic reaction is defined as a chemical reaction in which the type of chemical bonds broken in the reactant are the same as the type of bonds formed in the reaction product, while homodesmotic reactions are defined as a subclass of isodesmic reactions in which reactants and products contain equal numbers of carbon atoms in corresponding states of hybridization.

A limitation in the use of ΔH^f to determine resonance energies lies in the inaccuracy inherent to the difference of large numbers. For this reason, resonance energies calculated from heats of formation are reliable only for those compounds with high values of this parameter, such as aromatic molecules, but they are not very trustworthy for conjugated molecules like butadiene in which the additional stabilization from electron delocalization is expected to be small. For these molecules the second method cited above, namely the heat of hydrogenation appears to be more reliable. The calculation of resonance energies from heats of hydrogenation is based on the fact that the heats of hydrogenation of π -conjugated molecules are less (in absolute value) than those evaluated for an equal number of isolated double bonds. This means that π -conjugated molecules must be more stable than a system with the same number of independent C=C bonds. This additional stability is associated to the interaction between the conjugated double bonds, and the energy of stabilization is thus the resonance energy. As stated above, the resonance energies calculated from heats of hydrogenation are more reliable than those obtained from heats of formation since the numbers involved in the differences are much smaller. The delocalization (or resonance) energy of benzene, for example, can be obtained experimentally as the difference between the heat of hydrogenation of benzene and three times the heat of hydrogenation of cyclohexene.

$$RE_{\text{benzene}} = \Delta H_{\text{hydrog}}(\text{benzene}) - 3\Delta H_{\text{hydrog}}(\text{cyclohexene}) \quad (1.17)$$

This leads to the value $RE_{\text{benzene}} = 35.2 \text{ kcal mol}^{-1}$, which agrees perfectly the empirical resonance energy calculated from the heats of formation.

It is important to realize that the resonance energies determined as described above contain several contributions that cannot properly be ascribed to π -electron delocalization, and that therefore, render the comparison with the theoretical values not straightforward. First, the resonance energies contain an energy contribution from the change in hybridization of single bonds which cannot be clearly estimated. Second, the resonance energies also contain a contribution due to the change in hyperconjugative interactions of the σ -framework. Furthermore, the resonance energies contain an energy contribution from the compression of the σ -bonds, which is different between the reference structure and the π -conjugated molecule. The importance of these contributions has been discussed by Dewar [54], finding

for benzene that after the deletion of these contributions the resonance energy reduced to 13 kcal mol⁻¹.

Even if resonance or delocalization energies are, clearly, the reference parameter to quantify electron delocalization in π -conjugated systems, other parameters can be used to evaluate electron delocalization. A useful concept, in this regard, is the bond length alternation (BLA) defined as the average difference in length between adjacent bonds in a π -conjugated pathway. π -electron delocalization affects the molecular geometry by increasing the length of the C=C (or C \equiv C) bonds and by decreasing the length of C-C bonds. Therefore, the BLA decreases with increasing delocalization. In fact, according to Peierls [61] the band gap E_g of polyacetylene (PA) is directly proportional to the BLA, defined as the difference between long (C-C) and short (C=C) bonds (ΔR):

$$E_g = k\Delta R. \quad (1.18)$$

Brédas and co-workers [62] in the investigation of the first (α), second (β), and third (γ) order polarizabilities of a series of donor-acceptor polyenes using the sum-over-state approach showed that the distortion of the BLA from the polyene-like structure to a polymethine-like structure tunes the electronic and NLO characteristics of the chromophore because of the changes in π -delocalization. Many recent studies on several oligomeric and polymeric chromophores supported these results [63-68].

1.2.2 Theoretical Approaches

Recent approaches to the calculation of resonance or delocalization energies can be included in the VB or MO schemes. In the framework of MO theory, delocalization energies can be calculated as the difference between the energy of the delocalized wavefunction and the expectation value of a reference wavefunction in which the canonical orbitals are replaced by appropriate nonresonating, completely localized MOs.

Kollmar [69] examined three methods for the construction of nonresonating π -orbitals on several conjugated compounds: i) localized molecular orbitals transferred from an SCF calculation of ethylene to the conjugated system; ii) basis function coefficients of strictly

localized π MOs of the reference state obtained as the square roots of the corresponding diagonal elements of the bond order matrix of the π -conjugated system; iii) localization of the canonical π MO using the localization scheme of Boys [70]. The application of the three methods to 1,3-butadiene with a C-C single bond length of 1.48 Å leads to very similar values for the vertical delocalization energy (9.49, 9.59 and 9.51 kcal mol⁻¹, respectively).

Skaarup et al. [71] performed full geometry optimizations for planar and perpendicular conformations of 1,3-butadiene with the assumption that π -delocalization is suppressed at the highest point of the rotational barrier. Since in their calculations the C-C bond varied only by 0.07 Å between the *trans*-planar and the perpendicular conformation, in which π -delocalization should be switched off, they concluded that the shortening of the C-C bond of butadiene compared to that in an alkane is not due to the π -electron delocalization, but to the effects of rehybridization of carbon atoms from sp³ to sp². However, Daudey et al. [72] pointed out that hyperconjugation stabilizes the perpendicular form and tends to compensate the loss of direct π -electron delocalization.

Weinhold et al. [73] studied the electron delocalization in benzene using the Natural Bond Orbital (NBO) theory to generate the localized π -orbitals of the reference structure. The NBO theory and the approach for the calculation of delocalization energies using natural bond orbitals are the main subject of this thesis and will be explained in detail in the next chapter. The calculated vertical delocalization energy was equal to 147 kcal mol⁻¹, a value that was improperly compared with the experimental value of the adiabatic resonance energy. The deletion procedure of the NBO theory was also extensively used by Schleyer et al. [74-78] to study hyperconjugative effects in many molecular systems.

Mo and Schleyer [79-83] proposed a method which is based on an orbital deletion procedure (ODP) to study the delocalization effects in carbocations and boranes. The idea was quite simple: p orbitals of the positively charged carbon atoms (or the p orbital of boron in boranes) were “deactivated” by setting their one electron integrals very high and assigning a value of zero to their overlap integral with all other functions. The resulting localized wavefunction can also be subsequently optimized leading to geometries in which the effects of conjugation and hyperconjugation are excluded. A generalization of the ODP method valid for all molecular systems and named block-localized wavefunction (BLW) method has been

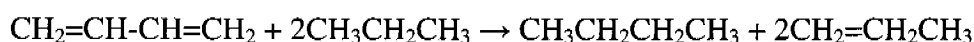
proposed by Mo and Peyerimhoff [84]. In this method, the wavefunction for the hypothetical and strictly localized structure is constructed based on the assumption that all electrons and primitive basis functions can be divided into selected subgroups. The molecular orbitals belonging to the same subgroup are constrained to be mutually orthogonal, while those belonging to different subgroups are free to overlap. This procedure produces final orthogonal orbitals which are expected to contain only an orthogonalization tail and no delocalization tail which are obtained, in turn, from the direct localization of canonical MOs [70, 85, 86]. The BLW approach has been first applied to the study of the conjugation and hyperconjugation effects in allyl ions and propene. Recently, a geometry optimization algorithm has been implemented in the BLW method [87], allowing to study delocalization effects not only on the energetic stability but also on the molecular geometries. Calculations on a series of *trans*-polyenes of increased chain length showed that the π -delocalization is, indeed, responsible for the shortening and lengthening of C-C and C=C bonds, respectively.

Mo et al. [88] used the bonded tableau unitary group valence bond approach to investigate on the π -electron delocalization of benzene cyclobutadiene and 1,3-butadiene. They found the vertical resonance energy (VRE) and the theoretical resonance energy (TRE) of benzene equal to 74.3 and 44.5 kcal mol⁻¹, respectively. The last value is in discrete agreement with the well-known experimental value of 36 kcal mol⁻¹. They also concluded that the driving force for the equalization of the C=C bonds is the π -electron delocalization, in contrast to the viewpoint of Shaik et al. [89] who suggested on the basis of VB calculations that the π electrons in benzene are distortive along a bond alternation mode, and that equalization of the C=C bonds is constrained by the σ frame. VRE and TRE calculated by Mo et al. for butadiene are equal to 9.37 and 8.52 kcal mol⁻¹, respectively, in good agreement with the experimental value of 7.2 kcal mol⁻¹ [90].

Another frequently adopted approach to theoretically estimate the stabilization due to the π -conjugation is the design of isodesmic [91, 92] or homodesmotic [93, 94] reactions, which have already been shortly introduced in the previous subsection (for the definition of isodesmic and homodesmotic reaction see the footnote on Pag. 15). For instance, the delocalization effect in butadiene can be calculated by the following reaction:



in which there is retention of the number of bonds of a given formal type but with a change in their relation to each other. However, as stated previously it has been recognized that the delocalization energies for the same molecular system depend on the selection of the reference molecules, where additional effects such strain and hyperconjugation, which may significantly contribute to the overall reaction, are hard to separate. In fact, if the following isodesmic reaction is considered:



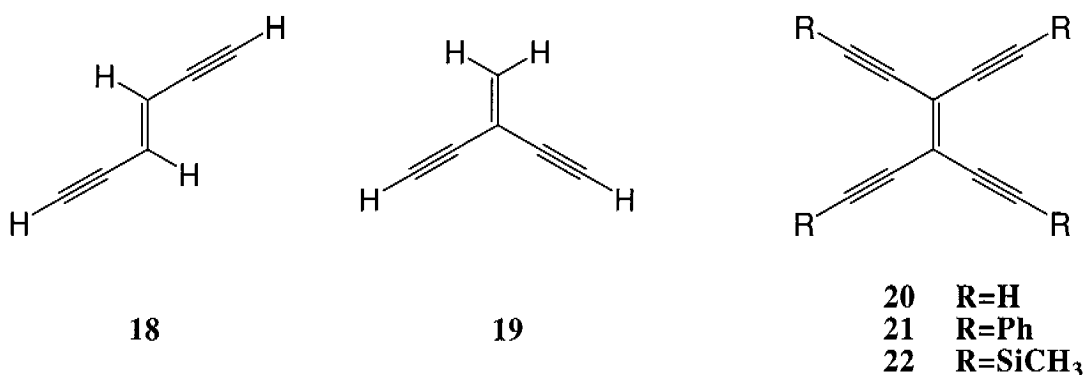
the enthalpy change is only $3.1 \text{ kcal mol}^{-1}$.

Various criteria, other than delocalization (or resonance) energies, based on geometrical, energetic and magnetic properties have been proposed to align the magnitude of electron delocalization effects among similar molecules [95, 96]. For example, Schleyer et al. [60, 97] proposed the use of the nucleus-independent chemical shift (NICS) calculated at the ring centre as a criterion to establish the aromatic or antiaromatic character of cyclic π -conjugated systems. The approach is based on the unusual protons chemical shifts of aromatic and antiaromatic molecules. In fact, the diatropic ring current of aromatic molecules produces modest displacements of the chemical shifts to lower magnetic field for protons located outside the aromatic rings, but much larger upfield displacements of protons located inside the aromatic rings, which resonate to negative values (for example, the δH of the six inner hydrogens of [18]-annulene is equal to -3.0 ppm vs $\delta\text{H} = 9.28$ for the outer protons). On the contrary, the paratropic ring currents of antiaromatic molecules gives rise to an inverted scheme; the inner protons resonate to much higher values than the outer ones (in the [18]-annulene dianion the δH of the two sets of inner protons is equal to 20.8 and 29.5 ppm while δH of outer protons is equal to -1.1 ppm). The evaluation of the NICS at the ring center, therefore, appears as a reliable criterion to investigate the aromaticity/antiaromaticity of a cyclic π -conjugated molecule since (in the NMR chemical shift convention) negative values are consistent with an aromatic character, while positive values are consistent with an antiaromatic character. Furthermore, Schleyer et al. showed that for a large set of aromatic/antiaromatic molecules the calculated NICS correlate fairly well with other

aromaticity criteria such as the aromatic stabilization energies and the magnetic susceptibility exaltations.

1.3 Acetylenic Carbon Rich Compounds as Example of Molecules with Extended π -Delocalization

Trans-diethynylethene [t-DEE; *Z*-exan-3-ene-1,5-diyne; **18**], *geminal*-diethynylethene [g-DEE; 2-ethynyl-butan-3-ene-1-yne; **19**] and tetraethynylethene [TEE; 3,4-ethynyl-exan-3-ene-1,5-diyne; **20**] and its derivatives represent a class of mono- and two-dimensionally conjugated building blocks with established potential as precursors to carbon-rich nanometer-sized compounds with unusual structures, high stability, and useful electronic and nonlinear optical properties [98, 99]. In 1969 Hori et al. [100] synthesized the tetrakis-(phenylethynyl)ethene (**21**) as the first member of this class and was followed several years later by the persilylmethylated derivative (**22**) synthesized by Hauptmann [101-103].



Hopf et al. [104] in 1991 proposed an alternative route to the synthesis of tetrakis-(phenylethynyl)ethene and reported its X-ray crystal structure. In the same year, Diederich et al. [105] reported the first synthesis of the parent unprotected TEE, C₁₀H₄ (**20**). In the last 15 years the synthetic flexibility inherent to the TEE core and the development of synthetic routes with various protecting and/or substitution patterns [106-109] allowed the use of DEEs and TEE as building blocks for the preparation of a broad range of new carbon-rich

compounds of nanometer scale such as rod-like linear polymers with the fully conjugated polytriacetylene (PTA) backbone [110-116] dendralenes [117], radialenes [118, 119] and dehydroannulenes [120, 121] (see Figure 1.3).

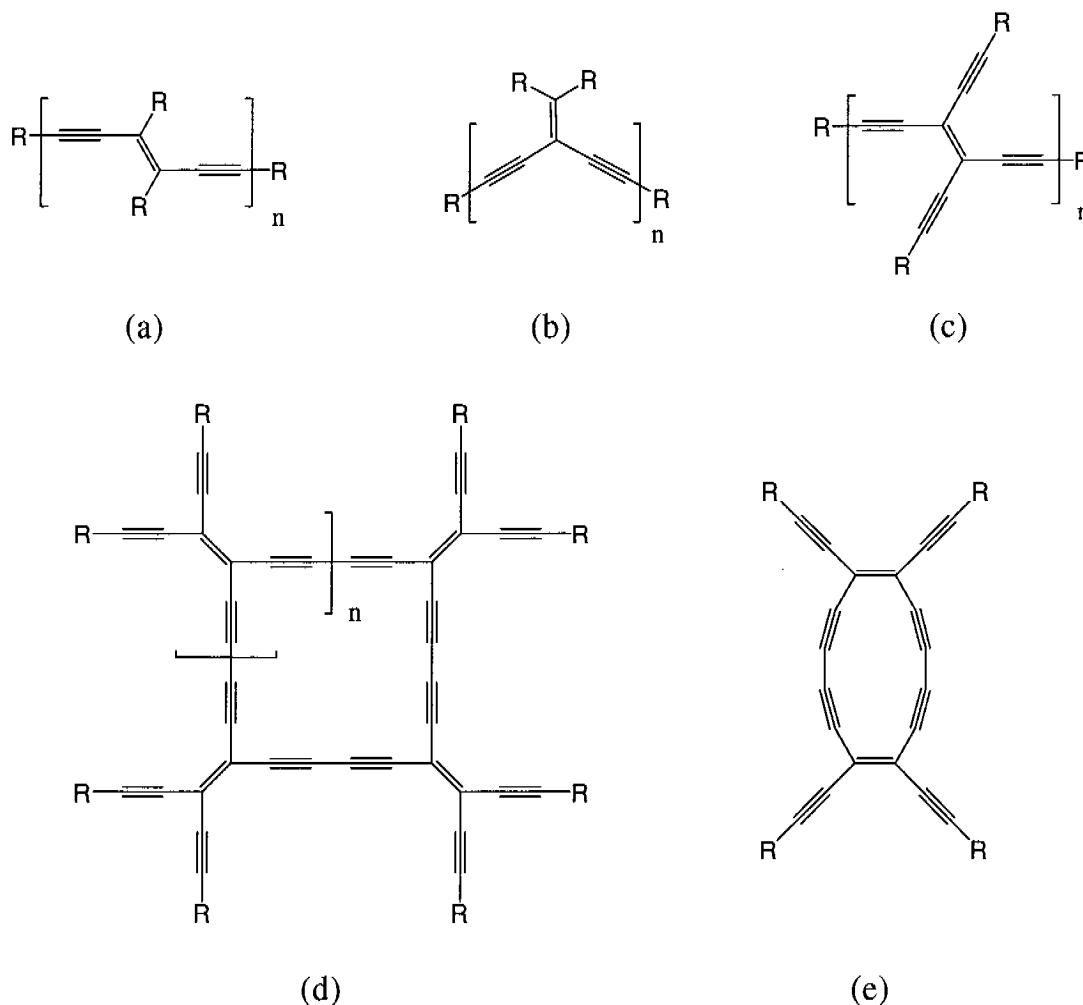


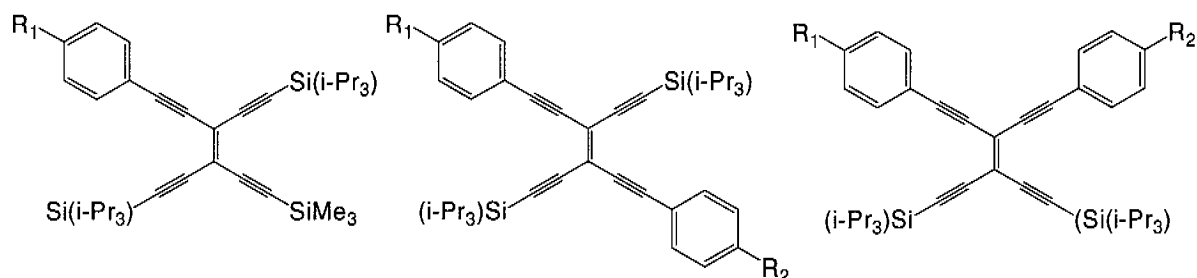
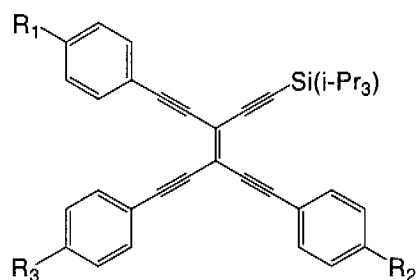
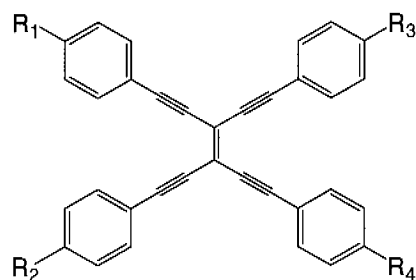
Figure 1.3: (a) linearly conjugated polytriacetylene (PTA) built with *t*-DEE monomer units. (b) cross-conjugated *iso*-polytriacetylene (*iso*-PTA) built with *g*-DEE monomer units. (c) Two dimensional perethynyl-polytriacetylene (*pe*PTA) built with TEE monomer units. (d) Expanded radialene. (e) Dehydroannulene.

PTA oligomers and polymers [110, 113] and their *cross*-conjugated isomers *iso*-polytriacetylene (*iso*-PTA) [122, 123] have also been synthesized from diethynylethenes **18**

and **19**, respectively. These are new members of a class of carbon-rich π -conjugated polymers with a non aromatic backbone, which ranges from polyacetylenes [PA's; $-(\text{CR}=\text{CR})_n-$], via polydiacetylenes [PDA's, $-(\text{C}\equiv\text{C}-\text{CR}=\text{CR})_n-$], to allotropic carbon polyyne [$-(\text{C}\equiv\text{C})_n-$]. In particular, *cross*-conjugation has been rarely considered for the preparation of highly π -conjugated oligomers and polymers because of the likely reduced extent of π -delocalization along the *cross*-conjugated carbon backbone. However it could represent an interesting alternative to the more prevalent linear π -conjugation for the possibility to generate desirable electronic characteristics such as an increased "optical transparency", which is essential for optical applications in the visible region of the spectrum [124-126].

Functionalization of the TEE core with donor and/or acceptor substituents renders these compounds promising materials for applications in molecular electronics and photonics. A broad library with mono- (**23**, **24**), di- (**25-30**), tri- (**31-32**), and tetra-functionalized (**33-38**) TEE derivatives has been created and used to investigate the effects of the nature, number, and position of the substituents on the selected properties such as electronic absorption [127, 128], redox behaviour [129, 130] and nonlinear optical responses [131-135].

These compounds are ideal for studying conjugation effects because in contrast to similar structures such as stilbenes [136-139] and tetraphenylethenes [140, 141], the TEEs have a fully planar, sterically unhindered framework. The acetylenic units keep the aromatic rings with donor or acceptor pendant functionalities far enough to prevent unfavourable steric interactions and thus electronic effects can be isolated from steric influences. This has been shown by X-ray structural analysis of several silyl- and arylated TEEs, which, in fact, reports nearly perfect planar structure for the entire π -conjugated skeleton, including the aryl rings [104-106, 127, 128, 142, 143]. The functionalization of the TEE core at different positions generates different π -conjugated pathways (*trans*, *cis* and *geminal*). The complete functionalization of TEE provides six possible π -conjugation pathways combining two *trans* (a), two *cis* (b), and two *geminal* (c) modes of conjugation (Figure 1.4). For such compounds the knowledge of how each π -conjugation pathway operates in the modulation of a selected property is, of course, of basic interest.

23 $R_1 = \text{NO}_2$ 24 $R_1 = \text{NMe}_2$ 25 $R_1 = R_2 = \text{NO}_2$ 26 $R_1 = R_2 = \text{NMe}_2$ 27 $R_1 = \text{NO}_2$; $R_2 = \text{NMe}_2$ 28 $R_1 = R_2 = \text{NO}_2$ 29 $R_1 = R_2 = \text{NMe}_2$ 30 $R_1 = \text{NO}_2$; $R_2 = \text{NMe}_2$ 31 $R_1 = R_2 = R_3 = \text{NO}_2$ 32 $R_1 = R_2 = \text{OMe}$; $R_3 = \text{NO}_2$ 33 $R_1 = R_2 = \text{OMe}$; $R_3 = \text{NO}_2$ 34 $R_1 = R_2 = R_3 = \text{H}$; $R_4 = \text{NO}_2$ 35 $R_1 = R_2 = \text{H}$; $R_3 = R_4 = \text{NO}_2$ 36 $R_1 = R_2 = \text{NO}_2$; $R_3 = R_4 = \text{NMe}_2$ 37 $R_1 = R_3 = \text{NO}_2$; $R_2 = R_4 = \text{NMe}_2$ 38 $R_1 = R_4 = \text{NO}_2$; $R_2 = R_3 = \text{NMe}_2$

An interesting application of TEE derivatives concerns the design of photo-switchable materials. Molecular switches are compounds which can exist in two stable forms that can be easily interconverted by an external influence such as pH, magnetic or electric fields, temperature, and light. Photoswitches can find application in data processing or information storage. TEE derivatives exhibit photo-induced *cis-trans* isomerization, and therefore, can act as photoswitch disclosing potential applications in the field of molecular electronics and

photonics. A series of donor-donor, acceptor-acceptor, and donor-acceptor TEE derivatives was synthesized and the influence of structure, solvent, and irradiation wavelength on the quantum yields of the *cis-trans* isomerization was investigated [144].

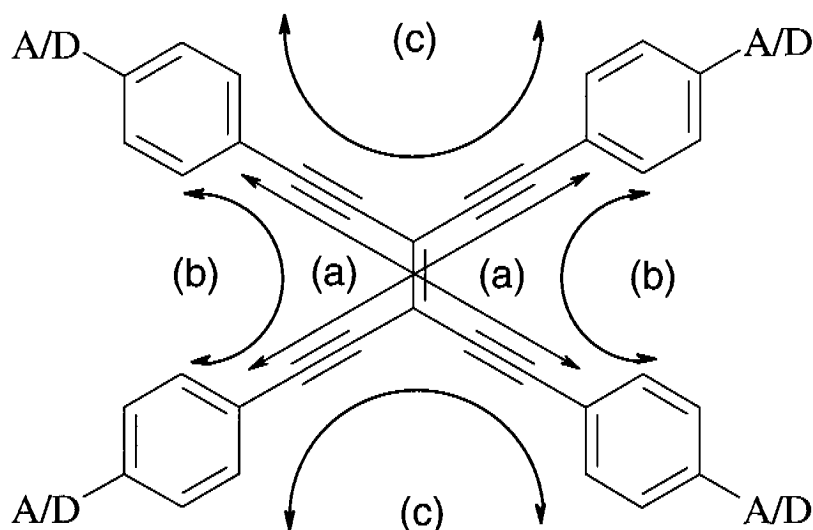
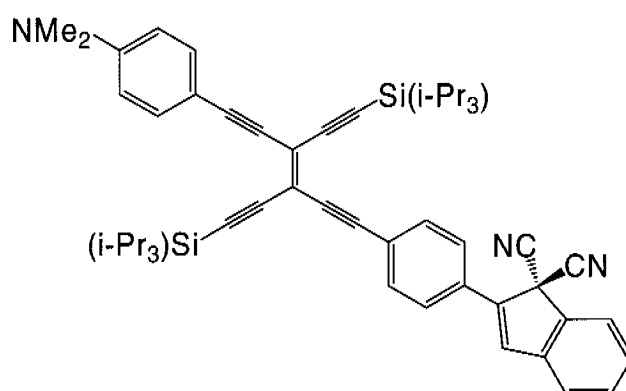


Figure 1.4: Schematic representation of the six possible π -conjugation pathways in donor/acceptor substituted tetraethynylethenes.

The preparation of compound **39** makes available a three-way molecular switch which is controlled by pH and light and which gives access to six different easily interconvertible states [145]. In fact, this compound shows *cis-trans* isomerization, reversible ring opening of the dihydroazulene unit to give vinylheptafulvene, and pH controlled protonotation of the amino group.

Further examples of DEE and TEE derivatives with their material and electronic properties can be found in the recent review of Diederich et al. [146].



39

1.4 Outline of the Thesis

Molecular and electronic properties of π -conjugated compounds, such as electronic absorption energies, polarizabilities, nonlinear optical coefficients (β and γ), ionization potentials, and electron affinities essentially depend on the extent of the π -delocalization in the molecule. The quantification of electron delocalization along different π -conjugated pathways is of crucial importance to establish quantitative structure-property relationships and for the rational design of materials for electronic and photonic applications. Prompted by these observations, we have developed an approach for the investigation of electron delocalization and calculation of delocalization energies. This approach will be applied to the investigation of electron delocalization of a series of molecules with expanded, π -conjugated carbon cores based on the DEE and TEE building blocks. Topological variables, such as the nature and the length of the conjugated backbone, the mode of π -conjugation (*trans*, *cis*, *cross*) and the type of substituents, are the degrees of freedom exploited and correlated to the physical observable through the quantification of electron delocalization.

In the next chapter, our approach for the analysis of electron delocalization will be presented and discussed in detail. In Chapter 3 the approach will be validated studying the

electron delocalization of selected prototypical systems. In Chapter 4 the approach will be then applied to the investigation of the electron delocalization and its correlation with molecular and electronic properties on extended π -conjugated molecular systems. Finally, a short outlook on the future improvements of the approach will be given in Chapter 5.

1.5 References

1. S. R. Marder, J. W. Perry, G. Bourhill, C. B. Gorman, B. G. Tiemann, K. Mansour, Relation Between Bond-Length Alternation and Second Electronic Hyperpolarizabilities of Conjugated Organic Molecules. *Science*, **1993**, 261, 186-189.
2. M. Jain, J. Chandrasekhar, Comparative Theoretical Evaluation of Hyperpolarizabilities of Push-Pull Polyenes and Polyynes. The Important Role of Configuration Mixing in the Excited States. *J. Phys. Chem.*, **1993**, 97, 4044-4049.
3. L.-T. Cheng, W. Tam, S. H. Stevenson, G. R. Meredith, G. Rikken, S. R. Marder, Experimental Investigations of Organic Molecular Nonlinear Optical Polarizabilities. 1. Methods and Results on Benzene and Stilbene Derivatives. *J. Phys. Chem.*, **1991**, 95, 10631-10643.
4. L.-T. Cheng, W. Tam, S. R. Marder, A. E. Steigman, G. Rikken, C. W. Spangler, Experimental Investigations of Organic Molecular Nonlinear Optical Polarizabilities. 2. A Study of Conjugation Dependence. *J. Phys. Chem.*, **1991**, 95, 10643-10652.
5. N. Matsuzawa, D. A. Dixon, Semiempirical Calculations of Hyperpolarizabilities for Donor-Acceptor Molecules: Comparison to the Experiment. *J. Phys. Chem.*, **1992**, 96, 6232-6241.
6. N. Matsuzawa, D. A. Dixon, Semiempirical Calculations of Hyperpolarizabilities for Extended π Systems: Polyenes, Polyynes, Polyphenyls. *Int. J. Quantum Chemistry*, **1992**, 44, 497-515.
7. J. O. Morley, V. J. Docherty, D. Pugh, Non-linear Optical Properties of Organic Molecules. Part 2. Effect of Conjugation Length and Molecular Volume on the Calculated Hyperpolarizabilities. *J. Chem. Soc., Perkin Trans. 2*, **1987**, 1351-1355.
8. I. D. L. Albert, J. O. Morley, D. Pugh, Further Studies on the Polarizabilities and Hyperpolarizabilities of the Substituted Polyenes and Polyphenyls. *J. Chem. Soc., Faraday Trans 2*, **1994**, 90, 2617-2622.
9. G. Bourhill, J.-L. Bredas, S. R. Marder, F. Meyers, J. W. Perry, B. G. Tiemann, Experimental Demonstration of the Dependence of the First Hyperpolarizability of

- Donor-Acceptor-Substituted Polyenes on the Ground-State Polarization and Bond Length Alternation. *J. Am. Chem. Soc.*, **1994**, *116*, 2619-2620.
10. F. Meyers, J.-L. Bredas, J. Zyss, Electronic Structure and Nonlinear Optical Properties of Push-Pull Polyenes: Theoretical Investigation of Benzodithia Polyenals and Dithiole Polyenals. *J. Am. Chem. Soc.*, **1992**, *114*, 2914-2921.
 11. I. D. L. Albert, J. O. Morley, D. Pugh, Comparative Study of Optical Nonlinearities in Substituted Polyynes versus the Corresponding Polyenes and Polyphenyls. *J. Phys. Chem. A*, **1997**, *101*, 2914-2921.
 12. J. O. Morley, Calculated Hyperpolarizabilities of Polythiophenes, Polyfurans and Polyphenyls. *J. Chem. Soc., Faraday Trans* **1991**, *87*, 1763-1766.
 13. D. R. Kanis, M. A. Ratner, T. J. Marks, Design and Construction of Molecular Assemblies with Large Second-Order Optical Nonlinearities. Quantum Chemical Aspects. *Chem. Rev.*, **1994**, *94*, 195-242.
 14. K. B. Wiberg, W. K. B. Rosenberg, P. R. Rablen, Butadiene. 2. Examination of the Energetic Preference for Coplanarity of Double Bonds. Comparison of Butadiene, Acrolein, and Vinylamine. *J. Am. Chem. Soc.*, **1991**, *113*, 2890-2898.
 15. C. Dehu, F. Meyers, J.-L. Bredas, Donor-Acceptor Diphenylacetylenes: Geometrical Structure, Electronic Structure, and Second-Order Nonlinear Optical Properties. *J. Am. Chem. Soc.*, **1993**, *115*, 6198-6206.
 16. C. Dehu, J.-L. Bredas, Theoretical Study of the Conjugation Effect on the Electronic and Second-Order Nonlinear Optical Properties of Amino-Nitro Diphenylacetylenes. *Int. J. Quantum Chem.*, **1994**, *52*, 89-96.
 17. J. O. Morley, Nonlinear Optical Properties of Organic Molecules. Calculations of the Hyperpolarizabilities of Donor-Acceptor Polyenes. *Int. J. Quantum Chem.*, **1993**, *46*, 19-26.
 18. J.-L. Brédas, C. Adant, P. Tackx, A. Persoons, B. M. Pierce, Third-Order Nonlinear Optical Response in Organic Materials: Theoretical and Experimental Aspects. *Chem. Rev.*, **1994**, *94*, 243-278.

19. I. D. W. Samuel, I. Ledoux, C. Dhenaut, J. Zyss, H. H. Fox, R. R. Schrock, R. J. Silbey, Saturation of Cubic Optical Nonlinearity in Long-Chain Polyene Oligomers. *Science*, **1994**, 265, 1070-1072.
20. D. Beljonne, Z. Shuai, J.-L. Bredas, Theoretical Evolution of the Third-Order Molecular Polarizabilities as a Function of Chain Length in Thiophene and Pyrrole Oligomers. *Int. J. Quantum Chem.*, **1994**, 52, 39-48.
21. D. Beljonne, F. Meyers, J.-L. Bredas, Excited States in Bis-Substituted Polyenes: Configuration Interaction Description of the Vertical Excitation Energies and Nonlinear Optical Properties. *Synt. Met.*, **1996**, 80, 211-222.
22. M. Faraday, *Phil. Trans. R. Soc. London* **1825**, 440.
23. A. Kekulé, *Bull. Soc. Chim. Paris* **1865**, 3, 98.
24. J. Thiele, *Liebigs Ann. Chem.*, **1899**, 306, 87.
25. K. Lonsdale, X-ray Evidence on the Structure of the Benzene Nucleus. *Trans. Faraday Soc.*, **1929**, 25, 352-366.
26. K. Lonsdale, The Structure of the Benzene Ring in Hexamethylbenzene. *Proc. R. Soc. London*, **1929**, A123, 494.
27. J. C. Slater, Directed Valence in Polyatomic Molecules. *Phys. Rev.*, **1931**, 37, 481-489.
28. J. C. Slater, Quantum Theory of Molecules and Solids. Vol. 1. 1963, New York: McGraw-Hill.
29. J. C. Slater, Note on the Structure of the Groups XO_3 . *Phys. Rev.*, **1931**, 38, 325-329.
30. J. C. Slater, Molecular Energy Levels and Valence Bonds. *Phys. Rev.*, **1931**, 38, 1109-1144.
31. J. C. Slater, Note on Molecular Structure. *Phys. Rev.*, **1932**, 41, 255-257.
32. L. Pauling, The Shared-Electron Chemical Bond. *Proc. Natl. Acad. Sci.*, **1928**, 14, 359-362.
33. L. Pauling, The Nature of the Chemical Bond. Application of Results Obtained from the Quantum Mechanics and from a Theory of Paramagnetic Susceptibility to the Structure of Molecules. *J. Am. Chem. Soc.*, **1931**, 53, 1367-1400.
34. L. Pauling, The Nature of the Chemical Bond II. The One-electron Bond and the Three-Electron Bond. *J. Am. Chem. Soc.*, **1931**, 53, 3225-3237.

-
35. R. S. Mulliken, The Assignment of Quantum Numbers for Electrons in Molecules. *Phys. Rev.*, **1928**, 32, 186-222.
 36. R. S. Mulliken, The Assignment of Quantum Numbers for Electrons in Molecules. II. Correlation of Molecular and Atomic Electron States. *Phys. Rev.*, **1928**, 32, 761-772.
 37. R. S. Mulliken, The Assignment of Quantum Numbers for Electrons in Molecules. III. Diatomic Hydrides. *Phys. Rev.*, **1929**, 33, 730-747.
 38. F. Hund, Symmetriecharaktere von Termen bei Systemen mit gleichen Partikeln in der Quantenmechanik. *Z. Phys.*, **1927**, 43, 788-804.
 39. L. Pauling, The Nature of the Chemical Bond. 3rd ed. ed. 1960, Ithaca, NY: Cornell University Press.
 40. L. Pauling, G. W. Wheland, The Nature of the Chemical Bond. V. The Quantum-Mechanical Calculation of the Resonance Energy of Benzene and Naphthalene and the Hydrocarbon Free Radicals. *J. Chem. Phys.*, **1933**, 1, 362-374.
 41. E. Hückel, Quantentheoretische Beiträge zum Benzol-Problem. I. Die Elektronenkonfiguration des Benzols und verwandter Verbindungen. *Z. Phys.*, **1931**, 70, 204-286.
 42. E. Hückel, Quantentheoretische Beiträge zum Benzol-Problem. II. Quantentheorie der induzierten Polaritäten. *Z. Phys.*, **1931**, 72, 310-317.
 43. E. Hückel, Quantentheoretische Beiträge zum Benzol-Problem. III. *Z. Phys.*, **1932**, 76, 628-648.
 44. E. Hückel, Quantentheoretische Beiträge zum Benzol-Problem. IV. *Z. Phys.*, **1933**, 83, 632.
 45. R. S. Mulliken, R. G. Parr, LCAO Molecular Orbital Computation of Resonance Energies of Benzene and Butadiene, with General Analysis of Theoretical versus Thermochemical Resonance Energies. *J. Chem. Phys.*, **1951**, 19, 1271.
 46. R. Breslow, E. Mohacsi, Studies on d-Orbital Conjugation. III. Non-aromaticity of a Derivative of the 1,3-Dithiepinyl Anion, a Ten pi-Electron Conjugated System. *J. Am. Chem. Soc.*, **1963**, 85, 431.
 47. L. Salem, The Molecular Orbital Theory of Conjugated Systems. 1965, New York: W. A. Benjamin Inc.

-
48. A. L. H. Chung, M. J. S. Dewar, Ground States of Conjugated Molecules. I. Semiempirical SCF MO Treatment and Its Application to Aromatic Hydrocarbons. *J. Chem. Phys.*, **1965**, *42*, 756-766.
 49. R. Pariser, R. G. Parr, A Semi-Empirical Theory of the Electronic Spectra and Electronic Structure of Complex Unsaturated Molecules. I. *J. Chem. Phys.*, **1953**, *21*, 466-471.
 50. M. J. S. Dewar, G. J. Gleicher, Ground States of Conjugated Molecules. II. Allowance for Molecular Geometry. *J. Am. Chem. Soc.*, **1963**, *87*, 685-692.
 51. M. J. S. Dewar, H. N. Schmeising, A Re-evaluation of Conjugation and Hyperconjugation: The Effects of Changes in Hybridisation on Carbon Bonds. *Tetrahedron*, **1959**, *5*, 166-178.
 52. M. J. S. Dewar, H. N. Schmeising, Resonance and Conjugation – II. Factors Determining Bond Lengths and Heats of Formation. *Tetrahedron*, **1960**, *11*, 96-120.
 53. M. J. S. Dewar, C. D. Llano, Ground States of Conjugated Molecules. XI. Improved Treatment of Hydrocarbons. *J. Am. Chem. Soc.*, **1969**, *91*, 789-795.
 54. M. J. S. Dewar, The Molecular Orbital Theory of Organic Chemistry. **1969**, New York: McGraw-Hill.
 55. L. J. Schaad, B. A. Hess Jr., Dewar Resonance Energy. *Chem. Rev.*, **2001**, *101*, 1465-1476.
 56. B. A. Hess Jr., L. J. Schaad, Hückel Molecular Orbital π Resonance Energies. A New Approach. *J. Am. Chem. Soc.*, **1971**, *93*, 305.
 57. R. Janoschek, Has a Benzene Molecule an Extra Stability ? *J. Mol. Struct. (Theochem)*, **1991**, *229*, 197-203.
 58. G. Merino, A. Vela, T. Heine, Description of Electron Delocalization Via the Analysis of Molecular Fields. *Chem. Rev.*, **2005**, in press.
 59. F. Bernardi, A. Bottoni, A. Venturini, An Ab Initio SCF-MO Study of the Aromaticity of Some Cyclic Compounds. *J. Mol. Struct. (Theochem)*, **1988**, *163*, 173-189.
 60. P. v. R. Schleyer, H. Jiao, What Is Aromaticity ? *Pure Appl. Chem.*, **1996**, *68*, 209-218.
 61. R. Peierls, Quantum Theory of Solids. **1956**, Oxford: Oxford University Press.

-
62. F. Meyers, S. R. Marder, B. M. Pierce, J.-L. Brédas, Electric Field Modulated non Linear Optical Properties of Donor-Acceptor Polyenes: Sum Over States Investigation and Relationship Between Molecular Polarizabilities (α , β , γ) and Bond Length Alternation. *J. Am. Chem. Soc.*, **1994**, *116*, 10703-10714.
 63. G. U. Bublitz, R. Ortiz, S. R. Marder, S. G. Boxer, Stark Spectroscopy of Donor/Acceptor Substituted Polyenes. *J. Am. Chem. Soc.*, **1997**, *119*, 3365.
 64. G. U. Bublitz, R. Ortiz, C. Runser, A. Fort, M. Barzoukas, S. R. Marder, S. G. Boxer, Acceptor Polyenes: Correlation with Non Linear Optical Measurements. *J. Am. Chem. Soc.*, **1997**, *119*, 2311.
 65. S. B. Allin, T. M. Leslie, R. S. Lumpkin, Effects of Molecular Hyperpolarizabilities Calculations. *Chem. Mater.*, **1996**, *8*, 428.
 66. J. Gao, C. Alhambra, Solvents Effects on the Bond Length alternation and Absorption Energy of Conjugated Compounds. *J. Am. Chem. Soc.*, **1997**, *119*, 2962.
 67. I. D. L. Albert, T. J. Marks, M. Ratner, Rational Design of Molecules with Large Hyperpolarizabilities. Electric field, Solvent Polarity, and Bond Length Alternation Effects on Merocyanine Dye Linear and Non Linear Optical Properties. *J. Phys. Chem.*, **1996**, *100*, 9714.
 68. G. Chen, S. Mukamel, Nonlinear Polarizabilities of Donor-Acceptor Substituted Conjugated Polyenes. *J. Phys. Chem.*, **1996**, *100*, 11080-11085.
 69. H. Kollmar, Direct Calculation of Resonance Energies of Conjugated Hydrocarbons with Ab Initio MO Methods. *J. Am. Chem. Soc.*, **1979**, *101*, 4832-4840.
 70. J. M. Foster, S. F. Boys, Canonical Configurational Interaction Procedure. *Rev. Mod. Phys.*, **1960**, *32*, 300-302.
 71. S. Skaarup, J. E. Boggs, P. N. Skancke, Contributions of Resonance, Hybridization, and Nonbonded Interactions to the Structure of Butadiene. *Tetrahedron* **1976**, *32*, 1179-1181.
 72. J. P. Daudey, G. Trinquier, J. C. Barthelat, J. P. Malrieu, Decisive Role of π Conjugation in the Central Bond Length Shortening of Butadiene. *Tetrahedron*, **1980**, *36*, 3399-3401.

-
73. E. D. Glendening, R. Faust, A. Streitwieser, K. P. C. Vollhard, F. Weinhold, The Role of Delocalization in Benzene. *J. Am. Chem. Soc.*, **1993**, *115*, 10952-10957.
 74. A. E. Reed, P. v. R. Schleyer, The Anomeric Effect with Central Atoms other than Carbon. 1. Strong Interactions Between Nonbonded Substituents in Polyfluorinated First- and Second-Row Hydrides. *J. Am. Chem. Soc.*, **1987**, *109*, 7362-7373.
 75. U. Salzner, P. v. R. Schleyer, A Successful Ab Initio Study of the Adiabatic Electron Affinity of the Methyl Radical. *Chem. Phys. Lett.*, **1992**, *190*, 401.
 76. A. E. Reed, P. v. R. Schleyer, Chemical Bonding in Hypervalent Molecules. The Dominance of Ionic Bonding and Negative Hyperconjugation over d-orbital Participation. *J. Am. Chem. Soc.*, **1990**, *112*, 1434-1445.
 77. U. Salzner, P. v. R. Schleyer, Generalized Anomeric Effects and Hyperconjugation in $\text{CH}_2(\text{OH})_2$, $\text{CH}_2(\text{SH})_2$, $\text{CH}_2(\text{SeH})_2$, and $\text{CH}_2(\text{TeH})_2$. *J. Am. Chem. Soc.*, **1993**, *115*, 10231-10236.
 78. U. Salzner, P. v. R. Schleyer, Ab Initio Examination of Anomeric Effects in Tetrahydropyrans, 1,3-Dioxanes, and Glucose. *J. Org. Chem.*, **1994**, *59*, 2138-2155.
 79. Y. Mo, H. Jiao, Z. Lin, P. v. R. Schleyer, Application of the Orbital Deletion Procedure (ODP) to Planar Carbocations. *Chem. Phys. Lett.*, **1998**, *289*, 383-390.
 80. H. Jiao, P. v. R. Schleyer, Y. Mo, M. A. McAllister, T. T. Tidwell, Magnetic Evidence for the Aromaticity and Antiaromaticity of Charged Fluorenyl, Indenyl, and Cyclopentadienyl Systems. *J. Am. Chem. Soc.*, **1997**, *119*, 7075-7083.
 81. Y. Mo, H. Jiao, P. v. R. Schleyer, Hyperconjugation Effect in Substituted Methyl Boranes: An Orbital Deletion Procedure Analysis. *J. Org. Chem.*, **2004**, *69*, 3493-3499.
 82. Y. Mo, P. v. R. Schleyer, H. Jiao, Z. Lin, Quantitative Evaluation of Hyperconjugation in the Cyclopropylcarbinyl Cation and in Cyclopropylborane. *Chem. Phys. Lett.*, **1997**, *280*, 439-443.
 83. Y. Mo, W. Wu, Q. Zhang, Study of Intramolecular Electron Transfer with a Two-State Model Based on the Orbital Deletion Procedure. *J. Chem. Phys.*, **2003**, *119*, 6448-6456.
 84. Y. Mo, S. D. Peyerimhoff, Theoretical Analysis of Electron Delocalization. *J. Chem. Phys.*, **1998**, *109*, 1687-1697.

-
85. C. Edmiston, K. Ruedenberg, Localized Atomic and Molecular Orbitals. *Rev. Mod. Phys.*, **1963**, 35, 457-464.
 86. J. Pipek, P. G. Mezey, A Fast Intrinsic Localization Procedure Applicable for Ab Initio and Semiempirical Linear Combination of Atomic Orbital Wave Functions. *J. Chem. Phys.*, **1989**, 90, 4916-4926.
 87. Y. Mo, Geometrical Optimization for Strictly Localized Structures. *J. Chem. Phys.*, **2003**, 119, 1300-1306.
 88. Y. Mo, W. Wu, Q. Zhang, Theoretical Resonance Energies of Benzene, Cyclobutadiene, and Butadiene. *J. Phys. Chem.*, **1994**, 98, 10048-10053.
 89. S. Shaik, A. Shurki, D. Danovich, P. C. Hiberty, A Different Story of π -Delocalization-The Distortivity of π -Electrons and Its Chemical Manifestations. *Chem. Rev.*, **2001**, 101, 1501-1539.
 90. L. A. Carreira, Determination of the Torsional Potential Function of 1,3-Butadiene. *J. Chem. Phys.*, **1975**, 62, 3851-3854.
 91. W. J. Hehre, R. Ditchfield, L. Radom, J. A. Pople, Molecular Orbital Theory of the Electronic Structure of Organic Compounds. V. Molecular theory of Bond Separation. *J. Am. Chem. Soc.*, **1970**, 92, 4796-4801.
 92. W. J. Hehre, L. Radom, P. v. R. Schleyer, J. A. Pople, Ab Initio Molecular Orbital Theory. **1986**, New York: Wiley.
 93. P. George, M. Trachtman, C. W. Bock, A. Brett, An Alternative Approach to the Problem of Assessing Destabilization Energies (Strain Energies) in Cyclic Hydrocarbons. *Tetrahedron*, **1976**, 32, 317-323.
 94. P. George, C. Bock, M. Trachtman, Empirical Resonance Energies for Benzene and Pyridine. *Tetrahedron Lett.*, **1985**, 26, 5667-5670.
 95. P. J. Garratt, Aromaticity. **1986**, New York: Wiley.
 96. V. I. Minkin, M. N. Glukhovtsev, B. Y. Simkin, Aromaticity and Antiaromaticity: Electronic and Structural Aspect. **1994**, New York: Wiley.
 97. P. v. R. Schleyer, C. Maerker, A. Dransfeld, H. Jiao, N. J. R. v. E. Hommes, Nucleus-Independent Chemical Shifts: A Simple and Efficient Aromatic Problem. *J. Am. Chem. Soc.*, **1996**, 118, 6317-6318.

-
98. F. Diederich, Y. Rubin, Synthetic Approaches to Molecular and Polymeric Carbon Allotropes. *Angew. Chem. Int. Ed.*, **1992**, *31*, 1101.
 99. F. Diederich, Carbon Scaffolding: Building Acetylenic All-Carbon and Carbon-Rich Compounds. *Nature*, **1994**, *369*, 199.
 100. Y. Hori, K. Noda, S. Kobayashi, H. Taniguchi, Synthesis and Properties of Tetrakis(phenylethynyl)ethylene. *Tetrahedron Lett.*, **1969**, 3563.
 101. H. Hauptmann, Tetraethynylethylenes. *Angew. Chem. Int. Ed.*, **1975**, *14*, 498.
 102. H. Hauptmann, Untersuchungen zu Baseninduzierten Reaktionen an Tetraäthynyläthanen. *Tetrahedron Lett.*, **1975**, 1931.
 103. H. Hauptmann, Diäthynylcarbene und 2, 4 Pentadiinylidene. *Tetrahedron*, **1976**, *32*, 1923.
 104. H. Hopf, M. Kreutzer, P. G. Jones, Zur Darstellung und Struktur von Tetrakis(phenylethynyl)ethen. *Chem. Ber.*, **1991**, *124*, 1471.
 105. Y. Rubin, C. B. Knobler, F. Diederich, Tetraethynylethene. *Angew. Chem. Int. Ed.*, **1991**, *30*, 698.
 106. R. R. Tykwinski, F. Diederich, Tetraethynylethene Molecular Scaffolding. *Liebigs Ann./Recueil*, **1997**, 649.
 107. F. Diederich, Modern Acetylene Chemistry, ed. P. J. Stang, F. Diederich. **1995**, Weinheim: Verlag Chemie. Chapter 13. Oligoacetylenes.
 108. F. Diederich, L. Gobbi, Cyclic and Linear Acetylenic Molecular Scaffolding. *Top. Curr. Chem.*, **1999**, *201*, 43-79.
 109. R. E. Martin, F. Diederich, Linear Monodisperse π -Conjugated Oligomers: Model Compounds for Polymers and More. *Angew. Chem. Int. Ed.*, **1999**, *38*, 1350-1377.
 110. M. Schreiber, J. Anthony, F. Diederich, M. E. Spahr, R. Nesper, M. Hubrich, F. Bommeli, L. Degiorgi, P. Wachter, P. Kaatz, C. Bosshard, P. Günter, M. Colussi, U. W. Suter, C. Boudon, J.-P. Gisselbrecht, M. Gross, Polytriacetylenes: Conjugated Polymers with a Novel All-Carbon Backbone. *Adv. Mater.*, **1994**, *6*, 786-790.
 111. M. Boldi, J. Anthony, V. Gramlich, C. B. Knobler, C. Boudon, J.-P. Gisselbrecht, M. Gross, F. Diederich, Acyclic Tetraethynylethene Molecular Scaffolding:

- Multinanometer-Sized Linearly Conjugated Rods with the Poly(triacetylene) Backbone and Cross-conjugated Expanded Dendralenes. *Helv. Chim. Acta*, **1995**, 78, 779-796.
112. J. Anthony, C. Boudon, F. Diederich, J. P. Gisselbrecht, V. Gramlich, M. Gross, M. Hobi, P. Seiler, Stable Soluble Conjugated Carbon Rods with Persilylethynylated Polytriacetylene Backbone. *Angew. Chem. Int. Ed.*, **1994**, 33, 763-766.
113. R. E. Martin, U. Gubler, C. Boudon, V. Gramlich, C. Bosshard, J.-P. Gisselbrecht, P. Gunter, M. Gross, F. Diederich, Poly(triacetylene) Oligomers: Synthesis Characterization, and Estimation of the Effective Conjugation Length by Electrochemical, UV/vis, and Nonlinear Optical Methods. *Chem. Eur. J.*, **1997**, 3, 1505-1512.
114. R. E. Martin, T. Mäder, F. Diederich, Monodisperse Poly(triacetylene) Rods: Synthesis of 11.9 nm Long Molecular Wire and Direct Determination of the Effective Conjugation Length by UV/vis and Raman Spectroscopies. *Angew. Chem. Int. Ed.*, **1999**, 38, 817-822.
115. R. E. Martin, U. Gubler, J. Cornil, M. Y. Balakina, C. Boudon, C. Bosshard, J.-P. Gisselbrecht, F. Diederich, P. Günter, M. Gross, J.-L. Brédas, Monodisperse Polytriacetylene Oligomers Extending from Monomer to Hexadecamer: Joint Experimental and Theoretical Investigation of Physical Properties. *Chem. Eur. J.*, **2000**, 6, 3622-3634.
116. U. Gubler, C. Bosshard, P. Günter, M. Y. Balakina, J. Cornil, J.-L. Brédas, R. E. Martin, F. Diederich, Scaling Law for Second-Order Hyperpolarizabilities in Poly(triacetylene) Molecular Wires. *Opt. Lett.*, **1999**, 24, 1599-1601.
117. E. Burri, F. Diederich, M. B. Nielsen, Synthesis and Characterization of Multinanometer-Sized Expanded Dendralenes with an iso-Poly(triacetylene) Backbone. *Helv. Chim. Acta*, **2002**, 85, 2169-2182.
118. J. Anthony, A. M. Boldi, C. Boudon, J. P. Gisselbrecht, M. Groos, P. Seiler, C. B. Knobler, F. Diederich, Macrocyclic Tetraethynylethene Molecular Scaffolding: Perethynylated aromatic Dodecahydro-[18]annulenes, Antiaromatic Octadehydro-[12]annulenes, and Expanded Radialenes. *Helv. Chim. Acta*, **1995**, 78, 797-817.

-
119. M. B. Nielsen, M. Schreiber, Y. G. Baek, P. Seiler, S. Lecomte, C. Boudon, R. R. Tykwinski, J. P. Gisselbrecht, V. Gramlich, P. J. Skinner, C. Bosshard, P. Günter, M. Gross, F. Diederich, Highly Functionalized Dimeric Tetraethynylethenes and Expanded Radialenes: Strong Evidence for Macrocyclic Cross-Conjugation. *Chem. Eur. J.*, **2001**, 7, 3263-3280.
 120. J. Anthony, C. B. Knobler, F. Diederich, Stable [12]- and [18]annulenes Derived from Tetraethynylethene. *Angew. Chem. Int. Ed.*, **1993**, 32, 406-409.
 121. F. Mitzel, C. Boudon, J. P. Gisselbrecht, M. Gross, F. Diederich, π -Electron Conjugation Effects in Antiaromatic Dehydro[12]- and Aromatic Dehydro[18]-annulenes. *Chem. Comm.*, **2002**, 2318-2319.
 122. Y. Zhao, R. McDonald, R. R. Tykwinski, Study of Cross-Conjugated *iso*-Polytriacylenes and Related Oligoenynes. *J. Org. Chem.*, **2002**, 67, 2805-2812.
 123. R. R. Tykwinski, Y. Zhao, Cross Conjugated Oligo(enynes). *Synlett*, **2002**, 1939-1953.
 124. C. R. Moylan, R. J. Twieg, V. Y. Lee, S. A. Swanson, K. M. Betterton, R. D. Miller, Nonlinear Optical Chromophores with Large Hyperpolarizabilities and Enhanced Thermal Stabilities. *J. Am. Chem. Soc.*, **1993**, 115, 12599-12600.
 125. I. Ledoux, J. Zyss, A. Jutand, C. Amatore, Non Linear Optical Properties of Unsymmetrical Polyphenyls: Efficiency versus Transparency Trade Off. *Chem. Phys.*, **1991**, 150(117-123)
 126. A. Slepko, F. Hegmann, Y. Zhao, R. R. Tykwinski, K. Kamada, Ultrafast Optical Kerr Effect Measurements of Third-Order Nonlinearities in Cross-Conjugated *iso*-Polydiacetylene Oligomers. *J. Chem. Phys.*, **2002**, 116, 3834-3840.
 127. R. R. Tykwinski, M. Schreiber, R. P. Carlón, F. Diederich, V. Gramlich, Donor/Acceptor-Substituted Tetraethynylethenes: Systematic Assembly of Molecules for Use as Advanced Materials. *Helv. Chim. Acta*, **1996**, 79, 2249-2281.
 128. R. R. Tykwinski, M. Schreiber, V. Gramlich, P. Seiler, F. Diederich, Donor-Acceptor Substituted Tetraethynylethenes. *Adv. Mater.*, **1996**, 8, 226-231.
 129. C. Boudon, J.-P. Gisselbrecht, M. Gross, J. Anthony, A. M. Boldi, R. Faust, T. Lange, D. Philp, J.-D. V. Loon, F. Diederich, Electrochemical Properties of Tetraethynylethenes, Fully *cross*-Conjugated π -Chromophores, and

- Tetraethynylethene-Based Carbon-Rich Molecular Rods and Dehydroannulenes. *J. Electroanal. Chem.*, **1995**, 294, 187-197.
130. A. Hilger, J.-P. Gisselbrecht, R. R. Tykwinski, C. Boudon, M. Schreiber, R. E. Martin, H. P. Lüthi, M. Gross, F. Diederich, Electronic Characteristics of Arylated Tetraethynylethenes: A Cooperative Computational and Electrochemical Investigation. *J. Am. Chem. Soc.*, **1997**, 119, 2069-2078.
131. C. Bosshard, R. Spreiter, P. Gunter, R. R. Tykwinski, M. Schreiber, F. Diederich, Structure-Properties Relationships in Nonlinear Optical Tetraethynylethenes. *Adv. Mater.*, **1996**, 8, 231-234.
132. R. Spreiter, C. Bosshard, G. Knöpfle, P. Günter, R. R. Tykwinski, M. Schreiber, F. Diederich, One- and Two-Dimensionally Conjugated Tetraethynylethenes: Structure versus Second-Order Optical Polarizabilities. *J. Phys. Chem. B*, **1998**, 102, 29-32.
133. U. Gubler, S. Concilio, C. Bosshard, I. Biaggio, P. Gunter, R. E. Martin, M. J. Edelmann, J. A. Wytko, F. Diederich, Third-Order Nonlinear Optical Properties of in-Backbone Substituted Conjugated Polymers. *Appl. Phys. Lett.*, **2002**, 81, 2322-2324.
134. R. R. Tykwinski, U. Gubler, R. E. Martin, F. Diederich, C. Bosshard, P. Günter, Structure-Property Relationships in Third-Order Nonlinear Optical Chromophores. *J. Phys. Chem. B*, **1998**, 102, 4451-4465.
135. U. Gubler, C. Bosshard, Molecular Design for Third-Order Nonlinear Optics. *Adv. Polym. Sci.*, **2002**, 158, 123-191.
136. G. Hohlneicher, B. Dick, Experimental Determination of the Low Lying Excited A States of *trans*-Stilbene. *J. Photochem.*, **1984**, 27, 215-231.
137. G. Orlandi, W. Siebrand, Model for the Direct Photo-Isomerization of Stilbene. *Chem. Phys. Lett.*, **1975**, 30, 352-354.
138. D. H. Waldeck, Photoisomerization Dynamics of Stilbenes. *Chem. Rev.*, **1991**, 91, 415-436.
139. G. Hohlneicher, M. Müller, M. Demmer, J. Lex, J. H. Penn, L. Gan, P. D. Loesel, 1,2 Diphenylcycloalkenes: Electronic and Geometric Structures in Gas Phase, Solution and Solid State. *J. Am. Chem. Soc.*, **1988**, 110, 4483-4494.

-
140. M. O. Wolf, H. H. Fox, M. A. Fox, Reduction of Acetylated Tetraphenylethylenes: Electrochemical Behaviour and Stability of the Related Reduced Anions. *J. Org. Chem.*, **1996**, *61*, 287-294.
141. D. A. Shultz, M. A. Fox, Structural Effects on the Disproportionation Equilibrium of Tethered Tetraphenylethylene Radical Anions. *J. Org. Chem.*, **1990**, *55*, 1047-1051.
142. F. Diederich, D. Philp, P. Seiler, π -complexes Incorporating Tetraphenyl-tetraethynylethene. *J. Chem. Soc., Chem. Commun.*, **1994**, 205-208.
143. D. Philp, V. Gramlich, P. Seiler, F. Diederich, π -Complexes Incorporating Tetrakis(phenylethynyl)ethene. *J. Chem. Soc., Perkin Trans. 2*, **1995**, 875-886.
144. R. E. Martin, J. Bartek, F. Diederich, R. R. Tykwinski, E. C. Meister, A. Hilger, H. P. Lüthi, Photochemical trans-cis Isomerization of Donor/Acceptor-Substituted (E)-hex-3-ene-1,5-diynes (1,2 diethynylethene, DEEs) and 3,4-diethynylhex-3-ene-1,5-diynes (tetraethynylethenes, TEEs). *J. Am. Chem. Soc., Perkin trans. 2*, **1998**, 233-241.
145. L. Gobbi, P. Seiler, F. Diederich, A Novel Three-Way Chromophoric Molecular Switch: pH and Light Controllable Switching Cycles. *Angew. Chem. Int. Ed.*, **1999**, *38*, 674-678.
146. M. B. Nielsen, F. Diederich, Conjugated Oligoenynes Based on Diethynylethene Unit. *Chem. Rev.*, **2005**, *105*, 1837-1867.

2 A New Approach for the Investigation of Electron Delocalization

As discussed in the previous chapter, various methods have been proposed for the analysis of electron delocalization in unsaturated or aromatic molecules. These methods range from simple bond length alternation (BLA) schemes to much more sophisticated approaches such as those based on magnetic shielding properties or on delocalization energies (see subchapter 1.2 and references therein).

In the framework of MO theory, electron delocalization can be expressed as the interaction between specific occupied fragment MOs in one part of the molecule with specific unoccupied fragment MOs in another part of the molecule. This intramolecular donor \rightarrow acceptor interaction, in which electron density is transferred from one set of MOs to another, renders a basis for the quantitative description of delocalization. The delocalization energy can then be calculated as the difference between the energy of the delocalized wavefunction and the energy of a reference wavefunction consisting of localized orbitals in which intramolecular donor \rightarrow acceptor interactions are deactivated. Based on this assumption, we developed a method which gives a measure of electron delocalization by means of delocalization energies [1-3], which is based on the Natural Bond Orbital (NBO) analysis of Weinhold [4-12]. In the following section the NBO theory is briefly described. Our method

of analysis of delocalization is then presented in detail. Two different protocols to evaluate the delocalization energies will be introduced. In addition, other indicators useful for the analysis of delocalization will be presented.

In the last section of the chapter the values as well as the drawbacks of the approach will be critically discussed in comparison to other methods. Examples of application of the approach to some prototypical systems will be the subject of the next chapter.

2.1 The Natural Bond Orbital (NBO) Approach

The NBO analysis of Weinhold [4-12] generates, departing from canonical MOs, a set of localized one centre (core, lone pairs) and two centre (π and σ bonds) strongly occupied orbitals, and a set of one centre (Rydberg) and two centre (σ^* , π^*) weakly occupied orbitals: the NBOs. The NBO analysis involves only the first-order density matrix (Γ_{ij}) which is the matrix representation of the density operator:

$$\hat{\Gamma}(1|1') = N \int \psi(1, 2, \dots, N) \psi^*(1', 2', \dots, N') d\tau_2 \dots d\tau_N \quad (2.1)$$

in the basis set of atomic orbitals:

$$\Gamma_{ij} = \int \chi_i^*(1) \Gamma(1|1') \chi_j(1') d\tau_1 d\tau_{1'} \quad (2.2)$$

and thus can be applied to any desired level of theory.

Wavefunctions transformed into NBO form are in agreement with the Lewis structure or with the basic Pauling-Slater-Coulson picture of bonds in molecules. The strongly occupied NBOs of the natural Lewis structure are therefore well adapted for describing covalency effects in molecules.



Figure 2.1: Sequence of transformations from the input basis set to the NLMOs.

The NBOs are obtained by a sequence of transformations from the input basis to give, first, the natural atomic orbitals (NAOs), then the hybrid atomic orbitals (NHOs), and finally the natural bond orbitals (NBOs) (see Figure 2.1). NBOs may be subsequently transformed to the natural localized molecular orbitals (NLMO). Each step of the sequence involves an orthonormal set that spans the full space of the input basis set and can be used to give an exact representation of the calculated wavefunction and properties of the system.

2.1.1 NAO Transformation; the Occupancy Weighted Symmetric Orthogonalization

The first step in the generation of the NBOs is the transformation of the atomic basis functions to a complete set of orthogonal atomic functions (NAOs). In this respect, the general objective is to orthogonalize the complete set of orbitals, while preserving their atomic-like character as close as possible. The NAOs are closely related to the natural orbitals (NOs) introduced originally by Löwdin [13]. Indeed, for isolated atoms these two sets of orbitals would be identical. However, for polyatomic molecules, NAOs and NOs differ since the latter are defined as the orthonormal *molecular* orbitals for a given wavefunction, and are obtained as eigenfunctions of the first order density matrix Γ . They therefore transform as irreducible representations of the full symmetry group of the molecule and are completely delocalized. On the contrary, the NAOs are orthogonal atomic (one centre) orbitals for a given wavefunction.

The construction of NAOs involves two essential steps: (i) diagonalization of one center angular symmetry block of the density matrix, and (ii) removal of interatomic overlap. In the first step, the density matrix is partitioned into blocks of basis function belonging to specific atomic centres (A, B, ..., L ...) as:

$$P = \begin{bmatrix} P_{AA} & P_{AB} & \cdots & P_{AL} & \cdots \\ P_{BA} & P_{BB} & \cdots & P_{BL} & \cdots \\ \vdots & \vdots & & & \\ P_{LA} & P_{LB} & \cdots & P_{LL} & \cdots \\ \vdots & \vdots & & & \end{bmatrix} \quad (2.3)$$

where P_{AA} , P_{BB} , ..., P_{LL} etc. are blocks of elements of the density matrix defined for atomic centres A, B, ..., L, etc., and P_{AB} , P_{AL} etc. are blocks of elements of the density matrix defined between atomic centres A and B, A and L, etc. The diagonalization of each one-centre block P_{AA} with respect to the associated overlap submatrix S_{AA} gives the set of orthonormal *pre*-NAOs ($h_i^{(A)}$):

$$P_{AA} h_i^{(A)} = n_i^{(A)} S_{AA} h_i^{(A)} \quad (2.4)$$

The eigenvalues $n_i^{(A)}$ (occupation numbers) are expected to have a value of about 2 for the core or lone pair orbitals, about 1 for orbitals available for covalent bonding, and near 0 for unfilled orbitals. Therefore, the *pre*-NAOs can be divided into two subsets: (i) the ‘*minimal*’ subset of orbitals with non zero occupancy in the atomic ground state electronic configuration and (ii) the subset of (formally) *unoccupied* Rydberg orbitals. The former represents the most compact description of the electronic ground state and constitutes the so called ‘*natural minimal basis*’, whereas the latter, composed by *unoccupied* orbitals in an isolated atom, but *weakly occupied* in the molecular environment, increases without limit as the basis set is enlarged.

The second step in the NAO construction is the removal of the overlap between *pre*-NAOs of different atoms. However, in this case it is important to treat the *strongly occupied* minimal set and the *weakly occupied* Rydberg set of orbitals (which have a little role in describing the atomic electron density) in a different manner. The goal is to preserve the forms of strongly occupied orbitals which *exactly* describe the atomic electron density. For this purpose, the method of the occupancy-weighted symmetric orthogonalization has been developed as a modification of the symmetric orthogonalization of Löwdin [13].

In the orthogonalization of Löwdin a set of nonorthogonal orbitals $\{\phi_i\}$ is transformed to the orthogonal set $\{\phi_i^o\}$ with the property:

$$\sum_i \|\phi_i^o - \phi_i\|^2 = \min \quad (2.5)$$

whereas in the occupancy-weighted symmetric orthogonalization to generate orthogonal orbitals $\{\phi_i^w\}$ Equation 2.5 takes the form:

$$\sum_i \omega_i \|\phi_i^w - \phi_i\|^2 = \min \quad (2.6)$$

where the weighting factor $\omega_i \geq 0$ is the occupancy of the orbital ϕ_i . Orbitals of low occupancy are then free to rotate significantly during the orthogonalization procedure, whereas orbitals with high occupancy will be strongly preserved.

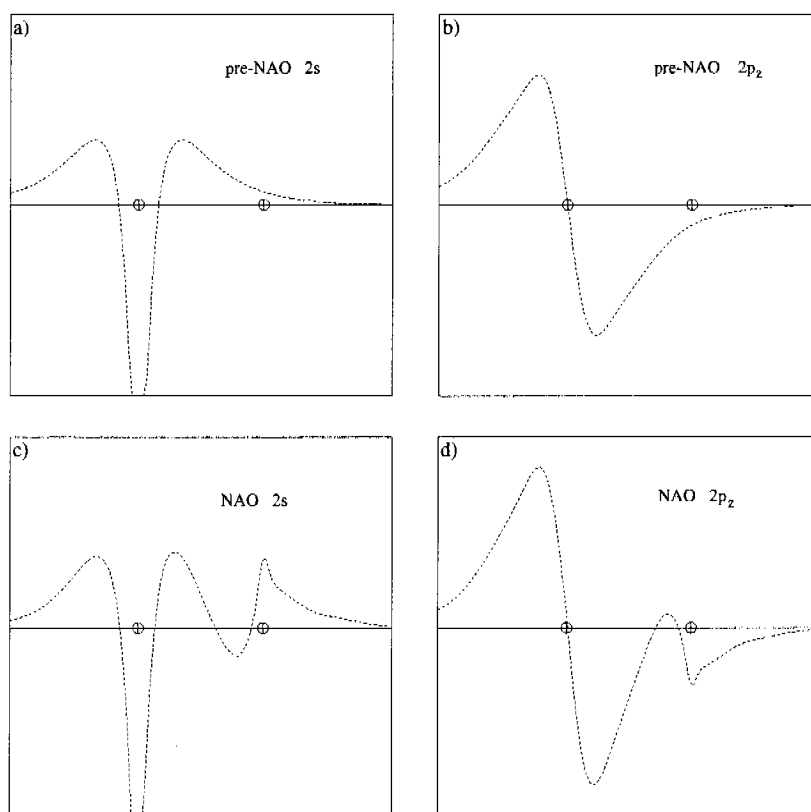


Figure 2.2: Profiles of the 2s and 2p_z pre-NAO (a and b, respectively) and the corresponding 2s and 2p_z NAO (c and d, respectively) centered on one carbon atom of ethylene computed at HF/STO-3G level of theory. The pre-NAO and NAO orbitals differ mainly near the adjacent C nucleus where NAOs exhibit additional nodal features, which render these orbitals orthogonal to the NAOs centered on the adjacent C atom.

The orthogonalization sequence leading from *pre*-NAO to NAO may be summarized as follows: (i) the set of functions is first separated into the minimal natural basis and Rydberg sets described above. (ii) The occupancy-weighted symmetric orthogonalization is performed on the minimal natural orbitals. (iii) The Rydberg orbitals are orthogonalized with respect to the minimal natural set by means of a Schmidt orthogonalization. (iv) Finally, the occupancy-weighted symmetric orthogonalization is performed on the Rydberg orbitals. The final NAO orbitals are then obtained as eigenfunctions of the one center angular symmetry density matrix block in this basis, and the NAO populations are their eigenvalues. It should be noted that the Schmidt orthogonalization is needed to avoid the overcounting problem that could otherwise affect the occupancy-weighted symmetric orthogonalization.

The effect of the transformation of *pre*-NAOs to NAO is shown in Figure 2.2 for the 2s and 2p_z orbitals centered on one carbon atom of ethylene. *pre*-NAOs and NAOs mainly differ in the region near the adjacent carbon nucleus where NAOs exhibit additional nodal features. In fact, *pre*-NAOs, which are orthogonal to the other orbitals centered on the same carbon atom but are not orthogonal to the orbitals centered on different atoms, pass smoothly through the region occupied by the electrons associated with the adjacent carbon atom. The occupancy-weighted symmetric orthogonalization renders NAOs orthogonal also to orbitals centered on the adjacent carbon atom by preserving as much as possible the form of the orbital.

The effect of these transformations is to describe each atomic orbital as nearly as possible in terms of natural minimal basis orbitals. The remaining electron density that cannot be described by the natural minimal basis orbitals is accommodated in the Rydberg orbitals that would have a zero occupancy for the ground state of an isolated atom. For this reason any nonzero occupation in Rydberg orbitals can be ascribed to atomic changes that take place when the atom is in the molecular environment.

2.1.2 NHO and NBO Transformation

Once the density matrix has been transformed to the NAO basis, bonds between atoms are identified from the off-diagonal blocks P_{AL} (see Equation 2.3). In this procedure, the NAOs

of very high occupancy (for example > 1.999) are identified as unhybridized core orbitals and removed from the density matrix. Then, NBOs are obtained by diagonalizing all two-center submatrices $P^{(AL)}$:

$$P^{(AL)} = \begin{pmatrix} P_{AA} & P_{AL} \\ P_{LA} & P_{LL} \end{pmatrix} \quad (2.7)$$

with respect to the associated overlap submatrices $S^{(AL)}$:

$$P^{(AL)} h_i^{(AL)} = n_i^{(AL)} S^{(AL)} h_i^{(AL)} \quad (2.8)$$

and searching for bond vectors σ_{AB} whose occupancy exceeds a given threshold (for example 1.90). The problems due to the near degeneracy of lone pairs on different atoms, which may lead to a significant mixing of the corresponding eigenvectors, is avoided by depleting $P^{(AL)}$ of lone-pair eigenvectors $h_i^{(A)}$ found in the diagonalization of P_{AA} :

$$\bar{P}^{(AL)} = P^{(AL)} - n_i^{(A)} h_i^{(A)} h_i^{(A)\dagger} \quad (2.9)$$

In the case of a single bond between A and L, the depleted matrix is expected to have a unique eigenvector $h_i^{(AL)}$ of about double occupancy ($n_i^{(AL)} \approx 2$) which is a linear combination of the hybrid orbitals on atoms A and L:

$$\bar{h}_i^{(AL)} = \begin{bmatrix} h_i^{(A)} \\ h_a^{(L)} \end{bmatrix} \quad (2.10)$$

Therefore, the orbital $h_i^{(AL)}$ represents the bond orbital between an hybrid $h_i^{(A)}$ on atom A and the corresponding hybrid $h_a^{(L)}$ on atom L. It should be noted that the hybrid orbitals computed in this way are not orthogonal and therefore they must be symmetrically orthogonalized to obtain the final natural hybrid orbitals for each center. In the orthogonalization procedure it is necessary to specify the minimal occupancy (n_{\min}) that will be accepted to constitute an electron “pair”.

At the end of these procedures, one center and two centers localized NBOs are generated. As discussed previously, these NBOs can be divided into two subsets; a set of strongly occupied orbitals (core, lone pairs, and bonding orbitals) and a set of weakly occupied orbitals (antibonding, and rydberg orbitals).

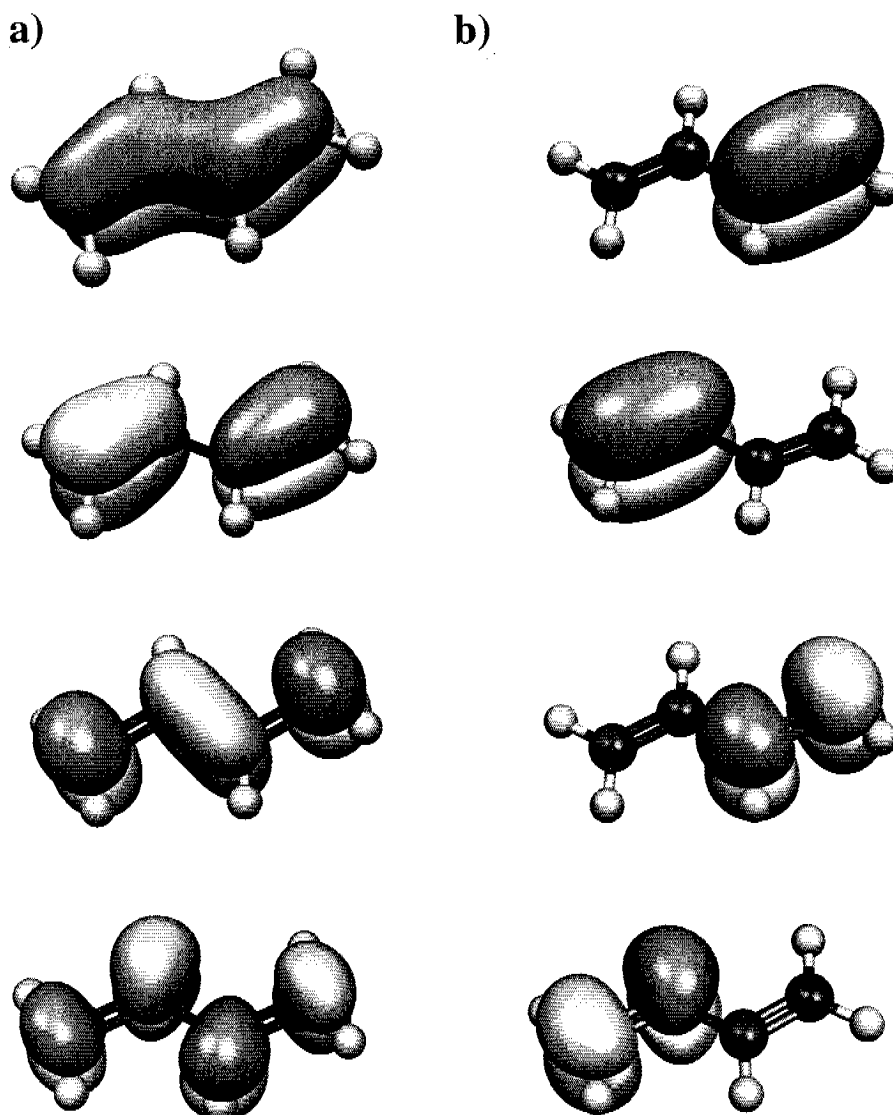


Figure 2.3: a) canonical delocalized π and π^* MOs and b) corresponding localized π and π^* NBOs of 1,3-butadiene computed at HF/6-31G(d,p) level of theory.

In Figure 2.3 are reported, as example, the two highest occupied and two lowest unoccupied canonical π MOs and the corresponding localized π and π^* NBOs of 1,3-butadiene computed at HF/6-31G(d,p) level of theory. The orbital occupancies of the canonical MOs are clearly 2 (occupied MOs) or 0 (unoccupied MOs), while those of NBOs

are 1.953 and 0.045 for the π and π^* orbitals, respectively. In the next section we will explain the protocols to use the NBOs for the evaluation of the delocalization energies.

2.2 A New Approach for the Analysis of Electron Delocalization Based on NBO Theory

2.2.1 Deletion Energies Protocol

The complete information contained in the first-order reduced density matrix $\Gamma(\mathbf{r}|\mathbf{r}')$ of an n -electron LCAO-MO wavefunction Ψ can be obtained by solving the eigenvalue equations

$$\hat{\Gamma} \theta_i = n_i \theta_i \quad (2.11)$$

where θ_i are natural orbitals and n_i are their occupancies. By searching for the highest-occupancy eigenorbitals in each diatomic region, one finds the optimal natural bond orbitals (NBOs) $\theta_i^{(AB)}$. As discussed in the previous section, this set of high-occupancy NBOs, each taken doubly occupied, is considered to represent the “natural Lewis structure” of the molecule, or according to Pauling’s resonance theory, the most stable resonance structure. The antibonding (σ^* and π^*) and Rydberg orbitals, which are also generated in the NBO analysis, should be unoccupied in the Lewis description of the molecule. Therefore, these orbitals, which are weakly occupied in the NBO description represent the irreducible departure from the *idealized* Lewis picture or, in terms of resonance theory, these orbitals represent the contribution given by the less stable resonance structures to the ‘real’ (delocalized) wavefunction of the system. The electron density accommodated in the antibonding and Rydberg orbitals is referred to as the “non-Lewis density”. The energy associated with these orbitals is calculated by deleting them from the NBO basis set and by recomputing the total energy (E'_{tot}) in the reduced orbital space. The deletion of all σ^* and π^* orbitals and the recomputation of the energy imposes on the non-Lewis electron density to move into bonding orbitals giving rise to a *perfect* Lewis representation of the molecule.

The deletion procedure is carried out by deleting the off-diagonal terms of the rows and columns corresponding to the selected orbitals from the Bond Orbital Fock matrix and by re-diagonalizing the Fock matrix to form a new density matrix (see Figure 2.4). This density is used to evaluate the energy in a single SCF cycle. This method is therefore not strictly self-consistent. However, Weinstock [14] showed that the complete SCF calculation in the truncated NBO basis, led to deletion energies within $0.1 \text{ kcal mol}^{-1}$ only.

$$F = \begin{bmatrix} f_{11} & f_{12} & \cdots & f_{1i} & \cdots \\ f_{21} & f_{22} & \cdots & f_{2i} & \cdots \\ \vdots & \vdots & & & \\ f_{i1} & f_{i2} & \cdots & f_{ii} & \cdots \\ \vdots & \vdots & & & \end{bmatrix}$$

Figure 2.4: Fock matrix in the NBO basis. The deletion of orbital i corresponds to the deletion of the row and column involving this orbital.

The total energy (E_{tot}), after the deletion of the weakly occupied (non-Lewis) orbitals, can be expressed as sum of Lewis (L) and non-Lewis (NL) contributions:

$$E_{tot} = E_L + E_{NL} \quad (2.12)$$

where:

$$E_L = E'_{tot} \quad (2.13)$$

and

$$E_{NL} = E_{tot} - E'_{tot} \quad (2.14)$$

This deletion procedure is a standard feature of the NBO program and it has been used by Weinhold and Schleyer to calculate the non-Lewis (NL) contribution on several hypervalent compounds [15-19] (see Section 1.2.2).

In linearly π -conjugated systems, the π^* and σ^* NBOs are considered to be responsible for electron delocalization. The energy associated with their deletion may thus be used as a measure of delocalization. In this picture, the delocalization energy, E_{deloc} , is obtained as:

$$E_{deloc} = E_{NL} - E_{strain} - E_{Rydberg}. \quad (2.15)$$

If the contributions of the Rydberg orbitals ($E_{Rydberg}$) and the steric repulsion (E_{strain}) are both negligible, then:

$$E_{deloc} = E_{NL} = E_{del}. \quad (2.16)$$

Therefore, E_{del} or E_{NL} are equivalent to E_{deloc} and may, for example, be used to quantitatively assess the delocalization energy differences in conformational isomers [1, 2]. In this case, the difference in delocalization energy (ΔE_{del}) for a pair of isomers A and B is given as:

$$\Delta E_{del} = \Delta E_{tot} - \Delta E_{strain} \quad (2.17)$$

where ΔE_{tot} and ΔE_{strain} denote the difference between A and B in total and in strain energies, respectively. For planar π -conjugated compounds studied here it will be shown that ΔE_{strain} is very small compared to ΔE_{del} , and therefore, can be neglected.

E_{del} , calculated by deleting all antibonding orbitals, is the energy associated to the σ and π electron delocalization from the single most stable Lewis representation of the molecule, and therefore has no experimental counterpart. Since the geometry of the reference structure is the same of the delocalized one, E_{del} corresponds to a *vertical resonance energy* (VRE).

One of the main features of the present approach is that, in the case of planar π -conjugated molecules, E_{del} can be decomposed into σ - and π -contributions [1] using the same deletion procedure on the specific σ and π sets of orbitals:

$$E_{del} = E_{del}(\sigma) + E_{del}(\pi). \quad (2.18)$$

In case where the in-plane π orbitals ($\pi_{=}$) can only interact with the σ framework, but not with the perpendicular orbitals (π_{\perp}), the delocalization energy can be further expressed as:

$$E_{del} = E_{del}(\sigma_{=}) + E_{del}(\pi_{\perp}) \quad (2.19)$$

where:

$$E_{del}(\sigma_{=}) = E_{del}(\sigma + \pi_{=}) \quad (2.20)$$

which means that the energy associated with $\sigma_{=}$ is calculated by deleting all the σ^* and $\pi_{=}^*$ orbitals simultaneously. The reliability of this decomposition scheme is confirmed by the fact

that the sum of $E_{del}(\sigma_{\pm})$ and $E_{del}(\pi_{\perp})$, which are obtained by deleting the σ and π sets of orbitals, is in fact, roughly equal to E_{del} obtained by deleting all antibonding orbitals.

The small discrepancy between E_{del} and the sum of $E_{del}(\sigma_{\pm})$ and $E_{del}(\pi_{\perp})$ is due to the different dimension of the reduced orbital spaces in which E_{del} (deletion of the total antibonding orbitals) and $E_{del}(\sigma_{\pm})$ or $E_{del}(\pi_{\perp})$ (deletion of a subset of the antibonding orbitals)

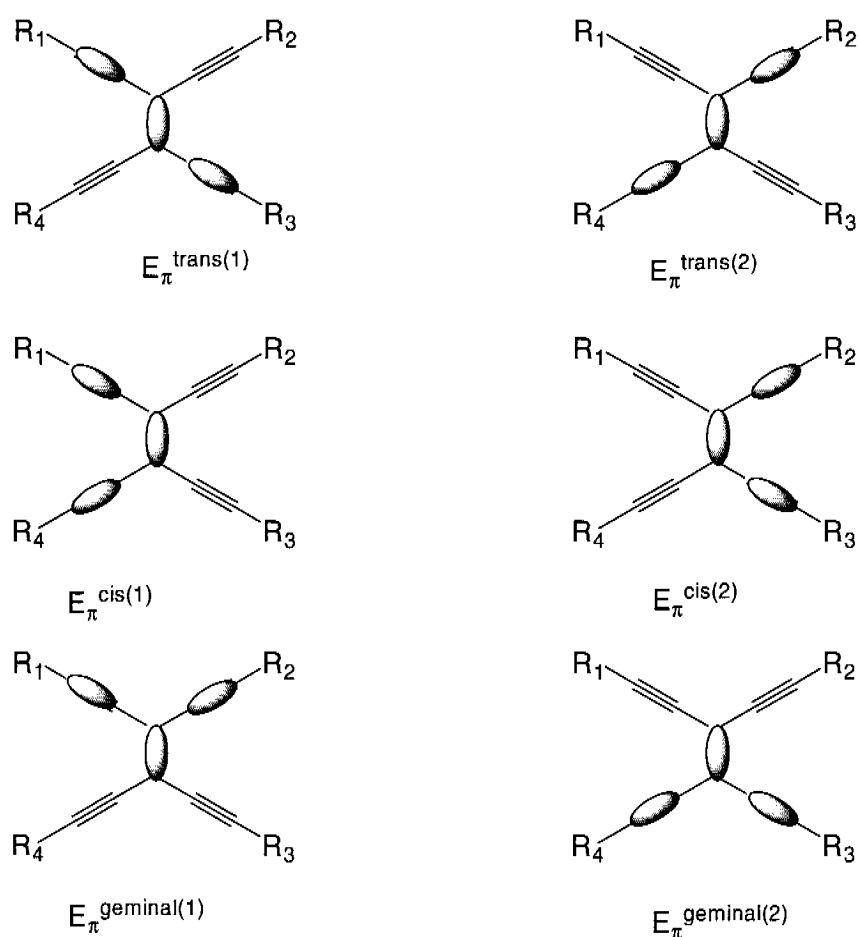


Figure 2.5: Schematic representation of the NBOs involved in the six different π -conjugated pathways of a tetraethynylethene derivative.

are calculated. This approach (Equation 2.20) has the advantage of giving an energy based measure for in-plane conjugation ($E_{del}(\sigma_-)$) and vertical π -conjugation ($E_{del}(\pi_-)$) at the same time. It even allows to quantitatively analyze electron delocalization in a given path within the same system. In fact, for a molecule characterized by *different* π -conjugated paths, it is possible to delete orbitals along a selected π -conjugated pathway, and therefore, to calculate a delocalization energy E_{del}^{path} for that pathway. For example, the six different π -conjugated pathways of a tetraethynylethene derivative (see Figure 2.5) can be investigated by deleting specific π^* orbitals along the two *cis*, two *trans* and two *geminal* π -conjugated pathways and computing the corresponding π -delocalization energies. The comparison of these energies can be used to measure the impact of the substituents, as well as the π -conjugated pathway on the π -delocalization.

Equation 2.20 can be further expanded to include contributions from individual localized orbitals in the path under consideration. However, in this case we will be confronted with non-additivity problems due to the orbital interactions. On the other hand, the decomposition of E_{del} into individual orbital contributions gives qualitative information beyond what we can learn from (2.20). In the present context, we will look at the contributions of the individual orbitals to the differences in the delocalization energies. Moreover, the attention will be also focused on local features such as differences in the bond lengths.

2.2.2 Second-Order Orbital Interaction Energies Protocol

In non-aromatic compounds, the non-Lewis contributions are typically very small compared to the Lewis-type ones, they amount to less than 1%. The corrections to the Lewis-type picture can thus be approximated by second-order perturbation theory.

A many-electron perturbation operator $\hat{H}^{(pert)}$ can be written as a sum of one-electron perturbations:

$$\hat{H}^{(pert)} = \hat{F}_1^{(pert)} + \hat{F}_2^{(pert)} + \dots + \hat{F}_n^{(pert)} \quad (2.21)$$

The substitution of Equation (2.21) into the general perturbation equations:

$$E^{(1)} = \langle \Psi^{(0)} | \hat{H}^{(pert)} | \Psi^{(0)} \rangle \quad (2.22a)$$

$$E^{(2)} \leq - \frac{\langle \Psi^{(0)} | \hat{H}^{(pert)} | \tilde{\Psi}^{(1)} \rangle}{\langle \tilde{\Psi}^{(1)} | \hat{H}^{(0)} - E^{(0)} | \tilde{\Psi}^{(1)} \rangle} \quad (2.22b)$$

leads to first and second-order corrections of the form:

$$E^{(1)} = \sum_i E_i^{(1)} \quad (2.23a)$$

$$E^{(2)} = \sum_i E_i^{(2)} \quad (2.23b)$$

where:

$$E_i^{(1)} = -n_i^{(0)} \langle \phi_i^{(0)} | \hat{F}^{(pert)} | \phi_i^{(0)} \rangle \quad (2.24a)$$

$$E^{(2)} \leq -n_i^{(0)} \frac{\langle \phi_i^{(0)} | \hat{F}^{(pert)} | \tilde{\phi} \rangle^2}{\langle \tilde{\phi} | \hat{H}^{(0)} - \epsilon_i^{(0)} | \tilde{\phi} \rangle} \quad (2.24b)$$

In these expressions $n_i^{(0)}$ is the number (0, 1, 2) of electrons occupying the spatial orbital $\phi_i^{(0)}$ in the wavefunction $\Psi^{(0)}$ and $\tilde{\phi}$ is a variational trial function (orthogonal to $\phi_i^{(0)}$) for the first order correction $\phi_i^{(1)}$. The expressions 2.24a and 2.24b allow us to treat the perturbative effects on an orbital-by-orbital basis. The treatment can be further simplified by noting that $E^{(1)}$ is a constant that can be added to $\hat{H}^{(0)}$, giving a shift in the zero of the energy scale for $E^{(0)}$ and making $E^{(1)} = 0$. Thus, it may be assumed that $\hat{H}^{(0)}$ and $\hat{F}^{(0)}$ are chosen to make the first order corrections vanish, so that Equation 2.24b is the leading correction. This equation can also simplify by noting that $\hat{F}^{(pert)}$ can be replaced in the numerator by \hat{F} , because $\langle \phi_i^{(0)} | \hat{F}^{(0)} | \tilde{\phi} \rangle = 0$ for any $\tilde{\phi}$ orthogonal to $\phi_i^{(0)}$. $\tilde{\phi}$ can further be chosen to be a normalized trial function, and define:

$$\tilde{\epsilon} = \langle \tilde{\phi} | \hat{F}^{(0)} | \tilde{\phi} \rangle \quad (2.25)$$

Then Equation 2.23b can be expressed as:

$$E^{(2)} \leq -n_i^{(0)} \frac{\langle \phi_i^{(0)} | \hat{F}^{(pert)} | \tilde{\phi} \rangle^2}{\langle \tilde{\phi} | \tilde{\mathcal{E}} - \mathcal{E}_i^{(0)} | \tilde{\phi} \rangle} \quad (2.26)$$

Moreover, it will often occur that the best possible trial function $\tilde{\phi}$ is dominated by a single unperturbed orbital $\phi_{j^*}^{(0)}$ (with $n_{j^*}^{(0)} = 0$, the asterisk denoting an initially unoccupied orbital), and therefore approximate:

$$\tilde{\phi} = \phi_{j^*}^{(0)} \quad (2.27a)$$

$$\tilde{\mathcal{E}} = \mathcal{E}_{j^*}^{(0)} \quad (2.27b)$$

The substitution of Equations 2.27a and 2.27b into Equation 2.24b leads to the formula for the second-order interaction energy (SOIE) for a pair of donor and acceptor NBOs

$$E^{(2)} = E_{SOIE_{ij}} = -n_i^{(0)} \frac{\langle \phi_i^{(0)} | \hat{F} | \phi_{j^*}^{(0)} \rangle^2}{\mathcal{E}_{j^*}^{(0)} - \mathcal{E}_i^{(0)}} \quad (2.28)$$

where $n_i^{(0)}$ is the donor orbital occupancy, $\mathcal{E}_{j^*}^{(0)}$ and $\mathcal{E}_i^{(0)}$ are the orbital energies of the acceptor and donor orbitals, respectively, and $\langle \phi_i^{(0)} | \hat{F} | \phi_{j^*}^{(0)} \rangle$ is the corresponding element of the Fock matrix in the NBO basis.

Using Equation 2.28 allows to examine all possible interactions between filled Lewis-type NBOs (donor orbitals) and weakly occupied non-Lewis-type NBOs (acceptor orbitals), and evaluate their relevance. These donor-acceptor interactions are responsible for the loss of occupancy in filled NBOs, and measure the deviation from the *idealized* Lewis structure. Therefore, they are also referred to as “delocalization corrections” to the natural Lewis structure.

For a system of two pairs of π orbitals (π_i and π_j), the leading second-order interaction terms are:

$$\pi_i \rightarrow \pi_j^* \quad \text{SOIE}_{ij}$$

$$\pi_j \rightarrow \pi_i^* \quad \text{SOIE}_{ji}$$

The $\pi_i \rightarrow \pi_i^*$ and $\pi_j \rightarrow \pi_j^*$ are usually very small and do not play an important role. The sum of SOIEs corresponds to the non-Lewis contribution to the total energy

$$E_{NL} = E_{SOIEij} + E_{SOIEji} + \text{higher order terms.} \quad (2.29)$$

From the above discussion, we can conclude that:

$$\sum_{ij} E_{SOIEij} = E_{NL} \quad (2.30)$$

as long as higher order contributions can be neglected, and therefore:

$$E_{del} = \sum_{ij} E_{SOIEij} \quad (2.31)$$

The approaches to calculate delocalization energies are summarized in Figure 2.6 where we schematically show the relationship between E_{deloc} , E_{NL} , E_{del} , and $\sum_{ij} E_{SOIEij}$.

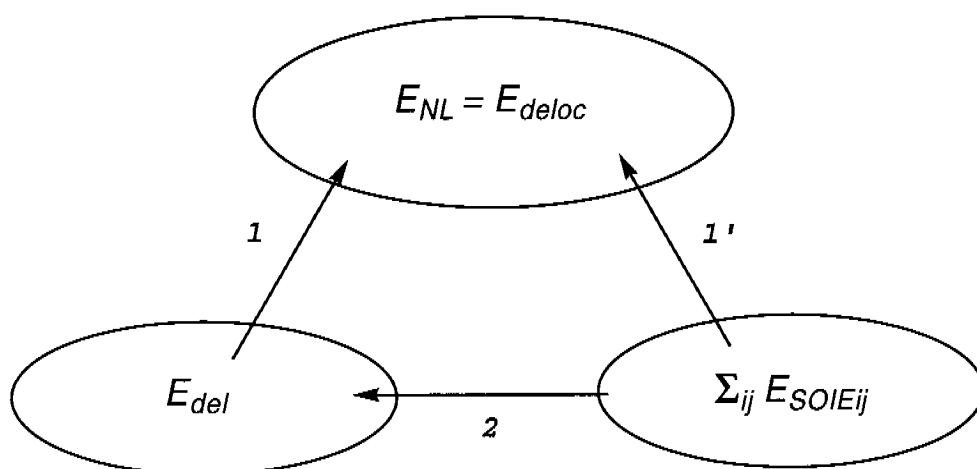


Figure 2.6: The relationship between E_{del} and $\sum_{ij} E_{SOIEij}$. Both E_{del} and $\sum_{ij} E_{SOIEij}$ allow to “measure” the total or the local delocalization energy (1,1’); the results, however, may not be identical (higher-order corrections).

In summary, while E_{NL} just gives the total delocalization energies, both the E_{del} and the sum of second-order energies ($\sum_{ij} E_{SOIE_{ij}}$) protocols allow to “measure” distinct conjugation paths, looking at delocalization as a local property. Moreover, the SOIE approach further allows to identify the donor/acceptor orbital interactions responsible for the delocalization energies observed.

2.2.3 Other Electron Delocalization Indicators

Additional very useful information for the investigation of electron delocalization is given by the population (or occupation numbers) of the bonding and antibonding NBOs. As discussed above, the NBO analysis generates a set of strongly occupied (with the electron population slightly lower than 2) core, lone pair and bonding orbitals, and a set of weakly occupied (with the electron population slightly larger than 0), antibonding and Rydberg orbitals. The values of these occupation numbers correspond to the flux of charge involved in the intramolecular donor \rightarrow acceptor interactions, and therefore, give qualitative information on the extent of delocalization. For example (as it will be shown in the next chapter), the population of the π^* orbitals in a conjugated molecular system linearly correlates with the C=C bond length, providing a link between molecular and electronic structure. In addition, the deletion of an acceptor orbital followed by recomputation of the new energies in the reduced space gives important qualitative information about the flow of charge (or relaxation) associated with the disablement of a certain delocalization pathway. Therefore, the changes of the occupation numbers associated to the orbital deletion provide a way to identify the orbitals involved in the donor-acceptor interaction.

The three approaches discussed above are equivalent, in the sense that they produce the same kind of information. However, one of these approaches is better than the others to investigate selected features of electron delocalization.

2.2.4 Values and Drawbacks of the Approach

An important drawback of the approach is that it is not designed to give absolute values for delocalization energies, but it is developed to reproduce differences between structural isomers or between backbones with different functionalizations. In fact, the absolute values calculated for the delocalization energies are generally larger than those obtained with other theoretical methods. For example, the π -delocalization energy calculated for the allyl cation and anion is about two times larger than that obtained by Peyerimhoff et al. using the BLW approach [20]. The authors explain this difference by arguing that the wavefunction of the Lewis structure in the NBO method, being deduced from the SCF wavefunction calculated for the real molecule, is not relaxed. However, the same authors noted that *“it is difficult to judge which set of data is more reliable since there is no direct experimental proof”*. On the other hand, in the next chapter, we will show that the approach is well suited for the investigation of configurational or conformational isomers for which the relative energies give accurate results due to a compensation of errors. For these reasons, in the following, we will discuss relative delocalization energies rather than absolute values. It should also be noted that, in the previous chapter we clearly emphasized the limits of any definition concerning delocalization energy. The delocalization energy is not a physical observable, and therefore, should not be overinterpreted. The importance of this descriptor lies in the ability to assist the interpretation of the effects played by topological variables to the physical properties of a molecule.

An important feature of this approach is the possibility to investigate different π -conjugated pathways within the same molecule, thus, allowing to identify the relevant contributions to conjugation in a given system, to assess the impact of donor or acceptor substituents and/or spacers, and to evaluate the response of a backbone to substitution. In addition, the approach can be easily implemented, is not time-consuming and can be applied to any mono-determinant SCF approach like HF and DFT methods.

2.3 References

1. M. Bruschi, M. G. Giuffreda, H. P. Lüthi, *Trans* versus *Geminal* Electron Delocalization in Tetra- and Di-Ethynylethenes. *Chem. Eur. J.*, **2002**, 8, 4216-4227.
2. M. G. Giuffreda, M. Bruschi, H. P. Lüthi, Electron Delocalization in Linearly π -Conjugated Systems: A Concept for Quantitative Analysis. *Chem. Eur. J.*, **2004**, 10, 5671.
3. M. Bruschi, M. G. Giuffreda, H. P. Lüthi, Electron Delocalization in Extended Linearly π -conjugated Systems: *Through* versus *Cross* Electron Delocalization in Polytriacetylene. *ChemPhysChem*, **2005**, 6, 511-519.
4. J. P. Foster, F. Weinhold, Natural Hybrid Orbitals. *J. Am. Chem. Soc.*, **1980**, 102, 7211-7218.
5. A. E. Reed, F. Weinhold, Natural Bond Orbitals of Near Hartree-Fock Water Dimer. *J. Chem. Phys.*, **1983**, 78, 4066.
6. A. E. Reed, R. B. Weinstock, F. Weinhold, Natural Population Analysis. *J. Chem. Phys.*, **1985**, 83, 735-746.
7. A. E. Reed, F. Weinhold, Natural Localized Molecular Orbitals. *J. Chem. Phys.*, **1985**, 83, 1736-1740.
8. A. E. Reed, L. A. Curtiss, F. Weinhold, Intermolecular Interaction from a Natural Bond Orbital, Donor-Acceptor Viewpoint. *Chem. Rev.*, **1988**, 88, 899-926.
9. F. Weinhold, Natural Bond Orbital Methods. Encyclopedia of Computational Chemistry. Vol. 3. ed. P. v. R. Schleyer, N. L. Allinger, T. Clark, J. Gasteiger, P. A. Kollman, H. F. Schaefer, III, P. R. Schreiner, **1998**, Chichester, UK: John Wiley & Sons. 1792-1811.
10. F. Weinhold, J. E. Carpenter, The Structure of Small Molecules and Ions, ed. Naaman, Z. Vager. **1988**, New York: Plenum. 227-236.
11. F. Weinhold, Computational Methods in Organic Photochemistry: Molecular and Supramolecular Photochemistry, ed. A. Kutateladze. **2003**, New York: Marcel Dekker.
12. F. Weinhold, C. R. Landis, Valency and Bonding: A Natural Bond Orbital Donor-Acceptor Perspective. **2005**, Cambridge: Cambridge University Press.

13. P. O. Löwdin, Quantum Theory of Many-Particle Systems. I. Physical Interpretations by Means of Density Matrices, Natural Spin-Orbitals, and Convergence Problems in the Method of Configurational Interaction. *Phys. Rev.*, **1955**, 97, 1474.
14. R. B. Weinstock, *PhD Thesis*. 1981, University of Wisconsin: Madison.
15. A. E. Reed, P. v. R. Schleyer, The Anomeric Effect with Central Atoms Other Than Carbon. 1. Strong Interactions Between Nonbonded Substituents in Polyfluorinated First- and Second-row Hydrides. *J. Am. Chem. Soc.*, **1987**, 109, 7362-7373.
16. A. E. Reed, P. v. R. Schleyer, Chemical Bonding in Hypervalent Molecules. The Dominance of Ionic Bonding and Negative Hyperconjugation over d-orbital Participation. *J. Am. Chem. Soc.*, **1990**, 112, 1434-1445.
17. U. Salzner, P. v. R. Schleyer, A Successful Ab Initio Study of the Adiabatic Electron Affinity of the Methyl Radical. *Chem. Phys. Lett.*, **1992**, 190, 401.
18. U. Salzner, P. v. R. Schleyer, Generalized Anomeric Effects and Hyperconjugation in $\text{CH}_2(\text{OH})_2$, $\text{CH}_2(\text{SH})_2$, $\text{CH}_2(\text{SeH})_2$, and $\text{CH}_2(\text{TeH})_2$. *J. Am. Chem. Soc.*, **1993**, 115, 10231-10236.
19. U. Salzner, P. v. R. Schleyer, Ab Initio Examination of Anomeric Effects in Tetrahydropyrans, 1,3-Dioxanes, and Glucose. *J. Org. Chem.*, **1994**, 59, 2138-2155.
20. Y. Mo, S. D. Peyerimhoff, Theoretical Analysis of Electron Delocalization. *J. Chem. Phys.*, **1998**, 109, 1687-1697.

3 The Validation of the Approach

In this chapter the approach for the analysis of electron delocalization described and discussed in Chapter 2 is validated on two test cases; the *1,3*-butadiene molecule, and the diethynylethene isomers. The analysis of *1,3*-butadiene focuses on the changes of delocalization energy for the rotation around the central C-C bond. In the case of the DEEs, the investigation concerns the differences between *linear (through)* and *cross π* -delocalization in the *trans* and *geminal* isomers. In both cases, the analysis is extended to related molecular systems in order to further check the reliability of the approach.

3.1 *1,3*-Butadiene: an Illustration of the Approach

3.1.1 Summary

The evaluation of electron delocalization in *1,3*-butadiene, which is the prototypical linear π -conjugated compound, represents a test case for the application of our approach based on the NBO theory. The results of the analysis show that, despite the calculated value of the delocalization energy is much larger than that found by other theoretical methods, the *cis-trans* rotational barrier is accurately reproduced by the changes in the delocalization energy.

We also show that the sum of the second-order interaction energies (SOIE) corresponds to the delocalization energy, proving that Equation 2.30 is fulfilled. The extension of the analysis to larger π -conjugated polyenes, up to $C_{16}H_{18}$, confirms the results reported for 1,3-butadiene. In addition, the approach is able to reproduce fine effects such as the position of the energy maximum at a C=C-C=C dihedral angle larger than 90° , and the non linear relationship between the extent of electron delocalization and the number of π -conjugated bonds in the molecule.

3.1.2 Introduction

1,3-butadiene is the simplest π -conjugated compound, and therefore, represents the reference system to validate the approach presented in the previous chapter. This molecule is poorly delocalized when compared with aromatic compounds, such as benzene, as confirmed by the strong bond length alternation. However, the two C=C bonds are longer than the C=C bond in ethylene and the central bond is significantly shorter than that of a single C-C bond in alkanes. These changes in bond lengths can be attributed to a weak π -electron delocalization between the double bonds (Figure 3.1). In linear olefins, a method to assign qualitative resonance stabilization values is the examination of rotational barriers. The basic assumption in this case is that no π -delocalization is present at the highest point of the rotational profile, and therefore, the stabilization energy should be equal to the rotational barrier. Values obtained with this method are not accurate since, as illustrated by Marks et al. [1], other factors such as steric effects and σ -frame conjugation influence the barrier height. Nevertheless, the rotational energy barrier has been employed as a measure of conjugation in systems such as allyl cation [2-8], radical [2, 7-10], and anion [2, 7, 8, 11], butadiene [12-15], butadiene radical cation [16, 17] and derivatives thereof [18-21].

1,3-butadiene has been the subject of a great number of conformational studies, and all of these found the most stable conformation to be the planar *trans* molecule [22-26]. The torsional potential function, determined using Raman spectroscopy and high intensity argon ion laser source, provided an energy barrier for the rotation around the C-C bond equal to 7.2

kcal mol⁻¹, and an energy difference between the *trans* and *cis* conformation equal to 2.5 kcal mol⁻¹ [27].

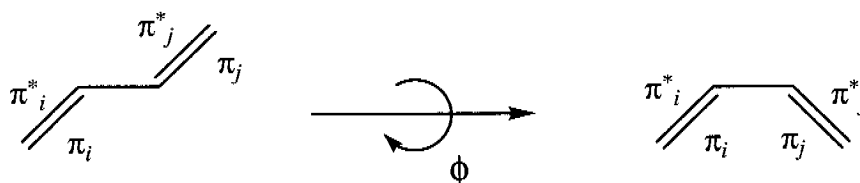


Figure 3.1: The *trans* and *cis* 1,3-butadiene. π_i and π_j are the two out-of-plane occupied orbitals, π_i^* and π_j^* are the corresponding unoccupied ones.

The goal of the present work is to use our approach in order to reproduce the *cis-trans* rotational barrier solely based on the change in the delocalization energy. The reader should be reminded that the planar *cis* structure is a transition state, and that the minimum for the *cis* structure is found at a torsional angle of 30.9 degrees (steric repulsion). Similarly, the maximum of the rotational barrier is shifted towards the *trans* structure, and it occurs at 100 degrees.

3.1.3 Computational Methods

In the present work the calculations were performed at the Density Functional Theory (DFT) level [28]. In the framework of DFT, the B3LYP functional has been used [29-33] together with the 6-31G(d,p) basis set [34]. The NBO analysis of 1,3-butadiene and larger polyenes has been performed on the geometry optimized in the planar structure at the same level of theory.

The delocalization energy E_{del} has been calculated by removing all the antibonding natural bond orbitals (NBO; σ^* and π^*) simultaneously (see Chapter 2). All energy differences (ΔE_{tot} , ΔE_{del}) are calculated with respect to the *trans* isomer (180 degrees), which is taken as reference structure. The delocalization energies are further broken down into orbital contributions for each type of bond. The π -delocalization energy calculated by deleting the π^*

antibonding orbitals is labeled E_π . For the σ backbone, $E\sigma_D$, $E\sigma_S$, $E\sigma_{C-H1}$ and $E\sigma_{C-H2}$ correspond to the delocalization energies calculated by deleting the σ antibonding orbitals of the C=C, C-C, -C-H and =C-H bonds, respectively.

All calculations have been carried out using Gaussian98 package [35]. The Natural Bond Orbital analysis has been performed with the program NBO 5.0 [36] included in Gaussian98.

3.1.4 Results and Discussion

1,3-butadiene. E_{tot} , E_{NL} ($\equiv E_{del}$), and E_L calculated at the B3LYP/6-31G(d,p) level of theory, with respect to the reference structure (*trans* isomer), as a function of the torsional angle ϕ , are displayed in Figure 3.2. The calculated energy barrier ($7.6 \text{ kcal mol}^{-1}$) is in close agreement with the experimental one ($7.2 \text{ kcal mol}^{-1}$). The graph shows that in the range 180 to 90 degrees, i.e. from the *trans* structure to the region slightly beyond the maximum, ΔE_{tot} and ΔE_{del} are nearly identical, indicating that Equation 2.17 is fulfilled. Moreover, the results show that the Lewis component of the energy (E_L) does remain constant during the rotation, and that the energy variation is exclusively due to the non-Lewis component (E_{NL}), i.e. the rotational barrier of 1,3-butadiene is entirely due to changes in the delocalization energy. On the other hand, in the range of $0 < \phi < 80$ degrees the discrepancy between $\Delta E_{del}(\phi)$ and $\Delta E_{tot}(\phi)$ is noticeably larger due to steric repulsion, which means that E_{strain} (Equation 2.17) is not any longer negligible. Furthermore, it is worth to note that both curves exhibit the maximum at the exact same angle, which means that the deletion approach predicts the transition state to occur at the correct dihedral angle.

Figure 3.3 shows the accuracy of the relationship between the sum of E_{SOIE} and E_{del} as well as E_{NL} . We find that all energies show the same pattern, and that they compare reasonably well also in a quantitative way. It is also evident that the E_{del} calculated from the sum of the single π^* deletions compares more favorably with E_{SOIE} than the deletion energies obtained by removing all the π^* orbitals simultaneously. In the first case, both E_{del} and E_{SOIE} consider only single orbitals, whereas in the latter case the deletion energy also takes into account the coupling between orbitals, which in general has the effect of reducing the interaction energy.

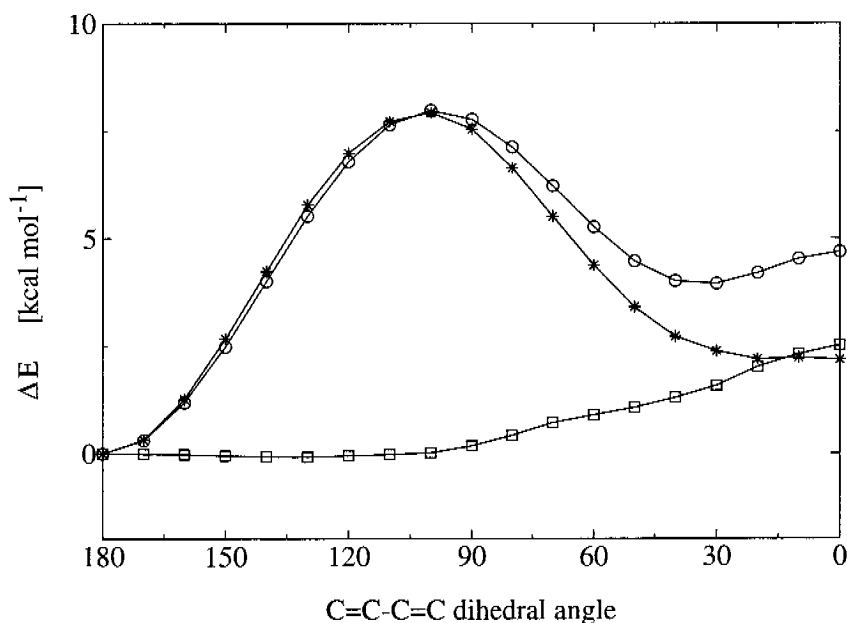


Figure 3.2: The calculated ΔE_{tot} (○), ΔE_{NL} (*), and ΔE_L (□) of the $C=C-C=C$ dihedral angle. The energies are computed for all the structures obtained after a rotation of 10 degrees about the single central bond. All energies are calculated with respect to the *trans* isomer (180 degrees), which is taken as reference structure.

Moreover, from Figure 3.3 we see that the discrepancy between the $\sum_{ij} E_{SOIE_{ij}}$ and E_{del} is larger for those structures with a dominant out-of-plane π - π conjugation. In fact the most significant energy difference is found for the *trans* isomer (180 degrees) and the planar *cis* one (0 degrees), where the out-of-plane conjugation is purely given by π - π interactions. This indicates that for these geometries the second-order energies are insufficient to describe accurately these interactions, and that higher-order terms should be taken into account (Equation 2.29).

As expected, the perpendicular conformation is more localized than the planar one (*trans* or *cis*). In fact, the non-Lewis orbital population reduces from 0.95% to 0.68% with respect to the total number of electrons. The decomposition of E_{del} into individual orbital contributions, as well as the changes of the orbital populations, give qualitative information on the intramolecular donor \rightarrow acceptor interactions involved in the electron delocalization. It should be noted that the calculated E_{π} in the *trans*-planar conformation ($24.7 \text{ kcal mol}^{-1}$) is significantly larger with respect to the one predicted by other approaches. Daudey et al. [37] and Mo et al. [38] reported values equal to 10.4 and $9.37 \text{ kcal mol}^{-1}$, respectively, which are only slightly larger than that of the energy barrier. E_{π} decreases from $24.7 \text{ kcal mol}^{-1}$ to $11.4 \text{ kcal mol}^{-1}$ when moving from the *trans*-planar conformation to the perpendicular ($\phi = 90^\circ$) one. The latter value indicates that in the perpendicular conformation the π^* orbitals are not completely turned off, but they are involved in hyperconjugative interactions with orbitals of the σ framework. This is confirmed by the fact that the π^* orbitals are also weakly populated

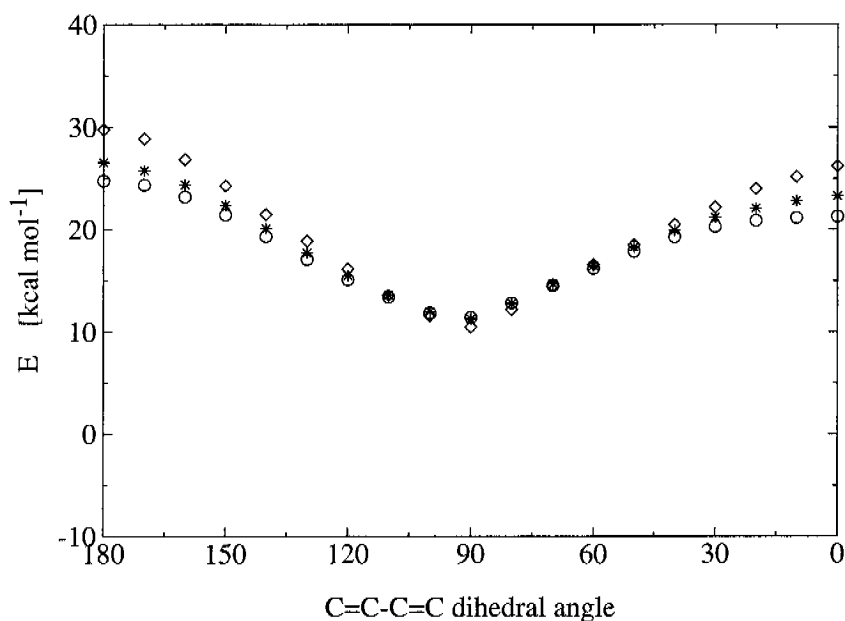


Figure 3.3: The $SOIE$, $E_{del(1)}$ (\circ) calculated by deletion of all π orbitals simultaneously, $E_{del(2)}$ (*) calculated as sum of deletion of single orbitals, and E_{SOIE} (\diamond) calculated as a sum of $SOIE$ s, as function of the $C=C-C=C$ dihedral angle.

in the perpendicular conformation (the π^* orbital population is equal to 0.072 in the *trans*-planar conformation and 0.021 in the perpendicular one). These hyperconjugative interactions, identified by the analysis of the changes in the orbital population upon the deletion of the π^* orbitals, are the result of the $\sigma_{\text{C-H}} \rightarrow \pi^*$ and $\sigma_{\text{D}} \rightarrow \pi^*$ charge transfers.

Polyenes. The accuracy of the relationship given by Equation 2.17 has further been checked by the study of the rotational barriers in larger polyenes up to $\text{C}_{16}\text{H}_{16}$. In fact, the energy barriers of polyenes of increasing chain length, calculated by the concerted rotation around all C-C bonds, match within a few tenths of a kcal mol^{-1} (see Table 3.1) the changes in delocalization energies, indicating that the relationship 2.17 is fulfilled also in the case of extended π -conjugated molecular systems. As example, in Figure 3.4 we report ΔE_{tot} and ΔE_{del} of the 1,3,5,7-octa-tetra-ene (C_8H_{10}) as function of the concerted rotation of the three $\text{C}=\text{C}-\text{C}=\text{C}$ torsional angles ϕ_n ($n = 1, 2, 3$).

Table 3.1: ΔE_{tot} and ΔE_{del} (in kcal mol^{-1}) calculated for a concerted rotation of 90 degrees of all $\text{C}=\text{C}-\text{C}=\text{C}$ torsional angles of polyenes of increasing chain length, at the B3LYP/6-31G(d,p) level of theory.

	ΔE_{tot}^a	ΔE_{del}^a
C_4H_6	7.6	7.8
C_6H_8	17.2	16.8
C_8H_{10}	27.4	26.7
$\text{C}_{12}\text{H}_{14}$	48.7	48.7
$\text{C}_{16}\text{H}_{18}$	68.2	69.1

a) All energies are calculated with respect to the trans isomer (180 degrees), which is taken as reference structure.

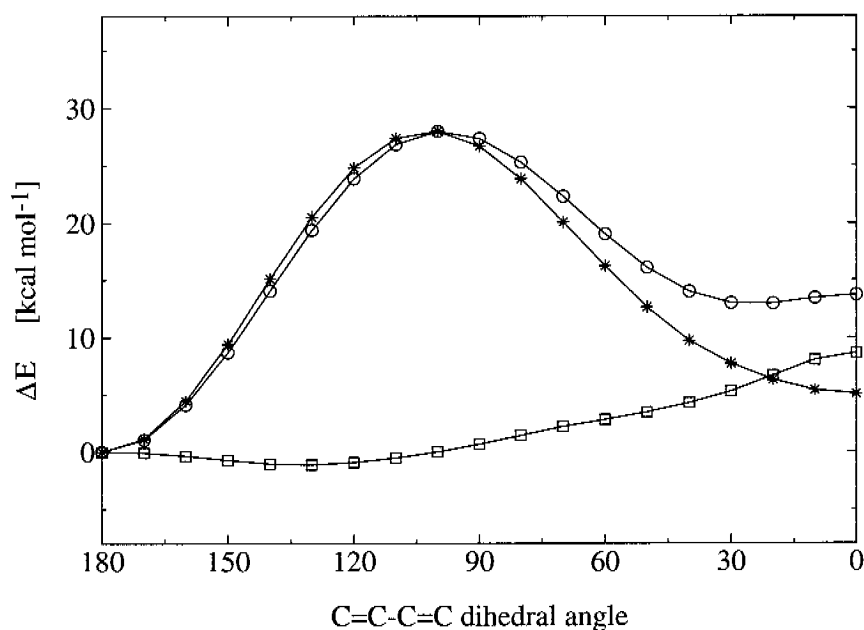


Figure 3.4: The calculated ΔE_{tot} (○), ΔE_{NL} (*), and ΔE_L (□) 1,3,5,7-octa-tetraene as function of the $C=C-C=C$ dihedral angle. The energies are computed for all the structures obtained after a rotation of 10 degrees about the single bonds. All energies are calculated with respect to the *trans* isomer (180 degrees), which is taken as reference structure.

Clearly, π -electron delocalization increases with increasing the length of the π -conjugated chain. In particular, one expects that for short polyenes, because of cooperative effects of π -conjugated orbitals, π -electron delocalization increases more than linearly as a function of the chain length, while for long polyenes, beyond the ECL the relationship between delocalization energy and chain length should be linear. The energy barrier calculated by the concerted rotation around all C-C bonds should reproduce these fine effects allowing to evaluate the extent of π -electron delocalization by increasing the chain length.

In fact, as shown in Table 3.1, the contribution of each rotation to the total energy barrier is more than additive. This is illustrated in Figure 3.5, in which E_{del} divided by the number of π -conjugated bonds ($E_{del}/C=C$) is reported as a function of the number of C=C bonds in the polyene. The value of $E_{del}/C=C$ rapidly increases for shorter polyenes, while for longer ones

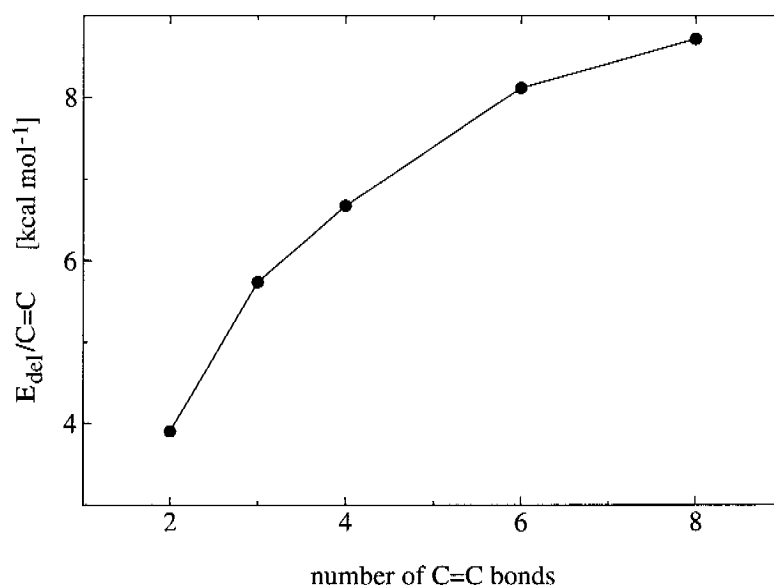


Figure 3.5: Evolution of $E_{\text{del}}/\text{C}=\text{C}$ as a function of the number of the $\text{C}=\text{C}$ bonds.

it approaches to an asymptotic value, for which the π -electron delocalization energy is an additive function with respect to the number of $\text{C}=\text{C}$ bonds.

3.1.5 Conclusions

1,3-butadiene has been used as test molecule to validate our approach for the quantification of electron delocalization. The approach appears to be suitable to reproduce differences between conformational and structural isomers and not to give absolute values for delocalization energies. The *cis-trans* rotational barrier of *1,3*-butadiene is accurately reproduced by changes in delocalization energy, indicating that the barrier is exclusively due to the reduction of electron delocalization in the perpendicular conformation. The analysis has been extended to larger polyenes, for which we showed that the increase of π -electron delocalization as a function of the π -conjugated chain length is more than additive; an effect that is ascribed to cooperative interactions of π -orbitals and should vanish at the effective conjugation length. Finally, we verified that Equation 2.30 is fulfilled.

3.2 *Through* versus *Cross* Electron Delocalization in Tetra- and Di-Ethynylethenes

3.2.1 Summary

Trans-diethynylethene [*Z*-exan-3-ene-1,5-diyne; **1a**], *geminal*-diethynylethene [2-ethynylbutan-3-ene-1-yne; **1b**] and tetraethynylethene [3,4 ethynyl-exan-3-ene-1,5-diyne; **2**] are flexible molecular building blocks for π -conjugated polymers with interesting electronic and photonic properties. The type of functionalization, the length of the polymer chain, as well as the choice of π -conjugation mode, plays a crucial role for the properties of these compounds. In order to rationalize the impact of the different delocalization pathways in the various types of isomers (*trans* or *geminal*) on the molecular and electronic structure, the approach presented in Chapter 2, based on the NBO analysis of Weinhold, is applied on these parent molecules. This approach is used to correlate the changes in molecular and electronic observables like the bond lengths and the absorption frequencies, with the molecular and electronic structures. It also shows that the difference between *trans* (or *through*) and *geminal* (or *cross*) conjugation is not only due to the vertical π -conjugation but also to the in-plane σ hyperconjugation. Moreover, this method allows us to predict how a certain substituent will affect the molecular structure as well as the electronic properties of a given backbone.

3.2.2 Introduction

In the recent past, the π -conjugated organic polymers have been widely explored as advanced materials for electronic and photonic applications [39-45]. Many of these compounds show considerable flexibility, ease of processing, and the possibility of tailoring material characteristics to match a desired property.

The *trans* and *geminal* diethynylethene **1a** and **1b**, as well as the tetraethynylethene **2**, introduced in Section 1.4 are extensively used as a ‘molecular construction kit’ in the

synthesis of new compounds with potential applications in the field of molecular devices [46].

The properties of these compounds strongly depend on the type of functionalization, on the length of the polymer chain, and also on the kind of π -conjugation modes or π -delocalization pathways these structures support. A detailed knowledge of electron delocalization and its impact on the parent compounds **1a-b** and **2** is therefore important for the rational optimization of the properties of these linear conjugated polymers.

As a second example for the validation of the method discussed in the previous chapter, in this section we will show that the deletion approach allows to discriminate between *geminal* and *trans* paths of **1a-b** and **2** (afterworth referred as reference or parent molecules). The resulting parameters will be also correlated with observables such as the molecular geometries and the excitation energies.

In the section "Results and Discussion", the molecular structures of **1a-b** and **2** are first analyzed with particular attention on the differences between the *cross* and *through* delocalization pathways. In fact, it is well established that the degree of the bond length alternation (BLA) strongly correlates with the extent of the electron delocalization [13]. Hence, the comparison of the molecular geometries of **1a-b** and **2** should give qualitative information about the differences in electron delocalization. In order to exclude artifacts in the data used for the analysis, it is important to study in great detail the dependence of the molecular structures on the level of theory applied. Furthermore, in this section, we also give theoretical values of some important electronic properties such as electron affinities, ionization potentials and first allowed excitation energies. The proposed method is then applied to our reference molecules and an analysis of the differences in delocalization energies between the *cross* and *through* conjugation pathways is presented. The electron delocalization is also discussed in terms of changes in occupation numbers of antibonding orbitals as well as in terms of the flow of the charge upon orbital deletion. Finally, some interesting correlations between molecular and electronic properties with electron delocalization are illustrated and discussed. The results from this work should give useful guidelines for the rational design of this class of materials.

3.2.3 Computational Methods

The full geometry optimizations of **3b**, **1a-b** and **2** have been performed using Density Functional (DFT) and *ab initio* approaches. In the *ab initio* calculations, the electron correlation has been taken into account by using the Møller-Plesset (MP) perturbation theory. Calculations at the second (MP2), third (MP3) and fourth (MP4 without triple excitation) orders have been performed using the 6-31G(d,p) basis set of Gaussian orbitals [34]. Moreover, the basis set convergence has been checked for **1a-b** at the MP2 level using the Dunning correlation consistent basis sets of double, triple and quadruple ζ quality [47, 48]. For the DFT [28] calculations, the B3LYP hybrid functional [29, 30, 49], consisting of the Becke's exchange functional [32] and the Lee Yang and Parr's correlation functional [33], has been used together with the 6-31G(d,p) basis set. All the structure optimizations of neutral species have been performed in the planar arrangement, which are shown to be pure minima by the vibrational analysis. In order to match a sufficient accuracy of the geometrical parameters, we have adopted a convergence threshold of 5.0×10^{-5} Hartree Bohr⁻¹ or Hartree Rad⁻¹.

The most appropriate level of theory for the geometry optimizations is selected by comparing the computed geometrical parameters of **3b** with its experimental gas-phase electron diffraction structure [50]. The theoretical and experimental parameters are reported in Table 3.2. At the Hartree-Fock (HF) level, as observed in similar studies (see for example Ref. [51]), the C3=C4 and C1≡C2 bond lengths are underestimated by 0.029 and 0.027 Å, respectively. When correlation is taken into account, both the DFT and *ab initio* results agree well with the experiment. In the worst case, i.e. MP3, the C3=C4 bond length is underestimated by 0.011 Å. In particular, the B3LYP and MP2 methods predict very similar geometries and they give the best agreement with the experiment. The calculations performed at the MP2 level using the correlated consistent basis set of Dunning up to the quadruple ζ quality (data not shown) indicate that the C≡C bond length, for which with the 6-31G(d,p) basis there is the largest difference between the MP2 and B3LYP approaches (0.013 Å), converges to the B3LYP value. Moreover, it should be noted that the changes between the *geminal* and the *trans* molecules are always very similar.

Table 3.2: The geometrical parameters (in Å and degrees) of 3b calculated at different levels of theory (see Figure 3.6 for the atom labels)

	HF/ 6-31G(d,p)	MP2/ 6-31G(d,p)	MP3/ 6-31G(d,p)	MP4(SDQ)/ 6-31G(d,p)	B3LYP/ 6-31G(d,p)	Experiment ^a
C3=C4	1.328	1.352	1.346	1.348	1.350	1.357
C2-C3	1.447	1.436	1.444	1.445	1.435	1.433
C1≡C2	1.188	1.223	1.209	1.215	1.210	1.215
C1-Ht	1.057	1.067	1.062	1.063	1.065	1.062
C3-C5	1.478	1.470	1.475	1.476	1.474	1.481
C5=C6	1.321	1.342	1.337	1.340	1.337	1.342
C-Hde1	1.075	1.067	1.083	1.085	1.088	1.091
C-Hde2	1.075	1.067	1.080	1.081	1.086	1.091
C-Hde3	1.075	1.067	1.079	1.080	1.085	1.091
C4-Hdi1	1.075	1.067	1.078	1.080	1.084	1.091
C4-Hdi2	1.075	1.067	1.080	1.081	1.085	1.091
C4=C3-C5	121.5	121.3	121.5	121.5	121.1	122.0
C3-C5=C6	125.7	124.6	124.7	125.0	125.5	126.0
C4=C3-C2	120.1	120.3	120.1	120.2	120.4	120.0
C5=C6-Hde2	119.8	121.0	121.5	121.6	121.5	120.0
C3=C4-Hdi1	121.6	121.5	121.6	121.6	121.7	123.0
C3-C2≡C1	179.7	178.5	179.0	179.0	179.1	180.0

a) Taken from Reference [50]

The excitation energies have been computed using the semiempirical intermediate neglected differential overlap (INDO/S) Hamiltonian parametrized by Zerner et al. [52-62] on

previously optimized geometries. The active space contained all the virtual and occupied orbitals (full Single CI calculation).

The adiabatic electron affinities (EA's) and ionization potentials (IP's) have been calculated as differences between the energies of the neutral and the ionic species at the equilibrium geometries. The B3LYP/6-31G(d,p) level of theory has been used for all structure optimizations. The open shell species have been calculated using the unrestricted formalism. The neutral molecules were optimized (as specified above) in the planar arrangement, whereas the anions were optimized in a lower non-planar symmetry. In fact, the vibrational analysis showed that the planar geometries are stationary points with two imaginary frequencies corresponding to a symmetric or asymmetric bend out of plane of the terminal hydrogens. The optimization of the structures in these two configurations leads to two genuine minima with an energy difference lower than $0.1 \text{ kcal mol}^{-1}$. The cations have been optimized in the planar geometries. The vibrational analysis confirmed that these are

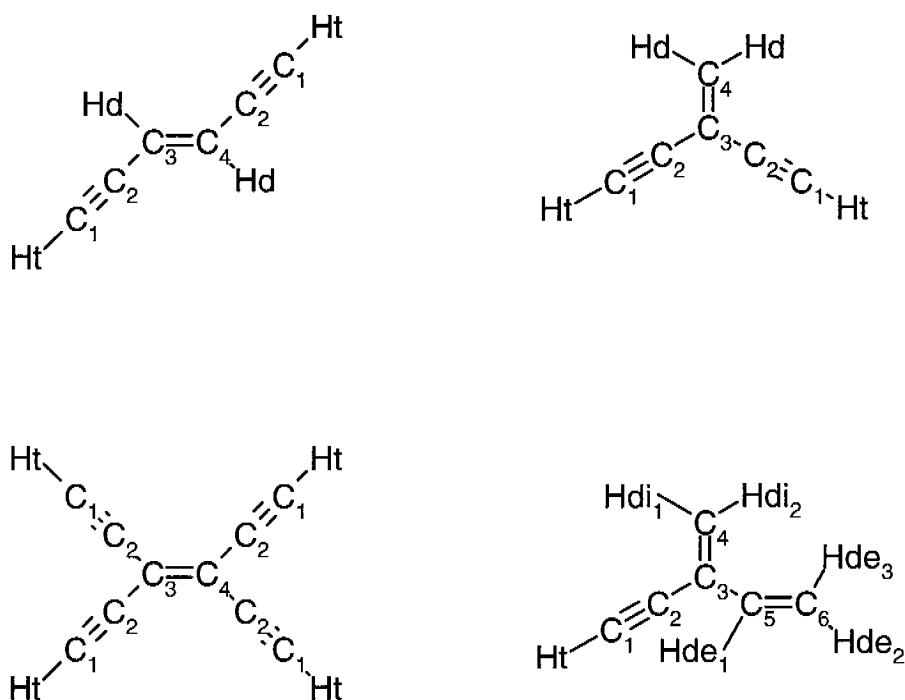


Figure 3.6: Atom labels of the *1a*, *1b*, *2*, and *3b* compounds.

pure minima.

For the anions, at the equilibrium geometries, single point energy calculations at the B3LYP/6-31+G(d,p) and BHandHLYP/6-31+G(d,p) levels have been performed. The addition of diffuse functions, however, leads to strong linear dependence in the basis set. This is due to the large overlap of the diffuse functions centered on the acetylenic carbon atoms. In order to avoid this problem, the acetylenic systems have been described using bond centered diffuse functions. The level of theory applied is represented as follows: B3LYP/6-31+G(d,p)//B3LYP/6-31G(d,p) for general atoms, and B3LYP/6-31+G(d,p)(Bq)//B3LYP/6-31G(d,p), where Bq stands for a single set of diffuse functions centered on the acetylenic bonds. Benchmark calculations on small molecular systems [63] and by us on nitrobenzenes (data not shown) have demonstrated that the BHandHLYP functional [31] in the framework of the DFT theory gives the best results, whereas the B3LYP functional generally overestimates the EA's.

All the calculations have been performed using the Gaussian98 package [64]. The Natural Bond Orbital analysis has been performed with the program NBO [65] as implemented in Gaussian98.

Discussion and Validation of the Method of Analysis.

All the structures considered in the present study are shown in Figure 3.7. Moreover, for the reference molecules, **1a-b** and **2**, and for **3b** the atom labeling is also provided in Figure 3.6. For all these molecular systems, the additivity in Equations 2.17 and 2.18 is well observed. For the pair of isomers **1a** and **1b**, the difference in total delocalization energies ΔE_{del} calculated by deleting at the same time all the antibonding orbitals and the difference in total energies ΔE_{tot} are within $0.6 \text{ kcal mol}^{-1}$ using orbitals optimized at the B3LYP/6-31G(d,p) level of theory (see Table 3.8). For this and later comparisons, we assume that the difference in strain (ΔE_{strain}) between the two isomers is zero. Noteworthy, also when ΔE_{del} is calculated from Equation 2.19, the deviation in Equation 2.17 is still within $0.5 \text{ kcal mol}^{-1}$.

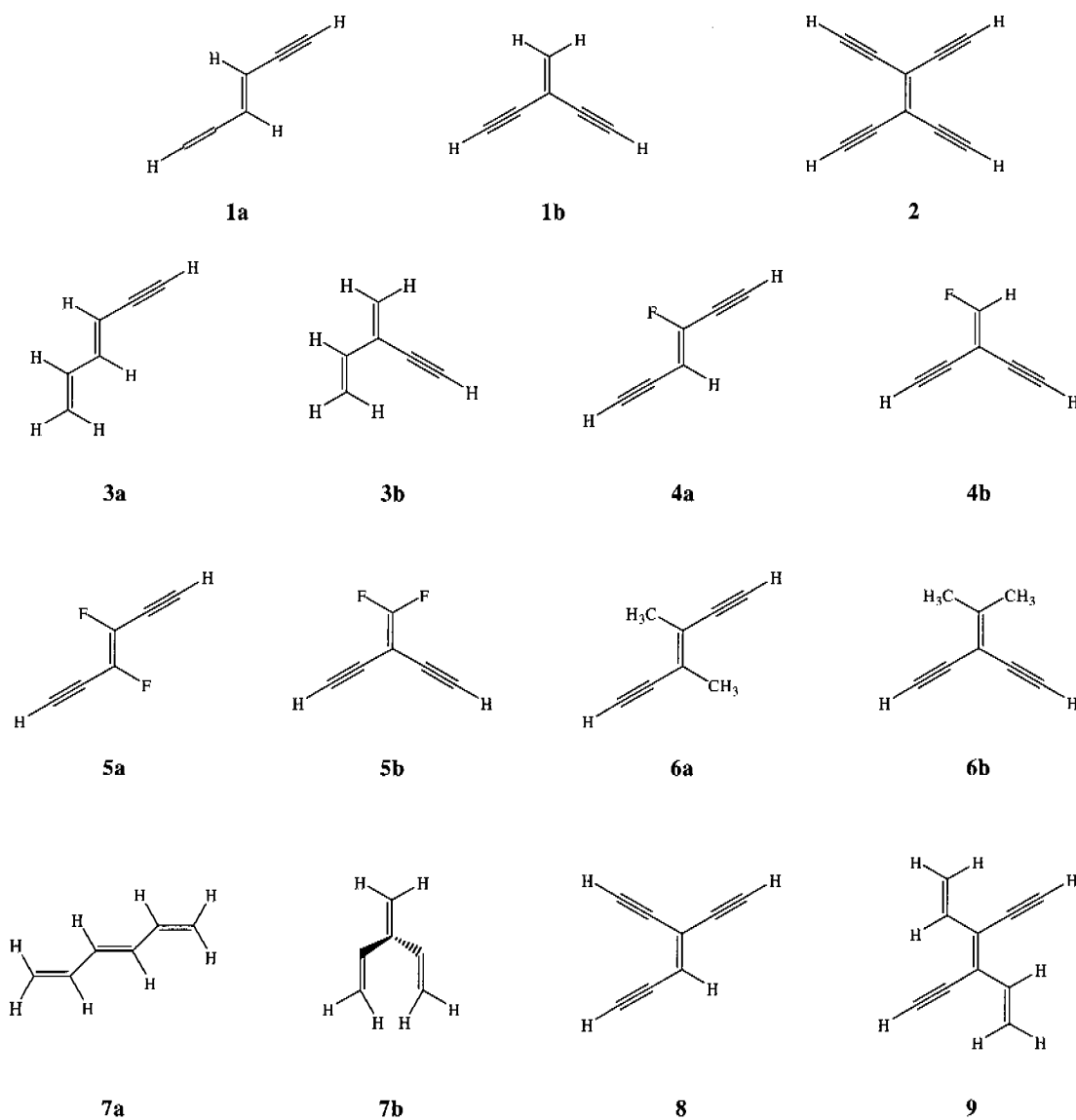


Figure 3.7: Pairs of isomers considered in this study.

Application of the method in the present context.

The procedure to apply our approach in the present context consists of three steps. In the first step, all the antibonding orbitals are deleted and the energy is recomputed in the reduced orbital space. The difference between the SCF energies calculated from the full and reduced

orbital space gives the 'total delocalization energy' and corresponds to E_{del} . In the second step, the delocalization energy is split into π and σ contributions by deleting all π^* orbitals perpendicular to the molecular plane and all the σ^* orbitals and π orbitals in the molecular plane, respectively. These two energies correspond to the $E\pi^*_{\perp}$ and $E\sigma^*_{\parallel}$ of Equation 2.19. The sum of $E\pi^*_{\perp}$ and $E\sigma^*_{\parallel}$ is labeled $E_{\pi+\sigma}$. Finally, the delocalization energies are broken down into orbital contributions for each type of bond. The deleted π^* antibonding orbitals are labeled according to the bond they are associated with, that is π^*_{D} , π^*_{T} and π^*_{\parallel} correspond to the π^* orbitals of the C=C and the vertical and in-plane C \equiv C bonds in **1a-b** and **2**. For the σ backbone, σ^*_{D} , σ^*_{S} , σ^*_{T} , σ^*_{Hd} and σ^*_{Ht} correspond to the σ antibonding orbitals of the C=C, C-C, C \equiv C, =C-H and \equiv C-H bonds, respectively. The energy obtained from the sum of all the orbital contributions is labeled $E_{\Sigma\text{orb}}$. Once again, it should be stressed that our interest is focused on delocalization energy differences between a pair of isomers rather than on absolute delocalization energies.

3.2.4 Results and Discussion

3.2.4.1 Molecular and Electronic Observables

In this section we report on the experimental and computed data that will be used for the analysis of delocalization in these compounds.

Molecular Structures: Experimental data.

To our knowledge until now there are no experimental studies on the structures of the parent compounds **1a** and **1b**. On the other hand, the structures of some derivatives of **2** have been determined by means of X-ray diffraction experiments [66, 67]. However, these structures appear to be strongly influenced by crystal packing forces resulting in two short and two long C-C bonds as well as two short and two long C \equiv C bonds. The central C=C bond ranges between 1.324 and 1.369 Å in the different derivatives. Given the uncertainty due to the solid state determination, these experimental geometries do not appear suitable for comparison with theoretical (gas phase) geometry determination. Up to now, there are only few theoretical studies on **1a-b** and **2** that have been published [68, 69].

The molecular structure of the 2-ethynyl-1,3-butadiene (**3b**, Figure 3.6 and Figure 3.7) has been determined experimentally using a gas phase electron diffraction technique [50]. For this reason, a calibration of the methods can be provided by comparison of the experimental geometry of **3b** with the geometries obtained at different levels of theory. Upon inspection of the results, it appears that the B3LYP functional combined with the 6-31G(d,p) basis set gives the best agreement with the experimental values, and therefore, will be extensively used in the present study. The geometrical parameters of **3b** calculated at different levels of theory are shown in Table 3.2

Geminal-diethynylethene (1b): The computed bond lengths and bond angles of **1a-b** and **2** are listed in Table 3.3. The structure of **3b** is similar to that of **1b** with the exception that in the former an ethynyl group has been replaced by a vinyl group. Comparing these two molecules, it has been noticed that the bond lengths remain practically unchanged. It appears, therefore, that there is no effect on the structure of the $\text{H}_2\text{C}=\text{C}-\text{C}\equiv\text{CH}$ moiety when an ethynyl group is replaced with a vinyl group in a *cross*-conjugated way.

Trans-diethynylethene (1a): A comparison of the *trans* and *geminal* isomers shows some interesting features. At the B3LYP/6-31G(d,p) level it has been found that the C=C and C≡C bond lengths in the *trans* isomer **1a** are 0.003 Å longer than those in **1b**. In order to study the impact of the π -delocalization on the C=C bond length, the ethylene has been taken as reference. Comparing the C=C bond lengths obtained for ethylene (1.330 Å) and for the isomers **1a** (1.354 Å) and **1b** (1.351 Å), it has been noted an increase of this bond length of 0.024 Å for **1a** and 0.021 Å for **1b**. These variations are rather large with respect to 0.003 Å observed between **1a** and **1b**. The effect of the electron delocalization on the C=C bond length appears to be very similar for **1b** and **1a** despite the different delocalization modes (*through* versus *cross*). Similar considerations apply to the C≡C bond lengths. Once again, the difference between the C≡C bond lengths of **1a** and **1b** is small compared to the elongation from the acetylene reference. Apparently for the isomers **1a-b** the length of the double and triple bonds is not a good hallmark for discriminating between *cross* and *through* electron delocalization.

Table 3.3: The geometrical parameters (in Å and degrees) of 1a, 1b and 2 calculated at different levels of theory (see Figure 3.6 for the atom labels)

	HF/6-31G(d,p)			MP2/6-31G(d,p)			MP3/6-31G(d,p)			MP4(SDQ)/6-31G(d,p)			B3LYP/6-31G(d,p)		
	1b	1a	2	1b	1a	2	1b	1a	2	1b	1a	2	1b	1a	2
C3=C4	1.327	1.328	1.345	1.352	1.355	1.381	1.346	1.347	1.367	1.349	1.349	1.369	1.351	1.354	1.384
C2-C3	1.445	1.435	1.438	1.436	1.423	1.426	1.444	1.432	1.437	1.444	1.433	1.436	1.435	1.417	1.424
C1≡C2	1.187	1.189	1.187	1.223	1.224	1.225	1.208	1.209	1.207	1.215	1.216	1.216	1.209	1.212	1.210
≡C1-Ht	1.057	1.057	1.057	1.063	1.063	1.063	1.062	1.061	1.062	1.063	1.063	1.063	1.065	1.065	1.066
=C4-Hd	1.074	1.076	---	1.080	1.084	---	1.078	1.081	---	1.080	1.083	---	1.084	1.088	---
C4=C3-C2	121.6	123.0	121.9	121.5	122.8	121.0	121.5	122.7	121.5	121.6	122.9	121.4	121.7	123.7	121.5
C3-C2≡C1	179.5	178.7	178.0	179.6	178.6	178.9	179.4	178.5	178.5	179.6	178.6	178.5	178.8	178.0	177.7
C2≡C1-Ht	179.9	179.6	179.4	179.9	179.3	179.8	179.8	179.3	179.6	179.9	179.3	179.6	179.6	179.2	179.3
C3=C4-Hd	120.9	120.2	---	120.6	119.3	---	120.8	119.9	---	120.8	119.8	---	120.8	119.3	---

In contrast to the very similar C=C and C≡C bond lengths discussed above the single C-C bond length shows the largest difference between **1b** and **1a**. At the B3LYP level the C-C bond of **1b** is 0.018 Å longer than in **1a**. The origin of this difference will be further investigated below.

Tetraethynylethene (2): In general, at all levels of theory, it has been found that the most important difference between **2** and the two isomers **1a-b** is a substantial lengthening of the C=C bond. In particular, at the B3LYP/6-31G(d,p) level the C=C bond length of **2** is about 0.030 Å longer than the corresponding ones in **1a** and **1b**. On the other hand, comparing the C≡C and C-C bond lengths of **2** and **1a**, it has been noticed that the triple bond of the former is 0.007 Å longer than that in the latter, whereas the single bond is 0.002 Å shorter. Hence, the C-C and C≡C bond lengths in **2** are inbetween those calculated for **1a** and **1b**.

Total energy differences (ΔE_{tot})

The computed total energy differences between the isomers **1a** and **1b** are shown in Table 3.4. At all levels of theory, **1a** is more stable than **1b**. The ΔE_{tot} value ranges from 2.70 (MP4) to 4.81 kcal mol⁻¹ (B3LYP).

Table 3.4: The energy difference ΔE_{tot} (in kcal mol⁻¹) between **1a** and **1b** calculated at different levels of theory

	ΔE_{tot}
HF/6-31G(d,p)	3.46
B3LYP/6-31G(d,p)	4.81
MP2/6-31G(d,p)	2.95
MP3/6-31G(d,p)	3.39
MP4(SDQ)/6-31G(d,p)	2.70
MP2/cc-pVDZ	3.02
MP2/cc-pVTZ	2.76
MP2/cc-pVQZ	2.83

Excitation energies

The first allowed transition energies of the reference molecules, computed using the geometries optimized at different levels of theory, are shown in Table 3.5. The computed excitation energies are particularly sensitive to the molecular geometries. For the isomer **1a**, an experimental value [70] of the first allowed transition energy is available. By comparison of the theoretical and experimental results, it has been found that the best agreement is obtained using the structure optimized at the B3LYP/6-31G(d,p) level. The first allowed transition energy difference (ΔE_{exc}) between **1a** and **1b** is equal to 8.30 kcal mol⁻¹, whereas the differences between **2** and **1a-b** are equal to 14.29 and 22.59 kcal mol⁻¹, respectively. In all cases, the HOMO \rightarrow LUMO transition gives the main contribution to the excited state.

Table 3.5: The first allowed excitation energy (in eV) of **1a-b**, and **2** calculated with the ZINDO/S Hamiltonian on the geometries optimized at different levels of theory

	ZINDO// HF/6-31G(d,p)	ZINDO// B3LYP/6-31G(d,p)	ZINDO// MP2/6-31G(d,p)	Experiment ^a
1b	4.80	4.56	4.45	
1a	4.50	4.20	4.12	4.18
2	3.90	3.58	3.50	

a) Taken from Reference [70]

Molecular Ions

The molecular structures of the anions and cations **1a-b** and **2** are listed in Table 3.6. Significant changes of the geometries with respect to the neutral molecules are observed in all cases considered. For **1b**⁻ it has been observed that the C=C bond length is 0.079 Å longer than that in the neutral species, the C-C bond length is shortened by 0.028 Å, and finally, the C≡C bond length is lengthened by 0.025 Å. On the other hand, the results obtained for **1a**⁻ show that the C=C bond length increases 0.066 Å with the respect to the neutral system, but

less than in the isomer **1b**⁺. Furthermore, the C-C bond length decreases of 0.036 Å compared to neutral counterpart, whereas the C≡C bond length increases of 0.039 Å. For the latter two bonds, the variation of the bond length is more pronounced than in the isomer **1b**⁺. In **2**⁺ the C=C bond length goes from 1.384 Å of the neutral system to 1.450 Å with a difference of 0.066 Å (exactly the difference observed in **1a**⁺). Finally, the C-C bond length shortens by 0.014 Å, whereas the C≡C one lengthens by 0.013 Å.

Despite the opposite charge of the molecules, the structural differences between the neutral molecules and the cations are similar to those described for the anions. For the species positively charged, the lengthening of the C=C and C≡C bonds is generally smaller than those in the anions, whereas the increase of the C-C bond lengths is larger.

Electron Affinities and Ionization Potentials

The calculated adiabatic electron affinities (EA's) and ionization potentials (IP's) are shown in Table 3.7. A substantial difference between the EA's of the isomers **1a** and **1b** has been found comparing the values obtained using the BHandHLYP functional together with the 6-31G(d,p) basis set. In fact, the EA is positive for **1a** and negative for **1b**, meaning that the extra-electron is bound in the former and unbound in the latter. As can be easily predicted, **2** with its extended delocalization pattern, shows the highest EA. The difference between the EA's of **1a** and **1b** is equal to 5.17 kcal mol⁻¹, whereas those calculated between **2** and **1a-b** are equal to 20.69 and 25.85 kcal mol⁻¹, respectively.

The IP's of the reference molecules have been calculated at the B3LYP/6-31G(d,p) level of theory. The highest and the lowest IP's are observed for the structure **1b** and **2**, respectively. It is important to note that the IP differences between **1a** and **1b**, and between **2** and **1a-b** are equal to 5.72, 22.88 and 28.60 kcal mol⁻¹, respectively. These values are similar to the differences observed for the EA's.

Table 3.6: The geometrical parameters (in Å and degrees) of 1a-1b and 2 anions and cations calculated at the B3LYP/6-31G(d,p) level of theory using the unrestricted formalism (atom labels in Figure 3.6)

	Anions			Cations		
	1b ⁻	1a ⁻	2 ⁻	1b ⁺	1a ⁺	2 ⁺
C3=C4	1.430	1.420	1.450	1.406	1.401	1.439
C2-C3	1.410	1.381	1.410	1.404	1.380	1.401
C1≡C2	1.237	1.251	1.223	1.219	1.226	1.216
≡C1-Ht	1.073	1.080	1.065	1.072	1.073	1.071
=C4-Hd	1.084	1.091		1.086	1.089	
C4=C3-C2	121.5	125.5	121.5	119.9	122.1	120.5
C3-C2≡C1	174.1	173.6	176.6	179.8	178.3	179.7
C2≡C1-Ht	148.1	138.4	165.2	179.8	179.6	179.6
C3=C4-Hd	120.6	117.0		120.4	119.5	

Table 3.7: The adiabatic electron affinities and ionization potentials (in eV) of 1a-b and 2 calculated at different levels of theory

	1b	1a	2
adiabatic electron affinities			
B3LYP/6-31G(d,p)// B3LYP/6-31G(d,p)	-0.489	-0.133	0.665
B3LYP/6-31+G(d,p)Bqc// B3LYP/6-31G(d,p)	0.144	0.345	1.017
BhandHLYP/6-31+G(d,p)Bqc// B3LYP/6-31G(d,p)	-0.157	0.067	0.964
adiabatic ionization potentials			
B3LYP/6-31G(d,p)// B3LYP/6-31G(d,p)	8.549	8.301	7.309

3.2.4.2 Analysis and Correlation of the Electron Delocalization with the Molecular and Electronic Properties

The delocalization energies have been calculated applying the method defined above. These energies for the reference molecules have been computed at the B3LYP/6-31G(d,p) level of theory and are shown in Table 3.8. The $\Delta E_{\text{del}(1\mathbf{a}-1\mathbf{b})}$ obtained deleting all the antibonding orbitals is 5.42 kcal mol⁻¹ in favor of the *trans* isomer. This is in very good agreement with the difference in stability calculated from the total energies ($\Delta E_{\text{tot}(1\mathbf{a}-1\mathbf{b})}=4.81$ kcal mol⁻¹).

According to Equation 2.19, the total delocalization energy can be expressed as a sum of the two components $E\pi^*_{\perp}$ and $E\sigma^*_{=}$. By this partition, it appears that the main contribution to the energy difference $\Delta E_{\text{del}(1\mathbf{a}-1\mathbf{b})}$ is due to the π -delocalization, e.g. $\Delta E\pi^*_{\perp}(1\mathbf{a}-1\mathbf{b})$. In fact, as shown in Table 3.8, the $\Delta E\sigma^*_{=(1\mathbf{a}-1\mathbf{b})}$ is of 0.35 kcal mol⁻¹ in favor of the *geminal* isomer **1b**, whereas the $\Delta E\pi^*_{\perp}(1\mathbf{a}-1\mathbf{b})$ is of 5.45 kcal mol⁻¹ in favor of the *trans* isomer **1a**. The sum of the $\Delta E\pi^*_{\perp}$ and $\Delta E\sigma^*_{=}$, e.g. $\Delta E_{\pi+\sigma}(1\mathbf{a}-1\mathbf{b})$, is equal to 5.10 kcal mol⁻¹ and matches nearly perfectly with both ΔE_{tot} and ΔE_{del} .

By inspection of the delocalization energies at the individual orbital level, it can be noted that in the σ skeleton significant differences are observed by deleting the σ^* orbitals corresponding to the C-C (σ_s^*) and =C-H (σ_{Hd}^*) bonds. In fact, the $E\sigma_s^*$ calculated for the *geminal* isomer **1b** is 15.96 kcal mol⁻¹ higher than that obtained for the *trans* isomer **1a**. This could also be related to the fact that the largest bond length difference between **1a** and **1b** is observed precisely for this particular bond. However, the advantage of the *geminal* isomer within the carbon σ skeleton is cancelled by the $E\sigma_{\text{Hd}}^*$, which for the *trans* isomer **1a**, has been found to be 12.54 kcal mol⁻¹ higher than that of the isomer **1b**. Here also, a slight difference in the =C-H bond length is observed. Another source of energy difference between the isomers **1a** and **1b** is the in-plane π^* C \equiv C orbitals ($\pi_{=}^*$). The $\Delta E\pi_{=}^*$ amounts to 2.98 kcal mol⁻¹ in favor of **1a**. In conclusion, the total difference in the delocalization energy is controlled by the π_{\perp} conjugation, however, the contribution due to the energy differences of the σ_s^* and σ_{Hd}^* orbitals are interestingly high, but due to their opposite sign, they cancel each other.

At the HF level, the same considerations are still valid (data not shown). As expected, the absolute values of the π delocalization energies (E_{del}) are in general smaller than those obtained at the B3LYP/6-31G(d,p) level. Finally, this HF inherent underestimation of the π -delocalization disfavors the *trans* isomer relatively more than the *geminal* isomer.

For **2**, the number of the bonding and antibonding orbitals is larger, and therefore, the computed delocalization energies are considerably higher. In order to obtain values directly comparable with those calculated for **1a** and **1b**, we compute delocalization energies deleting only the three π_{\perp}^* orbitals in a *trans* or in a *geminal* arrangement.

Table 3.8: The π and σ delocalization energies (in kcal mol⁻¹) of 1a-b and 2 calculated at the B3LYP/6-31G(d,p) level as described in the text. The number of the deleted antibonding orbitals is shown in parenthesis

	$E \pi^*_D$	$E \pi^*_T$	$E \sigma^*_D$	$E \sigma^*_S$	$E \sigma^*_T$	$E \sigma^*_{Hd}$	$E \sigma^*_{Ht}$	$E \pi^*_\perp$	$E \sigma^*_\perp$	$E \sigma^*_{orb}$	$E \pi+\sigma$	E_{del}	E_{tot}
1a	28.18 (1)	33.33 (2)	14.55 (1)	42.73 (2)	47.49 (2)	20.07 (2)	16.35 (2)	13.47 (2)	53.88 (3)	158.94 (11)	216.17 (14)	212.82 (14)	213.92 (14)
1b	23.14 (1)	29.48 (2)	14.76 (1)	58.69 (2)	46.48 (2)	7.53 (2)	16.66 (2)	10.49 (2)	48.43 (3)	159.29 (11)	207.23 (14)	207.72 (14)	208.50 (14)
ΔE_{1a-1b}	5.04	3.85	-0.21	-15.96	1.01	12.54	-0.31	2.98	5.45	-0.35	5.50	5.10	5.42
2	63.69 (1)	46.42 (4)	28.44 (1)	109.51 (4)	93.28 (4)		32.37 (4)	21.47 (4)	106.12 (5)	295.54 (17)	395.18 (22)	401.66 (14)	403.07 (22)
2-trans	63.69 (1)	29.25 (2)	28.44 (1)	56.15 (2)	46.32 (2)		16.17 (2)	10.98 (2)	82.29 (3)				
$\Delta E_{2trans-1a}$	35.51	-4.08	13.89	13.42	-1.17		-0.18	-2.49	28.41				
2-gem	63.69 (1)	32.43 (2)	28.44 (1)	55.33 (2)	46.58 (2)		16.17 (2)	10.69 (2)	82.86 (3)				
$\Delta E_{2gem-1b}$	40.55	-2.95	13.68	-3.36	0.10		-0.49	0.20	34.43				

As shown in Table 3.8, the *trans* and *geminal* π^*_{\perp} delocalization energies in **2** do not differ appreciably. The difference between the "*trans*" π^*_{\perp} delocalization energy in **2** and that calculated for **1a**, e.g. $\Delta E\pi^*_{\perp}(2\text{trans-1a})$ is equal to 28.41 kcal mol⁻¹. This value is a measure for the π_{\perp} delocalization energy due to the effect of the functionalization of the **1a** backbone with two acetylenic substituents. This can be a useful tool to study the impact of the functionalization on the electron delocalization of the π -conjugated molecular systems. This issue will be addressed in the next chapter.

The π^*_{\perp} delocalization energy has been further analyzed considering the π^*_D and π^*_T contributions. Since there is only one π_D orbital in all the three systems (**1a-b**, **2**), the delocalization energy obtained by deleting the π^*_D orbital is directly comparable. The $E\pi^*_D$ calculated for **2** is more than the double of that calculated for the **1b** or **1a** backbones. This large increase of the $E\pi^*_D$ suggests that the two additional acetylenic arms have a strong additive effect in promoting π -delocalization. On the other hand, the $E\pi^*_T$ computed by deleting the two π^*_T orbitals in the *trans* arrangement is lower than that computed for **1a**. This suggests a less efficient back-donation from π_D into π^*_T when the two acetylenic groups are added to the *trans* diethynylethene backbone.

Table 3.9: The energy differences (in kcal mol⁻¹) of the pair of isomers shown in Figure 3.7 and calculated at the B3LYP/6-31G(d,p) level of theory. The number of the deleted antibonding orbitals is provided in parenthesis

	$\Delta E\pi^*_{\perp}$	$\Delta E\sigma^*_{=}$	$\Delta E_{\pi+\sigma}$	ΔE_{del}	ΔE_{tot}
3a – 3b	5.95 (3)	-2.67 (11)	3.28 (14)	3.42 (14)	3.36
4a – 4b	2.49 (3)	1.29 (11)	3.78 (14)	3.57 (14)	3.67
5a – 5b	-5.85 (3)	-19.81 (11)	-25.66 (14)	-26.97 (14)	-5.28
6a – 6b	-0.05 (3)	1.20 (11)	1.15 (14)	1.38 (14)	2.26
7a – 7b	9.31 (3)	-4.49 (11)	4.82 (14)	4.68 (14)	7.41

The method described above has also been applied to the other isomers presented in Figure 3.7). E_{del} , $E\sigma^*$ and $E\pi^*$ contributions as well as the difference in stability calculated from the total energies are provided in Table 3.9. For the isomers **3a-b**, **4a-b** and **6a-b** the agreement between the difference in the delocalization and total energy is excellent, i.e. within 1 kcal·mol⁻¹. At this point, it should be noted that both σ and π components contribute to the difference in stability. For the isomers **3a-b**, the $\Delta E\pi^*$ of 5.95 kcal mol⁻¹ in favor of the *trans* isomer is mitigated by the $\Delta E\sigma^*$ contribution of 2.67 kcal mol⁻¹ in favor of the *geminal* isomer. Therefore, the decrease of ΔE_{tot} comparing **3a-b** with **1a-b** is mainly due to the differences in the σ delocalization rather than in the π -delocalization. In the mono-fluorinated isomers **4a-b**, both π^* and σ^* components favor the *trans* isomer, however, the $\Delta E\pi^*$ decreases to 2.49 kcal mol⁻¹. The di-fluorinated compounds **5a-b** are the only isomers which exhibit a significant difference between ΔE_{tot} and ΔE_{del} . The di-fluorinated compound in the *geminal* arrangement **5b** is more stable than that in the *trans* arrangement **5a** by 5.28 kcal mol⁻¹. The ΔE_{del} correctly predicts the inversion of the stability, but drastically overestimates the energy splitting (29 vs 5 kcal mol⁻¹). Despite we do not have a clear explanation for this large discrepancy, an analysis of single orbital deletions shows that the high value of $E\sigma^*$ in **5b** is due to the interaction between a lone pair of fluorine atoms and the σ^*_s orbitals. In sharp contrast to the molecules discussed above, the steric strain of **7b** is not negligible. In fact, B3LYP/6-31G(d,p) predicts for **7b** a non-planar structure of C_2 symmetry (**7b_{C2}**), whereas at the same level of theory the planar structure of C_{2v} symmetry (**7b_{C2v}**) is found to possess an imaginary frequency and, therefore, is a transition state. For this reason, a discrepancy between ΔE_{tot} and ΔE_{del} is expected. Indeed, for the isomers **7a** and **7b_{C2}** these two quantities differ by 2.73 kcal mol⁻¹. If we consider the steric strain of **7a** negligible, this value could be an estimation of the steric energy in **7b_{C2}**. The decomposition of E_{del} into π^* and σ^* shows that the $\Delta E\pi^*$ = 9.31 kcal mol⁻¹ in favor of the *trans* isomer is partially compensated by the $\Delta E\sigma^*$ = 4.49 kcal mol⁻¹ in favor of the *geminal* compound.

A more detailed investigation of the origin of the hyperconjugative interactions leading to the σ and π delocalization can be carried out considering the changes of the σ or π orbital occupations. The variation of the NBO occupations for **1a-b** and **2** are shown in Table 3.10.

The π_{\perp} delocalization energies are easily attributed to $\pi_{\text{T}} \rightarrow \pi_{\text{D}}^*$ and $\pi_{\text{D}} \rightarrow \pi_{\text{T}}^*$ donor-acceptor interactions. For **1b**, when the π_{\perp}^* orbitals are deleted, the electron population that moves from the π_{D}^* to the π_{T} (0.121) is larger than the population that moves from the π_{T}^* to the π_{D} orbital (0.110). For the **1a** isomer a similar, but more pronounced transfer is observed. Therefore, for both the molecules, there is a net increase of the π_{D}^* orbital and a corresponding decrease of the π_{T}^* orbital occupation, which confirms that the π_{T} orbitals act as π donors to the central C=C bond.

Table 3.10: Changes in the occupation of the π and σ orbitals by depleting selected π^* or σ^* orbitals

		1b	1a	2
Deleted Orbitals	Orbitals with changes in occupation	Orbital occupation changes		
π_{\perp}^*	π_{D}	0.110	0.131	0.213
	π_{D}^*	-0.121	-0.143	-0.292
	π_{T}	0.061	0.079	0.085
	π_{T}^*	-0.056	-0.075	-0.067
σ_{S}^*	σ_{D}	0.005	0.003	0.010
	σ_{Hd}	0.010	0.001	---
	σ_{T}	0.007	0.007	0.008
	$\pi_{=}$	0.008	0.002	0.009
	σ_{S}	~0.00	0.004	0.005
	σ_{S}^*	-0.034	-0.020	-0.030
$\pi_{=}$	σ_{D}	0.009	0.010	0.016
	σ_{Hd}	0.006	0.014	---
	σ_{S}	0.001	~0.00	0.006
	$\pi_{=}$	0.004	0.001	0.007
	$\pi_{=}^*$	-0.016	-0.020	-0.016
σ_{Hd}^*	σ_{D}	0.001	0.001	
	σ_{S}	0.004	~0.00	
	$\pi_{=}$	0.002	0.009	---
	σ_{Hd}^*	-0.006	-0.019	

In compound **2**, the occupation of the π_D^* is roughly double with respect to that calculated for the **1a** isomer. The addition of two acetylenic arms to the diethynylethene backbone leads to an additive effect (actually more than additive) which reflects into the π_D^* occupation. Considering the variation of the occupation numbers of the π_D^* orbitals, the order **1b** < **1a** < **2** is determined. On the other hand, for the π_T^* the order becomes **1b** < **2** < **1a**, which means that the back-donation $\pi_D \rightarrow \pi_T^*$ of **2** is in between that obtained for **1a** and **1b**. Finally, it is noteworthy that this behaviour can be correlated to the differences of the C=C and C≡C bond lengths. Similar considerations can be observed for the σ_s^* , σ_{Hd}^* and $\pi_{=}$ orbital occupations. In fact, the σ_s^* occupation number decreases in the order **1b** > **2** > **1a**; this agrees with the calculated $E\sigma_s^*$ as well as with the differences in C-C bond lengths.

Several donor \rightarrow acceptor interactions contribute to the occupation of the σ_s^* orbitals. For **1a-b**, the σ_{Hd} and $\pi_{=}$ orbitals give the strongest donor contribution. However, in **1a** the contributions are much lower. The differences in occupation of the in-plane π orbitals ($\pi_{=}$) is controlled by the hyperconjugative interactions with the σ orbitals of the backbones of the molecules. The only significant difference is in a stronger donor \rightarrow acceptor interaction with the σ_{Hd} orbitals. This means that the functionalization with the σ donors or acceptors should be most efficient when this functionalization is positioned at the double bond. The positioning of the σ donor/acceptor at the triple bond will be less effective. As outlined above, a strong correlation between the π^* and σ^* orbital occupations with the corresponding bond length distances can be observed. In order to further investigate this critical point, the occupation of the antibonding orbitals of all the molecules represented in Figure 3.7 (with the only exception of the di-fluorinated isomers **5a-b**) has been considered. The correlation between the π_D^* occupation numbers and the C=C bond lengths is shown in Figure 3.8. A straight line is obtained with a correlation coefficient equal to 0.990. However, a similar correlation is not found for the σ_D^* occupation numbers. This could suggest that, despite the differences in σ_D^* occupation numbers, the C=C bond lengths depend only (or mainly) on the occupation of the π^* orbitals. As shown in Figure 3.9, also for the C≡C bond, a linear correlation between the bond lengths and the π_T^* occupation is observed. Once again, a similar correlation is not found when σ_T^* or $\pi_{=}$ occupations are plotted against the bond

lengths. Noteworthy, as displayed in Figure 3.10, the σ_s^* occupation numbers correlate sufficiently well with the C-C bond lengths suggesting that, besides the π conjugation, also the hyperconjugative delocalization is relevant in the C-C bond length difference.

Considering the first allowed excitation energies (ΔE_{exc}) of the isomers **1a** and **1b**, it appears that the comparison with the $\Delta E\pi^*_{\perp}$ is rather satisfactory; in fact, they only differ by 2.88 kcal mol⁻¹. In Figure 3.11 it is shown that this correlation exists also for the other pairs of considered isomers. The computed ΔE_{exc} are systematically 2-3 kcal mol⁻¹ higher than the $\Delta E\pi^*_{\perp}$. At this point, the origin of this correlation is not yet fully understood.

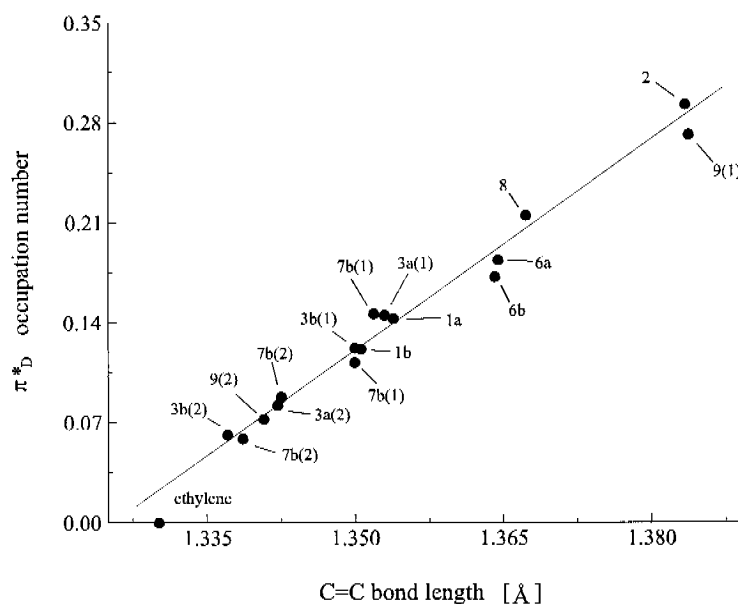


Figure 3.8: The π^*_D orbital occupation calculated by the NBO theory as function of the C=C bond lengths (in Å) for the molecules represented in Figure 3.7. For the molecules with different C=C bonds, the numbers in parenthesis indicate the specific C=C bond: (1) central, (2) peripheral.

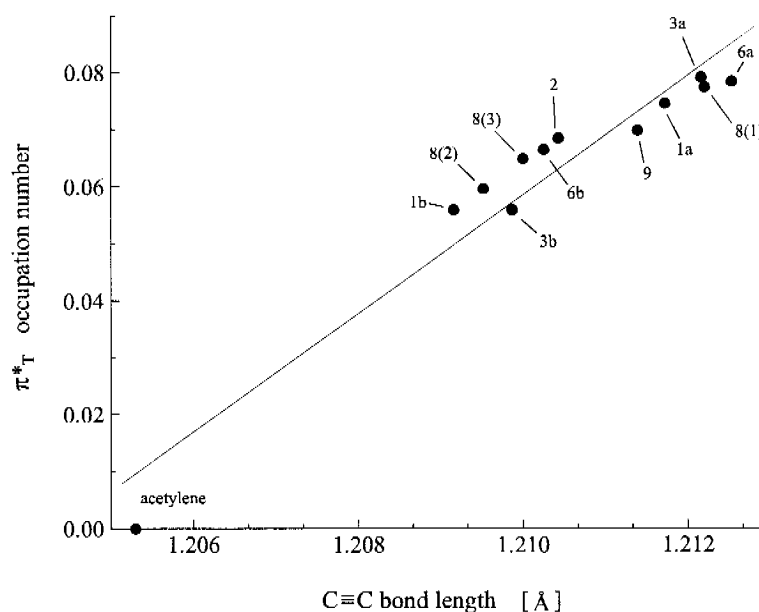


Figure 3.9: The π^*_T orbital occupation calculated by the NBO theory as function of the of C≡C bond lengths (in Å) for the molecules represented in Figure 3.7. For **8**, the three non-equivalent C≡C bonds are indicated with the numbers in parenthesis: (1) for the C≡C bond on the right, (2) for the C≡C bond lower on the left, and (3) for the C≡C bond upper on the left in Figure 3.7

For the anions and cations **1a-b** and **2**, the differences in the bond lengths can be interpreted on the basis of the calculated atomic spin densities shown in Table 3.11. In **1b⁻** the unpaired electron is highly localized on the atom C4 (atom labels in Figure 3.6). A small "fraction" of the electron is at the position C1, whereas atoms C2 and C3 exhibit a negligible spin density. In **1a⁻**, the atomic spin densities show that the unpaired electron is more delocalized along the carbon backbone. In particular, the spin density is high on the atoms C1 (0.233) and C3 (0.321) and, like in **1b⁻**, is negligible at the atoms C2. The spin density of **2⁻** is comparable to that of **1a⁻**, however, it increases on the two central atoms (C3 and C4) and decreases on the atoms C1. The spin densities of the cations are similar to those already discussed for the anions (see Table 3.11).

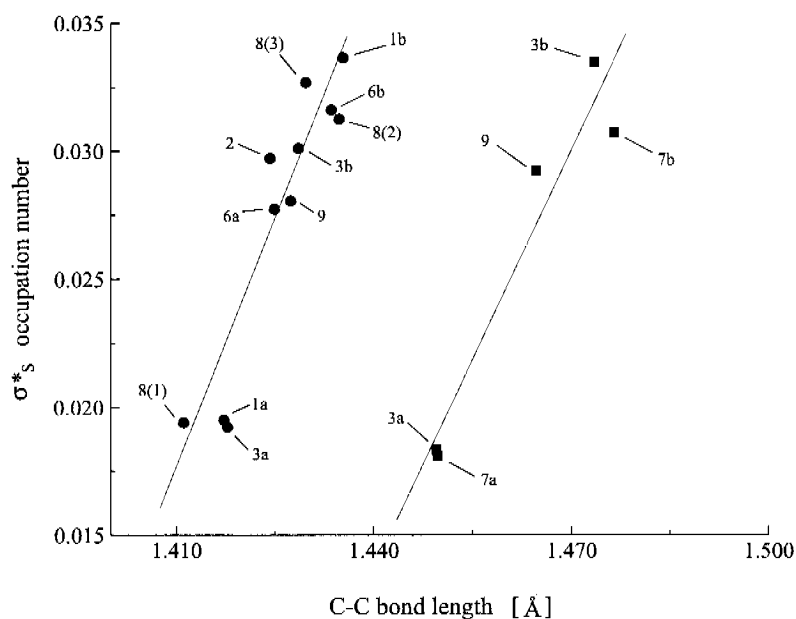


Figure 3.10: The σ_s^* orbital occupation calculated by the NBO theory as function of the C–C bond lengths (in Å) for the molecules represented in Figure 3.7. With (●) are indicated the C–C bonds which are in between C=C and C≡C bonds, whereas with (■) are indicated the C–C bonds which are in between two C=C bonds. For 8, the three non-equivalent C–C bonds are indicated as reported in the caption of Figure 3.9.

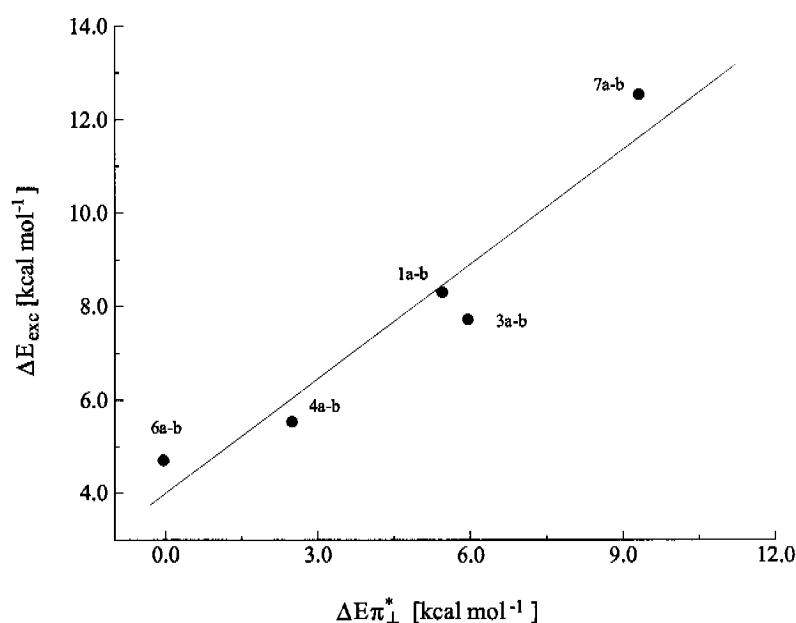


Figure 3.11: The calculated ΔE_{exc} between the trans and geminal isomers as function of the corresponding $\Delta E\pi_{\perp}^*$ (in kcal mol⁻¹).

Table 3.11: The total atomic spin densities of the anions and cations **1a**, **1b** and **2** calculated at the B3LYP/6-31G(d,p) level of theory using the unrestricted formalism (see Figure 3.6 for the atom labels)

	Anions			Cations		
	1b⁻	1a⁻	2⁻	1b⁺	1a⁺	2⁺
C4	0.728	---	---	0.569	---	---
C3	0.038	0.233	0.268	0.045	0.209	0.208
C2	-0.006	-0.057	-0.096	-0.006	-0.070	-0.071
C1	0.151	0.321	0.217	0.231	0.383	0.225
Ht	0.008	0.017	-0.006	-0.024	-0.009	-0.008
Hd	-0.036	-0.014	---	-0.008	-0.014	---

From this NBO picture it is possible to explain the differences in the bond lengths. In fact, in **1b⁻** the extra electron is localized on the atom C4 in the p_z orbital perpendicular to the molecular plane. This results in a reduction of the C=C bond order and a corresponding elongation of the bond. In **1a⁻** the extra electron is localized at the position C1 resulting in a larger elongation of the C≡C bond length and a shorter elongation of the C=C one with respect to **1b⁻**. Finally, in **2⁻** the extra electron has two more acetylenic arms to be delocalized on, therefore, the effect on all the bond lengths is rather small.

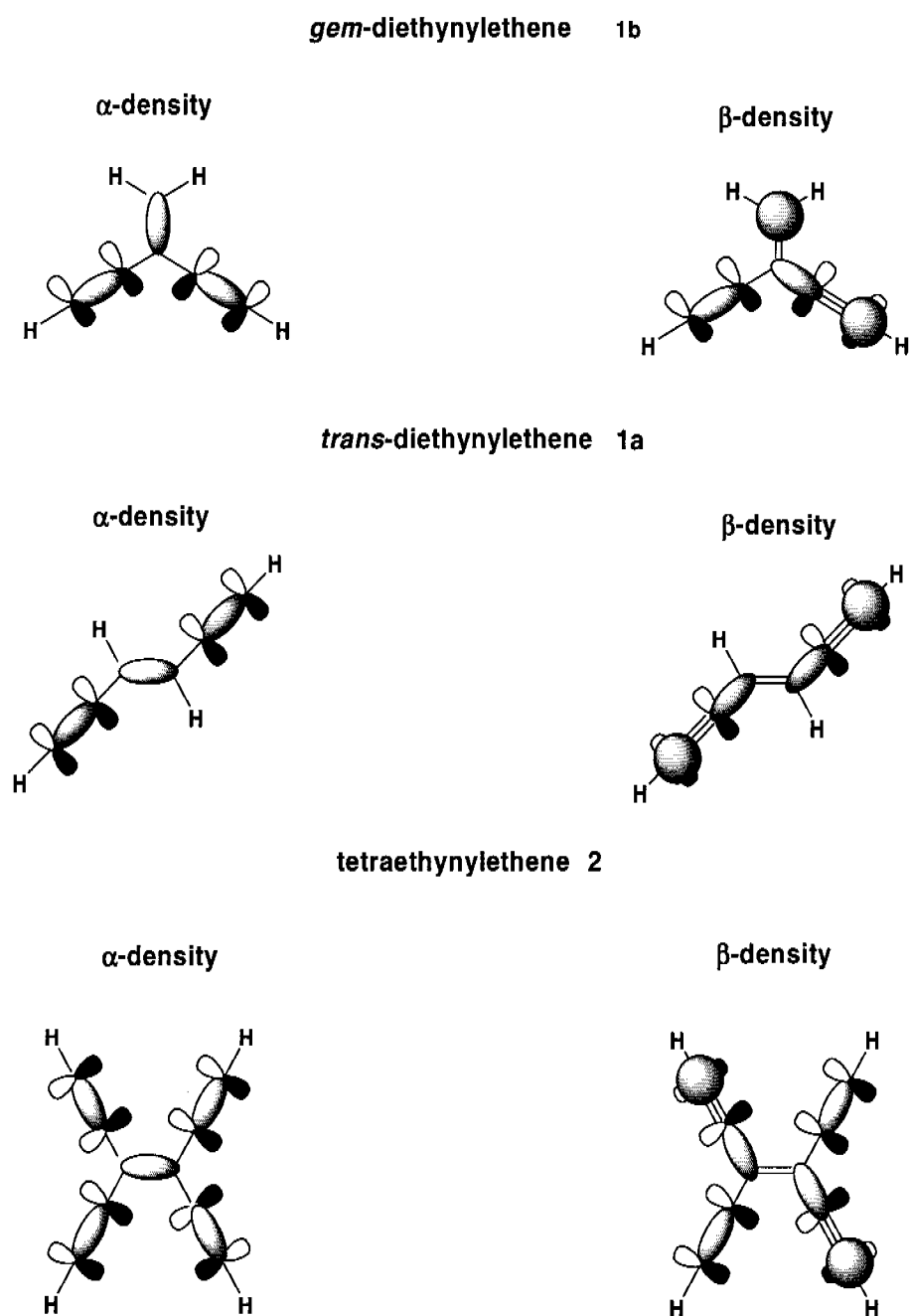


Figure 3.12: Schematic picture showing the α and β electron density of the localized NBO orbitals for 1a, 1b and 2.

3.2.5 Conclusions

In this section our approach to analyze electron delocalization in π -conjugated organic compounds has been validated using the compounds **1a-b** and **2**. As discussed in Chapter 2, the approach is not designed to give absolute values for delocalization energies, but is built to reproduce differences between structural isomers or between backbones with different functionalization. These differences can be correlated with structural features such as changes in bond lengths. It is also possible to (near-) quantitatively predict shifts in the electronic excitation energies based on the comparison of conjugation patterns.

With regard to its predictive power, we show that the approach not only allows to study the impact of a specific donor, acceptor, or spacer, but it also helps to identify the location on the backbone which is most sensitive to the action of a substituent. In this particular context, the idea of splitting the electron delocalization into vertical and parallel components has been shown to be very useful.

By applying the approach to the isomers **1a** and **1b**, it has been shown that the difference in stability between the *cross* and *through* conjugation is controlled by the vertical π delocalization, whereas the σ -delocalization appears to play a very minor role. However, the analysis of all the other compounds shows that the σ -delocalization cannot be neglected. In fact, it is often used as a way to discriminate between *geminal* and *trans* conjugation. This is confirmed by the significant differences in the σ -delocalization at the individual orbital level in **1a** and **1b**.

The importance of the σ -delocalization is also supported by the fact that the largest structural difference between *trans* and *geminal* isomers is not in the π bond lengths but rather in the σ bond lengths. In fact, in the *geminal* isomers the =C-C σ -bonds are consistently longer than those in the *trans* ones.

Compared to **1a-b**, in **2** the *geminal-trans* delocalization energy gap is reduced, as confirmed by the fact that the C-C and C \equiv C bond lengths in **2** fall in between those of **1a** and **1b**. Furthermore, the two acetylenic substituents act as strong π -donors determining a significant increase of the central C=C bond length.

3.3 References

1. G. R. Hutchinson, Y.-J. Zhao, B. Delley, A. J. Freeman, M. A. Ratner, T. J. Marks, Electronic Structure of Conducting Polymers: Limitations of Oligomer Extrapolation Approximations and Effects of Heteroatoms. *Phys. Rev. B*, **2003**, 68, 035204.
2. Y. Mo, Z. Lin, W. Wu, Q. Zhang, Delocalization in Allyl Cation, Radical and Anion. *J. Phys. Chem.*, **1996**, 100, 6469-6474.
3. J. B. Foresman, M. W. Wong, K. B. Wiberg, M. J. Frisch, Theoretical Investigation of the Rotational Barrier in Allyl and 1,1,3,3-tetramethylallyl Ions. *J. Am. Chem. Soc.*, **1993**, 115, 2220-2226.
4. H. Mayr, W. Forner, P. v. R. Schleyer, Methyl-Substituted Allyl Cations. A Comparison of Experimental Stability, Rotational Barrier and Solvolysis Data with Ab Initio Calculations. *J. Am. Chem. Soc.*, **1979**, 101, 6032-6040.
5. K. Raghavachari, R. A. Whiteside, J. A. Pople, P. v. R. Schleyer, Molecular Orbital Theory of Electronic Structure of Organic Molecules. 40. Structures and Energies of C1-C3 Carbocations Including Effects of Electron Correlation. *J. Am. Chem. Soc.*, **1981**, 103, 5649-5657.
6. M. E. Comoyer, W. L. Jorgensen, Solvent Effects on the Relative Energies of Carbonium ions. Solvation and Internal Rotation for the Allyl Cation in Liquid Hydrogen Fluoride. *J. Am. Chem. Soc.*, **1984**, 106, 5104-5112.
7. A. Gobbi, G. Frenking, Resonance Stabilization in Allyl Cation, Radical, and Anion. *J. Am. Chem. Soc.*, **1994**, 116, 9275.
8. Y. Mo, S. D. Peyerimhoff, Theoretical Analysis of Electron Delocalization. *J. Chem. Phys.*, **1998**, 109, 1687-1697.
9. D. Feller, E. R. Davidson, W. T. Borden, Allylic Resonance - When is it Unimportant ? *J. Am. Chem. Soc.*, **1984**, 106, 2513-2519.
10. P. B. Karadakov, J. Gerratt, G. Raos, D. L. Cooper, M. Raimondi, The Nature of the Carbon-Carbon Bonds in Cyclopropane and Cyclobutane: A Comparison Based on Spin-Coupled Theory. *J. Am. Chem. Soc.*, **1994**, 116, 7714-7721.

11. T. Clark, C. Rohde, P. v. R. Schleyer, Allyllithium, Allylsodium, and Allylmagnesium Hydride: Geometries and Bonding. A Comparative Ab Initio Study. *Organometallics*, **1983**, 2, 1344-1351.
12. K. B. Wiberg, W. K. B. Rosenberg, P. R. Rablen, Butadiene. 2. Examination of the Energetic Preference for Coplanarity of Double Bonds. Comparison of Butadiene, Acrolein, and Vinylamine. *J. Am. Chem. Soc.*, **1991**, 113, 2890-2898.
13. A. Karpfen, C. Choi, C. H. Kertesz, Single-Bond Torsional Potentials in Conjugated Systems: A Comparison of Ab Initio and Density Functional Results *J. Phys. Chem. A*, **1997**, 101, 7426-7433.
14. M. E. Squillacote, R. S. Sheridan, O. L. Chapman, F. A. Anet, Planar s-cis-1,3-Butadiene. *J. Am. Chem. Soc.*, **1978**, 101, 3657-3659.
15. M. A. Murcko, H. Castejon, K. B. Wiberg, Carbon-carbon Rotational Barriers in Butane, 1-butene, 1,3-butadiene. *J. Phys. Chem.*, **1996**, 100, 16162-16168.
16. J. Oxgaard, O. Wiest, Rehybridized 1,3-Butadiene Radical Cations: How Far will a Radical Cation go to Mantain Conjugation ? *J. Phys. Chem. A*, **2002**, 106, 3967-3974.
17. J. Oxgaard, O. Wiest, Symmetry, Radical Ions, and Butadienes: Exploring the Limits of Density Functional Theory. *J. Phys. Chem. A*, **2001**, 105, 8236-8240.
18. M. Traetteberg, P. Bakken, H. Hopf, R. Hanel, *Chem. Ber.*, **1994**, 127, 1469.
19. S. Tsuzuki, L. Schaefer, G. Hitoshi, E. D. Jemmis, H. Hosoya, K. Siam, K. Tanabe, E. Osawa, Investigation of Intramolecular Interactions in n-Alkanes. Cooperative Energy Increments Associated with GG and GTG' [G = gauche, T = trans] Sequences. *J. Am. Chem. Soc.*, **1991**, 113, 4665-4671.
20. A. Karpfen, Torsional Potentials of Perfluoro-1,3-Butadiene and Perfluoro-1,3,5-Hexatriene: A Comparison of Ab Initio and Density Functional Results. *J. Phys. Chem. A*, **1999**, 103, 2821-2827.
21. M. Traetteberg, H. Hopf, H. Lipka, R. Hanel, *Chem. Ber.*, **1994**, 127, 1459.
22. V. Schomaker, L. Pauling, The Electron Diffraction Investigation of the Structure of Benzene, Pyridine, Pyrazine, 1,3-Butadiene, Cyclopentadiene, Furan, Pyrrole, and Thiophene. *J. Am. Chem. Soc.*, **1939**, 61, 1769-1780.

-
23. D. R. Lide Jr, Microwave Studies of Butadiene Derivatives. I. Spectrum of Fluoroprene. *J. Chem. Phys.*, **1962**, 37, 2074-2079.
 24. D. R. Lide Jr., M. Jen, Microwave Studies of Butadiene Derivatives. II. Isoprene. *J. Chem. Phys.*, **1964**, 40, 252-253.
 25. R. L. Lipknick, E. W. Garbisch Jr., Conformational Analysis of 1,3-Butadiene *J. Am. Chem. Soc.*, **1973**, 95, 6370-6375.
 26. R. S. Rasmussen, R. R. Brattain, Infra-Red Absorption Spectra of Some C4 and C5 Dienes. *J. Chem. Phys.*, **1947**, 15, 131-135.
 27. L. A. Carreira, Determination of the Torsional Potential Function of 1,3-Butadiene. *J. Chem. Phys.*, **1975**, 62, 3851-3854.
 28. R. G. Parr, W. Yang, Density Functional Theory of Atoms and Molecules. **1989**, New York: Oxford University Press.
 29. A. D. Becke, Density-Functional Thermochemistry. I. The Effect of the Exchange-Only Gradient Correction. *J. Chem. Phys.*, **1992**, 96, 2155-2160.
 30. A. D. Becke, Density-Functional Thermochemistry. III. The Role of Exact Exchange. *J. Chem. Phys.*, **1993**, 98, 5648-5652.
 31. A. D. Becke, A New Mixing of Hartree-Fock and Local Density-functional Theories. *J. Chem. Phys.*, **1993**, 98, 1372-1377.
 32. A. D. Becke, Density-Functional Exchange-Energy Approximation with Correct Asymptotic Behavior. *Phys. Rev. A*, **1988**, 38, 3098-3104.
 33. C. Lee, W. Yang, R. G. Parr, Development of the Colle-Salvetti Correlation-Energy Formula into a Functional of the Electron Density. *Phys. Rev. B*, **1988**, 37, 785-789.
 34. W. J. Hehre, R. Ditchfield, J. A. Pople, Self-Consistent Molecular Orbital Methods. XII. Further Extensions of Gaussian-Type Basis Sets for Use in Molecular Orbital Studies of Organic Molecules. *J. Chem. Phys.*, **1972**, 56, 2257-2261.
 35. M. J. Frisch, G. W. Trucks, H. B. Schlegel, G. E. Scuseria, M. A. Robb, J. R. Cheeseman, V. G. Zakrzewski, J. A. Montgomery, R. E. Stratmann, J. C. Burant, S. Dapprich, J. M. Millam, A. D. Daniels, K. N. Kudin, M. C. Strain, O. Farkas, J. Tomasi, V. Barone, M. Cossi, R. Cammi, B. Mennucci, C. Pomelli, C. Adamo, S. Clifford, J. Ochterski, G. A. Petersson, P. Y. Ayala, Q. Cui, K. Morokuma, D. K.

- Malick, A. D. Rabuck, K. Raghavachari, J. B. Foresman, J. Cioslowski, J. V. Ortiz, B. B. Stefanov, G. Liu, A. Liashenko, P. Piskorz, I. Komaromi, R. Gomperts, R. L. Martin, D. J. Fox, T. Keith, M. A. Al-Laham, C. Y. Peng, A. Nanayakkara, C. Gonzalez, M. Challacombe, P. M. W. Gill, B. G. Johnson, W. Chen, M. W. Wong, J. L. Andres, M. Head-Gordon, E. S. Replogle, J. A. Pople, *Gaussian 98 (Revision A.7)*. 1998, Gaussian, Inc.: Pittsburgh PA.
36. E. D. Glendening, J. K. Badenhoop, A. E. Reed, J. E. Carpenter, J. A. Bohmann, C. M. Morales, F. Weinhold, *NBO 5.0*. 2001, Theoretical Chemistry Institute, University of Wisconsin: Madison.
37. J. P. Daudey, G. Trinquier, J. C. Barthelat, J. P. Malrieu, Decisive Role of π Conjugation in the Central Bond Length Shortening of Butadiene. *Tetrahedron*, **1980**, 36, 3399-3401.
38. Y. Mo, W. Wu, Q. Zhang, Theoretical Resonance Energies of Benzene, Cyclobutadiene, and Butadiene. *J. Phys. Chem.*, **1994**, 98, 10048-10053.
39. Electronic Properties of Conjugated Polymers III: Basic Models and Applications ed. H. Kuzmani, M. Mehring, S. Roth. **1989**, Berlin: Springer.
40. J. S. Miller, Conducting Polymers - Materials of Commerce. *Adv. Mat.*, **1993**, 5, 671-676.
41. Handbook of Conducting Polymers, Vols. 1, 2 ed. T. A. Skotheim. **1986**, New York: Dekker.
42. Conjugated Polymers and Related Materials. The Interconnection of Chemical and Electronic Structure ed. W. R. Salaneck, I. L. B. Rånby. **1993**, Oxford: Oxford University Press.
43. M. Liphardt, A. Goonesekera, B. E. Jones, S. Ducharme, J. M. Takacs, L. Zhang, High Performance Photorefractive Polymers. *Science*, **1994**, 263, 367-369.
44. N. C. Greenham, S. C. Moratti, D. D. C. Bradley, R. H. Friend, A. B. Holmes, Efficient Light-Emitting Diodes Based on Polymers with High Electron Affinities. *Nature*, **1993**, 365, 628-630.
45. H. S. Nalwa, Organic Materials for Third-Order Nonlinear Optics Advanced Materials. *Adv. Mat.*, **1993**, 5, 341-358.

-
46. L. Gobbi, P. Seiler, F. Diederich, A Novel Three-Way Chromophoric Molecular Switch: pH and Light Controllable Switching Cycles. *Angew. Chem. Int. Ed.*, **1999**, 38, 674-678.
 47. T. H. Dunning Jr., General Contraction of Gaussian Basis Sets. II. Atomic Natural Orbitals and the Calculation of Atomic and Molecular Properties. *J. Chem. Phys.*, **1990**, 92, 551-560.
 48. A. K. Wilson, T. v. Mourik, T. H. Dunning Jr., Gaussian Basis Sets for Use in Correlated Molecular Calculations. VI. Sextuple Zeta Correlation Consistent Basis Sets for Boron through Neon. *J. Mol. Struct.*, **1996**, 388, 339-349.
 49. P. J. Stevens, F. J. Devlin, C. F. Chablowksi, M. J. Frisch, Ab Initio Calculation of Vibrational Absorption and Circular Dichroism Spectra Using Density Functional Force Fields. *J. Phys. Chem.*, **1994**, 98, 11623-11627.
 50. M. Traetteberg, H. Hopf, Cross-Conjugation: A Theoretical and Experimental Study of the Molecular Structure of 2-Ethynyl-1,3-butadiene. *Acta Chem. Scand.*, **1994**, 48, 989-993.
 51. Ab Initio Molecular Orbital Theory. Ed. W. J. Hehre, L. Random, P. R. Scheleyer, J. A. Pople. **1986**, New York: John Wiley & Son.
 52. A. D. Bacon, M. C. Zerner, An Intermediate Neglect of Differential Overlap Theory for Transition Metal Complexes: Fe, Co, and Cu Chlorides. *Theor. Chim. Acta* **1979**, 53, 21.
 53. M. C. Zerner, Metal-Ligand Interactions. **1996**, Dordrecht, The Netherlands: Kluwer Academic Publishers.
 54. M. C. Zerner, G. H. Loew, R. F. Kirchner, U. T. Mueller-Westerhoff, An Intermediate Neglect of Differential Overlap Technique for Spectroscopy of Transition-metal Complexes. Ferrocene. *J. Am. Chem. Soc.*, **1980**, 102, 589-599.
 55. J. C. Culberson, P. Knappe, N. Rösch, M. C. Zerner, An Intermediate Neglect of Differential Overlap (INDO) Technique for Lanthanide Complexes: Studies on Lanthanide Halides. *Theor. Chim. Acta* **1987**, 71, 21-39.
 56. J. Ridley, M. C. Zerner, An Intermediate Neglect of Differential Overlap Technique for Spectroscopy: Pyrrole and the Azines. *Theor. Chim. Acta*, **1973**, 32, 111.

-
57. J. Ridley, M. C. Zerner, Triplet states via Intermediate Neglect of Differential Overlap: Benzene, Pyridine, and the Diazines. *Theor. Chim. Acta*, **1976**, *42*, 223.
 58. W. P. Anderson, T. Cundari, M. C. Zerner, An Intermediate Neglect of Differential Overlap Model for Second Row Transition Metal Species. *Int. J. Quantum Chem.*, **1991**, *39*, 31.
 59. W. P. Anderson, T. Cundari, R. S. Drago, M. C. Zerner, Utility of the Semiempirical INDO/1 Method for the Calculation of the Geometries of Second-row Transition-metal Species. *Inorg. Chem.*, **1990**, *29*, 1-3.
 60. L. K. Hanson, J. Fajer, M. A. Thompson, M. C. Zerner, Electrochromic Effects of Charge Separation in Bacterial Photosynthesis: Theoretical Models. *J. Am. Chem. Soc.*, **1987**, *109*, 4728-4730.
 61. M. C. Zerner, P. C. de Mello, M. Hehenberger, On the Convergence of the Self Consistent Field Method to Excited States. *Int. J. Quantum Chem.*, **1982**, *21*, 251-255.
 62. M. C. Zerner, Semi Empirical Molecular Orbital Methods. Reviews of Computational Chemistry, ed. K. B. Lipkowitz, D. B. Boyd. Vol. 2. **1991**, New York: VCH. 313-366.
 63. G. S. Tschumper, H. F. Schaefer, Predicting Electron Affinities with Density Functional Theory: Some Positive Results for Negative Ions. *J. Chem. Phys.*, **1997**, *107*, 2529-2541.
 64. R. E. Stratmann, G. E. Scuseria, M. J. Frisch, An Efficient Implementation of Time-Dependent Density-Functional Theory for the Calculation of Excitation Energies of Large Molecules. *J. Chem. Phys.*, **1998**, *109*, 8218-8224.
 65. E. D. Glendening, K. Badenhoop, A. E. Reed, J. E. Carpenter, J. A. Bohmann, C. M. Morales, F. Weinhold, *NBO 5.0*. 2001, Theoretical Chemistry Institute, University of Wisconsin: Madison.
 66. J. Anthony, A. M. Boldi, C. Boudon, J. P. Gisselbrecht, M. Groos, P. Seiler, C. B. Knobler, F. Diederich, Macrocyclic Tetraethynylethene Molecular Scaffolding: Perethynylated aromatic Dodecahydro-[18]annulenes, Antiaromatic Octadehydro-[12]annulenes, and Expanded Radialenes. *Helv. Chim. Acta*, **1995**, *78*, 797-817.
 67. R. R. Tykwinski, A. Hilger, F. Diederich, H. P. Lüthi, P. Seiler, V. Gramlich, J. P. Gisselbrecht, C. Boudon, M. Gross, Donor-Acceptor-Functionalized

- Tetraethynylethenes with Nitrothienyl Substituents: Structure-Property Relation-ships. *Helv. Chim. Acta*, **2000**, 83, 1484-1508.
68. A. Hilger, J.-P. Gisselbrecht, R. R. Tykwinski, C. Boudon, M. Schreiber, R. E. Martin, H. P. Lüthi, M. Gross, F. Diederich, Electronic Characteristics of Arylated Tetraethynylethenes: A Cooperative Computational and Electrochemical Investigation. *J. Am. Chem. Soc.*, **1997**, 119, 2069-2078.
69. B. Ma, H. M. Sulzbach, Y. Xie, H. F. Schaefer, III, π Electron Delocalization and Compression in Acyclic Acetylenic Precursors to Multidimensional Carbon Networks: Comparison with Experiment for the Recently Synthesized Tris(trimethylsilyl)-Substituted Tetraethynylmethane. Structures, Thermochemistry, Infrared Spectra, Polarizabilities, and Hyperpolarizabilities. *J. Am. Chem. Soc.*, **1994**, 116, 3529-3538.
70. M. Schreiber, J. Anthony, F. Diederich, M. E. Spahr, R. Nesper, M. Hubrich, F. Bommeli, L. Degiorgi, P. Wachter, P. Kaatz, C. Bosshard, P. Günter, M. Colussi, U. W. Suter, C. Boudon, J.-P. Gisselbrecht, M. Gross, Polytriacetylenes: Conjugated Polymers with a Novel All-Carbon Backbone. *Adv. Mater.*, **1994**, 6, 786-790.

4 Applications

The application of our approach to linearly π -conjugated compounds, such as those described in section 1.3, will be presented and discussed in this chapter. The three main degrees of freedom to design compounds of tailored properties (type and length of the π -conjugated backbone; mode of π -conjugation; nature, strength, number, and position of the substituents) will be explored in order to rationalize their impact on electron delocalization, and correspondingly, on physical observables such as electron affinities, ionization potentials, maximum absorption wavelengths, polarizabilities and hyperpolarizabilities.

In subchapter 4.1, we report a theoretical study of π -electron delocalization in two-dimensional substituted tetraethynylethene (TEE) model compounds, which are characterized by distinct π -conjugated paths, i.e. *geminal*, *cis*, and *trans*. Subchapter 4.2 concerns with the investigation of parent (unsubstituted) polytriacetylene (PTA) and *iso*-polytriacetylene (*iso*-PTA) oligomers of increasing chain length. The study focuses on the differences between the *through* and *cross* π -conjugation pathways. In subchapter 4.3 we examine the insertion of ethynyl units into the polyacetylene (PA) chain and its effect on π -electron delocalization. Finally, the impact on π -electron delocalization of the donor and/or acceptor functionalization of PTA and perethynyl-polytriacetylene (pePTA) oligomers of increasing chain length is the topic of subchapter 4.4.

4.1 Extended Systems: Electron Delocalization in Substituted Tetraethynylethene Model Compounds.

4.1.1 Summary

Donor and/or acceptor substituted π -conjugated systems represent an important class of compounds in organic chemistry. However, up to now, a general method to quantitatively address the efficiency of a conjugated path is still missing. In this section, the computational approach based on deletion energies and on second-order orbital interaction energies, presented and discussed in Chapter 2 is employed to quantitatively assess (“measure”) delocalization energies. Moreover, the purpose of this work is to assess the efficiency of distinct π -conjugated paths, i.e. *geminal*, *cis*, and *trans*, as well as to predict the impact of substituents on a given backbone. The study is focused on various mono-, di-, tri-, and tetra-substituted tetraethynylethenes (TEEs). These model systems are suitable for our analysis because they offer distinct conjugation paths within the same molecule, and can also be substituted in multiple ways. Differences between conjugation paths, the effect of neighbor paths, and the impact of donor and acceptor substituents on the various paths are discussed.

4.1.2 Introduction

Tetraethynylethene (TEE, 3,4-diethynylhex-3-ene-1,5-diyne) and its derivatives are compounds of great interest due to the acetylenic scaffolding which provides carbon-rich compounds with very interesting physicochemical properties (see section 1.3 and references therein). In fact, these systems, as well as other polyethynylethenes [1], give access to advanced materials for electronic and photonic applications, such as chromophores with nonlinear optical properties of higher order [2, 3]; molecular photochemical switches [4-8]; and extensive π -conjugated polymers [9-15].

TEE has been studied both theoretically and experimentally because of its use as building blocks of linearly conjugated polymers, i.e. polyacetylenes (PAs), polydiacetylenes (PDAs), and polytriacetylenes (PTAs) [16-27]. Moreover, it shows two relevant characteristics. First, it allows *through-* (or *trans*) and *cross-* (or *geminal*) conjugation. Second, it can easily be functionalized with a wide range of donor and acceptor substituents. The presence of donor and acceptor substituents has a strong effect on the properties of this system [28-33].

In this subchapter our method based on the NBO analysis of Weinhold [34-39] is applied to quantify the delocalization energy (σ or π) of distinct conjugation paths within a given TEE derivative. Furthermore, the method is used to address the issue of quantifying donor/acceptor substituent effects on given backbones, and finally, to evaluate the effect of neighboring paths on the conjugation pathway under consideration. Simple model compounds, such as TEE substituted with NO₂, CHO, and CN (acceptors), and OH, OCH₃, and NH₂ (donors) are considered to explore the effects of the donor-acceptor functional groups on the π -conjugated pathways.

The NBO analysis developed by Weinhold and coworkers [34-39] offers a way to quantify electron delocalization in terms of intramolecular donor-acceptor interactions. In our method we “measure” the delocalization energy by applying the orbital deletion procedure described in Chapter 2. The orbitals deleted are the π^* (or σ^*) NBOs responsible for the delocalization. The difference between the total energies before and after the deletion gives the delocalization energy, E_{deloc} , which represents the deviation from the idealized Lewis-structure. E_{del} , therefore, is closely related to the non-Lewis (NL) contribution to the total energy along the conjugation path considered, i.e. $E_{deloc} = E_{NL} = E_{del}$. These non-Lewis contributions can be approximated by the sum of second-order interaction energies between the strongly occupied Lewis-type NBOs (donor orbitals) and the weakly occupied non-Lewis NBOs (acceptor orbitals) involved in the path. These interactions are responsible for the loss of occupancy of the donor in favor of the acceptor orbitals, and hence, for the departure from the idealized Lewis-type structure description. In other words, they represent the non-Lewis corrections to the natural Lewis structure, i.e. $\sum_{ij} E_{SOI_{ij}} = E_{NL}$. Thus, these second-order

perturbation energies and the deletion energies can be viewed as descriptors to evaluate delocalization by means of single orbital interactions.

In the section “Results and Discussion” we use our approach to predict the impact of donor/acceptor substituents on distinct paths within the same system, as well as to characterize the differences between the *cross-* (*geminal*) and *through-* (*trans*) conjugation paths.

4.1.3 Computational Methods

In the present work, all calculations were performed at the DFT level of theory [40], using the B3LYP functional [41, 42]. The optimized geometries and the NBO data have been obtained at B3LYP level together with a correlation-consistent polarized valence double- ζ (cc-pVDZ) basis set [43] for the TEE and its derivatives. All calculations have been carried out using Gaussian98 package [44]. The natural bond orbital analysis has been performed with the program NBO 5.0 included in Gaussian98 [45].

In the present section, we will refer to delocalization energy (E_{deloc}) without distinction between E_{del} and $\sum_{ij} E_{SOIE_{ij}}$ unless otherwise mentioned.

4.1.4 Results and Discussion

Scope of the Study and Notation

Tetraethynylethene (TEE) and its substituted derivatives offer an example of compounds with several distinct conjugation paths within the same molecule. The donor/acceptor substituted TEEs furthermore allow us to address the effect of donor/acceptor functionalization on a specific path.

For this purpose, we studied the complete set of mono-, di-, tri-, and tetra-substituted TEEs (TEE- nX , $n=1-4$, Figure 4.1). The substituents considered are NO₂, CN, CHO (acceptor groups), and OH, OCH₃, NH₂ (donor groups). None of these compounds has been

studied experimentally. However, in the context of the validation of the analysis, it is sufficient to compare among computed data.

Table 4.1: The distinct paths (*geminal* and *trans* conjugation) in substituted and unsubstituted TEEs (TEE-*n*X with *n* = 0-4). The labels *a* and *b* indicate *geminal* and *trans* paths, respectively. Non-equivalent *geminal* and *trans* paths are marked as *a'* and *b'*, respectively. In parentheses are indicated the neighbor paths

<i>n</i>	Compound	Paths	Occurrence
0	2a	<i>a</i> : EE (EE) <i>b</i> : EE (EE)	2 2
1	2b	<i>a</i> : EE (EX) <i>a'</i> : EX (EE) <i>b</i> : EE (EX) <i>b'</i> : EX (EE)	1 1 1 1
2	2c	<i>a</i> : EX (EX) <i>b</i> : EE (XX) <i>b'</i> : XX (EX)	2 1 1
2	2d	<i>a</i> : EE (XX) <i>a'</i> : XX (EE) <i>b</i> : EE (EX)	1 1 2
3	2e	<i>a</i> : EX (XX) <i>a'</i> : XX (EX) <i>b</i> : EX (XX) <i>b'</i> : XX (EX)	1 1 1 1
4	2f	<i>a</i> : XX (XX) <i>b</i> : XX (XX)	2 2

The notation used in the following discussion is explained in Figure 4.1. Three types of paths are distinguished: *trans* (*a*), *geminal* (*b*), and *cis* (*c*). We refer to the pure ethynyl unit ($-\text{C}\equiv\text{C}-\text{H}$) as E, and to the ethynyl unit with a substituent ($-\text{C}\equiv\text{C}-\text{X}$) as X. We will not investigate *cis* conjugation (*c*) any further in the present study since the focus of this work is on *through-* (*cis*, *trans*) versus *cross-* (*geminal*) conjugation. *Through*-conjugation will be represented by *trans* conjugation. Moreover, the specific path considered is referred to as

conjugation path, whereas the other is always referred to as *neighbor* path. For example, if the *geminal* XX path (a') in 2d (Figure 4.1) is the analyzed conjugation path, the second *geminal* path EE (a) is the *neighbor* path. Finally, in the following discussion, we will label the orbitals according to the bond they are associated with, i.e. π_D and π_T are the vertical occupied π orbitals of the double bonds (D) C=C and the triple bonds (T) C \equiv C, whereas π_D^* and π_T^* are the corresponding antibonding orbitals.

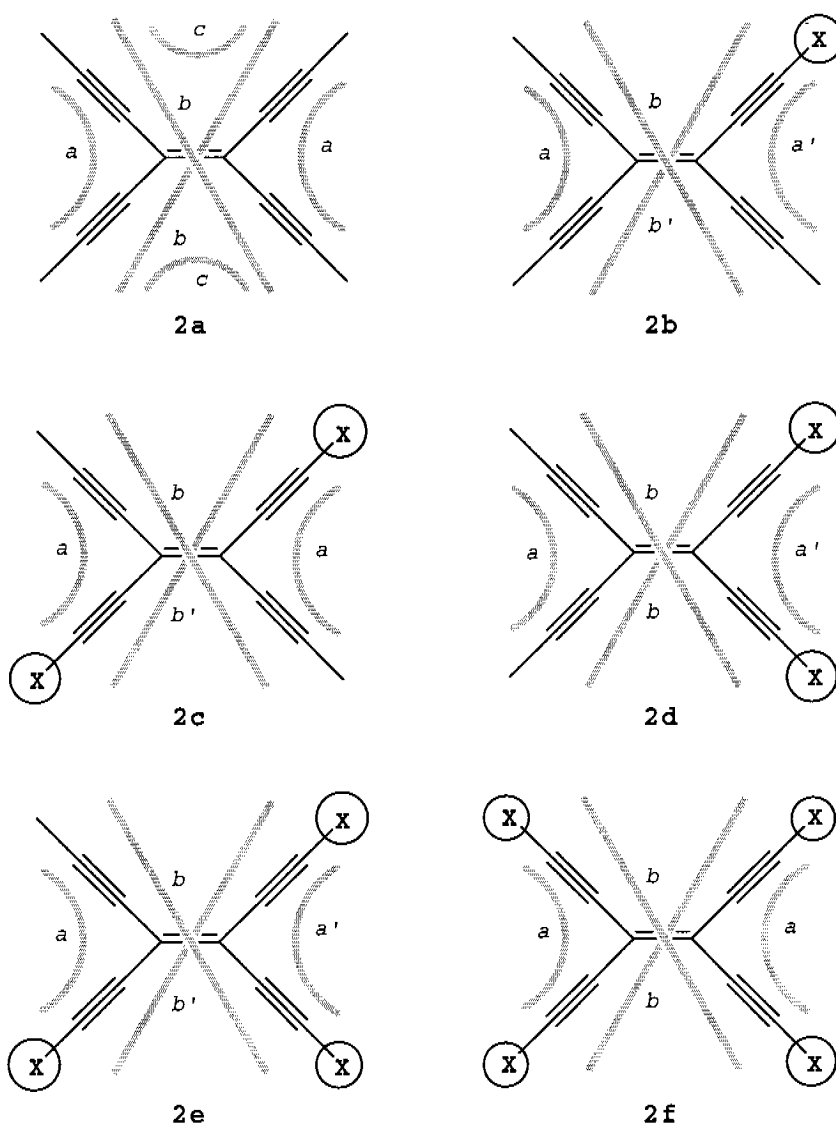


Figure 4.1: The tetraethynylethene derivatives (TEE- nX , $n = 0-4$ (2a-f)) studied in the present work ($X = , NO_2, CHO, CN, OH, OCH_3,$ and NH_2). The grey-shaded lines indicate the conjugation paths (trans and geminal) (see also Table 4.1).

Technical Details on the Analysis

For the comparison of SOIEs with deletion energies, one needs to consider carefully which orbital interactions have to be taken into account. Figure 4.2 shows the two *geminal* paths, i.e. EX (1) and EE (2), in a generic mono-substituted TEE. For example, the deletion energy $E_{del}(\text{EX})$ of the *geminal* path (1) should correspond to the SOIE given by the sum of all $\pi_T \rightarrow \pi_D^*$ contributions, of the $\pi_D \rightarrow \pi_T^*$ contributions involved in the EX path, and of the contributions due to the substituents, that is $Y_X \rightarrow \pi_T^*$. If X is a donor, Y_X stands for the donor lone pairs, whereas if X is an acceptor, Y_X stands for π_D or π_T depending on the nature of the substituents (see a , a' , b , and c in Figure 4.2, respectively). In the deletion procedure, removing the central π_D^* orbital in a specific path means deleting an orbital which is unavoidably affected by the neighbor path. Therefore, in order to have the appropriate comparison between E_{del} and E_{SOIE} , also the $\pi_T \rightarrow \pi_D^*$ contributions of the neighbor path need to be taken into account. Finally, the $\pi_T \rightarrow Y_X^*$ contributions do not need to be considered because the antibonding orbitals of X do not play an important role in characterizing the substituent effects on the backbone.

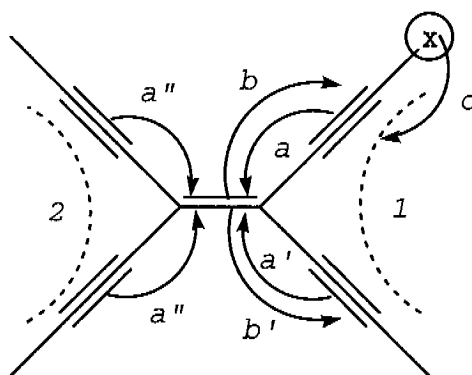


Figure 4.2: Geminal conjugated paths for a mono-substituted tetraethynylethene. 1 and 2 represent EX and EE conjugation paths, respectively. (a , a' , a'') are the $\pi_T \rightarrow \pi_D^*$ contributions; (b , b') are the $\pi_D \rightarrow \pi_T^*$ contributions; (c) are the $X_{\text{lonepair}} \rightarrow \pi_T^*$ or $\pi_{D(T)} \rightarrow \pi_T^*$ whether X is a donor or an acceptor, respectively.

Through- (Trans) versus Cross- (Geminal) Conjugation

By comparing distinct *geminal* or *trans* paths within TEE-*n*X, (*n* = 1-3), we observe considerable differences in the delocalization energies (Fig. 4.3-8 and 4.9-14). These energy differences are also summarized in Table 4.2.

For the *geminal* paths, in the acceptor substituted compounds, we observe conjugation energy splittings of 13-18, 25-35, and 11-18 kcal mol⁻¹ for the mono-, di-, and tri-substituted systems, respectively. However, this splitting between *geminal* paths is even larger when donor groups are attached to TEE. With X=OH or OCH₃, the splittings are 34 kcal mol⁻¹ for both TEE-X, about 68 kcal mol⁻¹ for TEE-2X, and, lastly, about 34 kcal mol⁻¹ for TEE-3X. TEE-*n*NH₂ (*n* = 1-3) show a behavior more similar to the acceptor groups than to the donor ones. In fact, the energy splitting is rather small, i.e. \approx 11, 22, and 11 kcal mol⁻¹ for the mono-, di-, and tri-substituted systems, respectively, compared to the other donors considered.

Table 4.2: The delocalization energy splitting (in kcal mol⁻¹) calculated at the B3LYP/cc-pVDZ level for TEE-*n*X with *n* = 1-3

TEE- <i>n</i> X	Splitting	Acceptors			Donors		
		NO ₂	CHO	CN	OH	OCH ₃	NH ₂
<i>n</i> =1							
<i>geminal</i>	EX-EE	15	13	18	34	34	11
<i>trans</i>	EX-EE	13	11	16	36	36	12
<i>n</i> =2							
<i>geminal</i>	XX-EE	30	25	35	68	67	22
<i>trans</i>	XX-EE	24	21	32	70	69	24
<i>n</i> =3							
<i>geminal</i>	XX-EX	15	11	18	34	33	11
<i>trans</i>	XX-EX	12	11	16	34	33	12

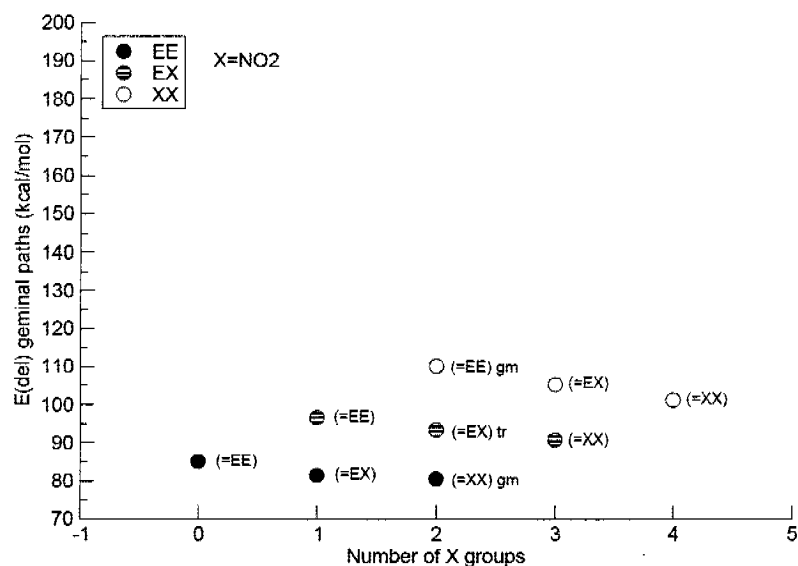


Figure 4.3: The geminal delocalization energies for all of the TEE- $n\text{NO}_2$, $n = 0-4$ (acceptor group). In the legend, full, striped, and empty circles represent the studied EE, EX, and XX conjugation paths, respectively, whereas in parentheses are displayed the neighbor paths.

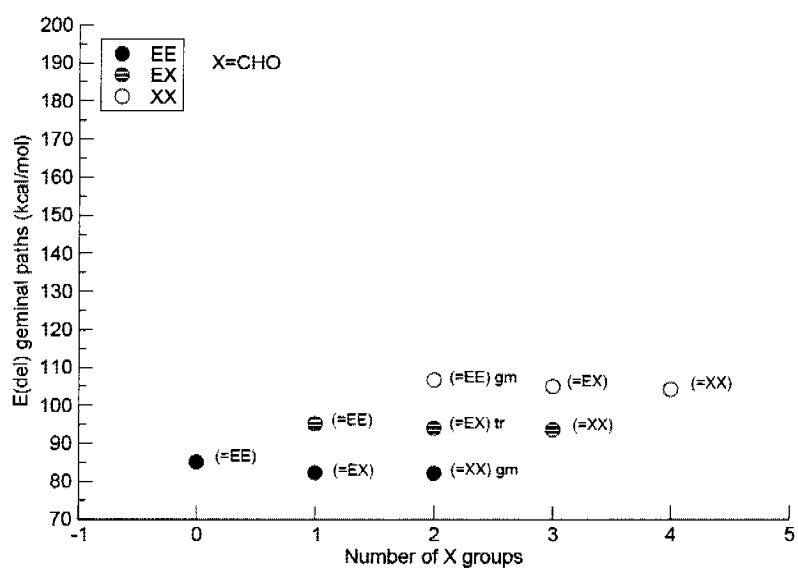


Figure 4.4: The geminal delocalization energies for all of the TEE- $n\text{CHO}$, $n = 0-4$ (acceptor group). In the legend, full, striped, and empty circles represent the studied EE, EX, and XX conjugation paths, respectively, whereas in parentheses are displayed the neighbor paths.

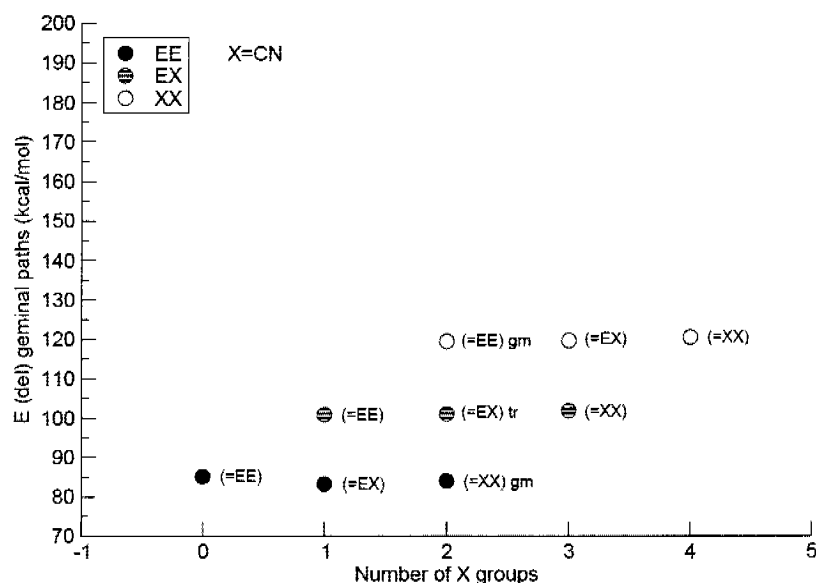


Figure 4.5: The geminal delocalization energies for all of the TEE- n CN, $n = 0-4$ (acceptor group). In the legend, full, striped, and empty circles represent the studied EE, EX, and XX conjugation paths, respectively, whereas in parentheses are displayed the neighbor paths.

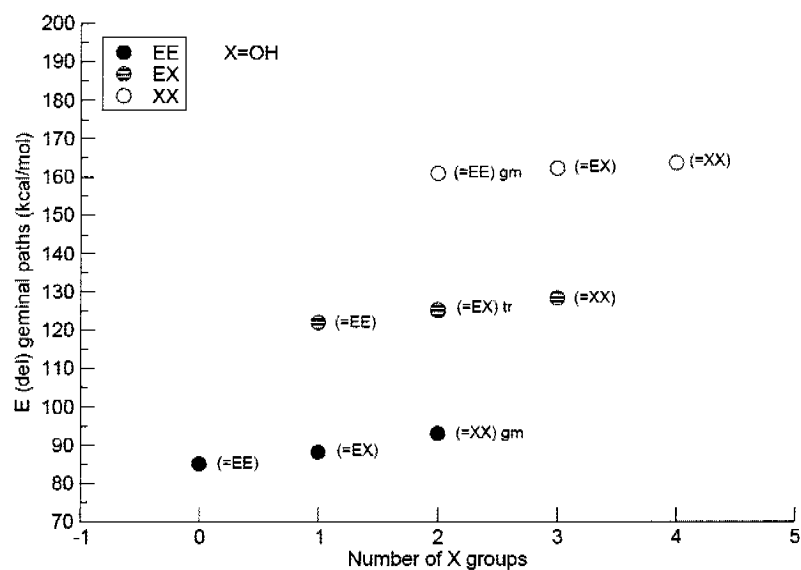


Figure 4.6: The geminal delocalization energies for all of the TEE- n OH, $n = 0-4$ (donor group). In the legend, full, striped, and empty circles represent the studied EE, EX, and XX conjugation paths, respectively, whereas in parentheses are displayed the neighbor paths.

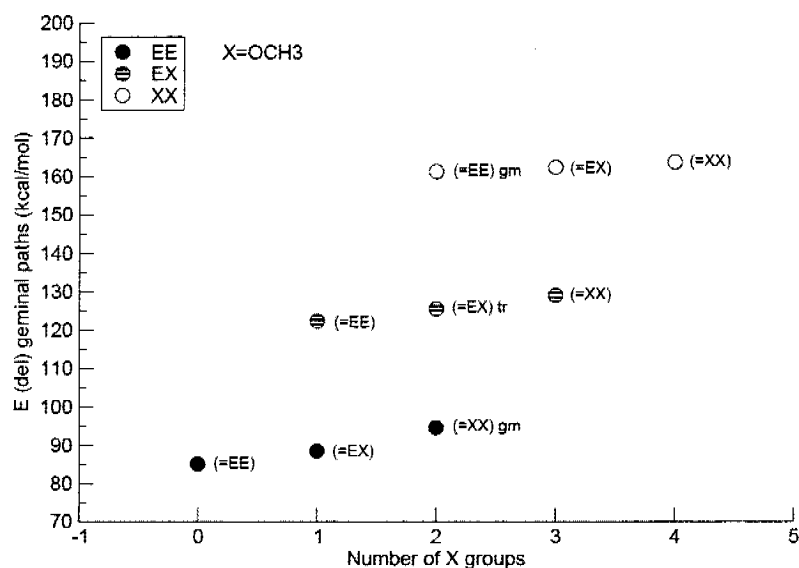


Figure 4.7: The geminal delocalization energies for all of the TEE-nOCH₃, $n = 0-4$ (donor group). In the legend, full, striped, and empty circles represent the studied EE, EX, and XX conjugation paths, respectively, whereas in parentheses are displayed the neighbor paths.

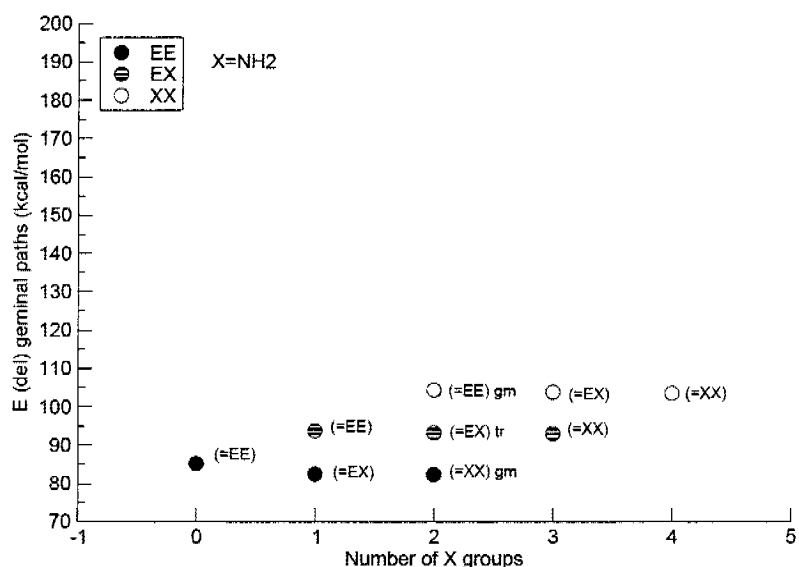


Figure 4.8: The geminal delocalization energies for all of the TEE-nNH₂, $n = 0-4$ (donor group). In the legend, full, striped, and empty circles represent the studied EE, EX, and XX conjugation paths, respectively, whereas in parentheses are displayed the neighbor paths.

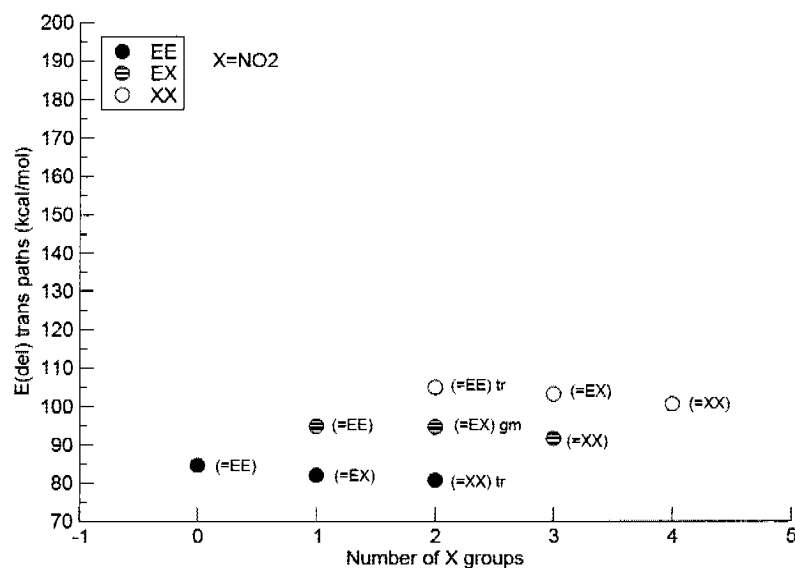


Figure 4.9: The trans delocalization energies for all of the TEE- n NO₂, $n = 0-4$ (acceptor group). In the legend, full, striped, and empty circles represent the studied EE, EX, and XX conjugation paths, respectively, whereas in parentheses are displayed the neighbor paths.

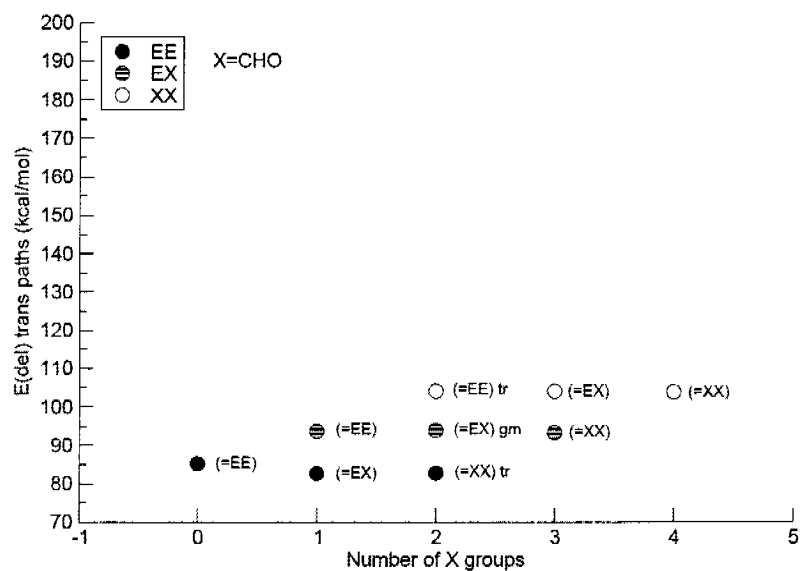


Figure 4.10: The trans delocalization energies for all of the TEE- n CHO, $n = 0-4$ (acceptor group). In the legend, full, striped, and empty circles represent the studied EE, EX, and XX conjugation paths, respectively, whereas in parentheses are displayed the neighbor paths.

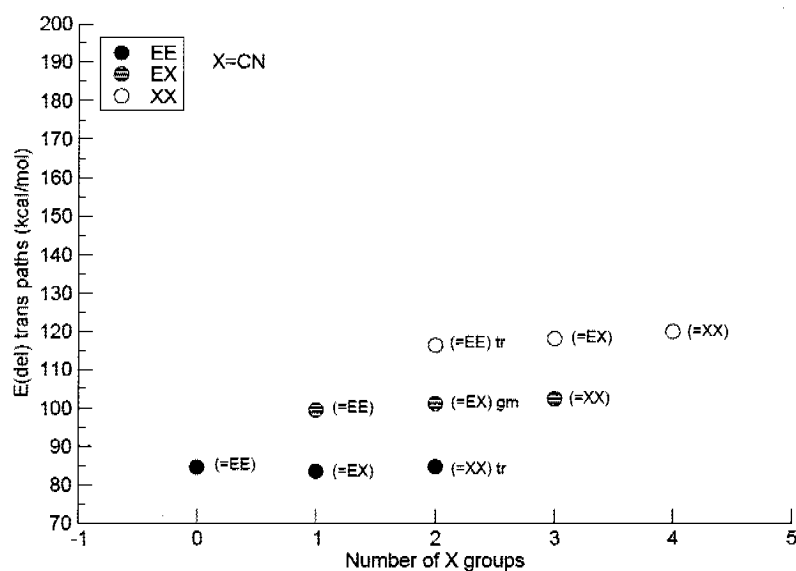


Figure 4.11: The trans delocalization energies for all of the TEE- $n\text{CN}$, $n = 0-4$ (acceptor group). In the legend, full, striped, and empty circles represent the studied EE, EX, and XX conjugation paths, respectively, whereas in parentheses are displayed the neighbor paths.

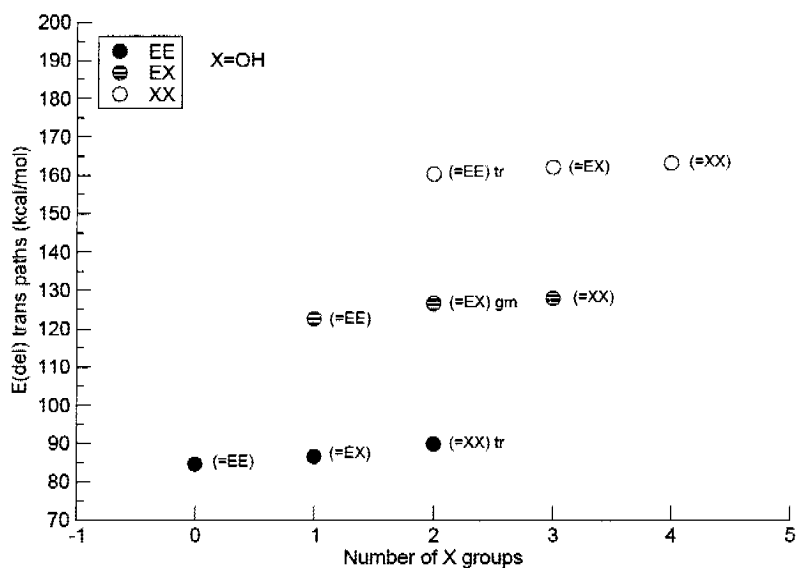


Figure 4.12: The trans delocalization energies for all of the TEE- $n\text{OH}$, $n = 0-4$ (donor group). In the legend, full, striped, and empty circles represent the studied EE, EX, and XX conjugation paths, respectively, whereas in parentheses are displayed the neighbor paths.

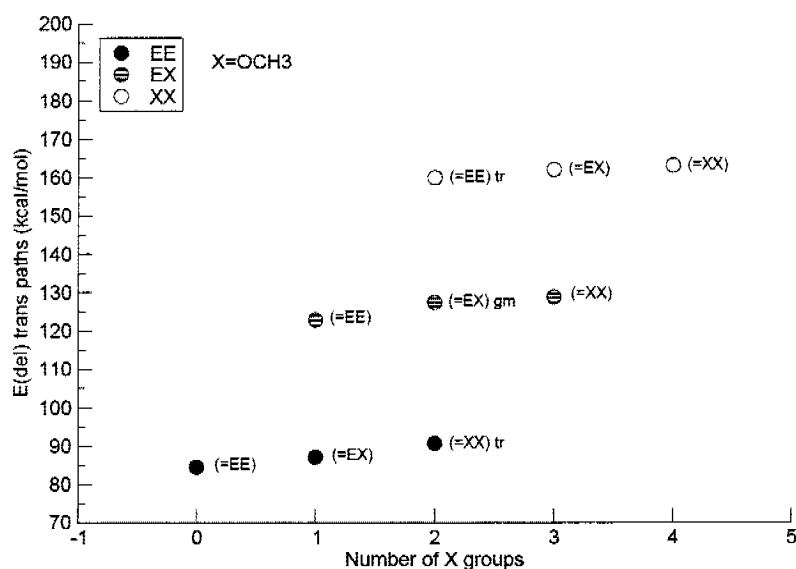


Figure 4.13: The trans delocalization energies for all of the $\text{TEE}-n\text{OCH}_3$, $n = 0-4$ (donor group). In the legend, full, striped, and empty circles represent the studied EE, EX, and XX conjugation paths, respectively, whereas in parentheses are displayed the neighbor paths.

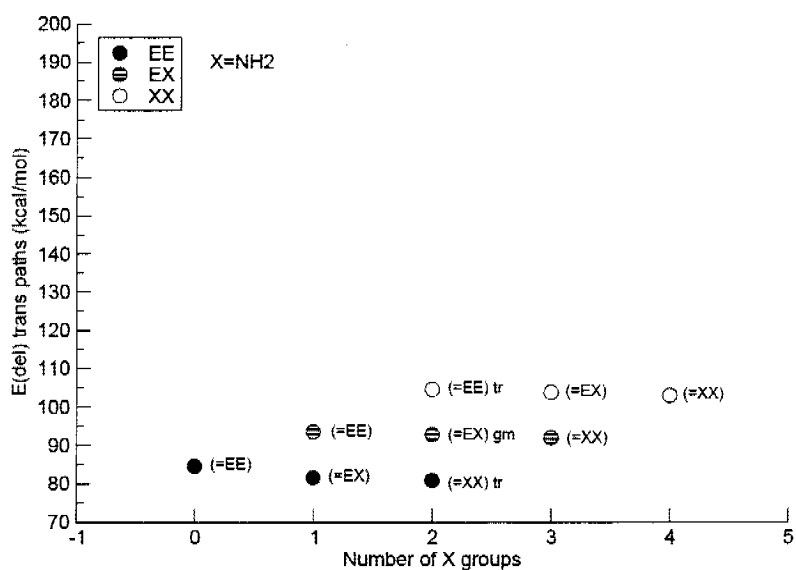


Figure 4.14: The trans delocalization energies for all of the $\text{TEE}-n\text{NH}_2$, $n = 0-4$ (donor group). In the legend, full, striped, and empty circles represent the studied EE, EX, and XX conjugation paths, respectively, whereas in parentheses are displayed the neighbor paths.

In Figure 4.9-14 we present the delocalization energies calculated for the *trans* paths of the same set of compounds. As also shown in Table 4.2, these results are similar to those obtained for the *geminal* pathways. In fact, for the acceptors, the energy splittings EX-EE, XX-EE, and XX-EX are in the range 11-16, 21-32, and 10-16 kcal mol⁻¹ for the mono-, di-, and tri-substituted systems, respectively. For the donors the same delocalization energy differences are 36 kcal mol⁻¹ for TEE-OH and TEE-OCH₃ mono-substituted, about 70 kcal mol⁻¹ for the di-substituted compounds, and about 34 kcal mol⁻¹ for the tri-substituted ones. TEE-*n*NH₂ show very small delocalization energy splitting, i.e. 12, 24, and 12 kcal mol⁻¹ for *n*=1, 2, and 3, respectively.

These data show three different aspects. First, the delocalization energies in the TEEs substituted with donors are much larger than those in the TEEs with acceptors for both *trans* and *geminal* pathways. The analysis of the SOIE data show that this is due to the interactions between the π_T^* of the backbone (TEE) and the lone pairs of the donors. This interaction is much stronger than the one of the $\pi_{D(T)}$ of the acceptors with the π_T^* of the backbone. This is consistent with the fact that the electronic population which moves from the lone pairs of the substituents to the π_T^* of the backbone is much larger than the charge which moves from the $\pi_{D(T)}$ (of the substituents) into the π_T^* of the backbone. Second, each substituent shows a different strength. In the case of the acceptor groups, the largest splitting is observed for the CN group, whereas the weakest delocalization energy differences between paths are found for CHO in all cases (*geminal*, *trans*). This indicates that the CN substituent is the strongest among the three acceptors considered here, promoting π -electron delocalization in TEE most effectively. For the donors (Figure 4.12, and Figure 4.13), there is not much difference in delocalization energies for the TEE-*n*OH and TEE-*n*OCH₃. Both of the two groups intensively enhance π -electron delocalization in TEE. Here NH₂ turns out to be a very weak π -donor also showing some acceptor character. Third, we note that in the acceptor-substituted TEE, the *geminal* paths are always more favorable by a few kcal mol⁻¹ than the *trans* ones, whereas in the donor-substituted TEE, the *trans* paths are preferred by 1-2 kcal mol⁻¹ with no exception. This peculiar behaviour of the acceptor-substituted TEE can be explained by the donor character of the neighbor ethynyl units, which in the *geminal* path are always in *trans* to the acceptor groups.

In summary, for the class of compounds studied here, the delocalization is determined by the type of substituent (donor versus acceptor), whereas the type of path considered (*through* versus *cross*) has a minor influence only.

Impact of Degree of Substitution

The analysis of Figure 4.3-14 reveals two more distinct trends. First, we see a significant increase of E_{deloc} when increasing the number of substituents in a *conjugation* path (“direct trend”). Second, we observe only a small variation of E_{deloc} when increasing the number of substituents in the *neighbor* path (“indirect trend”). In both cases, the best *geminal* and *trans* paths are always the XX paths, independently of the type of neighbor and of the type of substituents, i.e. donor or acceptor. In the XX paths the interactions between the substituents and the π^*_T of the backbone are doubled, thus strongly enhancing delocalization. For example, the delocalization energies of the *geminal* EE and EX paths of the TEE-OH are 86 and 122 kcal mol⁻¹, respectively. The contribution of the lone pair interacting with the π^*_T of TEE amounts to 37 kcal mol⁻¹ which accounts for most of the difference between the two conjugation paths. In the case of *geminal* TEE-2OH we observe similar numbers for the EE path (88 kcal mol⁻¹), and a very strong delocalization for the XX path (158 kcal mol⁻¹), which is dominated by the interactions between the lone pairs of the X groups and the π^*_T of the backbone (74 kcal mol⁻¹). In summary, the higher the number of substituents in a path, the larger is the corresponding delocalization energy.

By a more detailed analysis of the data presented in Table 4.3, we observe that in the acceptor case the energy difference of the *geminal* paths for the direct trend is 23 kcal mol⁻¹ on average for NO₂, 22 kcal mol⁻¹ for CHO, and 35 kcal mol⁻¹ for CN, whereas in the indirect trend the difference is 7, 2, and 1 kcal mol⁻¹ for NO₂, CHO, and CN, respectively. In the donor case, the energy variation in the direct trend is on average 74 and 73 kcal mol⁻¹ for OH and OCH₃, and 17 kcal mol⁻¹ for NH₂, whereas in the indirect trend it is 6 kcal mol⁻¹ for OH and OCH₃, and 2 kcal mol⁻¹ for NH₂. These data show that for a given conjugation path the neighborhood effects are small with respect to the substituent effects. In the case of the *trans* paths we observe similar numbers, however for the direct trend the *trans* paths are slightly

disfavored for TEE with acceptors, and slightly favored for TEE with donors, whereas in the indirect trend the *geminal* paths are always favored with the only exception of TEE-*n*CN. Thus, in TEE (as backbone) the π -delocalization in the *geminal* or *trans* path is enhanced by attaching donor groups rather than acceptor ones.

Table 4.3: The energy differences (in kcal mol⁻¹) in the direct and indirect trends calculated at the B3LYP/cc-pVDZ level for TEE-*n*X with *n* = 0-4. The degree of substitution *n* is shown in parenthesis in the first column

Energy Differences	Acceptors			Donors		
	NO ₂	CHO	CN	OH	OCH ₃	NH ₂
Direct Trend						
<i>Geminal</i>						
XX(2) – EE(0)	25	22	34	76	76	19
XX(3) – EE(1)	24	23	36	74	74	10
XX(4) – EE(2)	21	22	36	71	69	21
<i>Trans</i>						
XX(2) – EE(0)	20	20	32	76	75	20
XX(3) – EE(1)	21	21	35	73	75	22
XX(4) – EE(2)	20	21	35	73	72	22
Indirect Trend						
<i>Geminal</i>						
EE(2) – EE(0)	-5	-3	-1	8	9	-3
EX(3) – EX(1)	-6	-2	1	6	7	-1
XX(4) – XX(2)	-9	-2	1	3	2	-1
<i>Trans</i>						
EE(2) – EE(0)	-4	-2	0.1	5	6	-4
EX(3) – EX(1)	-3	-0.4	3	5	6	-2
XX(4) – XX(2)	-4	-0.2	4	3	3	-2

NH₂ represents a particular case. As known from the literature [46], and from our own study, this substituent behaves as a π -donor when attached to a phenyl group. Comparing the results obtained for our series of TEEs substituted with both donor and acceptor groups and TEE-*n*NH₂, it seems that the latter behaves more similarly to the acceptor groups rather than to the donor ones. By means of the SOIEs, it can be noted that the NH₂ is indeed a donor, but rather than being a π -donor, like in the case of Ph-NH₂, it is a σ -donor when attached to TEE.

Finally, we conclude from the data collected in Table 4.3, that the indirect trend - albeit small - consistently favors a less substituted neighbor path for the acceptor case and a more substituted neighbor path for the donor one. The only exceptions are CN and NH₂.

In summary, for the acceptor as well as for the donor substituted TEEs (Figure 4.3-14) we observe a strong dependence of the delocalization energy on the degree of substitution, and on the type of substituents attached (donors vs. acceptors). Somewhat surprisingly, the delocalization energy depends much less on the type of paths, i.e. *trans* vs. *geminal*. The impact of the neighboring path is clearly visible, but also much less pronounced.

4.1.5 Conclusions

A major focus of the present work was to validate our method of computing delocalization energies as presented in Chapter 2 [16] by means of the second-order orbital interaction energies (SOIE) approach. The study shows that the deletion energies, which represent the delocalization energy compare rather well with the second-order perturbation energies, both depicting the non-Lewis contribution to the total energy of the systems considered. The main advantage of the SOIE approach is that it offers higher depth of analysis allowing to identify the contributions to delocalization energies. However, in presence of very strong conjugation, higher-order perturbative corrections cannot be any longer neglected, therefore, the deletion approach becomes quantitatively more accurate.

To illustrate the capabilities of the method, an extensive study of mono-, di-, tri-, and tetra-donor/acceptor substituted TEEs was performed. We compared distinct conjugation paths, i.e. *geminal* (*cross*) or *trans* (*through*), within the same molecule. We also analyzed the effect of

each substituent on the TEE as backbone, and the impact of neighbor paths. From this analysis, we observed first that the delocalization is strongly dependent on the nature of the substituent (donor vs. acceptor) rather than on the type of path considered (*through* vs. *cross*). Second, we have found that the conjugation energy in a selected path is enhanced with increasing degree of substitution. In fact, the best *geminal* and *trans* paths are always the XX paths (X = donor or acceptor), regardless of the neighborhood. This is due to a strong contribution of the substituents into the π^*_T orbitals of the backbone, which is in general much larger with the donors than with the acceptors.

In this application of our approach we were restricting ourselves to model molecules because our goal mainly was to test our novel approach by showing that deletion energies and second-order orbital interaction energies can be used complementary to “measure” the delocalization energy in conjugated systems. By means of this method, we are able to understand why certain paths favor conjugation more than others. We are also able to quantify the effect of substituents on a backbone, and therefore, to predict how to enhance conjugation (π or σ) in a specific path.

4.2 Extended Systems: *Through* versus *Cross* Electron Delocalization in Polytriacetylene Oligomers

4.2.1 Summary

In this subchapter we report on a detailed theoretical investigation of the molecular and electronic properties of unsubstituted polytriacetylene (PTA) and *iso*-polytriacetylene (*iso*-PTA) oligomers, which are characterized by *through* and *cross* π -conjugation pathways, respectively. The goal of the study is the comparison of *through* versus *cross*-conjugation on the basis of the computed molecular geometries of the neutral, anionic, and cationic species, electron affinities, ionization potentials, excitation energies, and nonlinear optical properties for oligomers up to the nonamer. Differences in the effective conjugation length are directly related to electron delocalization in *cross*- and *through*-conjugated pathways.

As in the *through*-conjugated oligomers, i.e. the PTAs, the frontier orbitals of the *iso*-PTA oligomers are delocalized along the entire carbon backbone, suggesting that π -delocalization can extend through *cross*-linked carbon atoms. However, contrary to the PTA oligomers, the bond lengths remain strictly constant and the reduction of the energy gap beyond the trimer is completely due to the correlation contribution. On the other hand, in the anions and cations the bond lengths change significantly with increasing chain length. Therefore, oxidation or reduction of the *iso*-PTA oligomer appears to switch on delocalization through *cross*-linked carbon atoms.

4.2.2 Introduction

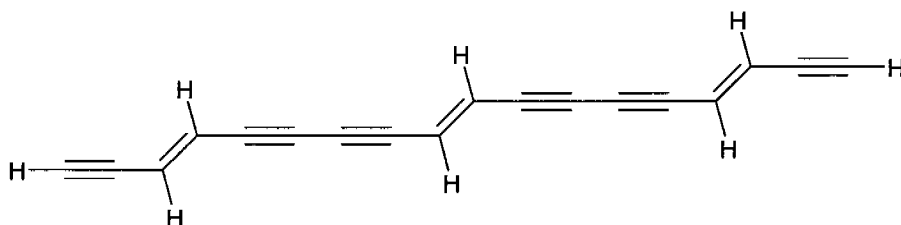
Polytriacyetylene [PTAs, $-(\text{C}\equiv\text{C}-\text{CR}=\text{CR}-\text{C}\equiv\text{C})_n-$] [17, 19, 47-52] and *iso*-polytriacyetylene [*iso*-PTAs, $-(\text{C}\equiv\text{C}-(\text{C}=\text{CR}_2)-\text{C}\equiv\text{C})_n-$] [27, 53-57] represent an example of π -conjugated polymers with potential application in the field of molecular electronics and photonics, due to their easy of processing and to the possibility of tailoring materials characteristics to suit a desired property. PTA and *iso*-PTA (Figure 4.15) are formed with the building blocks *trans*-diethynylethene [(E)-hex-3-ene-1,5-diyne] (hereafter referred to as t-DEE), and *geminal*-diethynylethene [3-ethynyl-but-3-ene-1-yne] (hereafter referred to as g-DEE), which molecular and electronic properties have been investigated in the previous chapter (see subchapter 3.2).

In this subchapter the investigation is extended to PTA and *iso*-PTA oligomers of increasing chain length. For that matter, it is important to understand how π -electron delocalization can extend along different pathways (*through*, *cross*), and how the extension of π -conjugation affects molecular and electronic properties such as bond length alternation, electron affinity, ionization potential, maximum absorption wavelength, and second-order hyperpolarizability. A critical parameter, in this respect, is the effective conjugation length (ECL), i.e. the length of the oligomer for which the property under consideration has converged to a limited value. The π -delocalization in the *cross*-conjugated compounds can be switched on and off at the *cross*-linked carbon atom depending on whether the ECL is reached or not.

Monodisperse PTA and *iso*-PTA oligomers of precisely defined length have recently been synthesized and characterized with regard to their structural, electronic, and optical properties [16-27, 56].

iso-PTAs are isomers of PTA characterized by a *cross* π -conjugated pathway (see Figure 4.15). Whereas the PTAs were the topic of a number of theoretical studies [47, 51], the *iso*-PTAs, so far, have not been explored computationally and relatively little is known about electron communication via *cross*-conjugation in general. The interest for these compounds is enhanced by the fact that this form of conjugation has only sparsely been considered in materials research. *Cross*-conjugated compounds could provide materials with significant transparency in the visible region potentially useful for application in molecular scale electronics.

a)



b)

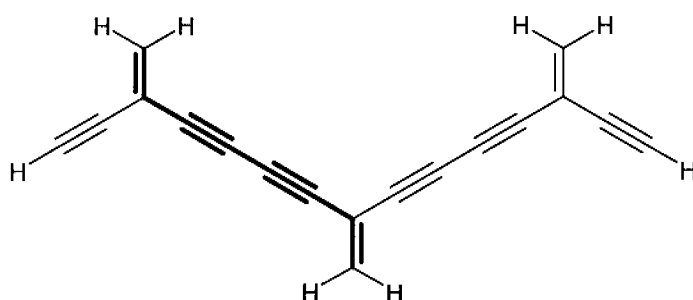


Figure 4.15: Schematic representation of the PTA (a) and *iso*-PTA (b) trimers. The longest linearly conjugated segment in the *iso*-PTA oligomers is shown in bold.

For π -conjugated polymers it is well known that there is a strong relationship between the structure and the electronic properties [58, 59]. According to Peierls [60], the band gap E_g of polyacetylene (PA) is directly proportional to the bond length alternation (BLA; hereafter referred also as ΔR), defined as the difference between long (C–C) and short (C=C) bonds:

$$E_g = k\Delta R \quad (4.1)$$

Ovchinnikov *et al.* [61] suggested that the inclusion of an electron correlation correction term (Δ_{correl}) in the Peierls expression results in more accurate prediction of E_g :

$$E_g = [(k\Delta R)^2 + \Delta_{correl}^2]^{1/2} \quad (4.2)$$

Kertesz *et al.* [62] have shown that for the PAs the correlation correction term is indeed very significant, and its inclusion leads to a better correlation between structure and properties. The same authors also showed that the value of k computed from Eq. 4.2 can be used to compare electron delocalization in different classes of conjugated systems [63].

Among the computational methods that include electron correlation, DFT and MP2 theories are the only ones which match high accuracy with acceptable computational cost for molecular systems composed of several tens of atoms. The numerous theoretical studies on PA and polydiacetylene (PDA) oligomers have shown that the DFT and MP2 levels of theory predict the geometrical parameters of π -conjugated compounds with good accuracy [62]. This also applies for the PTA and *iso*-PTA monomers studied in the previous Chapter [16]. Suhai has recently investigated the BLA of oligomers of PA using different exchange-correlation functionals [64] showing that hybrid functionals give results that are in reasonable agreement with experiment. In the section ‘Results and Discussion’ we first present a detailed comparison of the molecular geometries of the PTA and *iso*-PTA oligomers as a function of the chain length. The molecular and electronic structure of the negatively and positively charged oligomers are then analyzed in order to understand how the addition or the removal of an electron affects the extension of delocalization in different (*through* and *cross*) π -conjugation pathways. We will also discuss the computed values of electronic properties such as electron affinities, ionization potentials, electronic excitation energies, and second-order hyperpolarizabilities, for which the evolution as function of the chain length can be correlated with the extension of delocalization. Finally, our approach for the analysis of electron

delocalization is applied to the PTA and *iso*-PTA oligomers in order to find general correlations between molecular and electronic observables and the electronic structure.

4.2.3 Computational Methods

The full geometry optimizations of the neutral PTA and *iso*-PTA oligomers were performed using Density Functional Theory (DFT) and *ab initio* approaches. In the *ab initio* calculations, performed from the monomer (C_6H_4) up to the hexamer ($C_{36}H_{14}$), the electron correlation was taken into account using second-order Møller-Plesset (MP2) perturbation theory with the 6-31G(d,p) basis set of Gaussian orbitals [65]. For the DFT calculations, performed for the monomer (C_6H_4) up to the nonamer ($C_{54}H_{20}$), the B3LYP hybrid functional [41, 66, 67], consisting of the Becke's three parameters exchange functional [68, 69] and the Lee-Yang-Parr correlation functional [42] was used together with the same basis set. All the geometry optimizations were performed in the C_{2h} symmetry for the PTA oligomers, and C_{2h} or C_{2v} symmetry for the *iso*-PTA oligomers. In order to match sufficient accuracy for the geometrical parameters, a convergence threshold of 5.0×10^{-5} Hartree Bohr⁻¹ or Hartree Rad⁻¹ was adopted.

A full vibrational analysis of the shorter oligomers, up to the tetramer, characterized the optimized geometries as genuine minima on the potential energy surface. The geometry optimization of the cationic and anionic species, from the monomer to the nonamer was performed at the B3LYP/6-31G(d,p) level of theory. In the case of the cations, all geometry optimizations were computed in the C_{2h} or C_{2v} symmetry. For the anions, the planar arrangement of the monomers and dimers was characterized by the vibrational analysis to represent a stationary point with two imaginary frequencies corresponding to a symmetric and asymmetric out-of-plane bends of the terminal hydrogens. Following these vibrational modes, two genuine minima on the potential energy surfaces were found; the first in the C_i symmetry (asymmetric bent) and the second in the C_2 symmetry (symmetric bent) with an energy difference less than 0.1 kcal mol⁻¹. For the trimer and tetramer, the planar structure was shown by the vibrational analysis to be a genuine minimum.

The adiabatic EAs and IPs were calculated at the BHandHLYP/6-31+G(d,p) level of theory using the geometries optimized at the B3LYP/6-31G(d,p) level. Because of the addition of diffuse functions caused linear dependency in the basis set, due to the large overlap of basis functions centered on the acetylenic carbon atoms, the C \equiv C system was described a set of diffuse basis functions added only at the centre of the acetylenic bonds. It should be noted that in a recent review Schaefer et al. [70] showed, for a very large set of molecules, that the B3LYP functional gives the best agreement between computed and experimental EAs. However, they also showed that in the case of electron detachment from an open-shell anion to a closed-shell neutral species, as for the PTA and *iso*-PTA oligomers, B3LYP always significantly overestimates the EAs, whereas the BHandHLYP functional is in closer agreement with the experiment. In addition, we found that the B3LYP/6-31G(d,p)//BHandHLYP/6-31+G(d,p) level of theory gives the best agreement between computed and experimental EAs for a series of nitro-aromatic compounds (data not shown).

The linear optical absorption properties were computed from the monomer to the nonamer using the ZINDO/S level of theory [71-78], and from the monomer to the hexamer using the time-dependent DFT approach [79-81] with the BHandHLYP functional and the 6-31G(d) basis set. For the ZINDO calculations, all occupied and virtual orbitals were retained in the active space.

The second-order hyperpolarizabilities were computed from the monomer to the nonamer on the B3LYP geometries using the coupled-perturbed (CP) approach [82] and the MNDO Hamiltonian [83]. All calculations were performed with the Gaussian98 suite of programs [44], with the exception of the second-order hyperpolarizabilities for which the program MOPAC2000 was used [84].

4.2.4 Results and Discussion

Extension of definition of bond length alternation (δR)

PTA and *iso*-PTA contain alternating double, single, as well as triple bonds (see Figure 4.15). The traditional definition of the BLA needs to be extended. For this purpose, we introduce a generalized parameter δR defined as:

$$\delta R = (C_D - C_T + C_T - C_T)/2 - (C=C + C\equiv C)/2 \quad (4.3)$$

where $C_D - C_T$ and $C_T - C_T$ are the single bond lengths flanked by either a double and a triple bond or two triple bonds; $C=C$ and $C\equiv C$ are the double and triple bond lengths, respectively. For both *cross*- and *through*-conjugated compounds the single bonds shorten with the extension of the oligomer size, whereas the double and the triple bonds lengthen.

Molecular and electronic structure of neutral species

As expected, for the PTA oligomers (B3LYP/6-31G(d,p) level of theory) we observe a lengthening of the double and triple bonds by 0.013 and 0.015 Å, along with a shortening of the single bonds by 0.017 Å. MP2 theory predicts similar changes in the bond lengths; the $C=C$, $C-C$, and $C\equiv C$ bond lengths change by 0.010, 0.015 and 0.015 Å, respectively. From Figure 4.6, in which δR is plotted against the oligomer size (see also Table 4.4 and Table 4.5), we see that the ECL is reached at the octamer ($n = 8$; 24 conjugated bonds). For the PTA polymer of infinite length^a δR is equal to 0.078 and 0.079 Å at the B3LYP and MP2 levels of theory, respectively [85]. The same ECL was also found for the PDA oligomers^b. This value is slightly lower than that predicted experimentally on the basis of the saturation of electronic observables (maximum absorption wavelength and second-order hyperpolarizabilities) [47].

For the *cross*-conjugated oligomers, one certainly expects an extension of the linear π -conjugation pathway when going from the monomer to the dimer, and therefore, a reduction of the $C-C$ bonds and an elongation of the $C=C$ and $C\equiv C$ bonds. In fact, the $C=C$ and $C\equiv C$ bonds lengthen by about 0.003 and 0.010 Å, respectively, whereas the $C-C$ bonds shorten by about 0.007 Å. In the case of the *iso*-PTAs beyond the dimer, π -conjugation needs to go past one or several *cross*-linked carbon atoms (Figure 4.15b). Therefore, a reduction of the δR relative to the value of the dimer would actually suggest that *cross*-linked carbon atoms do promote π -delocalization. However, the results show that for the *iso*-PTA trimer, the $C-C$ and $C\equiv C$ bond lengths do not change significantly. This suggests that π -delocalization is switched off at the *cross*-linked carbon atom. The $C=C$ bond length still increases slightly when going from dimer to the trimer. This elongation can be explained by the fact that in the trimer this particular bond is involved in two different linear π -conjugation paths (Figure 4.15).

^a The single-double and single-triple BLAs for PTA of infinite chain length are extrapolated using the function $a/[1+b*\exp(-c/N)]$ as reported in Ref. [85].

^b We also performed the geometry optimizations of the PDA and *iso*-PDA oligomers from the monomer (C_6H_4) to the dodecamer ($C_{50}H_{26}$) and we calculated the BLAs (see next subchapter).

The extension of the oligomer size beyond the trimer has no effect on the bond lengths, and the δR is readily extrapolated for a polymer of infinite chain length to amount to 0.106 and 0.100 Å at the B3LYP and MP2 levels of theory, respectively.

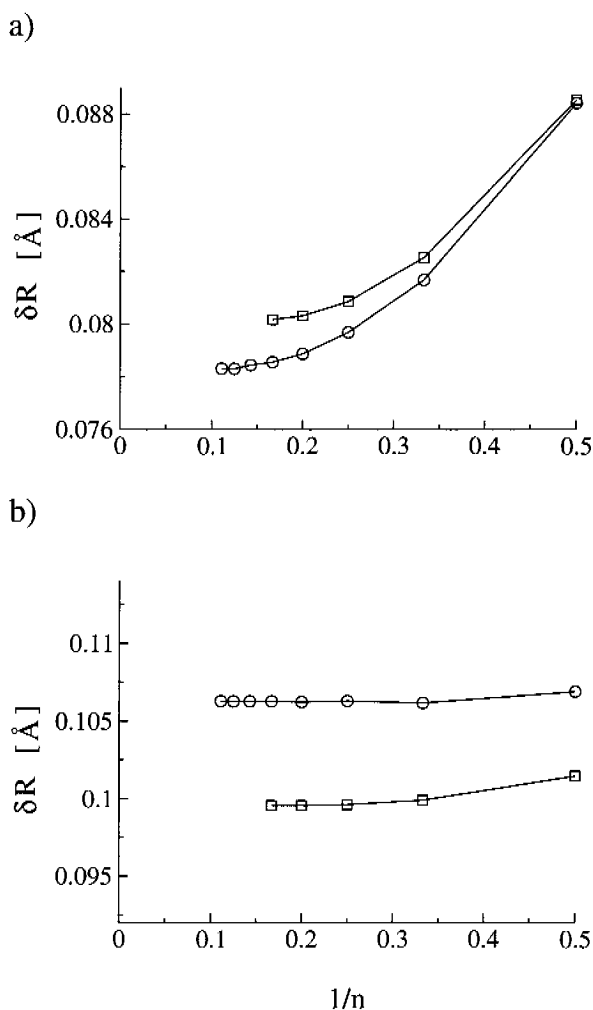


Figure 4.16: δR alternation parameter of PTA (a) and iso-PTA (b) oligomers as function of the reciprocal number of monomer units ($1/n$) at the B3LYP/6-31G(d,p) (□) and MP2/6-31G(d,p) (○) levels of theory. The alternation parameter has been calculated using the central bond lengths.

Table 4.4: The C=C, C_i-C_i,^a C≡C, and C_e-C_e,^a bond lengths (central / terminal) of the PTA oligomers at different levels of theory

	B3LYP/6-31G(d,p)					MP2/6-31G(d,p)				
	C=C	C _i -C _i ^a	C≡C	C _e -C _e ^a	δR	C=C	C _i -C _i ^a	C≡C	C _e -C _e ^a	δR
C ₆ H ₄	1.354	1.417	1.212	---	---	1.355	1.423	1.224	---	---
C ₁₂ H ₆	1.359	1.406/ 1.415	1.225/ 1.212	1.354	0.0884	1.359	1.413/ 1.420	1.236/ 1.225	1.360	0.0885
C ₁₈ H ₈	1.365/ 1.360	1.402/ 1.414	1.226/ 1.212	1.353	0.0817	1.364/ 1.359	1.409/ 1.420	1.238/ 1.225	1.358	0.0825
C ₂₄ H ₁₀	1.366/ 1.356	1.401/ 1.414	1.227/ 1.212	1.351/ 1.353	0.0797	1.365/ 1.359	1.408/ 1.420	1.238/ 1.225	1.357/ 1.358	0.0809
C ₃₀ H ₁₂	1.367/ 1.356	1.400/ 1.414	1.227/ 1.212	1.351/ 1.353	0.0789	1.365/ 1.359	1.408/ 1.420	1.239/ 1.225	1.356/ 1.358	0.0803
C ₃₆ H ₁₄	1.367/ 1.360	1.400/ 1.414	1.227/ 1.212	1.351/ 1.353	0.0786	1.365/ 1.359	1.408/ 1.420	1.239/ 1.225	1.356/ 1.358	0.0802
C ₄₂ H ₁₆	1.367/ 1.360	1.400/ 1.414	1.227/ 1.212	1.351/ 1.353	0.0784					
C ₄₈ H ₁₈	1.367/ 1.360	1.400/ 1.414	1.227/ 1.212	1.351/ 1.353	0.0783					
C ₅₄ H ₂₀	1.367/ 1.360	1.400/ 1.414	1.227/ 1.212	1.351/ 1.353	0.0783					

a) C_i-C_i and C_e-C_e are the single bonds flanked by either a double and a triple bond or by two triple bonds.

Table 4.5: The C=C, C_i-C_i^a, C≡C, and C_e-C_e^a bond lengths (central / terminal) of the iso-PTA oligomers at different levels of theory

	B3LYP/6-31G(d,p)					MP2/6-31G(d,p)				
	C=C	C _i -C _i ^a	C≡C	C _e -C _e ^a	δR	C=C	C _i -C _i ^a	C≡C	C _e -C _e ^a	δR
C ₁₂ H ₆	1.353	1.428/ 1.436	1.220/ 1.209	1.359	0.1062	1.355	1.429/ 1.436	1.234/ 1.223	1.362	0.1014
C ₁₈ H ₈	1.356/ 1.353	1.429/ 1.436	1.220/ 1.209	1.359	0.1063	1.357/ 1.355	1.429/ 1.436	1.234/ 1.223	1.362	0.0999
C ₂₄ H ₁₀	1.356/ 1.353	1.429/ 1.436	1.220/ 1.209	1.359/ 1.359	0.1062	1.357/ 1.355	1.429/ 1.436	1.234/ 1.223	1.361/ 1.362	0.0996
C ₃₀ H ₁₂	1.356/ 1.353	1.429/ 1.436	1.220/ 1.209	1.359/ 1.359	0.1063	1.357/ 1.355	1.429/ 1.436	1.234/ 1.223	1.362/ 1.362	0.0996
C ₃₆ H ₁₄	1.356/ 1.353	1.429/ 1.436	1.220/ 1.209	1.359/ 1.359	0.1063	1.357/ 1.355	1.429/ 1.436	1.234/ 1.223	1.362/ 1.362	0.0996
C ₄₂ H ₁₆	1.356/ 1.353	1.429/ 1.436	1.220/ 1.209	1.359/ 1.359	0.1063	1.357/ 1.355	1.429/ 1.436	1.234/ 1.223	1.362/ 1.362	0.0996
C ₄₈ H ₁₈	1.356/ 1.353	1.429/ 1.436	1.220/ 1.209	1.359/ 1.353	0.1063					
C ₅₄ H ₂₀	1.356/ 1.353	1.429/ 1.436	1.220/ 1.209	1.359/ 1.359	0.1063					

a) C_i-C_i and C_e-C_e are the single bonds flanked by either a double and a triple bond or by two triple bonds.

The extrapolated δR for the *cross*-conjugated polymer is thus significantly larger than that calculated for the *through*-conjugated compound. The larger δR values of *iso*-PTA are mainly due to the difference between the PTA and *iso*-PTA C–C bonds. In the section 3.2 [16] we showed that the elongation of the C–C bond in the *cross*-conjugated monomer (g-DEE) with respect to the *through* one (t-DEE) is not only due to vertical π -conjugation, but also to in-plane hyperconjugation. We therefore suggested that the δR of the *iso*-PTA can be modulated by a specific σ -donor or σ -acceptor substituent bound to the carbon atom of the double bond.

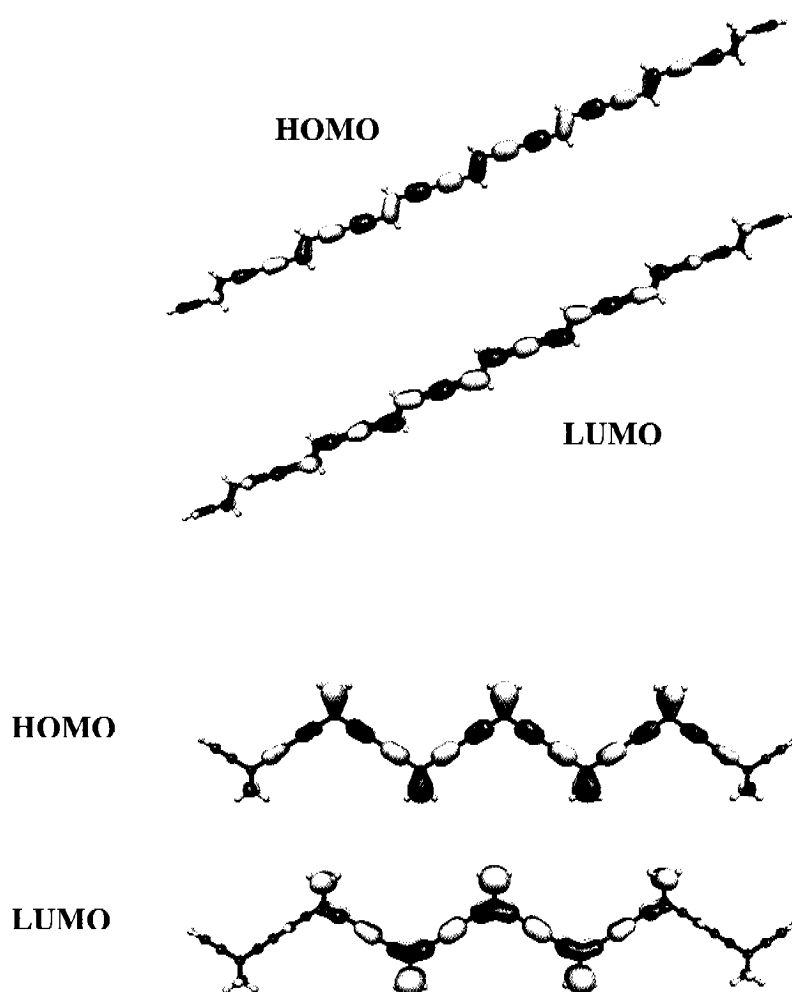


Figure 4.17: Highest occupied (HOMO) and lowest unoccupied (LUMO) molecular orbitals of the PTA and *iso*-PTA heptamers.

The frontier orbitals of the PTA and the *iso*-PTA heptamers are shown in Figure 4.17. The HOMO and LUMO of both compounds are delocalized over the entire carbon backbone. Even though δR has converged, the orbital energies, as well as the HOMO-LUMO energy gaps are still changing significantly (see Figure 4.18a).

In *iso*-PTA the reduction of the HOMO-LUMO gap is less pronounced. Using the expression of Ovchinnikov [see also the footnote (a)] (Equation 4.2), we find – somewhat surprisingly – that the values of k for PTA and *iso*-PTA oligomers are very similar.

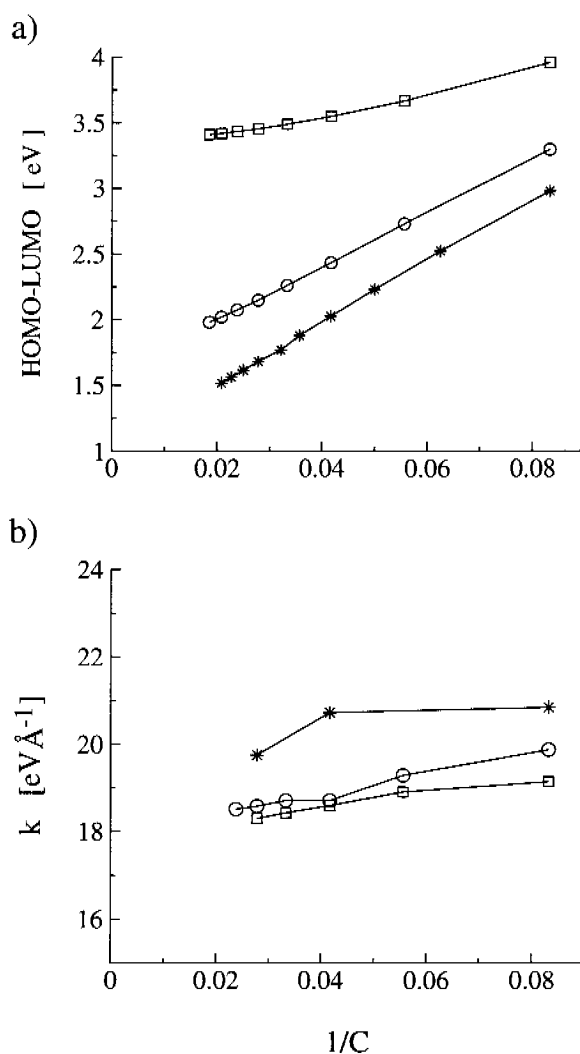


Figure 4.18: a) HOMO-LUMO energy gap of PTA (\square), *iso*-PTA (\circ) and PA ($*$) oligomers computed at the B3LYP/6-31G(d,p) level of theory as function of the reciprocal number of carbon atoms ($1/C$). b) k values of PTA, *iso*-PTA and PA oligomers computing using Equation 4.2 as function of the reciprocal number of carbon atoms ($1/C$).

^a Equation 2 was applied considering two energy gaps with the corresponding δR under the assumption that the correlation parameter Δ_{correl} is independent from the alternation parameter δR . The two energy gaps were taken from the B3LYP/6-31G(d,p)//B3LYP/6-31G(d,p) and BLYP/6-31G(d,p)//BLYP/6-31G(d,p) levels of theory (see also Ref. [62] and [63]).

The k slightly decreases with increasing oligomer size and finally approach a value of about $18 \text{ eV } \text{\AA}^{-1}$ for a polymer of infinite length. The fact that k is the same for both compounds indicates that the change in the energy gap is due to the correlation correction term (Δ_{correl}). Equation 4.2 tells us that all changes in E_g after convergence of δR are due to electron correlation effects. Whereas in *cross iso*-PTA the Peierls contribution to E_g has exhausted beyond the trimer, in the *through*-conjugated compounds this term still contributes to the energy gap.

Molecular and electronic structure of ionic species

The structures of the PTA and the *iso*-PTA anions are different from the ones computed for the neutral oligomers. They are both strongly cumulenic, with a drastic elongation of the C=C and C \equiv C bonds and a contraction of the C-C bonds (see Table 4.6 and Table 4.7).

For the PTA oligomers, the largest differences in the bond lengths between the anionic and neutral species are in the centre of the molecule and decrease towards the terminal bonds. Interestingly, the length of the central C=C bond is larger than that of any of the C-C bonds (Figure 4.19).

For the *iso*-PTA oligomers we find that the anion of the dimer has a structure only slightly less cumulenic than that of the corresponding *through*-conjugated compound, which can be explained by the similar length of the π -conjugation pathway. It is worth to note that by increasing the oligomer size all bond lengths of the various linearly conjugated segments are affected, suggesting that the additional electronic charge is delocalized over the entire *cross*-conjugated backbone. However, we observe that the larger the size of the oligomers, the smaller are the changes in geometry with respect to the neutral systems. Comparing the neutral oligomers with the corresponding anions, the variation of δR in the monomers amounts to 0.078 \AA , whereas in the nonamers it is reduced to 0.007 \AA . The structure of the PTA and *iso*-PTA cations is similar to that of the anions. Again, the removal of one electron from the neutral species leads to strongly cumulenic geometries. As shown in Figure 4.19, the effect of the ionization on the C=C and C \equiv C bonds is smaller than that observed for the anions. On the other hand, the C-C bond lengths of both charged species are very similar. A comparison of the δR of the neutral compounds with the cations shows that the changes in

geometry are larger for the monomers, i.e. 0.063 Å for *iso*-PTA and 0.067 Å for PTA, and reduce to 0.005 and 0.020 Å for *cross*- and *through*-conjugated nonamers, respectively. However, for the infinite chain size, we do not obtain convergence of the bond lengths for the PTAs, whereas it appears that we are close to converged values for the *iso*-PTAs.

The analysis of the spin density shows that in the PTA oligomers the spin for the anions as well as for the cations is highly delocalized. As expected, the spin is distributed over alternating carbon atoms. It is worth to note that the spin distribution of cations and anions is very similar for the *through*- and *cross*-conjugated compounds.

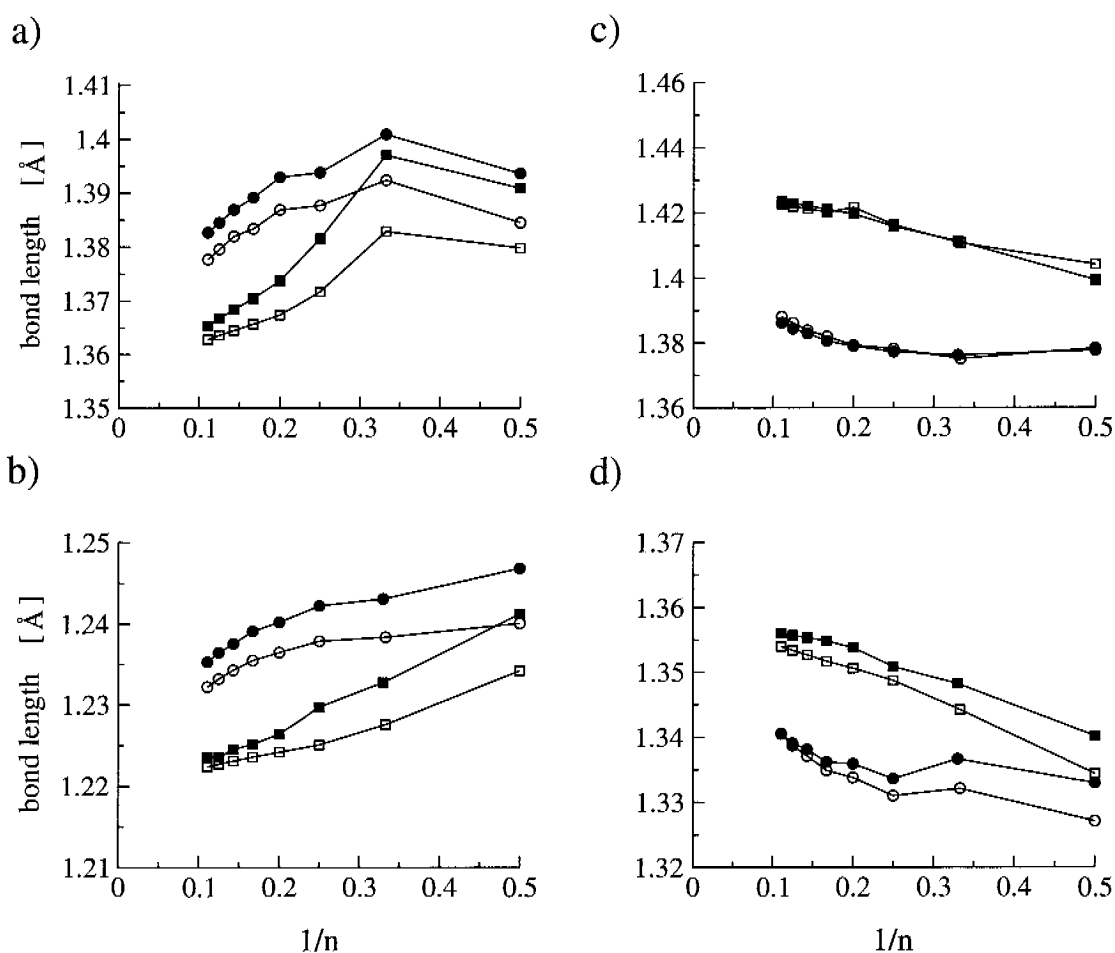


Figure 4.19: Evolution of the central (a) C=C, (b) C≡C, (c) C_D-C_T , and (d) C_T-C_T bond lengths of the PTA anions (●), *iso*-PTA anions (■), PTA cations (○), and *iso*-PTA cations (□) as function of the reciprocal number of monomer units ($1/n$) at the B3LYP/6-31G(d,p) level of theory.

Table 4.6: The C=C, C_I-C_I^a, C≡C, and C_e-C_e^a bond lengths (central / terminal) of the PTA and *iso*-PTA anion oligomers at the B3LYP/6-31G(d,p) level of theory. The values with the largest difference with respect to the neutral species are displayed in bold. For the largest *iso*-PTA oligomers the non central longest and shortest bond lengths are also reported

	PTA				<i>iso</i> -PTA			
	C=C	C _I -C _I ^a	C≡C	C _e -C _e ^a	C=C	C _I -C _I ^a	C≡C	C _e -C _e ^a
C ₆ H ₄	1.426	1.390	1.234	---	1.430	1.410	1.237	---
C ₁₂ H ₆	1.394	1.378/ 1.404	1.247/ 1.222	1.333	1.391	1.399/ 1.437	1.241/ 1.214	1.340
C ₁₈ H ₈	1.401/ 1.379	1.376/ 1.409	1.243/ 1.218	1.337	1.397/ 1.370	1.411/ 1.439	1.233/ 1.212	1.348
C ₂₄ H ₁₀	1.394/ 1.372	1.377/ 1.412	1.242/ 1.216	1.334/ 1.341	1.382/ 1.364	1.416/ 1.439	1.230/ 1.211	1.351/ 1.352
C ₃₀ H ₁₂	1.393/ 1.368	1.379/ 1.413	1.240/ 1.215	1.336/ 1.345	1.373/1.374/ 1.361	1.421/1.420/ 1.438	1.226/1.226/ 1.210	1.354/ 1.354
C ₃₆ H ₁₄	1.389/ 1.365	1.381/ 1.414	1.239/ 1.214	1.336/ 1.347	1.369/1.371/ 1.360	1.424/1.421/ 1.438	1.224/1.225/ 1.210	1.356/ 1.355
C ₄₂ H ₁₆	1.387/ 1.364	1.383/ 1.414	1.238/ 1.214	1.338/ 1.348	1.365/1.368/ 1.359	1.425/1.422/ 1.438	1.224/1.225/ 1.210	1.357/ 1.356
C ₄₈ H ₁₈	1.385/ 1.363	1.384/ 1.414	1.237/ 1.213	1.339/ 1.349	1.364/1.367/ 1.358	1.426/1.423/ 1.438	1.223/1.224/ 1.210	1.357/ 1.356
C ₅₄ H ₂₀	1.383/ 1.362	1.386/ 1.414	1.235/ 1.213	1.341/ 1.350	1.362/1.365/ 1.357	1.426/1.423/ 1.438	1.222/1.223/ 1.210	1.357/ 1.356

a) C_I-C_I and C_e-C_e are the single bonds flanked by either a double and a triple bond or by two triple bonds.

Table 4.7: The C=C, C_i-C_i^a, C≡C, and C_e-C_e^a bond lengths (central / terminal) of the PTA and *iso*-PTA cation oligomers at the B3LYP/6-31G(d,p) level of theory. The values with the largest difference with respect to the neutral species are displayed in bold. For the largest *iso*-PTA oligomers the non central longest and shortest bond lengths are also reported

	PTA				<i>iso</i> -PTA			
	C=C	C _i -C _i ^a	C≡C	C _e -C _e ^a	C=C	C _i -C _i ^a	C≡C	C _e -C _e ^a
C ₆ H ₄	1.401	1.380	1.226	---	1.406	1.404	1.219	---
C ₁₂ H ₆	1.385	1.378/ 1.394	1.240/ 1.217	1.327	1.380	1.404/ 1.423	1.234/ 1.210	1.334
C ₁₈ H ₈	1.392/ 1.375	1.375/ 1.401	1.238/ 1.215	1.332	1.383/ 1.366	1.411/ 1.428	1.228/ 1.209	1.344
C ₂₄ H ₁₀	1.388/ 1.369	1.378/ 1.405	1.238/ 1.214	1.331/ 1.337	1.372/ 1.362	1.419/1.416/ 1.430	1.225/1.225/ 1.209	1.350/ 1.349
C ₃₀ H ₁₂	1.393/ 1.368	1.240/ 1.215	1.379/ 1.413	1.336/ 1.345	1.365/1.367/ 1.360	1.422/1.422/ 1.431	1.223/1.224/ 1.209	1.353/ 1.351
C ₃₆ H ₁₄	1.383/ 1.365	1.382/ 1.409	1.236/ 1.213	1.335/ 1.343	1.363/1.366/ 1.432	1.424/1.420/ 1.432	1.222/1.224/ 1.209	1.355/ 1.352
C ₄₂ H ₁₆	1.382/ 1.364	1.384/ 1.410	1.234/ 1.213	1.337/ 1.345	1.361/1.365/ 1.358	1.435/1.421/ 1.433	1.221/1.223/ 1.209	1.356/ 1.353
C ₄₈ H ₁₈	1.380/ 1.363	1.386/ 1.410	1.233/ 1.213	1.339/ 1.346	1.360/1.364/ 1.357	1.425/1.422/ 1.433	1.221/1.223/ 1.209	1.356/ 1.353
C ₅₄ H ₂₀	1.378/ 1.362	1.388/ 1.411	1.232/ 1.212	1.340/ 1.347	1.360/1.363/ 1.357	1.426/1.423/ 1.433	1.221/1.222/ 1.209	1.356/ 1.354

a) C_i-C_i and C_e-C_e are the single bonds flanked by either a double and a triple bond or two triple bonds.

This is clearly visible from Figure 4.20, in which we report the spin density for each atom of the PTA and *iso*-PTA octamers along the carbon backbone. For all the PTA oligomers, the atomic spin density has a tendency to decrease when moving from terminal to central carbon atoms, with the maximum values localized at one and three quarter of the oligomer chain and the lowest values localized at the centre of the oligomer.

In the case of *iso*-PTA, however, the spin is delocalized over the entire backbone but confined over the equivalent primary carbon atoms involved in the C=C bonds (Figure 4.20).

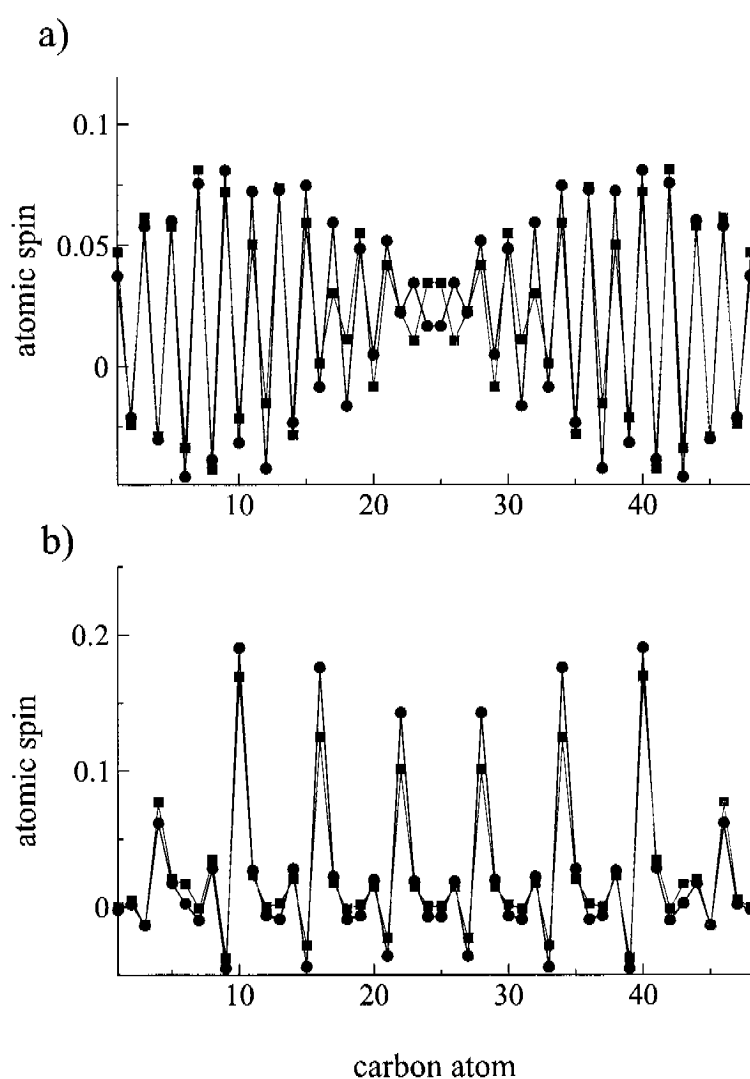


Figure 4.20: Atomic spin density along the carbon backbone of the (a) anionic (●) and cationic (■) PTA octamer; (b) anionic (●) and cationic (■) *iso*-PTA octamer.

Electron Affinities and Ionization Potentials

In Figure 4.21 the adiabatic EAs of the PTA and *iso*-PTA oligomers computed at the BHandHLYP/6-31+G(d,p) level of theory up to the nonamer are plotted against the inverse of the oligomer length. The choice of this level of theory is explained in detail in the section ‘Computational Methods’.

The EAs of the *through*-conjugated oligomers from the dimer to the hexamer increase almost linearly with the inverse of the oligomer size. At the heptamer, the curve finally starts to flatten, indicating inward saturation. For the largest oligomer considered, the calculated EA is equal to 2.441 eV, about 1.22 eV larger than that computed for the dimer.

The EAs of the *cross*-conjugated oligomers also respond to the extension of the chain size, but to a lesser extent than the PTA oligomers. For the transition from the dimer to the trimer, the EA increases by as much as 0.3 eV, indicating that π -delocalization does not appear to be switched off by a *cross*-linked carbon atom. As shown in Figure 4.21a, the EA keeps increasing and it is still not converged even for the largest oligomer considered. At that point the EA has increased by about 0.57 eV with respect to the dimer.

Adiabatic IPs of PTA and *iso*-PTA oligomers are also reported in Figure 4.21. We observe that the IPs are less affected by the extension of the chain length compared to the EAs for both types of conjugations. In fact, when moving from the dimer to the nonamer, the IP of PTA and *iso*-PTA changes by 0.86 and 0.35 eV, respectively, 0.36 and 0.22 eV less than the EA (Figure 4.21a). A similar trend was observed in the work of van Walree [86], who reported an increase of the oxidation potential with the oligomer size in a series of *p*-phenylvinilydene *cross*-conjugated oligomers. In the case of the *iso*-PTA oligomers the ECL as measured by the evolution of the IP has been reached at the octamer. However, for the PTAs no ECL has been reached yet. In Figure 4.21b we also report the vertical IPs and EAs calculated at the B3LYP/6-31G(d,p) level of theory according to Koopmans’ theorem. We note that the trend agrees closely with the adiabatic EA and IP.

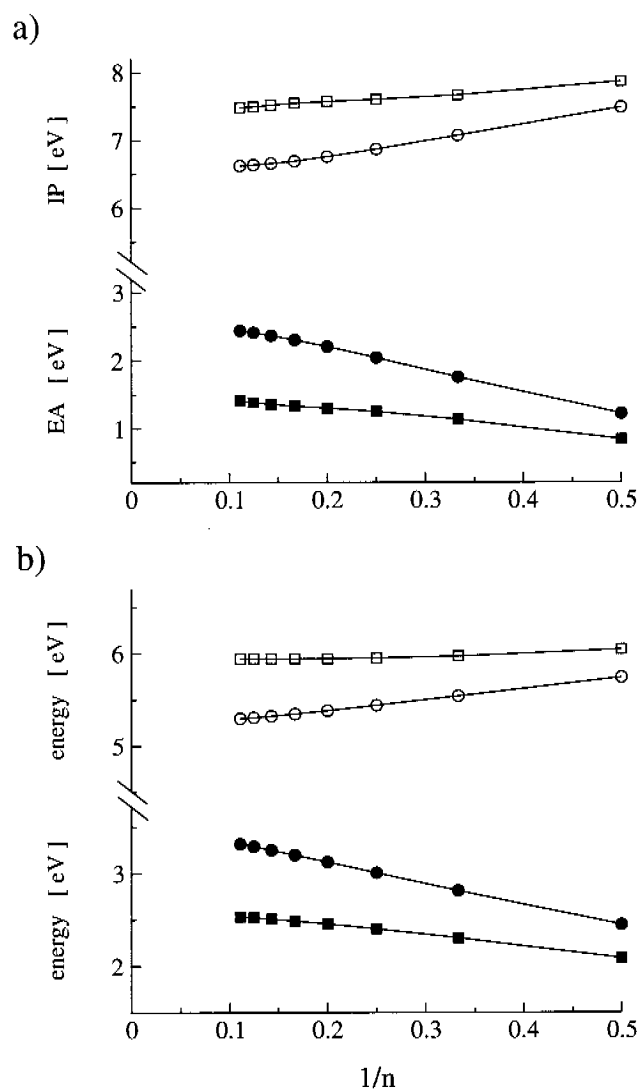


Figure 4.21: a) Evolution of the adiabatic EAs and IPs of the PTA (● EA; ○ IP) and iso-PTA (■ EA; □ IP) oligomers as function of the reciprocal number of monomer units ($1/n$) at the BHandHLYP/6-31+G(d,p) level of theory; b) Evolution of LUMO and HOMO energies (with opposite sign) of the PTA (● LUMO; ○ HOMO) and iso-PTA (■ LUMO; □ HOMO) oligomers as function of the reciprocal number of monomer units ($1/n$) at the B3LYP/6-31G(d,p) level of theory.

Excitation Energies

The maximum absorption wavelengths of the PTA and iso-PTA oligomers computed at the ZINDO and the time-dependent (TD) DFT levels of theory are shown in Table 4.8 and

Table 4.9, respectively. In Figure 4.22 the first allowed excitation energy (λ_{\max}) for both series of compounds is plotted against the inverse of the number of monomer units. As reported by Martin et al. [47] for the PTA oligomers, the lowest optical excitation energies computed at the ZINDO level [71-77, 87] are in good agreement with experiment.

Table 4.8: Lowest allowed excitation energy (eV, nm) of the PTA oligomers computed at different levels of theory

ZINDO				TD-BHandHLYP		
	Sym	Energy	Oscillator strength	Sym	Energy	Oscillator strength
C ₆ H ₄	B _u	4.201 (295.1)	0.353	B _u	4.851 (255.6)	0.575
C ₁₂ H ₆	B _u	3.013 (411.5)	0.541	B _u	3.508 (353.5)	1.177
C ₁₈ H ₈	B _u	2.753 (450.3)	1.212	B _u	3.004 (412.8)	2.358
C ₂₄ H ₁₀	B _u	2.613 (474.5)	1.868	B _u	2.724 (455.1)	3.532
C ₃₀ H ₁₂	B _u	2.531 (489.8)	2.500	B _u	2.556 (485.0)	4.680
C ₃₆ H ₁₄	B _u	2.480 (499.9)	3.118	B _u	2.448 (506.6)	5.808
C ₄₂ H ₁₆	B _u	2.446 (506.9)	3.726			
C ₄₈ H ₁₈	B _u	2.422 (512.0)	4.329			
C ₅₄ H ₂₀	B _u	2.405 (515.5)	4.923			

Here we report slightly different values since in our calculations we are using geometries optimized at the B3LYP/6-31G(d,p) rather than at the AM1 level [47]. We observe the same trends: the only difference is a small but consistent enhancement of the red shift of the absorption wavelengths. Here we also report λ_{max} computed at the TD-BHandHLYP/6-31G(d) level of theory. As shown in Figure 4.22b, the agreement with the experiment is slightly less satisfactory than that observed using the ZINDO method. In particular, λ_{max} decreases with the inverse of n more steeply than observed experimentally.

The calculation of the excitation energies for oligomers larger than nonamer is crucial for an accurate determination of the ECL. However, the computer demanding for the geometry optimization of these large oligomers is a limit in this investigation. On the other hand, since, as shown before, the geometry parameters are well converged for the largest oligomer considered, the molecular structure of oligomers beyond the nonamer has been designed by adding repeatedly a monomer unit at the centre of the oligomer constructed with the extrapolated bond lengths and angles. The excitation energies calculated on these series of PTA oligomers appear to converge for a value of ECL equal to about 40 conjugated bonds ($n = 13$) (data not shown).

For the *iso*-PTAs, starting with the trimer, λ_{max} stays nearly constant, i.e. no red shift is seen as in the PTAs for both levels of theory. We need to point out that there is no satisfactory quantitative agreement between computed and experimental λ_{max} ^a; the trend, however, remains the same. The discrepancies between theory and experiment could be partly due to the different terminal groups (H in this work and cyclohexylidene in Ref. [19]). Tykwinsky *et al.* [57] reported the synthesis of *iso*-PTA dimer with terminal methyl groups for which λ_{max} was at about 3.82 eV in fair agreement with the BHandHLYP value. Moreover, the λ_{max} calculated at the ZINDO level are overestimated by about 30 nm, whereas at the BHandHLYP level they are underestimated by about 20 nm.

Table 4.9: Low lying allowed excitation energies (eV, nm) of the iso-PTA oligomers

ZINDO				TD-BHandHLYP		
	Sym	Energy	Oscillator strength	Sym	Energy	Oscillator strength
C ₆ H ₄	A ₁	4.561 (271.8)	0.172	A ₁	5.502 (225.3)	0.277
C ₁₂ H ₆	B _u	3.272 (378.9)	0.130	B _u	4.027 (307.9)	0.373
C ₁₈ H ₈	B ₂	3.260 (380.3)	0.055	A ₁	3.993 (310.5)	0.394
	A ₁	3.281 (377.9)	0.187	B ₂	4.021 (308.3)	0.324
C ₂₄ H ₁₀	B _u	3.255 (380.9)	0.079	B _u	3.977 (311.8)	0.456
	B _u	3.286 (377.3)	0.279	B _u	4.022 (308.3)	0.638
C ₃₀ H ₁₂	B ₂	3.253 (381.1)	0.097	A ₁	3.971 (312.2)	0.525
	A ₁	3.289 (377.0)	0.359	B ₂	4.019 (308.5)	0.748
C ₃₆ H ₁₄	B _u	3.252 (381.2)	0.119	B _u	3.969 (312.4)	0.570
	B _u	3.291 (376.8)	0.444	B _u	4.018 (308.6)	1.043
C ₄₂ H ₁₆	B ₂	3.251 (381.3)	0.140			
	A ₁	2.292 (376.6)	0.523			
C ₄₈ H ₁₈	B _u	3.251 (381.4)	0.164			
	B _u	2.293 (376.5)	0.604			
C ₅₄ H ₂₀	B ₂	3.251 (381.4)	0.186			
	A ₁	3.294 (376.4)	0.681			

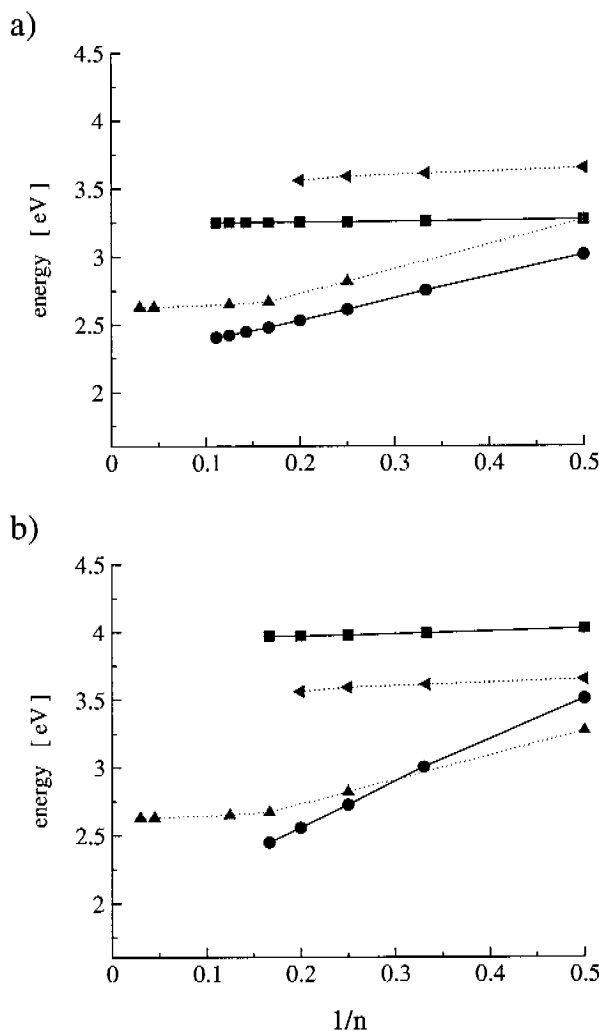


Figure 4.22: Evolution of the maximum absorption wavelength (λ_{\max}) as function of the reciprocal number of monomer units ($1/n$) for the PTA (●) and iso-PTA (■) oligomers at (a) ZINDO and (b) TD-BHandHLYP/6-31G(d) levels of theory. (▲) corresponds to the experimental values for the PTAs [47] and (◄) to the experimental values for the iso-PTAs [54].

However, a new feature is observed: in the *cross*-conjugated compounds the absorption at λ_{\max} is split into two allowed transitions; one characterized by an energy slightly lower, (hereafter referred to as λ_{\max}) and the other characterized by an energy slightly larger (hereafter referred to as $\lambda_{\max-1}$) with respect to that computed for the dimer. As shown in

Table 4.9, the intensity of the λ_{\max} is significantly smaller than that of the $\lambda_{\max-1}$. For each monomer unit added a new low intensity transition emerges between λ_{\max} and $\lambda_{\max-1}$. This is also observed at the TD-BHandHLYP/6-31G(d) level of theory. Whereas $\lambda_{\max-1}$ is mainly due to a HOMO \rightarrow LUMO transition, λ_{\max} is characterized by a combination of $\pi \rightarrow \pi^*$ excitations. The sum of the oscillator strengths of the λ_{\max} and $\lambda_{\max-1}$ per monomer unit ($\Sigma f/n$; f = oscillator strength, n = number of monomer units in the oligomer) is roughly constant, as observed experimentally. This suggests that the experimental band observed at λ_{\max} is due to two very close lying transitions. This could explain the unequivocal interpretation of the spectra.

Table 4.10: Second-order hyperpolarizabilities ($10^{-36} \text{ cm}^{-7} \text{ esu}$) of the PTA and the *iso*-PTA oligomers computed at the CPHF-MNDO level of theory. The geometries are optimized at the B3LYP/6-31G(d,p) level

	PTA		<i>iso</i> -PTA
	Calc.	Exp. ^a	Calc.
C ₁₂ H ₆	64	77	17
C ₁₈ H ₈	262		38
C ₂₄ H ₁₀	589	583	63
C ₃₀ H ₁₂	1033		90
C ₃₆ H ₁₄	1524	1130	118
C ₄₂ H ₁₆	2050		147
C ₄₈ H ₁₈	2599	2180	176
C ₅₄ H ₂₀	3151		206

a) taken from ref. [51]

Nonlinear optical properties

The second-order hyperpolarizabilities γ of the PTA and *iso*-PTA oligomers up to nonamer are reported in Table 4.10 and Figure 4.23. An experimental and quantum chemical investigation of the γ for the PTA oligomers using an MNDO Hamiltonian was previously reported [51]. For the PTA oligomers we note an increase of the γ following a power law $\gamma = \gamma_m n^a$ for short oligomer length ($a = 2.43$), in reasonable agreement with the experiment. For the *iso*-PTA oligomers the addition of linearly π -conjugated segments is expected to produce a linear increase of γ only. A response beyond linear would obviously be due to an interaction between linear segments across the *cross*-conjugated carbon atoms. This enhancement, as shown in Figure 4.23, is indeed predicted by our calculations using the same MNDO Hamiltonian. In fact, the values of γ/n per monomer unit added increase by about $15 \cdot 10^{-34} \text{ cm}^{-7} \text{ esu}$ from the dimer to the nonamer. This enhancement, compared to that observed for the PTA oligomers, is very limited but is still suggesting a weak communication across the *cross*-linked carbon atoms. Furthermore, we observe that the curve flattens for the largest oligomers and has effectively reached the asymptote at the nonamer.

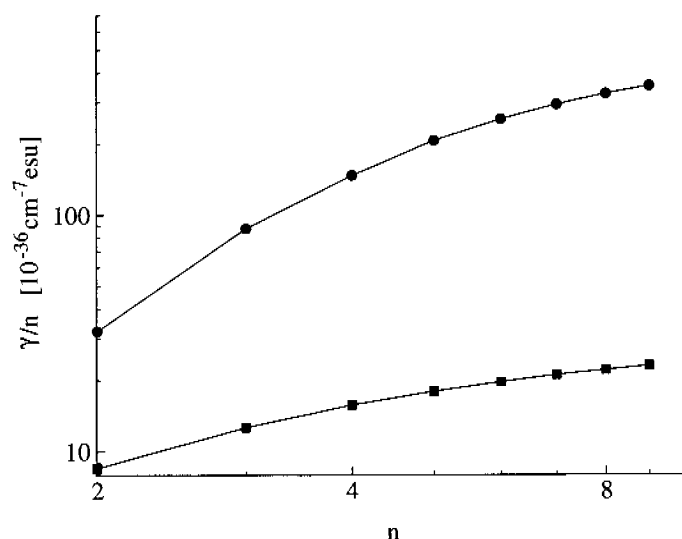


Figure 4.23: Evolution of the static second-order hyperpolarizability γ as function of the monomer units (n) (in logarithmic scale) of the PTA (●) and *iso*-PTA (■) oligomers computed at CP-MNDO level of theory.

Analysis of electron delocalization

The electron delocalization in PTA and *iso*-PTA oligomers has been investigated using the approach presented in Chapter 2 and based on the NBO analysis. As expected, the total amount of delocalization energy (E_{del}), for both PTA and *iso*-PTA oligomers, increases with increasing the oligomer size. In the previous chapter we showed that the difference in stability between the parent *t*-DEE and *g*-DEE isomers (ΔE_{tot}) is totally ascribed to the difference in delocalization energy (ΔE_{del}). However, the calculated ΔE_{del} values evolve more rapidly than the corresponding ΔE_{tot} values (see Figure 4.24) for the larger oligomer. The partitioning of ΔE_{del} into vertical ($\Delta E_{\pi_{\perp}}$) and in-plane (ΔE_{σ}) contributions shows that the ΔE_{del} is essentially controlled by the π -electron delocalization, even though the in-plane delocalization cannot be neglected. In fact, ΔE_{σ} slowly increases with increasing the oligomer size (Figure 4.24). It is interesting to note that the Lewis energy term ($\Delta E_{\text{L}} = \Delta E_{\text{tot}} - \Delta E_{\text{NL}}$) favors the *iso*-PTA isomers. The stabilization of PTA with respect to *iso*-PTA is totally due to the much larger delocalization energy of the former, or in other words, that without the stabilization given by the electron delocalization, the *iso*-PTA isomers should be more stable than the *trans* ones. This suggests that the relative stability of the two isomers could be modulated by tuning the extent of π -electron delocalization of the *trans* form, for example, through the insertion of spacers into the linearly π -conjugated pathway. The reduction of π -electron delocalization in the linear oligomers could give rise to an inversion of the order of stability of the two isomers.

The total amount of π -delocalization energy (E_{π}) is not a useful descriptor for the evaluation of the ECL as E_{π} monotonically increases with increasing the π -conjugated length, for both PTA and *iso*-PTA oligomers. Normalization of E_{π} by dividing it for the number of monomer units of the oligomer (E_{π}/n) also does not allow the evaluation of the ECL since it can be shown that E_{π}/n must increase beyond the ECL. On the other hand, the increase of E_{π} upon addition of a further monomer unit to the oligomer n , to give the oligomer $n + 1$, should converge to a saturation value at the ECL. In this respect, it is useful to define the parameter $\Delta E_{\pi_{\perp}}[n]$ as:

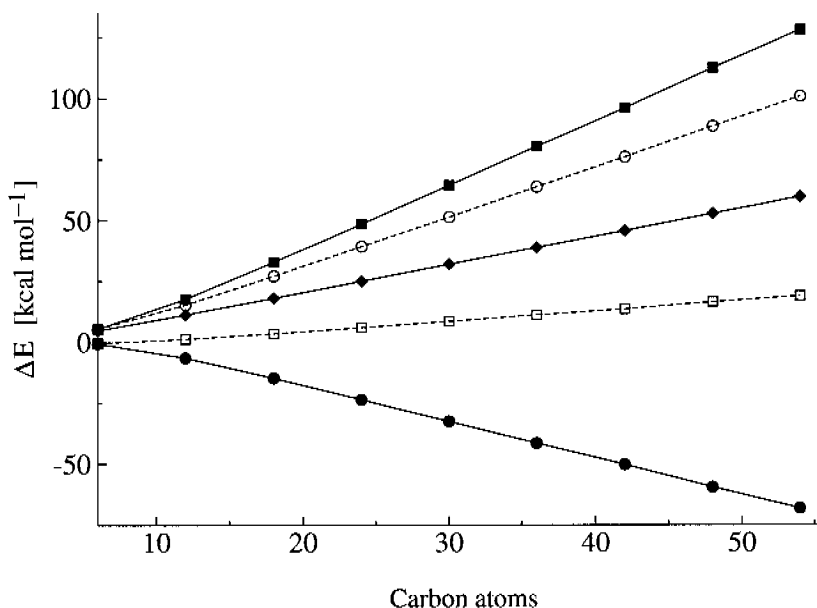
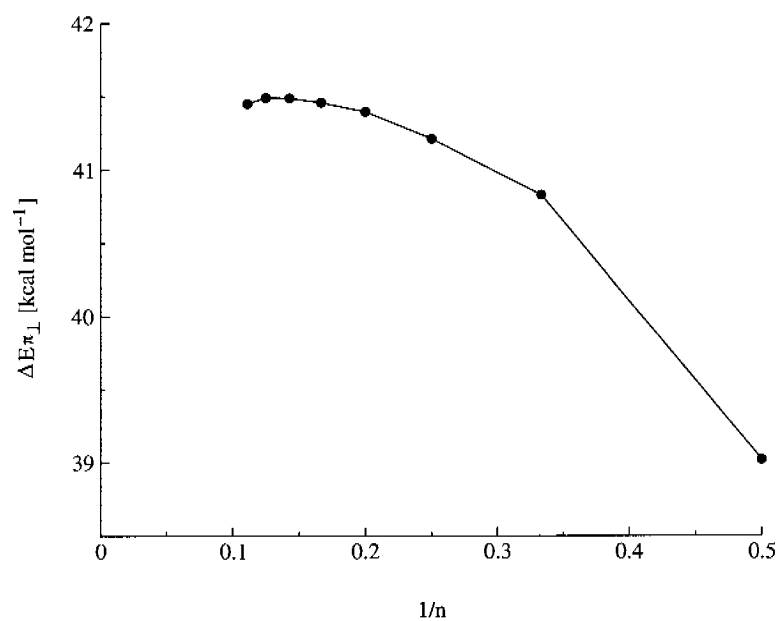


Figure 4.24: Energy differences between PTA and corresponding *iso*-PTA isomers as a function of number of carbon atoms of the π -conjugated chain. ΔE_{tot} (◆) is the SCF energy difference; ΔE_{del} (ΔE_{NL}) (■) is the delocalization energy (non-Lewis energy) difference; ΔE_L (●) is the Lewis energy difference; $\Delta E_{\pi_{\perp}}$ (○) is the π -vertical contribution to the delocalization energy difference; ΔE_{σ} (□) is the in-plane contribution to the delocalization energy difference.

$$\Delta E_{\pi}[n] = E_{\pi_{\perp}}[n] - (E_{\pi_{\perp}}[n-1] + E_{\pi_{\perp}}[1]). \quad (4.4)$$

that is as a difference between the π -delocalization of oligomer n and the sum of the π -delocalization energy of the oligomer $n-1$ and the monomer. $\Delta E_{\pi}[n]$ is plotted against the inverse number of monomer units in Figure 4.25. It is interesting to note that the values of $\Delta E_{\pi_{\perp}}[n]$ for the PTA oligomers reach a maximum at the octamer and then slightly decrease. This corresponds to the ECL of 24 conjugated bonds ($n = 8$), in perfect agreement with the value determined from the bond length alternation (δR), and close to that determined by the experimental investigation [47]. For the *iso*-PTA oligomers (Figure 4.25b) the $\Delta E_{\pi_{\perp}}[n]$ values are tightly constant beyond the dimer; a result which confirms that the π -electron delocalization is switched off at the *cross*-conjugated carbon atoms.

a)



b)

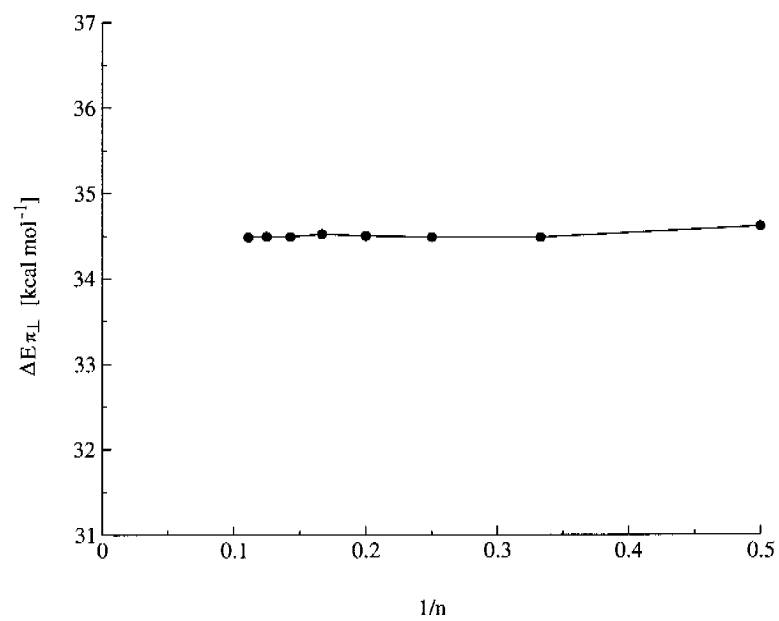


Figure 4.25: a) $\Delta E_{\pi_{\perp}}[n]$ parameter of PTA (a) and iso-PTA (b) oligomers as a function of the inverse number of monomer units

4.2.5 Conclusions

The present study shows that the effect of *through* and *cross*-conjugation on the geometrical and electronic properties of the PTA oligomers is specific and depends on the observable considered. The ECL, as determined on the basis of the molecular structure, (i.e. δR), and delocalization energies (i. e. E_π), amounts to 24 conjugated bonds ($n = 8$) in PTA, and only to 6 conjugated bonds ($n = 3$) in *iso*-PTA. Also, the extended alternation parameter δR proposed in this study appears to be properly defined.

The response of the frontier orbitals as well as the HOMO-LUMO gap to the length of the *iso*-PTA backbone indicates that electron delocalization effects also *cross*-conjugated oligomers. The fact that the HOMO-LUMO gap in the *cross*-conjugated compounds continues to change even after convergence of δR – in violation with the Peierls relation – is obviously due to the Δ_{correl} term in Equation 4.2.

Extended electron delocalization is observed, however, for the positively and negatively charged *iso*-PTA oligomers, there the π -conjugation through *cross*-linked carbon atoms is *definitely* switched on: the geometry of the ions is affected by the extension of the oligomer size. Similarly there is a significant change in the EAs (increase) and IPs (decrease) with the extension of the chain length even though to a lesser extent with respect to the PTA isomers. Therefore, the EA and IP might be the properties that can be rationally modified through selective functionalization of the *iso*-PTA backbone.

The analysis of the spin density of the *iso*-PTA oligomers reveals that in both the cationic and the anionic species the spin is not spread along the carbon backbone, but that it is mainly localized over the equivalent primary carbon atoms involved in the C=C bonds. The accumulation of the spin density on these atoms, seems to be the cause of the strong electronic and structural rearrangement of the *cross*-conjugated oligomer. Also for the optical excitation energies as well as the nonlinear properties (γ), there is some evidence for a weak interaction between conjugated segments.

4.3 Extended Systems: The Impact of Length and Type of Backbone on Electron Delocalization of Polyacetylene, Polydiacetylene, and Polytriacetylene

4.3.1 Summary

π -conjugated organic polymers are widely explored as advanced materials for electronic and photonic applications. In this respect, the type and length of the π -conjugated backbone are crucial degrees of freedom which can be modified to suit compounds with tailored properties. In order to rationalize the effects of the insertion of ethynyl groups into a polyacetylene (PA) chain on specific physical observables, in this subchapter we present a detailed theoretical investigation of electron delocalization in polydiacetylene (PDA), polytriacetylene (PTA) and perethynyl-polytriacetylene (pePTA) oligomers of increasing chain length. The results are then compared to those calculated for the PA oligomers of the same length. The study includes the analysis of the molecular geometries, excitation energies and nonlinear optical properties, and their correlation to the extent of π -delocalization, which is evaluated with the computational approach presented in Chapter 2.

We found that the incorporation of ethynyl groups into the PA chain, to give polydiacetylene (PDA) and polytriacetylene (PTA), increases the total amount of π -delocalization but, on the other hand, reduces the efficiency with which π -electron delocalization extends along the backbone. Furthermore, the lateral addition of ethynyl groups to PTA oligomers, as expected, significantly affects the total amount of π -delocalization, and correspondingly, the values of physical observables like the first allowed excitation energies and the bond length alternation. However, the evolution of these properties with the elongation of the π -conjugated chain is not enhanced with respect to that of PTA.

4.3.2 Introduction

Linearly π -conjugated polymers, such as polyenes and polyynes, are very promising materials with potential applications in the field of molecular electronics and photonics [9-14, 88]. In this class of materials, polyacetylene [PA; $-(\text{CH}=\text{CH})_n-$] is the prototypical compound. Since the discovery of the high conductivity in doped PA [89-92] an enormous amount of experimental [9, 10, 93-97] and theoretical work [62, 64, 85, 89, 91, 93, 98-108] has been devoted to this compound. However, technical applications of PA have been limited by the insolubility in all solvent and the instability under ambient conditions. The incorporation of ethynyl groups into the PA scaffold leads to rod-like polymers, such as polydiacetylenes [PDA, $-(\text{C}\equiv\text{C}-\text{CR}=\text{CR})_n-$] [23, 24] and polytriacetylenes [PTAs, $-(\text{C}\equiv\text{C}-\text{CR}=\text{CR}-\text{C}\equiv\text{C})_n-$] [17, 19, 47-52] (see Figure 4.26), which experience a larger thermal stability, and in addition, the capability to form functional derivatives with fully planar, sterically unhindered frameworks. On the other hand, the incorporation of ethynyl groups into the PA chain strongly affects the molecular and electronic structure which could be modified to match a desired property. For instance, differing from PA, PDAs and PTAs are not conducting upon doping but still show large third-order nonlinear optical responses [14].

Different theories, such as the Su-Schrieffer-Heeger (SSH) model [58, 102, 103], the semiempirical valence effective hamiltonian (VEH) [109], and the crystalline orbital periodic DFT method with several functionals [64, 104, 110-113], have been applied to the investigation of PA and PDA polymers of infinite chain length. PTA has been the subject of much less theoretical investigations since it has only recently been available. Many of these studies focused on the solitonic-excitonic structure and on the correlation between molecular and electronic properties of these polymers.

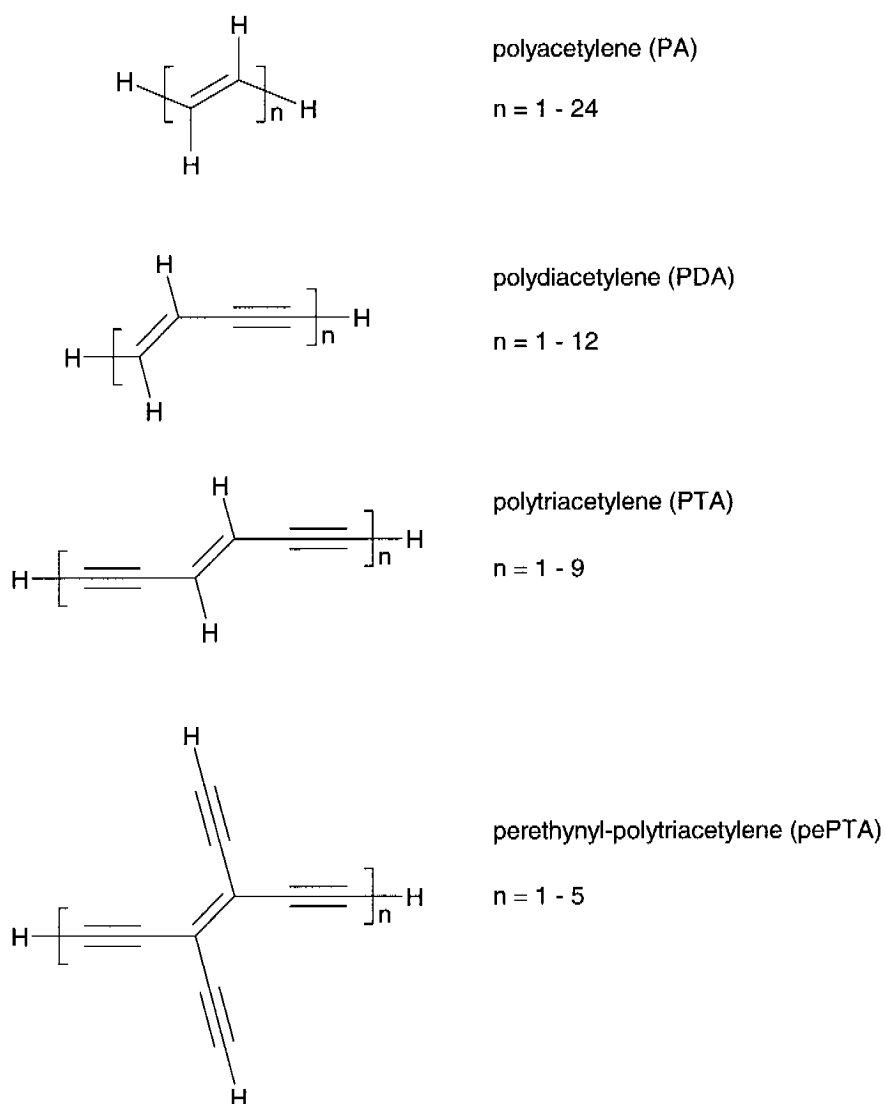


Figure 4.26: *The series of oligomers considered in this study.*

Another approach to the investigation of polymeric systems is the oligomeric technique, which is based on molecular-like calculations on oligomers of increasing size and on the extrapolation of the molecular and electronic properties to the polymeric values. Although some limitations to this “oligomer approach” has been outlined [114], it has been used many times due to the simplicity of the methodology. Another interest in the study of π -conjugated

oligomers of precisely defined lengths arises from their potential applications in the molecular scale electronics.

The “oligomer approach” enables the evaluation of the effective conjugation length (ECL) i.e. the length of the oligomer for which the property under consideration has converged to a constant value, which is a critical parameter for the understanding of many properties of π -conjugated compounds. The ECL of PA has been evaluated, from third harmonic generation (THG) measurements, to occur at approximatively 120 double bonds [115], and from optical properties of PA films to occur at 38 double bonds [105]. The latter value is in much better agreement with the value of 45 ± 5 and 38 theoretically predicted [101, 106]. In the case of both PDA and PTA the ECL has been calculated, on the basis of the saturation of the BLA, to occur at about 20-22 double-triple bonds [116, 117] (see also subchapter 4.2). Clearly, the difference in the ECL parameters, as well as the differences observed in the evolution of molecular and electronic properties, suggests that the incorporation of ethynyl groups into PA considerably affects both the amount of π -electron delocalization and its evolution as a function of the chain length.

These observations prompted us to investigate the impact of the insertion, or lateral addition, of ethynyl units into the backbone (PA, PDA, PTA, pePTA) on the extent of π -electron delocalization using our approach. The results presented and discussed in this work will be useful to get a better knowledge of the electronic and molecular structure in view of the rational design of compounds of multianometer length.

In our approach the delocalization energy is evaluated by applying the orbital deletion procedure described in Chapter 2 [16]. The orbitals deleted are the π^* NBOs responsible for the π -delocalization. The difference between the total energies before and after the deletion of these orbitals gives the π -delocalization energy (E_π), representing the deviation from the idealized Lewis-structure. These non-Lewis contributions, as shown in previous chapters, can also be approximated by the sum of second-order orbital interaction energies (SOIE) between the strongly occupied Lewis-type NBOs (donor orbitals) and the weakly occupied non-Lewis NBOs (acceptor orbitals) involved in the path [118].

In the first part of the section ‘Results and Discussion’ our method is briefly reviewed and detailed definitions for the delocalization parameters used in the present context are given. In

the second part, the physical observables which are generally used for the evaluation of the π -electron delocalization (bond length alternation, first allowed excitation energy, polarizability, and second-order hyperpolarizability) are analyzed and discussed as a function of the oligomer size. Our approach is then applied to the oligomers investigated. Finally, some interesting correlations between molecular and electronic properties with electron delocalization are illustrated and discussed.

4.3.3 Computational Methods

In the present work, all geometry optimizations and the NBO data analysis were performed in the Density Functional Theory (DFT) scheme [40], using the B3LYP functional [41, 42] with the 6-31G(d,p) basis set of Gaussian orbitals [65].

The linear optical absorption properties were computed using the ZINDO/S level of theory [71-77, 87] on the geometry optimized at the B3LYP/6-31G(d,p) level. In the ZINDO calculations, all occupied and virtual orbitals were retained in the active space. Frequency dependent polarizability and second-order hyperpolarizability were computed on the B3LYP geometries using the Coupled-Perturbed (CP) approach [82] and the semiempirical MNDO Hamiltonian [83] at the 1907 nm incident wavelength radiation. The longitudinal polarizability and hyperpolarizability corresponds to the tensor element in the direction of the charge transfer axis (α_{zz} and γ_{zzzz} in our reference system) of the molecule, while the transversal polarizability and second-order hyperpolarizability corresponds to the tensor element in the direction perpendicular to the charge transfer axis and in the molecular plane (α_{xx} and γ_{xxxx} in our reference system). In order to compare computed and measured γ values, the theoretical values have been multiplied by factors derived from the phenomenological approach [119]. Geometry optimizations, NBO analysis and excitation energy calculations have been carried out using the Gaussian98 package [44] and the program NBO 5.0 [45], while the calculation of polarizabilities and second-order hyperpolarizabilities have been performed with the MOPAC2000 program [84].

4.3.4 Results and Discussion

4.3.4.1 Technical Details of the Analysis:

The method used for the analysis of electron delocalization for the oligomers considered in this study is based on the NBO analysis and is explained in detail in Chapter 2. A value for the total amount of π -delocalization along the π -conjugated backbone, is obtained by calculating the E_π energies, given by deleting all vertical π^* orbitals of the backbone. In the case of the pePTA oligomers, only those π^* orbitals are deleted that are part of the PTA chain. To allow a direct comparison of the E_π parameters for the different oligomers, the E_π values are normalized by dividing them for the number of $\pi \rightarrow \pi^*$ donor-acceptor interactions involving π^* orbitals that were deleted ($E_\pi^{\text{norm}} = E_\pi / n$; where n = number of $\pi \rightarrow \pi^*$ interaction; see Figure 4.27). These normalized E_π^{norm} values should be considered a measure of the π -delocalization density per ‘interaction unit’.

Another quantity useful in the present context is the response of the backbone to the extension of the π -conjugated pathway, that is used to study the effects on π -delocalization due to the elongation of the chain length. For this purpose we use the second-order orbital interaction energies (SOIE) between π donor and π^* acceptor orbitals in the conjugation path. SOIEs are given by the formula (see Chapter 2):

$$E(2) = E_{\text{SOIE}_{ij}} = \Delta E_{ij} = q_i \frac{F(i, j)^2}{\epsilon_i - \epsilon_j} \quad (4.5)$$

where i and j are the donor and the acceptor NBOs considered, respectively, ϵ_i , ϵ_j are the corresponding orbital energies, q_i is the donor orbital occupancy, and $F(i, j)$ is the element of the Fock matrix in the NBO basis. The sum of SOIEs is equivalent to the delocalization energy as long as second-order perturbation theory is valid [118]. The oligomers are partitioned in a core backbone and in two terminal π -conjugated units, as shown for PTA in Figure 4.28. Then, we introduce the parameter $\Delta E\pi_{\text{SOIE}}$ defined as:

$$\Delta E\pi_{\text{SOIE}} = \sum E\pi_{\text{SOIE}}^{\text{core}}(n+2) - \sum E\pi_{\text{SOIE}}(n) \quad (4.6)$$

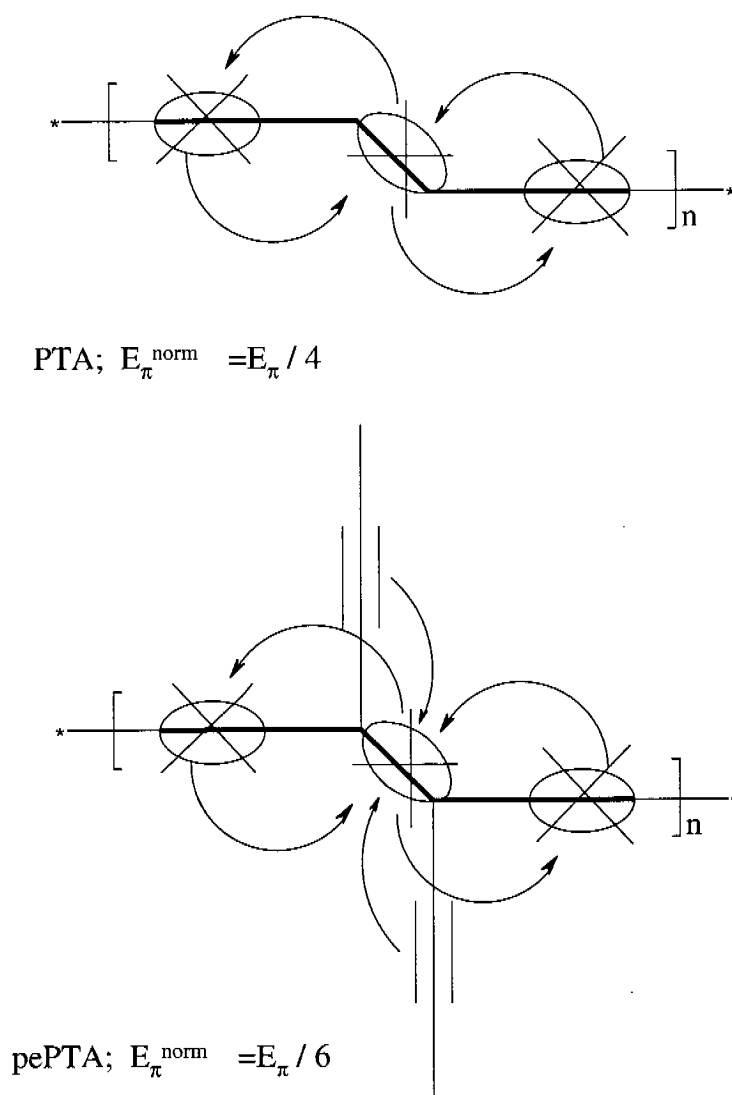


Figure 4.27: Schematic representation of the PTA and pePTA polymers with the $\pi \rightarrow \pi^*$ interactions accounted for the calculation of E_{π}^{norm} .

where $\sum E\pi_{\text{SOIE}}^{\text{core}}(n+2)$ is the sum of the $E\pi_{\text{SOIE}}$ energies between vertical π orbitals of the core backbone in the oligomer $n+2$, at which two extra terminal units are added to the core, and $\sum E\pi_{\text{SOIE}}(n)$ is the sum of the E_{SOIE} energies between vertical π orbitals of the oligomer n . The choice of the size of the terminal π -conjugated units, which carry three unsaturated bonds for all oligomers, is motivated by the fact that this is the number of unsaturated bonds

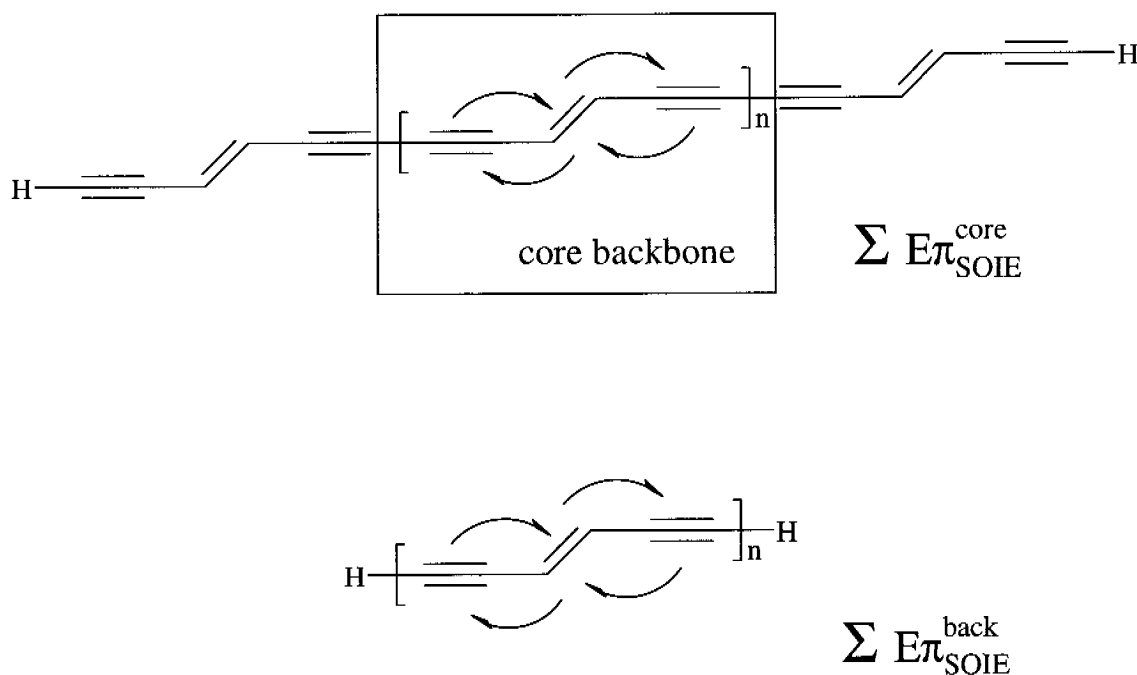


Figure 4.28: Schematic representation of the partitioning of a PTA oligomer into a core backbone and two terminal π -conjugated units. $\Delta E\pi_{\text{SOIE}}$ is calculated as the difference between the $E\pi_{\text{SOIE}}$ of the core backbone ($\sum E\pi_{\text{SOIE}}^{\text{core}}$) and the $E\pi_{\text{SOIE}}$ of an oligomer without the two terminal units ($\sum E\pi_{\text{SOIE}}^{\text{back}}$).

in the largest monomer (PTA) considered in this study. Clearly, the values of $\Delta E\pi_{\text{SOIE}}$ depend on the size of the terminal units adopted in the definition. However, we found that for different lengths of the terminal segments, the comparison of the values of $\Delta E\pi_{\text{SOIE}}$ and their evolution with respect to the reciprocal number of carbon atoms is very similar, thus leading to the same observations. The $E\pi_{\text{SOIE}}$ interactions to be considered in the summations are explained in Figure 4.28. It should be noted that the calculation of $\Delta E\pi_{\text{SOIE}}$ involves only interactions within the backbone and not the direct interaction between the backbone and the terminal units. Therefore, $\Delta E\pi_{\text{SOIE}}$ is a measure of the response of the backbone to the extension of the π -conjugated pathway due to the addition of the two extra terminal units. The reference system is the geometry optimized oligomer n . This means that $\Delta E\pi_{\text{SOIE}}$ takes also into account the contribution of the geometry relaxation in response to the extension of π -delocalization.

Finally, for the calculation of the bond length alternation we introduce a generalized parameter δR defined for the PTA oligomers as:

$$\delta R = (C_D - C_T + C_T - C_T)/2 - (C=C + C\equiv C)/2 \quad (4.7)$$

where $C_D - C_T$ and $C_T - C_T$ are the single bond lengths flanked by a double and a triple bond and by two triple bonds, respectively. Equation 4.7 reduces, in the case of PDA and PA, to:

$$\delta R = (C_D - C_T) - (C=C + C\equiv C)/2 \quad (4.8)$$

and

$$\delta R = (C-C) - (C=C) \quad (4.9)$$

respectively.

4.3.4.2 π -Electron Delocalization in PA, PDA, PTA, and pePTA Oligomers

Bond length alternation, Linear, and Nonlinear Optical Properties

The extent of electron delocalization in π -conjugated compounds is investigated experimentally analyzing the evolution of physical observables like the BLA, the first allowed excitation energy and the nonlinear optical properties as a function of the π -conjugated chain length. A detailed theoretical study of these properties for PTA and *iso*-PTA oligomers is reported in the previous subchapter [117]. Here, the study is extended to PA, PDA and pePTA oligomers in order to get a deeper understanding of the effects of π -electron delocalization on the different molecular backbones. It is important to realize that the BLA is a structural property that involves only the ground state of the molecule, whereas the excitation energy is an electronic property that involves both the ground and the excited state. Static polarizabilities and hyperpolarizabilities computed in the coupled perturbed (CP) scheme, which is based on the direct determination of the self-consistent first-order density matrix under the perturbation of a static electric field, are formally involving only the electron density of the ground state.

In Figure 4.29 the evolution of δR , as defined by Equations 4.7-4.9, is reported as a function of the reciprocal number of carbon atoms in the oligomers. On account of the different definitions given in the previous section, only the evolution of the δR parameters as a function of the chain length can be compared. PA starts from a low value (i.e. strong conjugation) and decreases more rapidly than any of the other oligomers, while for PDA and PTA, the curves, which are strictly parallel, rapidly flatten with the increasing of the oligomer length. The π -electron delocalization of these two oligomers seems to evolve poorly. It should be noted that, for both PDA and PTA, the slope of the curves has nearly converged to zero at the same oligomer length. Therefore, the effective conjugation length of PDA, determined on the basis of geometrical parameters, is equal to that of PTA, and corresponds to about 20-22 conjugated double-triple bonds. On the other hand, for PA, the curve is still decreasing for the largest oligomer investigated, indicating a larger ECL.

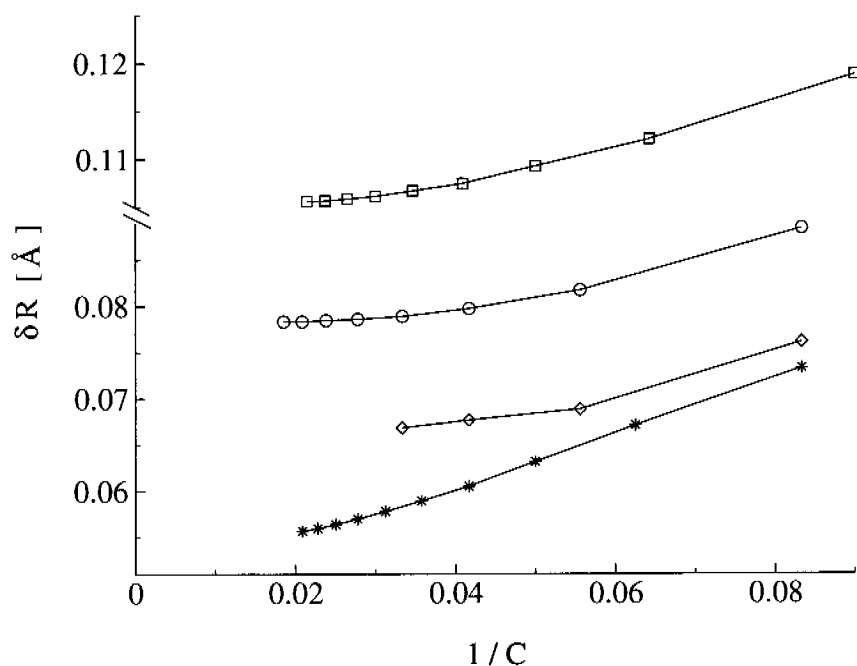


Figure 4.29: Evolution of the δR parameter as function of the reciprocal number of carbon atoms ($1/C$) for the PA (*), PDA (\square), PTA (\circ), and pePTA (\diamond) oligomers at the B3LYP/6-31G(d,p) level of theory. The alternation parameter has been calculated using the central bond lengths and Equations 4.7-4.9.

The evolution of the δR values of pePTA is also nearly parallel to that of PTA and PDA in the range within dimer and pentamer, the latter being the largest pePTA oligomer investigated. The values of δR are lower with respect to those of the corresponding PTA, as expected by the effect of the ethynyl arms on bond lengths, however, the curve appears to converge at the same oligomer length of PTA and PDA. This indicates that the ethynyl groups have a significant effect on the value of δR but not on its evolution as a function of the oligomer length.

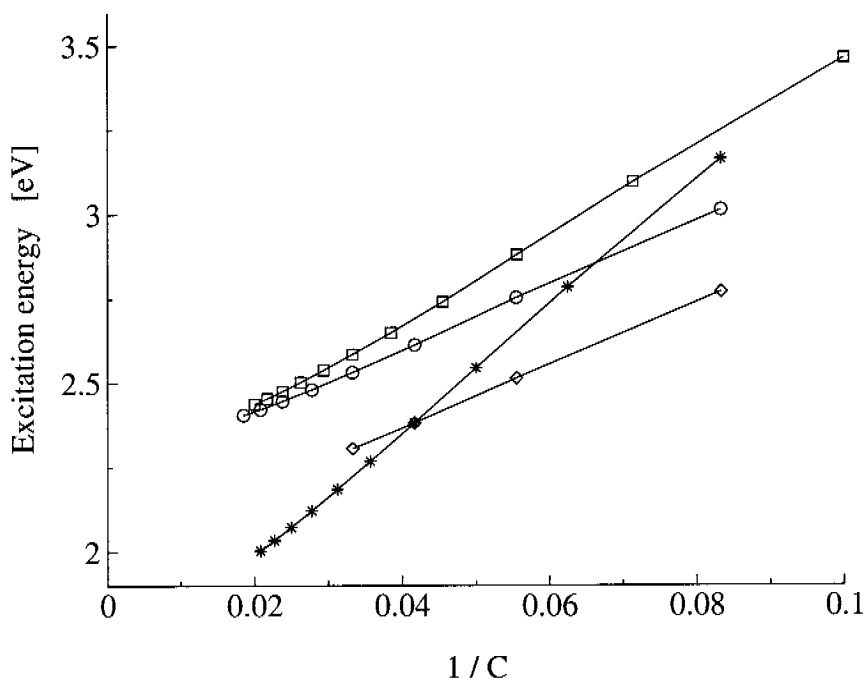


Figure 4.30: Evolution of the first allowed excitation energy (E_{\max}) (in eV) as function of the reciprocal number of carbon atoms ($1/C$) for the PA (*), PDA (□), PTA (○), and pePTA (◇) oligomers computed with the ZINDO Hamiltonian on the geometry optimized at B3LYP/6-31G(d,p) level of theory.

The evolution of the first allowed excitation energy (E_{\max}) as a function of the reciprocal number of carbon atoms in the oligomers investigated is reported in Figure 4.30. For the shorter oligomers the excitation energy depends on the number of triple bonds incorporated

into the backbone and on the presence of lateral ethynyl arms. pePTA has the lowest excitation energy, followed in order by PTA, PDA, and PA. However, as the oligomer chain increases, the excitation energy of PA decreases more rapidly than that of the other oligomers, and for the largest oligomers considered in this study it is significantly lower than that calculated for any other oligomers. On the other hand, the values of the excitation energy of PTA evolve slightly slower with respect to those of PDA, even though, they appear to converge to the same value (see Figure 4.30). The curve of the excitation energy of pePTA, as observed for δR , is parallel to that of PTA supporting the finding that the ethynyl groups affect significantly the values of the electronic and molecular properties but not their evolution as a function of the oligomer length.

The longitudinal polarizability α_L of a linearly π -conjugated compound is proportional to the length of the system for large oligomers [99, 100, 120-122]. This means that the polarizability per unit length approaches to an asymptotic finite value, for which it is an intensive quantity. Indeed, for all of the oligomers investigated in this work, the values of α_L divided by the number of carbon atoms of the backbone (α_L/C) appear to slowly converge to an asymptotic limit (Figure 4.31). For shorter oligomers the values of α_L/C are very similar. However, the value of α_L/C of PA evolves more rapidly, with increasing the oligomer size, than that of any other oligomers. Furthermore, it converges slower to the asymptotic limit. The extrapolated ECL of PA amount to 35÷40 double bonds, a value significantly higher than that extrapolated for PDA and PTA (25÷30 double/triple bonds), and in good agreement with the experiment [105] and the other theoretical predictions [101, 106]. It should be noted that the value of α_L/C of PDA evolves slower than that of PTA; a trend opposite to that observed for the excitation energy.

In contrast to the rod-like PA, PDA, and PTA, the pePTA oligomers have a significant transversal contribution to the polarizability. Accordingly, the average polarizability ($\bar{\alpha} = \frac{1}{3}(\alpha_{xx} + \alpha_{yy} + \alpha_{zz})$) of pePTA is significantly larger than that of the other compounds. However, the transversal polarizability per carbon atom (α_T/C) of pePTA oligomers is tightly constant with increasing the oligomer length, while the longitudinal polarizability per carbon atom (α_L/C) is parallel and very close to that of PTA (see Figure 4.31). Interestingly, this

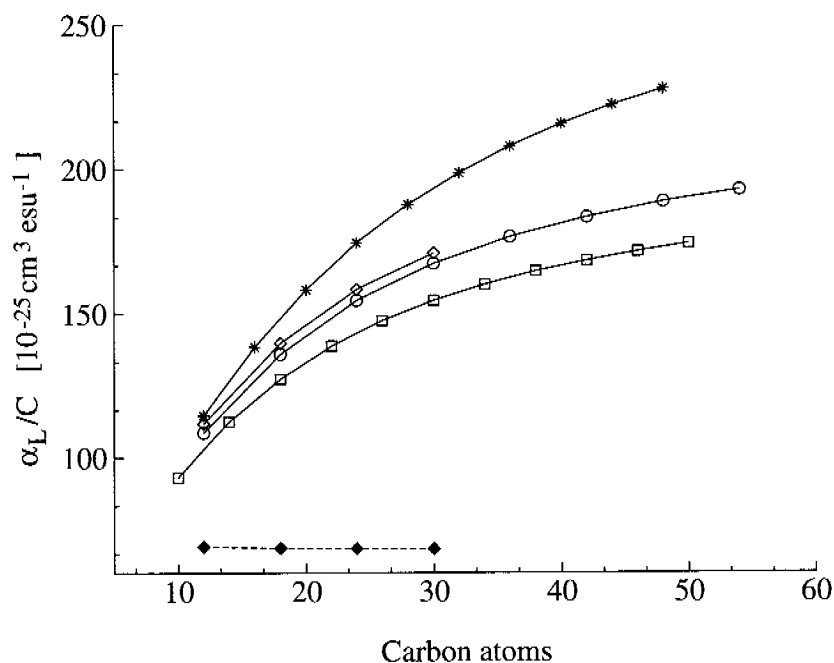


Figure 4.31: Evolution of the longitudinal polarizability per carbon atom of the backbone (α_L/C) (in $10^{-25} \text{ cm}^3 \text{ esu}^{-1}$) as a function of the number of carbon atoms for the PA (*), PDA (\square), PTA (\circ), and pePTA (\diamond) oligomers computed at the CP-MNDO level of theory. The Figure also reports the transversal polarizability per carbon atom of the backbone (α_T/C) for the pePTA (\blacklozenge) oligomers.

result points out that the lateral addition of ethynyl groups to the PTA backbone does not affect significantly the values of α_L/C , as well as their evolution with increasing the oligomer size.

The longitudinal second-order hyperpolarizability γ_L , for short π -conjugated oligomers, follows the power law $\gamma_L = \gamma_m n^a$ (where n is the number of oligomer units, and γ_m and a are constants) [109, 123, 124], while for large oligomers the γ_L values deviate from the power law, thus indicating inward saturation. In section 4.2 we showed that the γ values calculated for the PTA oligomers are in acceptable agreement with those determined from THG measurements [51]. Figure 4.32 reports the evolution of the values of γ_L per carbon atom of the backbone (γ_L/C), with respect to the oligomer size. The trend is similar to that discussed above for α_L/C . The γ_L/C value of PA evolves much more rapidly than that of any other oligomers. The γ_L/C values of the PDA and PTA oligomers are very similar and appear to

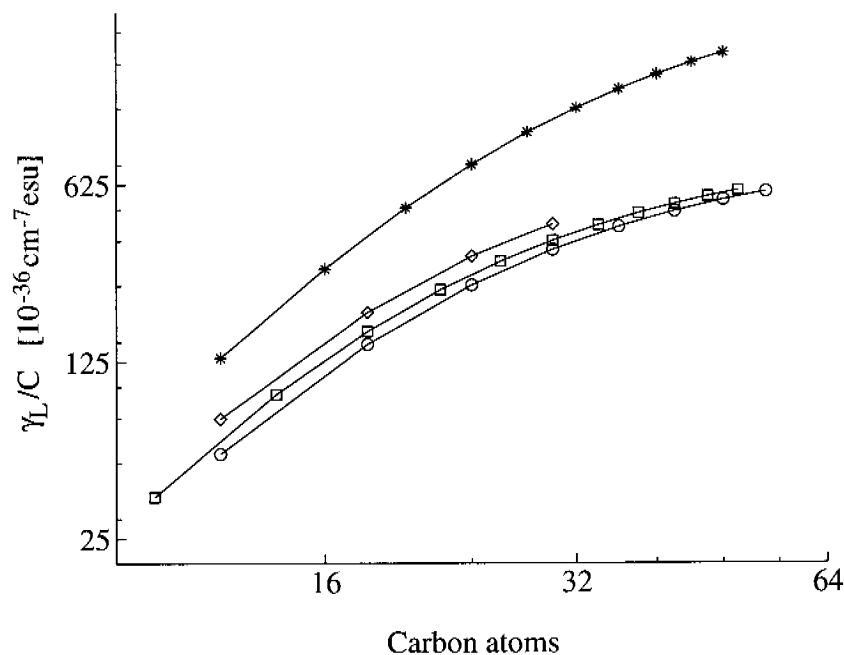


Figure 4.32. Evolution of the longitudinal second-order hyperpolarizability per carbon atom of the backbone (γ_L/C) (in $10^{-36} \text{ cm}^{-7} \text{ esu}$) as function of the number of carbon atoms for the PA (*), PDA (□), PTA (○), and pePTA (◇) oligomers computed at the CP-MNDO level of theory.

converge to the same saturation value. Again, the lateral extension of the π -conjugation in the pePTA oligomer does not result in a significant improvement of the longitudinal component of γ . Finally, it should be noted that the γ_L/C values of PTA and PDA have nearly converged to the saturation value for the largest oligomers investigated, allowing the extrapolation of ECL to a number of π -conjugated double/triple slightly larger than that evaluated from the δR parameter and equal to that discussed above for the polarizability.

Analysis of π -delocalization

For all of the compounds investigated, the amount of π -delocalization evaluated by E_{π}^{norm} increases with increasing the oligomer size and depends on the number of triple bonds incorporated into the backbone (Figure 4.33). In fact, for short oligomers, PTA has the largest value of E_{π}^{norm} followed by pePTA, PDA, and finally by PA. However, the slope of the curve

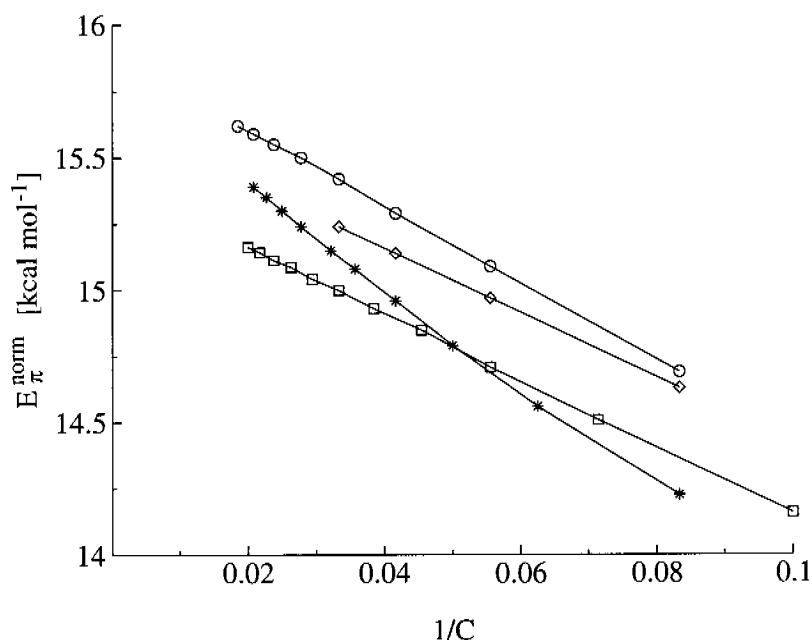


Figure 4.33: E_{π}^{norm} values (for details see Figure 4.27) as a function of reciprocal number of (backbone) carbon atoms for the PA (*), PDA (□), PTA (○), and pePTA (◇) oligomers, computed at the B3LYP/6-31G(d,p) level of theory.

corresponding to PA increases more rapidly than that of any other oligomers, and it crosses, for large oligomers, the curve corresponding to PDA. This result shows that the incorporation of triple bonds into the PA chain increases the total amount of π -delocalization, however, π -delocalization is promoted more efficiently in PA. It is also interesting to note that the calculated values of E_{π}^{norm} for pePTA oligomers are slightly lower than those calculated for PTA. As discussed above, the E_{π}^{norm} parameter does not measure the total amount of π -electron delocalization of the pePTA oligomers, which of course is significantly larger with respect to that of PTA, but the π -delocalization per $\pi \rightarrow \pi^*$ interaction along the PTA backbone. This finding could suggest that the promotion of π -delocalization in pePTA is slightly less efficient than in PTA, and it should account for the nearly parallel evolution of the physical observables discussed above.

A deeper analysis of π -electron delocalization can be carried out by considering the individual $\pi \rightarrow \pi^*$ orbital interactions calculated using SOIEs. The profile of the $\pi \rightarrow \pi^*$ SOIE for a set of oligomers with a π -conjugated backbone of 30 carbon atoms is illustrated in Figure 4.34. We note that the $\pi_{C\equiv C} \rightarrow \pi_{C\equiv C}^*$ (T \rightarrow T) and the $\pi_{C=C} \rightarrow \pi_{C\equiv C}^*$ (D \rightarrow T) interaction energies in PTA and PDA are larger than the $\pi_{C=C} \rightarrow \pi_{C=C}^*$ (D \rightarrow D) interaction energies in PA, while the $\pi_{C\equiv C} \rightarrow \pi_{C=C}^*$ (T \rightarrow D) interaction energies are significantly smaller, giving rise to the alternating profile of PDA and PTA shown in Figure 4.34. The sum of SOIEs gives the largest total π -electron delocalization energy for PTA followed by PDA (for shorter oligomers) and finally PA. Therefore, the total delocalization energy is expected to increase by increasing the number of triple bonds in the backbone. The larger SOIEs calculated for the $\pi_{C\equiv C} \rightarrow \pi_{C\equiv C}^*$ (T \rightarrow T) interactions with respect to the $\pi_{C=C} \rightarrow \pi_{C\equiv C}^*$ (D \rightarrow D) ones is supported by the recent work of Schleyer et al. [125] in which they reported a π -delocalization energy of 1,3-butadiyne slightly larger than that of 1,3-butadiene from calculation of heats of hydrogenation and isodesmic reactions.

The SOIEs profile of pePTA is similar to that of PTA with the significant exception of the $\pi_{C=C} \rightarrow \pi_{C\equiv C}^*$ (D \rightarrow T) interactions for which the SOIE of pePTA is about 2 kcal mol⁻¹ lower than that of PTA. In the pePTA oligomers, the $\pi_{C=C}$ and $\pi_{C\equiv C}^*$ orbitals are involved in two additional interactions with the $\pi_{C\equiv C}$ and $\pi_{C\equiv C}^*$ orbitals of the lateral ethynyl groups. The analysis of orbital occupancies in pePTA shows that the $\pi_{C\equiv C}^*$ orbitals accommodate additional electron density transferred from the lateral $\pi_{C\equiv C}$ orbitals (T \rightarrow D interactions), while the $\pi_{C=C}$ orbitals only transfer a fraction of the electron density, which is shifted along the backbone to the lateral $\pi_{C\equiv C}^*$ orbitals (D \rightarrow T interactions). In this respect, the lateral ethynyl groups act as good electron-donors, while the C=C bonds behave as good electron-acceptors but poor electron-donors. This accounts for the smaller values of $\pi_{C=C} \rightarrow \pi_{C\equiv C}^*$ (D \rightarrow T) SOIEs along the backbone and supports the assumption that the promotion of π -delocalization in pePTA is slightly less efficient than in PTA. Furthermore, it also explains the significant lengthening of the C=C bonds in the pePTA oligomers, with respect to those in PTA; the increase of the π -charge of the C=C bond of pePTA when compared to PTA ($q_\pi = 0.012$ and 0.082, respectively for the pentamer) is almost totally due to the increase of the π^*

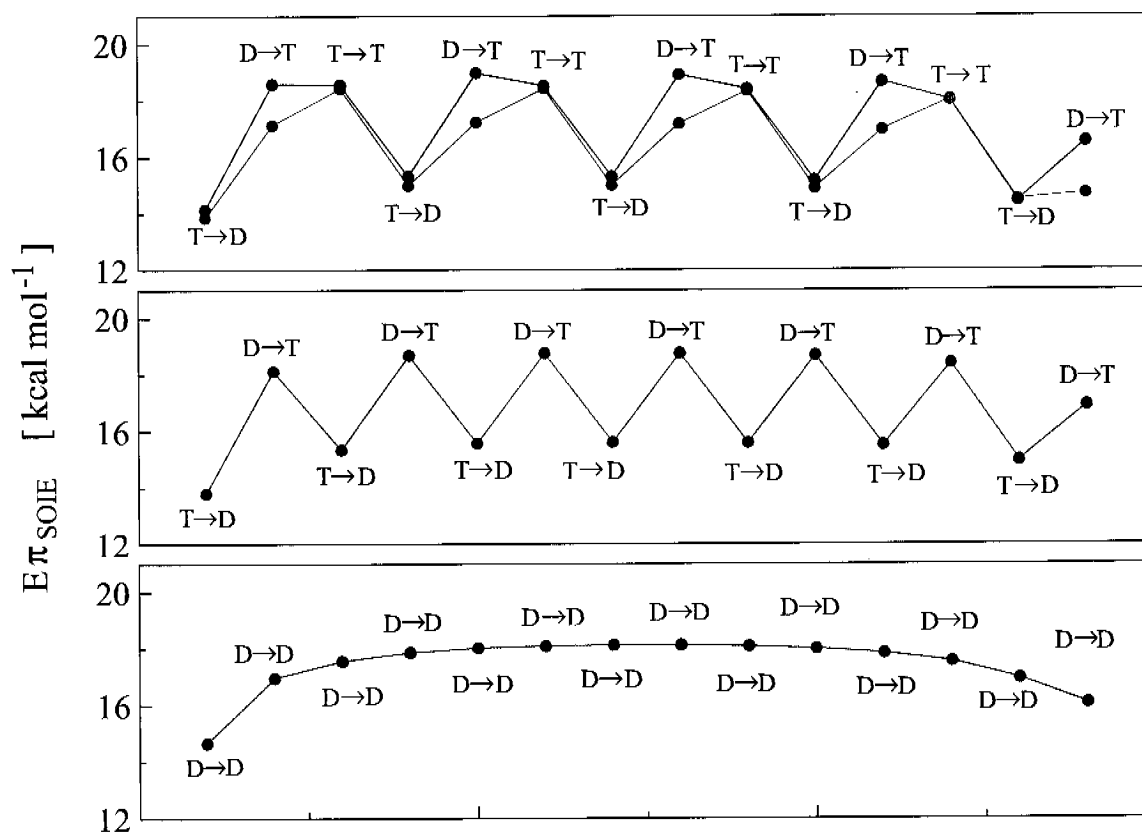


Figure 4.34: $\pi \rightarrow \pi^*$ SOIEs profile along the 30 carbon atoms backbone of the PA (●), PDA (●), PTA (●) and pePTA (●) oligomer. The labels $D \rightarrow D$, $T \rightarrow D$, $T \rightarrow T$, and $D \rightarrow T$ stand for the $\pi_{C=C} \rightarrow \pi_{C=C}^*$, $\pi_{C=C} \rightarrow \pi_{C=C}^*$, $\pi_{C=C} \rightarrow \pi_{C=C}^*$ and $\pi_{C-C} \rightarrow \pi_{C-C}^*$ interactions, respectively. The graph only reports one half of total $\pi \rightarrow \pi^*$ SOIEs, determined by the 'scanning' of the backbone in one direction. The profile corresponding to the 'scanning' in opposite direction is the mirror image to the one reported.

population, to which corresponds a significant reduction of the $C=C$ bond order. This analysis also explains the small shortening of the $C \equiv C$ bonds and lengthening of the $C-C$ bonds along the backbone of the pePTA oligomers compared to the PTA ones.

As discussed in the previous section, $\Delta E\pi_{SOIE}$, defined by Equation 4.6, is a measure of the response of the backbone to the elongation of the chain length and is a useful parameter for the evaluation of the ECL. As expected, for all of the oligomers investigated, $\Delta E\pi_{SOIE}$ converges to an asymptotic value, indicating that the addition of two further terminal units has only a constant local effect on the backbone and does not lead to an enhancement of π -

delocalization along the chain. As shown in Figure 4.35, the $\Delta E\pi_{\text{SOIE}}$ of PA increases, upon elongation of the chain length more rapidly with respect to that of any other oligomers. The evolution of $\Delta E\pi_{\text{SOIE}}$ of PDA and PTA is similar; with the latter evolving slightly slower with respect to the former and converging to a value 2 kcal mol⁻¹ lower (see Figure 4.35). Interestingly, the evolution of $\Delta E\pi_{\text{SOIE}}$ for the linearly π -conjugated oligomers can be qualitatively correlated to the evolution of the excitation energies: the slope of the $\Delta E\pi_{\text{SOIE}}$ curves increases in the order PA \gg PDA $>$ PTA \geq pePTA, which is exactly the same order observed for the evolution of excitation energies (see Figure 4.30).

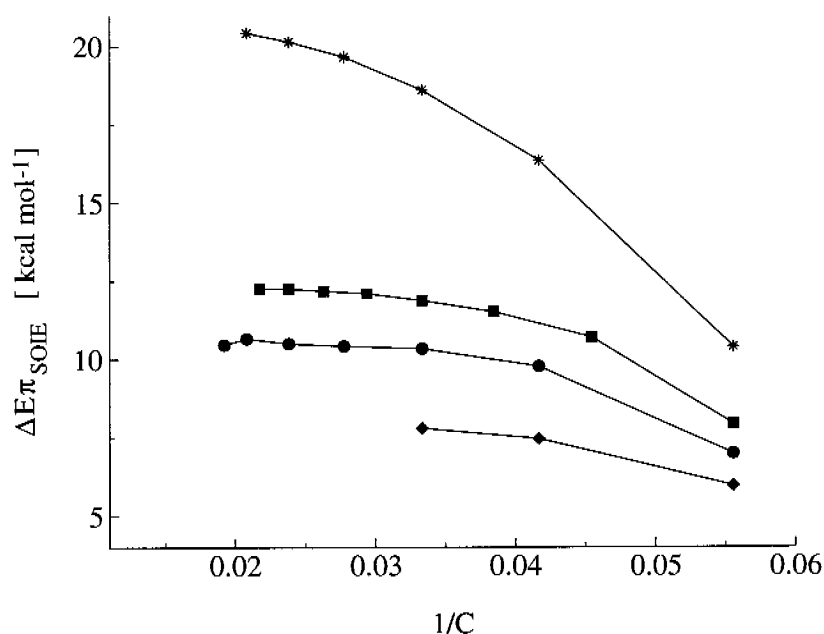


Figure 4.35: Evolution of $\Delta E\pi_{\text{SOIE}}$, as defined by Equation 4.6, as function of reciprocal number of (backbone) carbon atoms for the PA (*), PDA (■), PTA (●), and pePTA (◆) oligomers computed at the B3LYP/6-31G(d,p) level of theory. The definition of backbones and terminal groups is explained in the section 4.3.4.1.

In summary, for all the properties investigated above, we showed that the incorporation of an ethynyl group into the PA chain has a dramatic effect on the evolution of the physical properties investigated and on π -delocalization. On the other hand, the insertion of a second

triple bond (PDA \rightarrow PTA) does not significantly affect the values of the properties investigated, even as far as their evolution as a function of the chain length is concerned. In fact, for PDA and PTA, the values of all the calculated properties converge at the same ECL, and, for the excitation energy and second-order hyperpolarizability also to the same saturation value.

In addition, the results presented in this work, clearly show that the amount of π -electron delocalization is not *per se* the suitable parameter for the evaluation of the efficiency in promoting π -delocalization, but that also the evolution of π -electron delocalization as a function of the backbone length is a valuable parameter to be considered in order to get a better understanding of the extent of electron delocalization in π -conjugated molecular systems.

4.3.5 Conclusions

The present study shows that the insertion of ethynyl groups into the PA chain, to give PDA and PTA, increases the total amount of π -electron delocalization, but on the other hand, reduces significantly the efficiency with which π -electron delocalization is promoted. The triple bond act as spacer which controls the extent of π -electron delocalization along the backbone. Accordingly, all the physical observables computed for PA evolve as a function of the oligomer size more rapidly and converge to a saturation value for a larger ECL than those computed for PTA and PDA. We also showed that the insertion of a second ethynyl group into the PDA monomer units does not further affect the efficiency with which π -electron delocalization is promoted.

The addition of lateral ethynyl groups to PTA significantly increases the π -electron delocalization, but does not improve the evolution of the molecular and electronic properties as a function of the chain size. On the contrary, our analysis of delocalization reveals that the promotion of π -electron delocalization is slightly less efficient in pePTA than in PTA, an effect that should be ascribed to the competition between the additional 'local' conjugation pathways and the main conjugation path along the backbone.

4.4 Extended Systems: the Impact of Donor and/or Acceptor Functional Groups on Electron Delocalization of Polytriacetylene and Perethynyl-Polytriacetylene Oligomers

4.4.1 Summary

π -conjugated systems functionalized with electron donor and/or acceptor substituents are valuable materials with potential application in the field of molecular electronics and photonics. The type of functionalization, the length of the π -conjugated chain, as well as, the choice of the π -conjugation mode, play a crucial role for the properties of these compounds. A detailed knowledge of electron delocalization and its impact on molecular and electronic properties is therefore important for the rational optimization of the electronic characteristics of these materials.

In this subchapter the investigation of electron delocalization in π -conjugated compounds is extended to the donor and/or acceptor functionalized derivatives of polytriacetylene (PTA) and perethynyl-polytriacetylene (pePTA) oligomers of increasing chain length. Physical observables such as BLA, first allowed excitation energies, polarizabilities and second-order hyperpolarizabilities have been calculated and correlated with the degree of π -electron delocalization. The analysis of delocalization has been performed by applying our computational approach based on deletion energies and on second-order orbital interaction energies in the natural bond orbital (NBO) scheme as presented in Chapter 2 [16, 117, 118]. The analysis allows to evaluate which combination of substituents is more efficient in promoting π -electron delocalization.

4.4.2 Introduction

Monodisperse oligomers with precisely defined length and constitution are interesting as model compounds for π -conjugated polymers since they bridge the gap between oligomer and polymer domains, enabling the investigation of the physical properties in the region

where they start to show saturation. For this purpose a series of triethylsilyl-end-capped polytriacetylene (PTA) oligomers, up to the hexadecamer, have been synthesized and characterized by Diederich et al. [47, 50]. The study of their physical properties as a function of the oligomer size provided an estimate of the effective conjugation length (ECL) of 7-10 monomer units, a value in agreement with our theoretical calculations (see subchapters 4.2 and 4.3) [117]. Recently, a series of donor–donor (D/D; D = 4-(dimethylamino)-phenyl), and acceptor–acceptor (A/A; A = 4-nitrophenyl) terminally functionalized derivatives of PTA oligomers, ranging from monomer to hexamer, have been prepared in order to study the effects of the functionalization on the physical properties [126]. Both, the A/A and D/D derivatives showed saturation with respect to the first reduction potential for $n = 10$, a value equal to that determined for the parent (unsubstituted) PTA. However, for the D/D derivatives, the ECL evaluated from the deconvoluted maximum absorption wavelength was found to be equal to only 4 monomer units, while for the A/A derivatives a value of $n = 10$ was determined. In addition, the evolution of the second-order hyperpolarizability γ showed a strange behaviour: for both the D/D and A/A derivatives, the values of γ per monomer unit (γ_L) significantly increase up to tetramer and then drop drastically for the pentamers and hexamers. This peculiar behaviour, might originate from the experimental conditions (solvent, etc.), and in order to get a better insight into the relationships between physical observables and π -electron delocalization we carried out a computational study on the same compounds investigated experimentally (with the N-methyl groups of the donor substituent replaced by hydrogen atoms), as well as on the donor-acceptor (A/D) terminally functionalized derivatives of PTA oligomers. Our investigation also covers the corresponding functionalized derivatives of perethynyl-polytriacetylene (pePTA) oligomers (see Figure 4.36), in order to assess the effects of the lateral addition of ethynyl groups to the PTA backbone.

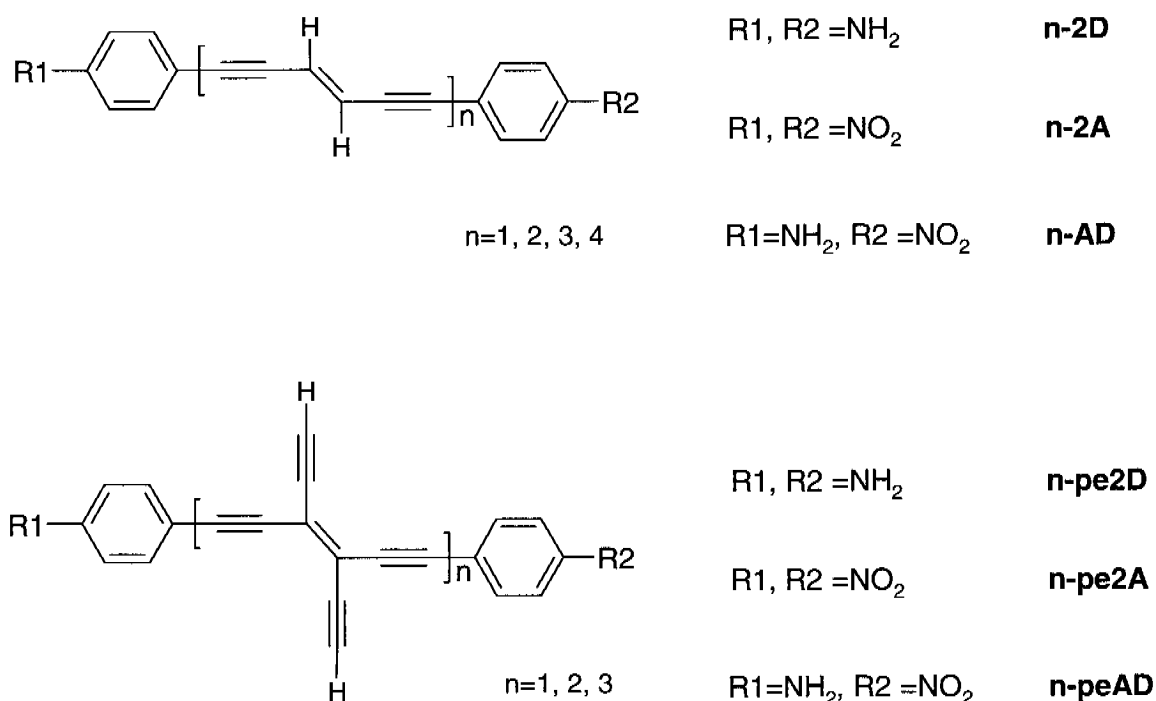


Figure 4.36: The compounds considered in this study and their corresponding labels

In the section “Results and Discussion” the delocalization parameters used in the present analysis of π -electron delocalization are first introduced. Calculated physical observables such as BLA, first allowed excitation energy, polarizability, and second-order hyperpolarizability are then presented and discussed as function of the oligomer size. Finally, the extent of electron delocalization is investigated using our approach and correlated to the evolution of the physical properties.

4.4.3 Computational Methods

All geometry optimizations and NBO analysis were performed in the Density Functional Theory (DFT) scheme [40], using the B3LYP functional [41, 42] together with 6-31G(d,p) basis set of Gaussian orbitals [65].

The linear optical absorption properties were computed at the ZINDO/S level of theory [71-77, 87] on the geometries optimized at the B3LYP/6-31G(d,p) level. In the ZINDO calculations, all occupied and virtual orbitals were retained in the active space.

Frequency dependent polarizabilities (α) and third harmonic generation (THG) hyperpolarizabilities (γ_{THG}) have been calculated using the coupled-perturbed (CP) scheme [82] with the MNDO Hamiltonian [83] at the 1907 nm (0.65 eV) incident wavelength radiation. In the following we will discuss the linear and nonlinear optical coefficients in terms of the averaged polarizability ($\bar{\alpha}$) and hyperpolarizability ($\bar{\gamma}$), defined as:

$$\bar{\alpha} = \frac{1}{3}(\alpha_{xx} + \alpha_{yy} + \alpha_{zz}), \text{ and} \quad (4.10)$$

$$\bar{\gamma} = \frac{1}{15}(\gamma_{zzzz} + \gamma_{yyyy} + \gamma_{xxxx} + 2\gamma_{zzxx} + 2\gamma_{zzyy} + 2\gamma_{xxyy}) \quad (4.11)$$

respectively, where z is the charge transfer axis, and α_{ii} and γ_{ijij} are elements of the polarizability and hyperpolarizability tensor, respectively. In order to compare computed and measured γ values, the theoretical values were multiplied by factors derived from phenomenological approach [119].

Geometry optimizations and excitation energy calculations have been carried out using the Gaussian98 package [45]. The natural bond orbital analysis has been performed with the program NBO 5.0 [44] included in Gaussian98. Polarizability and second-order hyperpolarizability calculations have been performed with the program MOPAC2000 [84] on the geometries optimized at the B3LYP/6-31G(d,p) level of theory.

4.4.4 Results and Discussion

4.4.4.1 Technical details of the analysis

For the evaluation of the extent of π -electron delocalization upon the addition of the functional groups, it is useful to introduce the quantity ΔE_{π} defined as:

$$\Delta E_{\pi} = E_{\pi}^{\text{tot}} - (E_{\pi}^{\text{bb}} + E_{\pi}^{\text{funct}}) \quad (4.12)$$

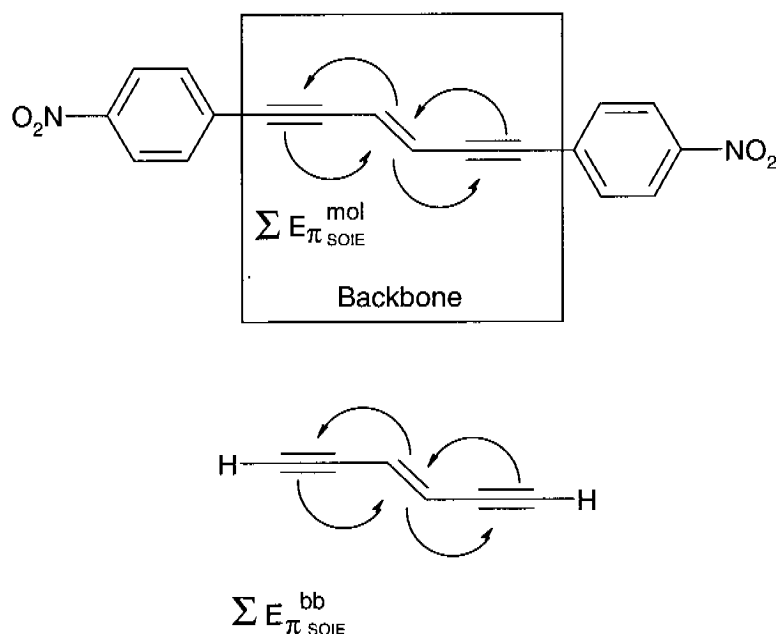
where E_{π}^{tot} is the delocalization energy calculated by deleting all perpendicular π^* NBOs of the molecule, E_{π}^{bb} is the delocalization energy calculated by deleting the perpendicular π^* NBOs of the backbone only, and E_{π}^{funct} is calculated by deleting the perpendicular π^* NBOs of the functional groups. For instance, ΔE_{π} of **1-2A** (see Figure 4.37) is obtained by subtracting from E_{π}^{tot} , calculated by deleting all the eleven π^* NBOs of the molecule, the sum of E_{π}^{bb} and E_{π}^{funct} , calculated by deleting the three π^* NBOs of the PTA backbone and the eight π^* NBOs of the two nitrophenyl groups, respectively. ΔE_{π} thus, corresponds to the change of the π -delocalization energy of the functionalized derivative with respect to backbone and functional groups considered as three non-interacting fragments.

Another quantity useful in the present context is the response of the backbone to the functionalization. For this purpose we use the second-order orbital interaction energies (SOIE) between donor and acceptor orbitals in the conjugation path, introducing the parameter $\Delta E\pi_{SOIE}$ defined as:

$$\Delta E\pi_{SOIE} = \sum E\pi_{SOIE}^{mol} - \sum E\pi_{SOIE}^{bb} \quad (4.13)$$

where $\sum E\pi_{SOIE}^{mol}$ is the sum of the E_{SOIE} energies between vertical π orbitals of the backbone in the functionalized derivative, and $\sum E\pi_{SOIE}^{bb}$ is the sum of the E_{SOIE} energies between vertical π orbitals of the parent PTA oligomer. The E_{SOIE} interactions to be considered in the summations are explained in Figure 4.37.

$\Delta E\pi_{SOIE}$ is equivalent to the parameter described in section 4.3.4, with the ‘terminal π -conjugated units’ of the oligomers replaced by the donor and/or acceptor functional groups.



$$\Delta E\pi_{SOIE} = \sum E\pi_{SOIE}^{mol} - \sum E\pi_{SOIE}^{bb}$$

Figure 4.37: Schematic representation of the partitioning of **1-2A** into a core backbone and two terminal functional groups. $\Delta E\pi_{SOIE}$ is calculated as the difference between the sum of $E\pi_{SOIE}$ of the **1-2A** backbone ($\sum E\pi_{SOIE}^{mol}$) and the sum of $E\pi_{SOIE}$ of the parent oligomer ($\sum E\pi_{SOIE}^{bb}$).

Finally, for the calculation of the BLA of the backbone we introduce the generalized parameter δR defined as:

$$\delta R = (C_D - C_T) - (C=C + C\equiv C)/2 \quad (4.14)$$

while for the evaluation of the BLA of the aromatic rings (quinoid character) we define the δC parameter as:

$$\delta C = \frac{(b - a) + (c - a)}{2} \quad (4.15)$$

where a, b, and c are the bond length shown in Figure 4.38. The δC values calculated for the references aniline and p-nitrobenzene are equal to 0.003 and 0.008 Å, respectively.

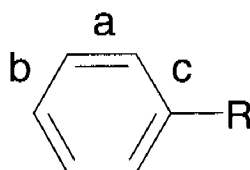


Figure 4.38: Labels of the bonds referred to Equation 4.15

4.4.4.2 π -delocalization in the functionalized PTA and pePTA oligomers

Molecular structure of neutral species. The functionalization of the parent DEE with donor and/or acceptor moieties significantly affects the geometrical parameters of the backbone. For **1-2A**, the C=C and C \equiv C bonds of the backbone lengthen by about 0.010 and 0.005 Å, respectively, while the C–C bond shorten by about 0.010 Å (see Table 4.11 for the geometrical parameters of the functionalized derivatives, and

Table 4.4 for the geometrical parameters of the parent PTA oligomers). The δR parameter decreases from 0.134 in the parent DEE to 0.117 in **1-2A** indicating strong delocalization in the functionalized compound. For the D/D and A/D derivatives **1-2D** and **1-AD**, the effects are even larger (see Table 4.11). The evolution of δR as a function of the chain length of the backbone is illustrated in Figure 4.39. The values of δR decrease with increasing chain length of the backbone and appear to converge to the saturation value calculated for the parent PTA oligomers. In the case of the A/D and D/D functionalized derivatives, the curve rapidly flatten and is nearly converged at the level of the trimer and tetramer, respectively, while for the A/A derivatives the curve appears to converge more slowly i. e. for larger number of monomer units. These results can be correlated with the experimentally determined Raman-

active stretches of the C \equiv C bonds ($\tilde{\nu}_{\text{C}\equiv\text{C}}$) obtained for the A/A and D/D derivatives of PTA oligomers [126]. The values of $\tilde{\nu}_{\text{C}\equiv\text{C}}$ decrease with increasing length of the backbone and finally converge to the same value measured for the parent PTA oligomers. The $\tilde{\nu}_{\text{C}\equiv\text{C}}$ values measured for the D/D derivatives are systematically lower than those of the A/A derivatives and converge at the trimer.

As already discussed in the previous subchapter, the lateral addition of ethynyl units to the PTA backbone leads to a significant lengthening of the C=C bonds (about 0.03 Å; see Table 4.11), while the C \equiv C and C–C bonds along the backbone pathway, slightly shorten. This peculiar behaviour has been explained with the competition between the additional short conjugation pathways and the main conjugation path along the backbone.

The δR parameters of the functionalized pePTA compounds are distinctly smaller than those of the corresponding PTA derivatives. However, as shown in Figure 4.39, their evolution as a function of the backbone length is nearly parallel to that discussed for the PTA derivatives; the δR values evolve slowly with increasing the backbone length and again appear to converge to the same value as the parent pePTA oligomers.

In Table 4.11 we also report the values of the δC parameter (Equation 4.15) which, as stated above, gives a measure of the quinoid character of the aromatic rings. The δC parameter increases significantly upon functionalization of the parent DEE, for both donor (0.015 Å) and acceptor (0.013 Å) substituents. However, the further extension of the backbone size has only a little effect on δC . In the case of the D/D derivatives, δC rises up to the tetramer, whereas for the A/A derivatives δC increase up to the trimer and then slightly decrease. The addition of the lateral ethynyl groups to the backbone does not affect the value of δC .

Table 4.11: Selected geometrical parameters of D/D, A/A and A/D functionalized derivatives of PTA and pePTA oligomers.

	C=C	C≡C	C-C	δR^a	δC^b
1-2D	1.362	1.220	1.409	0.1162 (0.1344)	0.023
2-2D	1.365	1.227	1.403	0.1068 (0.1142)	0.024
3-2D	1.367	1.227	1.401	0.1037 (0.1065)	0.025
4-2D	1.367	1.227	1.400	0.1032 (0.1045)	0.025
1-2A	1.361	1.219	1.408	0.1173 (0.1344)	0.016
2-2A	1.364	1.226	1.402	0.1075 (0.1142)	0.017
3-2A	1.366	1.226	1.401	0.1045 (0.1065)	0.017
4-2A	1.367	1.227	1.400	0.1037 (0.1045)	0.016
1-AD	1.363	1.221	1.406	0.1137 (0.1344)	0.025-0.018
2-AD	1.365	1.227	1.401	0.1054 (0.1142)	0.026-0.017
3-AD	1.367	1.227	1.400	0.1029 (0.1065)	0.026-0.017
4-AD	1.367	1.227	1.400	0.1029 (0.1045)	0.026-0.018
1-pe2D	1.393	1.219	1.413	0.1071 (0.1274)	0.024
2-pe2D	1.396	1.225	1.409	0.0984 (0.1058)	0.025
3-pe2D	1.398	1.226	1.407	0.0957 (0.0980)	0.026
1-pe2A	1.392	1.218	1.414	0.1094 (0.1274)	0.016
2-pe2A	1.394	1.225	1.409	0.0997 (0.1058)	0.016
3-pe2A	1.397	1.225	1.408	0.0965 (0.0980)	0.016
1-peAD	1.394	1.219	1.412	0.1053 (0.1274)	0.026-0.017
2-peAD	1.396	1.226	1.408	0.0973 (0.1058)	0.027-0.017
3-peAD	1.398	1.226	1.407	0.0949 (0.0980)	0.027-0.017

a) In parentheses are reported the δR values of the corresponding parent PTA and pePTA oligomers.

*b) For the **n-AD** derivatives are reported the δC parameter for both the nitro-phenyl (left) and anilino (right) aromatic rings.*

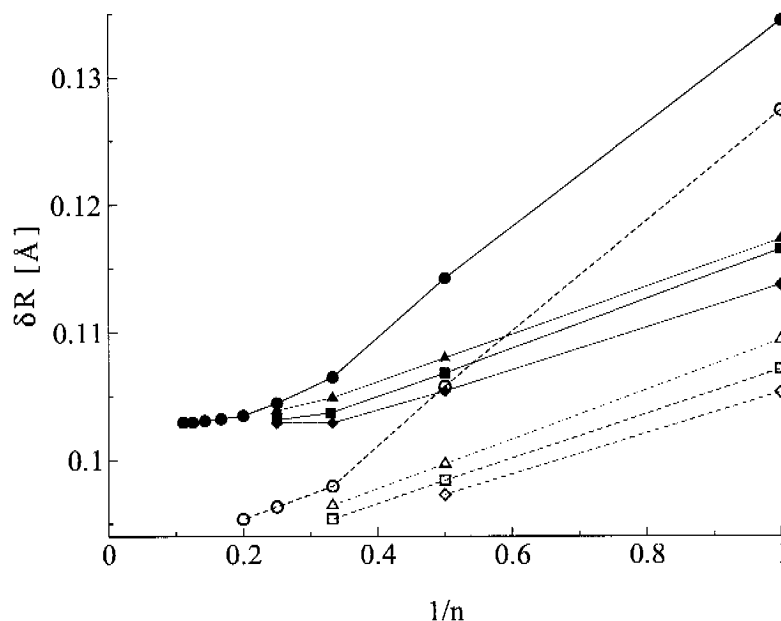


Figure 4.39: The BLA expressed in terms of the δR parameter of D/D (**n-2D**; $n=1-4$; ■), A/A (**n-2A**; $n=1-4$ ▲), A/D (**n-AD**; $n=1-4$; ◆) PTA derivatives and D/D (**n-2D**; $n=1-3$; □), A/A (**n-2A**; $n=1-3$; △), A/D (**n-AD**; $n=1-3$; ◇) pePTA derivatives as a function of the inverse of the number of monomer units of the backbone, computed at the B3LYP/6-31G(d,p) level of theory. In the Figure are also reported the δR parameters of the parent PTA (●) and pePTA (○) oligomers.

Linear and Nonlinear Optical Properties. Linear and nonlinear optical data of PTA and pePTA functionalized derivatives are reported in Table 4.12. The functionalization of the parent DEE leads to a substantial bathochromic shift of the maximum absorption wavelength (λ_{\max}). This bathochromic shift is larger for the A/A and A/D derivatives than for the D/D one. The evolution of the values of the excitation energies is quite slower than that of the corresponding parent oligomers and appears to converge to the same saturation value (see Figure 4.40); a trend similar to that discussed for the δR parameters. In addition, the impact of the type of functionalization on the calculated excitation energies is reduced with increasing the chain length of the PTA backbone, indicating that the excitation energies are increasingly dominated by the length of the backbone and not by the type of functionalization. In the case of the derivatives of the PTA tetramer, all calculated excitation energies are very similar, suggesting that beyond the tetramer the choice of the donor and/or acceptor substitution is no longer discriminating with respect to the excitation energies. The

calculated values of excitation energy are in acceptable agreement with the experiment (calculated and experimental values are always within 0.2 eV). However, they are in a qualitative disagreement, as the experimental excitation energy of the A/A derivatives is larger than that of the D/D ones, while the reverse order is found for the calculated values (see Table 4.12 and Figure 4.40). Furthermore, the faster saturation of λ_{max} versus n of the D/D substituted oligomers [126] is not reproduced by the calculated excitation energies. The discrepancy between the experimental and calculated values could be explained considering that in our model compounds the nitrogen atom of the $\text{R}_2\text{NC}_6\text{H}_4$ group is substituted by two hydrogen atoms ($\text{R} = \text{H}$), while in the molecules investigated experimentally the nitrogen atom is substituted by two methyl groups ($\text{R} = \text{CH}_3$). In this respect, Diederich et al. found that the N-substitution of the $\text{R}_2\text{NC}_6\text{H}_4$ donor group strongly influence the position of the maximum absorption wavelength [32]. In particular, the substitution of two hydrogen atoms with two methyl groups produces a bathochromic shift of about 20 nm in donor-acceptor substituted tetrakis-arylated TEE. Preliminary calculations, to investigate this effect show that the two methyl groups in the N-methyl substituted compounds, are sterically hindered inducing a larger sp^2 character on the nitrogen atom, and correspondingly, increasing the electron-releasing strength of the donor group.

Table 4.12: Electronic, linear, and nonlinear optical data of D/D, A/A and A/D functionalized derivatives of PTA and pePTA oligomers

	HOMO ^{a,d}	LUMO ^{a,d}	$\lambda_{\text{max}}^{\text{b,d}}$	$\lambda_{\text{max}}^{\text{expt. d,g}}$	$\alpha^{\text{c,e}}$	$\gamma^{\text{c,f}}$	$\gamma^{\text{expt. f,h}}$
1-2D	-4.60	-1.40	3.17	3.03	773	108	123
2-2D	-4.74	-2.07	2.75	2.72	1231	349	430
3-2D	-4.82	-2.45	2.60	2.64	1723	748	740
4-2D	-4.88	-2.70	2.51	2.62	2230	1272	1320
1-2A	-6.26	-3.21	2.99	3.08	813	117	88
2-2A	-5.90	-3.29	2.70	2.88	1265	359	220
3-2A	-5.71	-3.34	2.58	2.72	1751	742	460

Table 4.12: Electronic, linear, and nonlinear optical data of D/D, A/A and A/D functionalized derivatives of PTA and pePTA oligomers (continued)

	HOMO ^{a,d}	LUMO ^{a,d}	$\lambda_{\max}^{\text{b,d}}$	$\lambda_{\max}^{\text{expt. d,g}}$	$\alpha^{\text{c,e}}$	$\gamma^{\text{c,f}}$	$\gamma^{\text{expt. f,h}}$
4-2A	-5.60	-3.38	2.51	2.69	2250	1233	720
1-AD	-5.31	-2.60	2.94	2.75	811	164	250
2-AD	-5.20	-2.85	2.69	2.71	1264	415	465
3-AD	-5.15	-3.01	2.57		1749	805	
4-AD	-5.66	-3.60	2.50		2243	1284	
1-pe2D	-4.70	-1.92	2.88	2.70	899	137	
2-pe2D	-4.79	-2.53	2.51	2.55	1473	517	
3-pe2D	-4.88	-2.87	2.37		2092	1207	
1-pe2A	-6.28	-3.08	2.86	3.07	924	140	
2-pe2A	-5.83	-3.52	2.50	2.72	1479	485	
3-pe2A	-5.67	-3.61	2.37		2107	1134	
1-peAD	-5.31	-2.77	2.74	2.65	924	196	
2-peAD	-5.21	-3.10	2.48	2.58	1502	602	
3-peAD	-5.17	-3.29	2.36		2113	1278	

a) HOMO and LUMO are calculated at the B3LYP/6-31G(d,p) level of theory on the geometries optimized at the same level. b) λ_{\max} are calculated at the ZINDO level of theory on the geometries optimized at the B3LYP/6-31G(d,p) level. c) α and γ are calculated at the CP-MNDO level of theory on the geometries optimized at the B3LYP/6-31G(d,p) level. d) in eV. e) in $10^{-25} \text{ cm}^3 \text{ esu}^{-1}$. f) in $10^{-36} \text{ cm}^7 \text{ esu}$. g) Longest-wavelength absorption maximum in CHCl_3 at 20°C obtained by deconvolution of the absorption spectra. h) Obtained from third harmonic experiments (THG) at a fundamental wavelength of $\lambda=1907 \text{ nm}$.

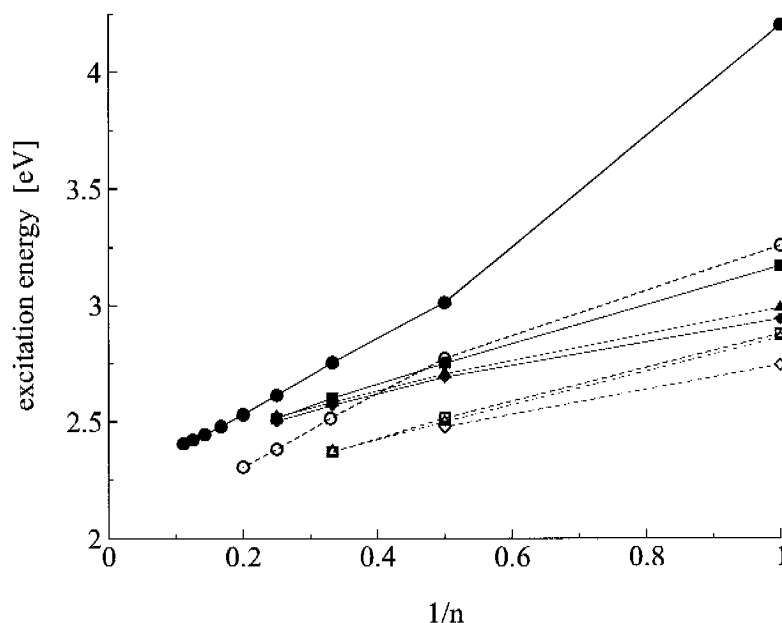


Figure 4.40: First allowed excitation energies of D/D (*n*-2D; *n*=1-4; ■), A/A (*n*-2A; *n*=1-4 ▲), A/D (*n*-AD; *n*=1-4; ◆) PTA derivatives and D/D (*n*-2D; *n*=1-3; □), A/A (*n*-2A; *n*=1-3; △), A/D (*n*-AD; *n*=1-3; ◇) pePTA derivatives as a function of the inverse of the number of monomer units of the backbone, computed at the ZINDO level. In the Figure are also reported the first allowed excitation energies of the parent PTA (●) and pePTA (○) oligomers.

The substitution of the donor and/or acceptor functional groups in DEE has a dramatic effect on the calculated polarizability α . Notably, for all of the type of functionalization, the values of α are larger than the saturation value calculated for the parent PTA oligomers (see Figure 4.41). The extension of the π -conjugated backbone gives rise to a peculiar evolution of the values of α . As the absolute values of α increase with increasing the backbone size, the values divided by the number of monomer units (α_n) decrease, slowly approaching to a value slightly larger than that of the parent PTA (see Figure 4.41). This is clearly due to the dominant control of the backbone on the values of α . However, it is interesting to note that, contrary to the δR and excitation energy, the functional groups seem to slightly affect the α_n values also beyond the ECL. As shown in Figure 4.40, the calculated polarizability of the A/A, D/D and A/D derivatives are very similar indicating that the value of α_n is not discriminated by the type of the functionalization.

The second-order hyperpolarizabilities γ , in the range within monomer and tetramer, increases with the power law $\gamma = \gamma_m n^a$, where γ_m and a are constants (see Table 4.12 and Figure 4.42) [109, 123, 124]. The functionalization of the parent DEE with donor and/or acceptor groups significantly increases the nonlinearity, up to 11, 10, and 16 times for the D/D, A/A and A/D derivatives, respectively. The two dimensional extension of the backbone core (DEE \rightarrow TEE) increases the γ values. However, the enhancement with respect to the parent TEE (7, 7, and 10 times for the D/D, A/A and A/D derivatives, respectively) is smaller than that calculated for the DEE ones. As observed for the other physical properties investigated, the values of γ divided for the number of monomer units (γ_n) increase quite slower than the corresponding values of the parent PTA oligomers and appear to converge to the same value calculated for the parent PTA. The values of γ_n calculated for the donor and/or

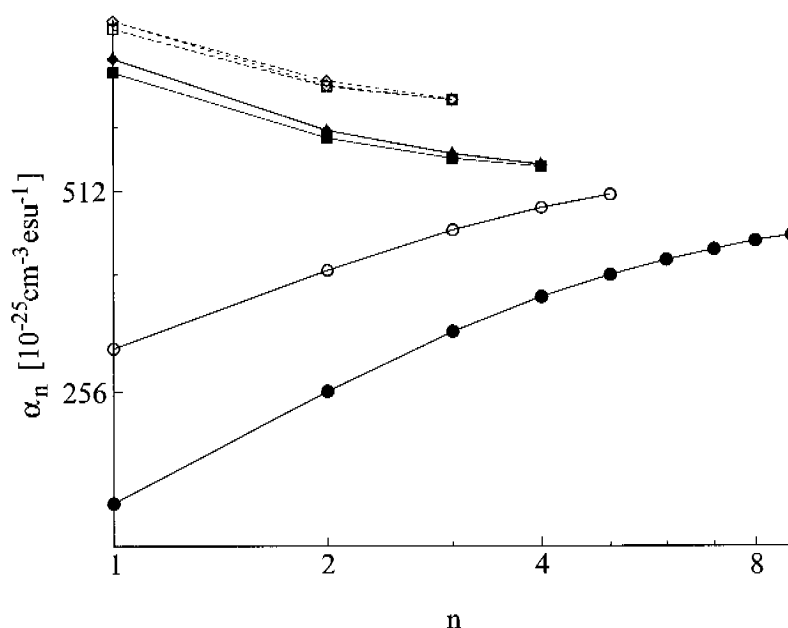


Figure 4.41: Polarizability per monomer unit (α_n) of D/D (**n-2D**; $n=1-4$; ■), A/A (**n-2A**; $n=1-4$ ▲), A/D (**n-AD**; $n=1-4$; ◆) PTA derivatives and D/D (**n-2D**; $n=1-3$; □), A/A (**n-2A**; $n=1-3$; △), A/D (**n-AD**; $n=1-3$; ◇) pePTA derivatives as a function of the number of monomer units of the backbone, computed at the CP-MNDO level. In the Figure are also reported the α_n of the parent PTA (●) and pePTA (○) oligomers.

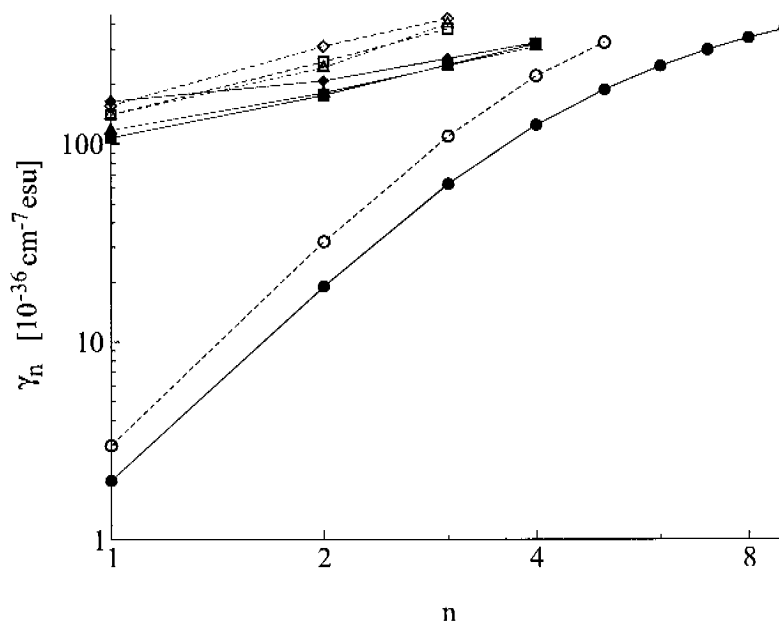


Figure 4.42: Second-order hyperpolarizability per monomer unit (γ_n) of D/D (**n-2D**; $n=1-4$; ■), A/A (**n-2A**; $n=1-4$ ▲), A/D (**n-AD**; $n=1-4$; ◆) PTA derivatives and D/D (**n-2D**; $n=1-3$; □), A/A (**n-2A**; $n=1-3$; △), A/D (**n-AD**; $n=1-3$; ◇) pePTA derivatives as a function of the number of monomer units of the backbone, computed at the CP-MNDO level. In the Figure are also reported the γ_n of the parent PTA (●) and pePTA (○) oligomers.

acceptor functionalized tetramers are very similar and slightly lower than the saturation value extrapolated for the parent PTA oligomers (see Figure 4.42), therefore, suggesting that the effective conjugation length, based on the evolution of γ_n is attained at $n = 5-6$. It is worth to note that the values of γ_n calculated at the CP-MNDO level of theory on the B3LYP optimized geometries, are in acceptable agreement with the experimental THG values (see Table 4.12); the trends are well reproduced with the exception of the γ_n values of the A/A derivatives which, contrary to the experiment, are larger than those calculated for the D/D compounds. The experimentally determined ECL value of $5 \div 6$ should also be well reproduced, even though the investigation of the pentamer and hexamer derivatives will be necessary to confirm these results.

Analysis of π -delocalization

The values of ΔE_π for the PTA and pePTA functionalized derivatives, calculated according to Equation 4.12, are reported in Figure 4.43. In order to consider the effects of the extension of the backbone chain on π -delocalization, in Figure 4.43 we also report the ΔE_π values calculated by replacing the functional groups by two extra monomer units.

Interestingly, the value of ΔE_π calculated for the addition of two extra monomer units to the parent DEE (PTA trimer) is about twice as large as that computed for the addition of D/D and A/D functional groups. This result clearly suggests that the extension of the linear π -conjugation of the PTA backbone promotes π -delocalization more than the functionalization with acceptor and/or donor substituents. Among the functionalized derivatives, the larger

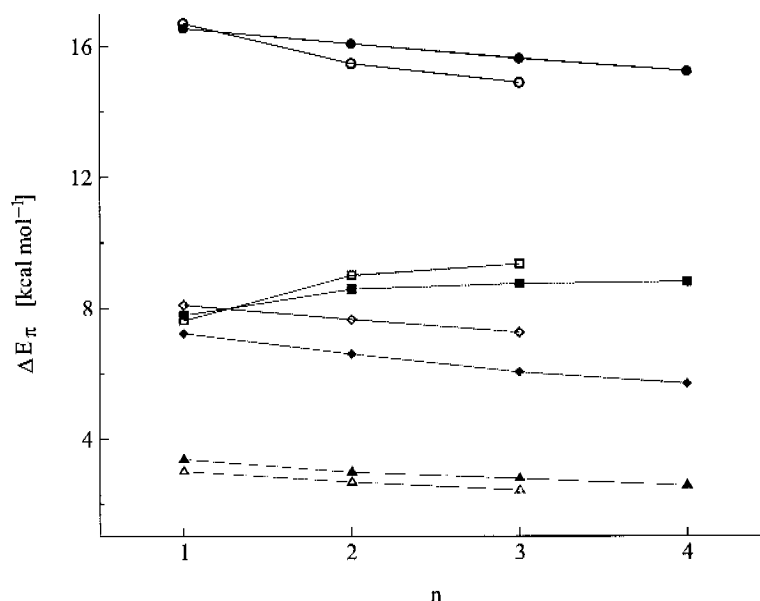
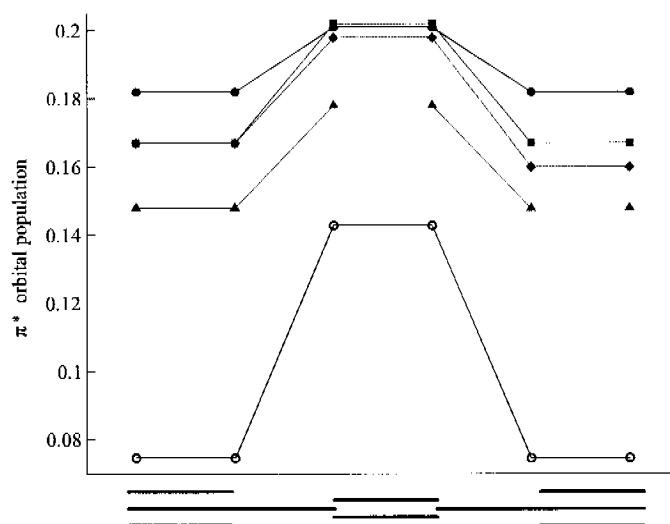


Figure 4.43: ΔE_π values, as defined by Equation 4.12, of D/D (*n*-2D; *n*=1-4; ■), A/A (*n*-2A; *n*=1-4 ▲), A/D (*n*-AD; *n*=1-4; ◆) PTA derivatives and D/D (*n*-2D; *n*=1-3; □), A/A (*n*-2; *n*=1-3; △), A/D (*n*-AD; *n*=1-3; ◇) pePTA derivatives as a function of the number of monomer units of the backbone. (●) and (○) stand for the ΔE_π values of the parent PTA and pePTA oligomers, respectively, to which two extra monomer units have been added

ΔE_{π} value is calculated for **1-2D** (7.8 kcal mol⁻¹), while a value about 0.5 kcal mol⁻¹ lower is calculated for **1-AD**. The ΔE_{π} of **1-2A** is equal to 3.4 kcal mol⁻¹; a value more than 4 kcal mol⁻¹ lower than that of **1-2D** derivative.

The ΔE_{π} values of all the compounds but the D/D derivatives slightly decrease (within 2 kcal mol⁻¹) with increasing oligomer size and rapidly approach to a saturation. This indicates

a)



b)

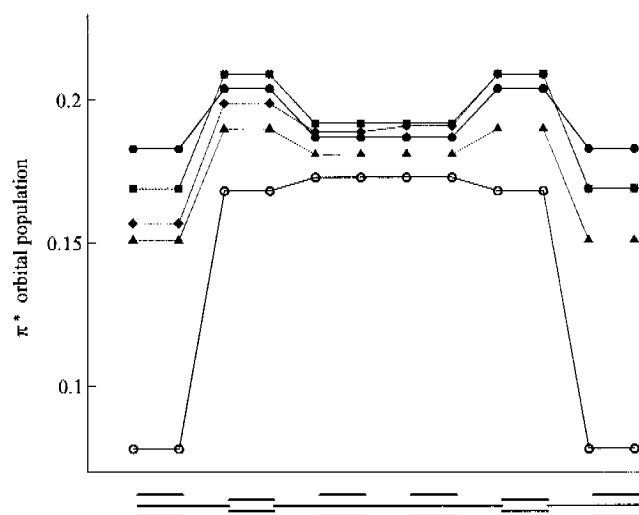


Figure 4.44: π^* orbital population along the a) DEE backbone and b) PTA dimer for D/D (■), A/A (▲), A/D (◆) terminally functionalized derivatives. In the Figure we also report the π^* orbital population of the parent backbone (○) and of the backbone to which two extra monomer units have been added (●).

that ΔE_{π} is governed by the local interaction between the backbone and the functional groups (see Figure 4.43) which rapidly approach to a constant value. A smaller term accounts for the relaxation along the backbone chain. This latter term decreases slightly since the extension of the backbone length favours the relaxation within the backbone, and therefore, compensates the effects provided by the addition of the functional groups. However, for the D/D derivatives ΔE_{π} slightly increases with the elongation of the chain length, indicating that the donor functional group provides a peculiar enhancement of π -delocalization in the functionalized derivative. To further investigate this effect in Figure 4.44 we report the π^* orbital population profile along the backbone for the functionalized derivatives of the PTA monomer (DEE) and dimer. As expected, the **n-AA** compounds have a small π^* orbital occupation, an observation which accounts for the lower values of ΔE_{π} . Interestingly, the addition of two monomer units to the PTA chain supplies the larger π^* orbital population in the vicinal (terminal) C \equiv C bonds of the backbone, while the D/D functionalization promotes the larger orbital population for the other π^* orbitals within the backbone (see Figure 4.44). This effect is more evident in the **2-DD** derivative, for which the π^* orbital occupancies within the core backbone are slightly larger than that of the PTA trimer, while only the π^* orbital population of the terminal C \equiv C bonds is significantly larger for the latter. This points out that, comparing the extension of PTA chain length with the D/D functionalization, the larger ΔE_{π} value found for the former is largely due to the local interaction at the backbone-functional group boundary. On the other hand the D/D functionalization promotes π -electron delocalization slightly better along the backbone. This result is explained by considering that the linearly π -conjugated units added to the backbone act as good donors and good acceptors, while the D/D functional groups act as good donors but poor acceptors. In terms of intramolecular donor \rightarrow acceptor interactions, this means that, for the former, the electron density transferred from the 'functional group' to the backbone is compensated by a similar electron density transferred from the backbone to the 'functional group', while for the latter, the accumulation of the charge transferred from the functional group can only be dispersed along the backbone. Interestingly, these results suggest that a functional group which behaves

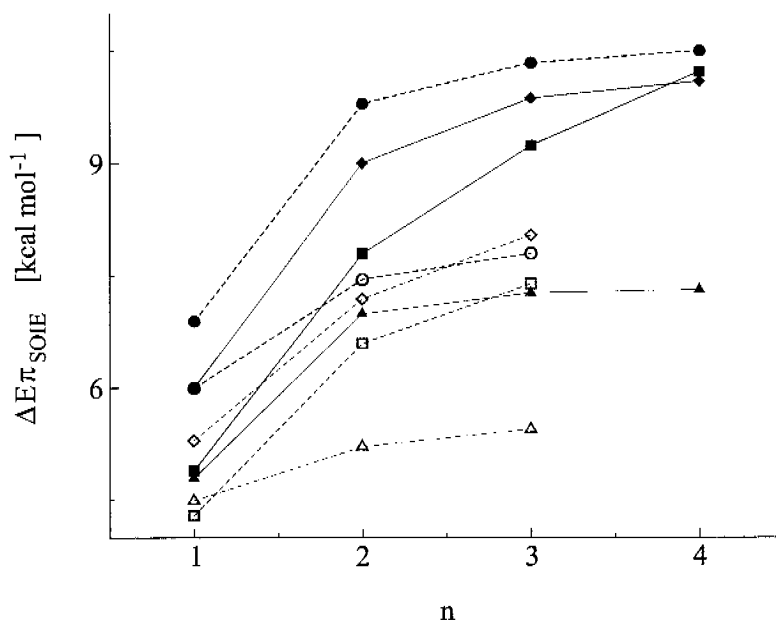


Figure 4.45: $\Delta E\pi_{S0IE}$ values, as defined by Equation 4.13, of D/D (*n*-2D; *n*=1-4; ■), A/A (*n*-2A; *n*=1-4 ▲), A/D (*n*-AD; *n*=1-4; ◆) PTA derivatives and D/D (*n*-2D; *n*=1-3; □), A/A (*n*-2A; *n*=1-3; △), A/D (*n*-AD; *n*=1-3; ◇) pePTA derivatives as a function of the number of monomer units of the backbone. (●) and (○) stand for the $\Delta E\pi$ values of the parent PTA and pePTA oligomers, respectively, to which two extra monomer units have been added.

both as a good donor and acceptor is not efficient in promoting π -delocalization along a conjugated chain.

In the case of the A/D derivatives, the π^* orbital occupancies are in between those calculated for the A/A and D/D substituted compounds; exactly equal to that of the D/D derivative in the segment of the backbone near to the donor functional group (indicating the dominant effect of this group) but larger than that calculated for the A/A derivative in the segment near to the acceptor functional group (see Figure 4.44). This accounts for the lower $\Delta E\pi$ values calculated for the A/D derivatives with respect to the D/D ones. It should be noted however that the asymmetric substitution produces an asymmetric charge distribution along the backbone, and therefore a larger charge separation. This effect explains the linear and

nonlinear optical properties calculated and measured experimentally for this class of compounds.

The trend observed for the pePTA derivatives is quite parallel to that discussed above for the PTA derivatives. In addition, the values of ΔE_π are very similar to those of the PTA derivatives (see Figure 4.43). In this respect, it is interesting to note that the addition of the acetylenic arms in the pePTA backbone has only a little effect on the values of ΔE_π .

A better insight into the ability of the different functional groups to promote π -delocalization into the backbone can be obtained by the analysis of the second-order orbital interaction energies $\Delta E\pi_{\text{SOIE}}$ (Equation 4.13), which measure the response of the backbone to functionalization, and which also take into account the geometry relaxation induced by the increase of π -delocalization (see Figure 4.45). As for the ΔE_π values, the extension of the linear conjugation in the PTA monomer leads to a larger value of $\Delta E\pi_{\text{SOIE}}$. The functionalization with electron acceptors and donors leads to the following order of the $\Delta E\pi_{\text{SOIE}}$ values; $A/D > D/D > A/A$. The extension of the PTA backbone chain leads to a systematic increase of the $\Delta E\pi_{\text{SOIE}}$ values, which converge to an asymptotic value when the functional groups do not further affect the π -delocalization within the backbone. As expected, in the case of the A/A derivatives, the extension of the backbone chain length has a small effect on the $\Delta E\pi_{\text{SOIE}}$ compared to that of the other derivatives (see Figure 4.45). The addition of the A/A functional groups to the PTA backbones gives both, lowest $\Delta E\pi_{\text{SOIE}}$ values and weakest response of the backbone to the elongation of the chain length. This indicates that the effect on π -delocalization into the backbone given by the acceptor functional group is rapidly saturated and that the further evolution of π -delocalization is governed by the backbone itself. The control of the backbone over π -delocalization explains the slower evolution of the physical observables discussed above and observed experimentally. The best response on the extension of the backbone is observed for the D/D derivatives, which appear to promote π -delocalization more efficiently than any other class of compounds (see Figure 4.45) and should explain the rapid saturation to the asymptotic value measured from the experiment.

The trend of the pePTA derivatives is parallel to that described for the PTA ones (see Figure 4.45). The $\Delta E\pi_{\text{SOIE}}$ values are systematically lower than the corresponding values for

the PTA derivatives suggesting a slightly less efficient promotion of π -delocalization into the backbone. The ethynyl arms increases the total amount of π -delocalization, but the competition between the additional “local” conjugation pathways and the main conjugation path reduces the efficiency in promoting π -delocalization. It could also lead to a ‘dispersion’ of delocalization into the backbone, reducing the effects given by the additional functional groups.

4.4.5 Conclusions

The donor/acceptor terminal functionalization of PTA and pePTA oligomers produces dramatic effects on the molecular and electronic properties as long as the bridge between the two functional groups (backbone) is short. These effects reduce with increasing the chain length. All of the properties investigated (with the only exception of the polarizability) appear to converge to the same saturation value as for the parent oligomers suggesting that the π -delocalization is governed by the π -conjugated backbone for large oligomers. Furthermore, with the exception of the δR parameter, beyond a number of backbone monomer units of 4-5, the values of the physical observables investigated are no longer discriminated by the type of functionalization.

The analysis of electron delocalization shows a peculiar behavior of the donor functional group that could account for the rapid saturation of the physical observables observed experimentally for the D/D functionalized derivatives. In fact, we found that the donor functional group promotes π -delocalization along the backbone more efficiently than any other substituent investigated in this work.

Finally, we showed that the evolution of the computed δR and γ values are in close agreement with the experimental finding, while for the first allowed excitation energies are in qualitative disagreement. This discrepancy has been explained by the fact that in the model compounds the two N-substituted methyl groups have been replaced by two hydrogen atoms.

4.5 References

1. U. H. F. Bunz, Poly(aryleneethynylene)s: Syntheses, Properties, Structures, and Applications. *Chem. Rev.*, **2000**, *100*, 1605-1644.
2. Modern Acetylene Chemistry, ed. P. J. Stang, F. Diederich. **1995**, Weinheim: VCH.
3. Carbon Rich Compounds II. Vol. 201, ed. A. d. Meijere.. **1999**, Berlin: Springer.
4. D. L. Pearson, J. S. Schumm, J. M. Tour, Iterative Divergent/Convergent Approach to Conjugated Oligomers by a Doubling of Molecular Length at Each Iteration. A Rapid Route to Potential Molecular Wires. *Macromolecules*, **1994**, *27*, 2348-2350.
5. J. S. Schumm, D. L. Pearson, J. M. Tour, Iterative Divergent/Convergent Doubling Approach to Linear Conjugated Oligomers. A Rapid Route to a 128 * Long Potential Molecular Wire. *Angew. Chem. Int. Ed. Engl.*, **1994**, *33*, 1360-1363.
6. J. M. Tour, Conjugated Macromolecules of Precise Length and Constitution. Organic Synthesis for the Construction of Nanoarchitectures. *Chem. Rev.*, **1996**, *96*, 537-553.
7. T. Bartik, B. Bartik, M. Brady, R. Dembinski, J. A. Gladsyz, A Step-Growth Approach to Metal-Capped One-Dimensional Carbon Allotropes: Syntheses of C12, C16, and C20 -Polyynediyl Complexes. *Angew. Chem. Int. Ed.* , **1996**, *35*, 414-417.
8. L. Jones II, D. L. Pearson, J. S. Schumm, J. M. Tour, Synthesis of Well-Defined Conjugated Oligomers for Molecular Electronics. *Pure Appl. Chem.* , **1996**, *68*, 145-148.
9. Handbook of Conducting Polymers, Vols. 1, 2 ed. T. A. Skotheim. **1986**, New York: Dekker.
10. Electronic Properties of Conjugated Polymers III: Basic Models and Applications ed. H. Kuzmani, M. Mehring, S. Roth. **1989**, Berlin: Springer.
11. Conjugated Polymers and Related Materials. The Interconnection of Chemical and Electronic Structure ed. W. R. Salaneck, I. L. B. Rånby. **1993**, Oxford: Oxford University Press.

12. N. C. Greenham, S. C. Moratti, D. D. C. Bradley, R. H. Friend, A. B. Holmes, Efficient Light-emitting Diodes Based on Polymers with High Electron Affinities. *Nature*, **1993**, 365, 628-630.
13. M. Liphardt, A. Goonesekera, B. E. Jones, S. Ducharme, J. M. Takacs, L. Zhang, High Performance Photorefractive Polymers. *Science*, **1994**, 263, 367-369.
14. H. S. Nalwa, Organic Materials for Third-Order Nonlinear Optics Advanced Materials. *Adv. Mat.*, **1993**, 5, 341-358.
15. M. B. Nielsen, F. Diederich, The Art of Acetylenic Scaffolding: Rings, Rods, and Switches. *Chem. Rec.*, **2002**, 2, 189-198.
16. M. Bruschi, M. G. Giuffreda, H. P. Lüthi, *Trans* versus *Geminal* Electron Delocalization in Tetra- and Di-Ethynylethenes. *Chem. Eur. J.*, **2002**, 8, 4216-4227.
17. M. Schreiber, J. Anthony, F. Diederich, M. E. Spahr, R. Nesper, M. Hubrich, F. Bommeli, L. Degiorgi, P. Wachter, P. Kaatz, C. Bosshard, P. Günter, M. Colussi, U. W. Suter, C. Boudon, J.-P. Gisselbrecht, M. Gross, Polytriacylenes: Conjugated Polymers with a Novel All-Carbon Backbone. *Adv. Mater.*, **1994**, 6, 786-790.
18. J. Anthony, A. M. Boldi, C. Boudon, J. P. Gisselbrecht, M. Groos, P. Seiler, C. B. Knobler, F. Diederich, Macrocyclic Tetraethynylethene Molecular Scaffolding: Perethynylated aromatic Dodecahydro-[18]annulenes, Antiaromatic Octadehydro-[12]annulenes, and Expanded Radialenes. *Helv. Chim. Acta*, **1995**, 78, 797-817.
19. M. Schreiber, R. R. Tykwinski, F. Diederich, R. Spreiter, U. Gubler, C. Bosshard, I. Poberaj, P. Günter, C. Boudon, J.-P. Gisselbrecht, M. Gross, U. Jonas, H. Ringsdorf, Tetraethynylethene Molecular Scaffolding: Nonlinear Optical, Redox, and Amphiphilic Properties of Donor Functionalized Polytriacylene and Expanded Radialenes. *Adv. Mater.*, **1997**, 9, 339-343.
20. H. Shirakawa, S. Ikeda, Infrared Spectra of Poly(acetylene). *Polymer. J.*, **1971**, 2, 231.
21. T. Ito, H. Shirakawa, S. Ikeda, Simultaneous Polymerization and Formation of Polyacetylene Film on the Surface of Concentrated Soluble Ziegler-Type Catalyst Solution. *J. Polym. Sci., Polym. Chem. Ed.*, **1974**, 12, 11-20.
22. G. Wegner, *Z. Naturforsch* **1969**, B24, 824-832.

-
23. Polydiacetylenes, ed. H. J. Cantow. **1984**, Berlin: Springer-Verlag, and references therein.
 24. M. Nijhoff, Polydiacetylenes, ed. D. Blood, R. R. Chance. **1985**, Dordrecht, and references therein.
 25. D. J. Sandman, Semiconducting Polymers and Their Solid State Properties: Are These Materials Semiconductors or Large Conjugated Molecules ? *Trends Polym. Sci.*, **1994**, 2, 44-55.
 26. S. Okada, H. Matsuda, H. Nakanishi, Polymeric Materials Encyclopedia, ed. J. C. Salomone. **1996**, Boca Ranton, FL, pag. 8393 and references therein: CRC Press.
 27. R. R. Tykwinski, Y. Zhao, Cross Conjugated Oligo(enynes). *Synlett*, **2002**, 1939-1953.
 28. R. R. Tykwinski, A. Hilger, F. Diederich, H. P. Lüthi, P. Seiler, V. Gramlich, J. P. Gisselbrecht, C. Boudon, M. Gross, Donor-Acceptor-Functionalized Tetraethynylethenes with Nitrothienyl Substituents: Structure-Property Relationships. *Helv. Chim. Acta*, **2000**, 83, 1484-1508.
 29. Y. Rubin, C. B. Knobler, F. Diederich, Tetraethynylethene. *Angew. Chem. Int. Ed.*, **1991**, 30, 698.
 30. R. R. Tykwinski, M. Schreiber, V. Gramlich, P. Seiler, F. Diederich, Donor-Acceptor Substituted Tetraethynylethenes. *Adv. Mater.*, **1996**, 8, 226-231.
 31. C. Bosshard, R. Spreiter, P. Gunter, R. R. Tykwinski, M. Schreiber, F. Diederich, Structure-Properties Relationships in Nonlinear Optical Tetraethynylethenes. *Adv. Mater.*, **1996**, 8, 231-234.
 32. R. R. Tykwinski, M. Schreiber, R. P. Carlón, F. Diederich, V. Gramlich, Donor/Acceptor-Substituted Tetraethynylethenes: Systematic Assembly of Molecules for Use as Advanced Materials. *Helv. Chim. Acta*, **1996**, 79, 2249-2281.
 33. R. Spreiter, C. Bosshard, G. Knöpfle, P. Günter, R. R. Tykwinski, M. Schreiber, F. Diederich, One- and two-Dimensionally Conjugated Tetraethynylethenes: Structure versus Second-Order Optical Polarizabilities. *J. Phys. Chem. B*, **1998**, 102, 29-32.
 34. T. K. Brunck, F. Weinhold, Quantum-mechanical Studies on the Origin of Barriers to Internal Rotation about Single Bonds. *J. Am. Chem. Soc.*, **1978**, 101, 1700-1709.

-
35. J. P. Foster, F. Weinhold, Natural Hybrid Orbitals. *J. Am. Chem. Soc.*, **1980**, *102*, 7211-7218.
 36. A. E. Reed, R. B. Weinstock, F. Weinhold, Natural Population Analysis. *J. Chem. Phys.*, **1985**, *83*, 735-746.
 37. A. E. Reed, F. Weinhold, Natural Localized Molecular Orbitals. *J. Chem. Phys.*, **1985**, *83*, 1736-1740.
 38. A. E. Reed, L. A. Curtiss, F. Weinhold, Intermolecular Interaction from a Natural Bond Orbital, Donor-Acceptor Viewpoint. *Chem. Rev.*, **1988**, *88*, 899-926.
 39. F. Weinhold, C. R. Landis, Valency and Bonding: A Natural Bond Orbital Donor-Acceptor Perspective. **2005**, Cambridge: Cambridge University Press.
 40. R. G. Parr, W. Yang, Density Functional Theory of Atoms and Molecules. **1989**, New York: Oxford University Press.
 41. A. D. Becke, Density-Functional Thermochemistry. III. The Role of Exact Exchange. *J. Chem. Phys.*, **1993**, *98*, 5648-5652.
 42. C. Lee, W. Yang, R. G. Parr, Development of the Colle-Salvetti Correlation-energy Formula into a Functional of the Electron Density. *Phys. Rev. B*, **1988**, *37*, 785-789.
 43. T. H. Dunning Jr., Gaussian Basis Sets for Use in Correlated Molecular Calculations. I. The Atoms Boron through Neon and Hydrogen. *J. Chem. Phys.*, **1989**, *90*, 1007-1023.
 44. M. J. Frisch, G. W. Trucks, H. B. Schlegel, G. E. Scuseria, M. A. Robb, J. R. Cheeseman, V. G. Zakrzewski, J. A. Montgomery, R. E. Stratmann, J. C. Burant, S. Dapprich, J. M. Millam, A. D. Daniels, K. N. Kudin, M. C. Strain, O. Farkas, J. Tomasi, V. Barone, M. Cossi, R. Cammi, B. Mennucci, C. Pomelli, C. Adamo, S. Clifford, J. Ochterski, G. A. Petersson, P. Y. Ayala, Q. Cui, K. Morokuma, D. K. Malick, A. D. Rabuck, K. Raghavachari, J. B. Foresman, J. Cioslowski, J. V. Ortiz, B. B. Stefanov, G. Liu, A. Liashenko, P. Piskorz, I. Komaromi, R. Gomperts, R. L. Martin, D. J. Fox, T. Keith, M. A. Al-Laham, C. Y. Peng, A. Nanayakkara, C. Gonzalez, M. Challacombe, P. M. W. Gill, B. G. Johnson, W. Chen, M. W. Wong, J. L. Andres, M. Head-Gordon, E. S. Replogle, J. A. Pople, *Gaussian 98 (Revision A.7)*. 1998, Gaussian, Inc.: Pittsburgh PA.

-
45. J. E. D. Glendening, K. Badenhop, A. E. Reed, J. E. Carpenter, J. A. Bohmann, C. M. Morales, F. Weinhold, *NBO 5.0*. 2001, Theoretical Chemistry Institute, University of Wisconsin: Madison.
 46. C. Dehu, F. Meyers, J.-L. Bredas, Donor-Acceptor Diphenylacetylenes: Geometrical Structure, Electronic Structure, and Second-Order Nonlinear Optical Properties. *J. Am. Chem. Soc.*, **1993**, *115*, 6198-6206.
 47. R. E. Martin, U. Gubler, J. Cornil, M. Y. Balakina, C. Boudon, C. Bosshard, J.-P. Gisselbrecht, F. Diederich, P. Günter, M. Gross, J.-L. Brédas, Monodisperse Polytriacetylene Oligomers Extending from Monomer to Hexadecamer: Joint Experimental and Theoretical Investigation of Physical Properties. *Chem. Eur. J.*, **2000**, *6*, 3622-3634.
 48. R. E. Martin, F. Diederich, Linear Monodisperse π -Conjugated Oligomers: Model Compounds for Polymers and More. *Angew. Chem. Int. Ed.*, **1999**, *38*, 1350-1377.
 49. R. E. Martin, T. Mäder, F. Diederich, Monodisperse Poly(triacetylene) Rods: Synthesis of 11.9 nm Long Molecular Wire and Direct Determination of the Effective Conjugation Length by UV/vis and Raman Spectroscopies. *Angew. Chem. Int. Ed.*, **1999**, *38*, 817-822.
 50. R. E. Martin, U. Gubler, C. Boudon, V. Gramlich, C. Bosshard, J.-P. Gisselbrecht, P. Gunter, M. Gross, F. Diederich, Poly(triacetylene) Oligomers: Synthesis Characterization, and Estimation of the Effective Conjugation Length by Electrochemical, UV/vis, and Nonlinear Optical Methods. *Chem. Eur. J.*, **1997**, *3*, 1505-1512.
 51. U. Gubler, C. Bosshard, P. Günter, M. Y. Balakina, J. Cornil, J.-L. Brédas, R. E. Martin, F. Diederich, Scaling Law for Second-Order Hyperpolarizabilities in Poly(triacetylene) Molecular Wires. *Opt. Lett.*, **1999**, *24*, 1599-1601.
 52. M. B. Nielsen, F. Diederich, Conjugated Oligoenynes Based on Diethynylethene Unit. *Chem. Rev.*, **2005**, *105*, 1837-1867.
 53. M. Boldi, J. Anthony, V. Gramlich, C. B. Knobler, C. Boudon, J.-P. Gisselbrecht, M. Gross, F. Diederich, Acyclic Tetraetynylethene Molecular Scaffolding:

- Multinanometer-sized Linearly Conjugated Rods with the Poly(triacetylene) Backbone and Cross-conjugated Expanded Dendralenes. *Helv. Chim. Acta*, **1995**, 78, 779-796.
54. E. Burri, F. Diederich, M. B. Nielsen, Synthesis and Characterization of Multinanometer-Sized Expanded Dendralenes with an *iso*-Poly(triacetylene) Backbone. *Helv. Chim. Acta*, **2001**, 85, 2169-2182.
55. Y. Zhao, R. McDonald, R. R. Tykwinski, Study of Cross-Conjugated *iso*-Polytriacetylenes and Related Oligoenynes. *J. Org. Chem.*, **2002**, 67, 2805-2812.
56. Y. Zhao, A. D. Slepko, C. O. Akoto, R. McDonald, F. A. Hegmann, R. R. Tykwinski, Structure, and Nonlinear Optical Properties of Cross-Conjugated Perphenylated *iso*-Polydiacetylene. *Chem. Eur. J.*, **2005**, 11, 321-329.
57. M. B. Nielsen, M. Schreiber, Y. G. Baek, P. Seiler, S. Lecomte, C. Boudon, R. R. Tykwinski, J. P. Gisselbrecht, V. Gramlich, P. J. Skinner, C. Bosshard, P. Günter, M. Gross, F. Diederich, Highly Functionalized Dimeric Tetraethynylethenes and Expanded Radialenes: Strong Evidence for Macrocyclic Cross-Conjugation. *Chem. Eur. J.*, **2001**, 7, 3263-3280.
58. A. J. Heeger, S. Kivelson, J. R. Schrieffer, W.-P. Su, Solitons in Conducting Polymers. *Rev. Mod. Phys.*, **1988**, 60, 782-850.
59. M. Kertesz, Electronic Structure of Polymers. *Adv. Quantum Chem.*, **1982**, 15, 161.
60. R. Peierls, Quantum Theory of Solids. **1956**, Oxford: Oxford University Press.
61. A. A. Ovchinnikov, I. I. Ukrainskii, G. F. Kvenstel, Theory of One-Dimensional Mott Semiconductors and the Electronic Structure of Long Molecules with Conjugated Bonds. *Usp. Fiz. Nauk*, **1972**, 108, 81-111.
62. C. H. Choi, M. Kertesz, A. Karpfen, The Effects of Electron Correlation on the Degree of bond Alternation and Electronic Structure of Oligomers of Polyacetylene. *J. Chem. Phys.*, **1997**, 107, 6712-6721.
63. C. H. Choi, M. Kertesz, Bond Length Alternation and Aromaticity in Large Annulenes. *J. Chem. Phys.*, **1998**, 108, 6681-6688.
64. S. Suhai, Electron Correlation and Dimerization in *trans*-Polyacetylene: Many-Body Perturbation Theory versus Density-Functional Methods. *Phys. Rev. B*, **1995**, 51, 16553-16557.

-
65. W. J. Hehre, R. Ditchfield, J. A. Pople, Self-Consistent Molecular Orbital Methods. XII. Further Extensions of Gaussian-Type Basis Sets for Use in Molecular Orbital Studies of Organic Molecules. *J. Chem. Phys.*, **1972**, 56, 2257-2261.
 66. A. D. Becke, Density-Functional Thermochemistry. I. The Effect of the Exchange-Only Gradient Correction. *J. Chem. Phys.*, **1992**, 96, 2155-2160.
 67. P. J. Stevens, F. J. Devlin, C. F. Chablowksi, M. J. Frisch, Ab Initio Calculation of Vibrational Absorption and Circular Dichroism Spectra Using Density Functional Force Fields. *J. Phys. Chem.*, **1994**, 98, 11623-11627.
 68. A. D. Becke, Density-functional Exchange-Energy Approximation with Correct Asymptotic Behavior. *Phys. Rev. A*, **1988**, 38, 3098-3104.
 69. A. D. Becke, A New Mixing of Hartree-Fock and Local Density-functional Theories. *J. Chem. Phys.*, **1993**, 98, 1372-1377.
 70. J. C. Rienstra-Kiracofe, G. S. Tschumper, H. F. Schaefer, Atomic and Molecular Electron Affinities: Photoelectron Experiments and Theoretical Computations. *Chem. Rev.*, **2002**, 102, 231-282.
 71. A. D. Bacon, M. C. Zerner, An Intermediate Neglect of Differential Overlap Theory for Transition Metal Complexes: Fe, Co, and Cu Chlorides. *Theor. Chim. Acta* **1979**, 53, 21.
 72. M. C. Zerner, Metal-Ligand Interactions. **1996**, Dordrecht, The Netherlands: Kluwer Academic Publishers.
 73. M. C. Zerner, G. H. Loew, R. F. Kirchner, U. T. Mueller-Westerhoff, An Intermediate Neglect of Differential Overlap Technique for Spectroscopy of Transition-Metal Complexes. Ferrocene. *J. Am. Chem. Soc.*, **1980**, 102, 589-599.
 74. J. C. Culberson, P. Knappe, N. Rösch, M. C. Zerner, An Intermediate Neglect of Differential Overlap (INDO) Technique for Lanthanide Complexes: Studies on Lanthanide Halides. *Theor. Chim. Acta* **1987**, 71, 21-39.
 75. J. Ridley, M. C. Zerner, An Intermediate Neglect of Differential Overlap Technique for Spectroscopy: Pyrrole and the Azines. *Theor. Chim. Acta*, **1973**, 32, 111.
 76. J. Ridley, M. C. Zerner, Triplet states via Intermediate Neglect of Differential Overlap: Benzene, Pyridine, and the Diazines. *Theor. Chim. Acta*, **1976**, 42, 223.

-
77. W. P. Anderson, T. Cundari, M. C. Zerner, An Intermediate Neglect of Differential Overlap Model for Second Row Transition Metal Species. *Int. J. Quantum Chem.*, **1991**, 39, 31.
 78. W. P. Anderson, T. Cundari, R. S. Drago, M. C. Zerner, Utility of the Semiempirical INDO/1 Method for the Calculation of the Geometries of Second-Row Transition-Metal Species. *Inorg. Chem.*, **1990**, 29, 1-3.
 79. R. E. Stratmann, G. E. Scuseria, M. J. Frisch, An Efficient Implementation of Time-Dependent Density-Functional Theory for the Calculation of Excitation Energies of Large Molecules. *J. Chem. Phys.*, **1998**, 109, 8218-8224.
 80. R. Bauernschmitt, R. Ahlrichs, A Direct Implementation of the GIAO-MBPT(2) Method for Calculating NMR Chemical Shifts. Application to the Naphthalenium and Anthracenium Ions. *Chem. Phys. Lett.*, **1996**, 256, 454-464.
 81. M. E. Casida, C. Jamorski, K. C. Casida, D. R. Salahub, Molecular Excitation Energies to High-Lying Bound States from Time-Dependent Density-Functional Response Theory: Characterization and Correction of the Time-Dependent Local Density Approximation Ionization Threshold. *J. Chem. Phys.*, **1998**, 108, 4439-4449.
 82. H. A. Kurtz, J. J. P. Steward, K. M. Dieter, Calculations of the Nonlinear Optical Properties of Molecules. *J. Comp. Chem.*, **1990**, 11, 82-87.
 83. M. J. S. Dewar, W. Thiel, Ground States of Molecules. 38. The MNDO Method. Approximations and Parameters. *J. Am. Chem. Soc.*, **1977**, 99, 4899-4907.
 84. J. J. Stewart, *MOPAC2000*. 1999, Fujitsu Limited: Tokyo, Japan.
 85. E. A. Perpète, B. Champagne, Determination of the Bond Length Alternation of Polyacetylene, Polydiacetylene and Polybutatriene from MP2 Oligomeric Investigations. *J. Mol. Struct. (Theochem)* **1999**, 487, 39-45.
 86. M. Klokkenburg, M. Lutz, A. L. Spek, J. H. van der Maas, C. A. van Walree, Electron Delocalization in Cross-Conjugated p-Phenylenevinylidene Oligomers. *Chem. Eur. J.*, **2003**, 9, 3544-3554.
 87. W. P. Anderson, T. Cundari, R. S. Drago, M. C. Zerner, *Inorg. Chem.*, **1989**, 29, 150.
 88. J. S. Miller, Conducting Polymers - Materials of Commerce. *Adv. Mat.*, **1993**, 5, 671-676.

-
89. H. Shirakawa, E. J. Louis, A. G. MacDiarmid, C. K. Chiang, A. J. Heeger, Synthesis of Electrically Conducting Organic Polymers: Halogen Derivatives of Polyacetylene, $(\text{CH})_x$, *J. Chem. Soc. Chem. Commun.*, **1977**, 16, 578-580.
 90. A. J. Heeger, Semiconducting and Metallic Polymers: The Fourth Generation of Polymeric Materials (Nobel lecture). *Angew. Chem. Int. Ed.*, **2001**, 40, 2591-2611.
 91. H. Shirakawa, The Discovery of Polyacetylene Film: The Dawning of an Era of Conducting Polymers (Nobel lecture). *Angew. Chem. Int. Ed.*, **2001**, 40, 2575--2581.
 92. A. G. MacDiarmid, "Synthetic Metals": A Novel Role for Organic Polymers (Nobel lecture). *Angew. Chem. Int. Ed.*, **2001**, 40, 2581-2590.
 93. Conjugated Polymers : The Novel Science and Technology of Highly Conducting and Nonlinear Optically Active Materials (Hardcover), ed. J. L. Brédas, R. Silbey. **1991**, Dordrecht ; Boston: Kluwer Academic Publishers.
 94. Conjugated Polymer & Molecular Interfaces, ed. W. R. Salaneck, K. Seki, A. Kahn, J.-J. Pireaux, W. R. Salaneck. **2001**, New York: Marcel Dekker.
 95. Handbook of Organic Conductive Molecules and Polymers ed. H. S. Nalwa. Vol. 1-4. **1997**, Chinchester: Wiley.
 96. S. Roth, D. Carroll, One-Dimensional Metals : Conjugated Polymers, Organic Crystals, Carbon Nanotubes. **2004**, Weinheim: John Wiley & Sons.
 97. Electronic Processes in Organic Crystals and Polymers ed. M. Pope, C. E. Swenberg. **1999**, Oxford: Oxford University Press.
 98. W. Barford, Electronic And Optical Properties of Conjugated Polymers. International Series of Monographs on Physics. **2005**, Gloucestershire: Clarendon Press.
 99. B. Champagne, E. A. Perpète, S. J. A. Gisbergen, E.-J. Baerendsen, J. G. Snijders, C. Soubra-Ghaoui, K. Robins, B. Kirtman, Assessment of Conventional Density Functional Schemes for Computing the Polarizabilities and Hyperpolarizabilities of Conjugated Oligomers: An ab initio Investigation of Polyacetylene Chains. *J. Chem. Phys.*, **1998**, 109, 10489-10498.
 100. B. Champagne, E. A. Perpète, Bond Length Alternation Effects on the Static Electronic Polarizability and Second Hyperpolarizability of Polyacetylene Chains. *Int. J. Quantum Chem.*, **1999**, 75, 441-447.

-
101. D. Q. Lu, B. Marten, M. Ringnalda, R. A. Friesner, W. A. Goddard, Saturation of the Second Hyperpolarizability for Polyacetylenes. *Chem. Phys. Lett.*, **1996**, 257, 224-228.
 102. W. P. Su, J. R. Schrieffer, A. J. Heeger, Solitons in Polyacetylene. *Phys. Rev. Lett.*, **1979**, 42, 1698-1701.
 103. W. P. Su, J. R. Schrieffer, A. J. Heeger, Soliton Excitations in Polyacetylene. *Phys. Rev. B*, **1980**, 22, 2099-2111.
 104. J. W. Mintmire, C. T. White, Local-Density-Functional Results for the Dimerization of trans-Polyacetylene: Relationship to the Band-Gap Problem. *Phys. Rev. B*, **1987**, 35, 4180-4183.
 105. A. Fujii, R. Hydarat, T. Sonoda, T. Fujisawa, M. Ozaki, Z. V. Vardeny, M. Teraguchi, T. Masuda, K. Yoshino, Optical Properties of Disubstituted Polyacetylene Thin Films *Synt. Met.*, **2001**, 116, 95-99.
 106. J. Ma, S. Li, J. Y, A Time-Dependent DFT Study on Band Gaps and Effective Conjugation Lengths of Polyacetylene, Polyphenylene, Polypentafulvene, Polycyclopentadiene, Polypyrrole, Polyfuran, Polysilole, Polyphosphole, and Polythiophene. *Macromolecules*, **2002**, 35, 1109-1115.
 107. S. Tretiak, S. Mukamel, Density Matrix Analysis and Simulation of Electronic Excitations in Conjugated and Aggregated Molecules. *Chem. Rev.*, **2002**, 102, 3171-3212.
 108. J.-L. Bredas, D. Beljonne, V. Coropceanu, J. Cornil, Charge-Transfer and Energy-Transfer Processes in π -Conjugated Oligomers and Polymers: A Molecular Picture. *Chem. Rev.*, **2004**, 104, 4971-5004.
 109. J.-L. Brédas, C. Adant, P. Tackx, A. Persoons, B. M. Pierce, Third-Order Nonlinear Optical Response in Organic Materials: Theoretical and Experimental Aspects. *Chem. Rev.*, **1994**, 94, 243-278.
 110. M. Tobita, S. Hirata, R. J. Bartlett, A Crystalline Orbital Study of Polydiacetylenes. *J. Chem. Phys.*, **2001**, 114, 9130-9141.
 111. K. N. Kudin, G. E. Scuseria, Linear-Scaling Density-Functional Theory with Gaussian Orbitals and Periodic Boundary Conditions: Efficient Evaluation of Energy and Forces via Fast Multipole Method. *Phys. Rev. B*, **2000**, 61, 16440-16453.

-
112. S. Hirata, H. Torii, M. Tasumi, Density-Functional Crystal Orbital Study on the Structures and Energetics of Polyacetylene Isomers. *Phys. Rev. B*, **1998**, 57, 11994-12001.
 113. M. Springborg, Structural and Electronic Properties of Fluorinated and Chlorinated Polyacetylene. *J. Am. Chem. Soc.*, **1999**, 121, 11211-11216.
 114. G. R. Hutchinson, Y.-J. Zhao, B. Delley, A. J. Freeman, M. A. Ratner, T. J. Marks, Electronic Structure of Conducting Polymers: Limitations of Oligomer Extrapolation Approximations and Effects of Heteroatoms. *Phys. Rev. B*, **2003**, 68, 035204.
 115. I. D. W. Samuel, I. Ledoux, C. Dhenaut, J. Zyss, H. H. Fox, R. R. Schrock, R. J. Silbey, Saturation of Cubic Optical Nonlinearity in Long-Chain Polyene Oligomers. *Science*, **1994**, 265, 1070-1072.
 116. R. Giesa, R. Schultz, Alternating All-trans Polyenyne - Model Compounds for Poly(diacetylene)s with Defined Conjugation Length. *Polym. Int.*, **1994**, 33, 43-60.
 117. M. Bruschi, M. G. Giuffreda, H. P. Lüthi, Electron Delocalization in Extended Linearly π -conjugated Systems: *Through* versus *Cross* Electron Delocalization in Polytriacetylene. *ChemPhysChem*, **2005**, 6, 511-519.
 118. M. G. Giuffreda, M. Bruschi, H. P. Lüthi, Electron Delocalization in Linearly π -Conjugated Systems: A Concept for Quantitative Analysis. *Chem. Eur. J.*, **2004**, 10, 5671.
 119. Willetts, A. Rice, J. E. Burland, D. M. Shelton, , Problems in Comparison of Theoretical and Experimental Hyperpolarizabilities. *J. Phys. Chem.*, **1992**, 97, 7590-7598.
 120. E. A. Perpète, B. Champagne, Linear and Nonlinear Polarizabilities of Polydiacetylene and Polybutatriene Chains: An Ab Initio Coupled Hartree-Fock Investigation. *J. Chem. Phys.*, **1997**, 107, 2463-2479.
 121. K. N. Kudin, R. Car, R. Resta, Longitudinal Polarizability of Long Polymeric Chains: Quasi-One-Dimensional Electrostatics as the Origin of Slow Convergence. *J. Chem. Phys.*, **2005**, ASAP
 122. B. Champagne, D. Mosley, M. Vračko, J.-M. André, Electron Correlation Effects on the Longitudinal Polarizability of Polymeric Chains. *Phys. Rev. A*, **1995**, 52, 178-188.

-
123. D. R. Kanis, M. A. Ratner, T. J. Marks, Design and Construction of Molecular Assemblies with Large Second-Order Optical Nonlinearities. Quantum Chemical Aspects. *Chem. Rev.*, **1994**, 94, 195-242.
 124. J. O. Morley, Nonlinear Optical Properties of Organic Molecules. Calculations of the Hyperpolarizabilities of Donor-Acceptor Polyenes. *Int. J. Quantum Chem.*, **1993**, 46, 19-26.
 125. P. D. Jarowski, M. D. Wodrich, C. S. Wannere, P. v. R. Schleyer, K. N. Houk, How Large is the Stabilization of Diynes ? *J. Am. Chem. Soc.*, **2004**, 126, 15036-15037.
 126. R. E. Martin, U. gubler, C. Boudon, C. Bosshard, J.-P. Gisselbrecht, P. Günter, M. Gross, F. Diederich, Synthesis and Physical Investigation of Donor-Donor Acceptor-Acceptor End-Functionalized Monodisperse Poly(triacetylene) Oligomers. *Chem. Eur. J.*, **2000**, 6, 4400-4412.

5 Outlook

Since the development of quantum chemistry, many attempts have been made to evaluate electron delocalization in π -conjugated compounds. Despite all these efforts, none of the delocalization parameters ever suggested allowed for a unique description of electron delocalization. The reason behind all these efforts is that it has been well recognized that physical observables are tightly correlated to the extent of electron delocalization. Therefore, the evaluation of electron delocalization renders an important descriptor to correlate physical observables with the topological degrees of freedom, which can be manipulated to suit a desired property of the molecule.

The value of the approach proposed in this thesis lies in the easy implementation (the required code is already implemented in several quantum mechanical packages), in the applicability for large molecular systems, and in the inclusion of correlation effects in the framework of the DFT scheme. An important feature of this approach regards the analysis of electron delocalization of distinct π -conjugated paths, i.e. *geminal*, *cis*, and *trans*, within the same molecule, as well as the assessment of the impact of substituents on a given backbone, thus enabling the identification of the relevant contributions to conjugation in a given system. Furthermore, the different protocols (delocalization energies, second-order interaction energies, and orbital occupation numbers) illustrated in this thesis allow a detailed analysis of electron delocalization, as they provide an equivalent picture, but, at the same time, they can be addressed to investigate selected features of electron delocalization.

On the other hand, some drawbacks have still to be addressed. As pointed out in this thesis, our approach is not designed to give absolute values for delocalization energies, but, at this stage of development, it is designed to reproduce differences between structural and conformational isomers or between backbones with different functionalizations; in this case the approach gives accurate results. The overestimation of the absolute values of delocalization energy in comparison to that calculated with other theoretical approaches can be related to the lack of relaxation of the NBO orbitals upon the deletion procedure. Thus, a further development of the approach should be the implementation of a procedure for the

orbital relaxation in the calculation of delocalization energies. However, a different explanation for the overestimation of the absolute values deserves to be considered and further investigated in the future. In Chapter 1 we clearly outlined that the definition of a proper reference structure is a critical point to be assessed for the evaluation of delocalization energies. Several attempts, in fact, have been made to find an alternative reference structure which accounts for the overestimation of delocalization energies, but further study is still needed. The application of our approach to the study of aromatic compounds could be very useful to check these assumptions. It should be noted that preliminary calculations on a series of aromatic compounds lead to a fairly good linear relationship between calculated and experimental delocalization energies (data not shown), in which, however, the computed values are significantly overestimated.

Applying the method, we were able to explain or even to suggest “design rules” for the synthesis of the types of compounds considered here. For example, the functionalization of ethynylethenes with donors and acceptors showed that a donor functional group promote π -electron delocalization within the molecular backbone more efficiently than an acceptor one. This suggests that the π -electron delocalization in a push-pull chromophore can be enhanced by a functionalization with donor groups in selected positions of the backbone. In a study which is not covered by this thesis, we were able to show that geminal conjugation is not necessarily inferior to through conjugation, and that targeted substitution of these compounds may actually bring geminal conjugation to the same level of through conjugation in terms of delocalization energies.

Another topic that deserves further study is the in-plane conjugation. The contents of this thesis focus on the vertical π -conjugation since, as it is well known, the physical properties of interest in the design of new materials for electronic and photonic applications are tightly correlated to the extent of the π -delocalization. However, the in-plane conjugation cannot be neglected, and in particular, we observed that the in-plane conjugation can affect the extent of π -delocalization through the modulation of the bond lengths. The role of the in-plane conjugation could be further addressed in the future by the investigation of the effects of different σ -substituents on the π - and σ -delocalization.

Finally, the approach discussed in this thesis can be extended beyond the investigation of electron delocalization in π -conjugation molecular systems. For example, this approach is well designed to study intermolecular donor \rightarrow acceptor interactions in supramolecular assemblies. Furthermore, in a study not included in this thesis the approach has been applied to the investigation of metal – ligand interactions in coordination compounds. In this respect, the definition of a model in which the metal – ligand bonds are described by intermolecular donor \rightarrow acceptor interactions provides a useful representation of the metal complexes in the framework of the ligand field theory. A further extension of this study, in the next future, will concern with the analysis of possible correlations between the NBO parameters calculated within the model defined above and the “hardness” and “softness” concepts.

Curriculum Vitae

Personal data

Name	Maurizio Bruschi
Date of birth	August 17, 1970
Place of birth	Milano, Italy
Citizenship	Italian

Education

1985-1990	Technical School in Chemistry
1990-1996	Degree in Industrial Chemistry; University of Milan Thesis: Computational modeling of zeolite systems and their use in the chemioadsorbition of biatomic and small organic molecules
1999-2005	PhD studies at the Institute of Physical Chemistry, ETH, Zurich, Switzerland, supervised by Prof. H. P. Lüthi

Practical Experience

1996-1997	Fellowship in the lab. of Prof. P. Fantucci; Department of Inorganic Chemistry, University of Milano, Milan, Italy
1997-1998	Fellowship in the lab. of Enzyme research; Pharmacological Institute 'Mario Negri', Milan, Italy.
1997 -1998	Consultant of Chemical Software; Campoverde srl, Gigalabo Division; Milan, Italy.
Since October 2000	Researcher at the Department of Environmental Science, University of Milano-Bicocca, Milan, Italy.

Complete List of Publications

E. Bolzacchini, M. Bruschi, J. Hjorth, S. Meinardi, M. Orlandi, G. Restelli, B. Rindone
Tropospheric Chemistry of Aromatic Compounds: Evidence for a Rate Determining Addition of NO₃ and OH to Substituted Toluenes

H. Powers, T. Trabassi, C. A. Brebbia Eds, Air Pollution V, Computational Mechanism Publications, **1997**, 893-902.

S. Demontis, M. Terao, M. Brivio, S. Zanotta, M. Bruschi, E. Garattini
Isolation and Characterization of the Gene Coding for Human Cytidine Deaminase
Biochimica et Biophysica Acta - Gene Structure and Expression **1998**, 1443(3), 323-333.

M. Salmona, P. Malesani, L. De Gioia, S. Gorla, M. Bruschi, A. Molinari, F. Della Vedova, M. A. Marrani, T. Awan, O. Bugiani, G. Forloni, F. Tagliavini
Molecular Determinants of the Physicochemical Properties of a Critical Prion Protein Region Comprising Residues 106-126
Biochemical Journal **1999**, 342, 207-214.

G. Gini, M. Lorenzini, E. Benfenati, P. Grasso, M. Bruschi
Predictive Carcinogenicity: A Model for Aromatic Compounds, with Nitrogen-Containing Substituents, Based on Molecular Descriptors Using an Artificial Neural Network
Journal of Chemical Information and Computer Science **1999**, 39(6), 1076-1080.

G. G. Ying, P. Proost, J. van Damme, M. Bruschi, M. Introna, J. Golay
Nucleolin, a novel partner for the Myb transcription factor family that regulates their activity
Journal of Biological Chemistry **2000**, 275(6), 4152-4158.

E. Bolzacchini, M. Bruschi, J. Hjorth, S. Meinardi, M. Orlandi, B. Rindone, E. Rosenbohm
Gas-Phase Reaction of Phenol with NO₃
Environmental Science & Technology **2001**, 35(9), 1791-1797.

E. Bolzacchini, M. Bruschi, J. Hjorth, S. Meinardi, M. Orlandi, B. Rindone, E. Rosenbohm
Nitrophenols in the Troposphere

Atmospheric Diagnostics in Urban Regions (J. P. Lay, K. H. Becker, W. Hauthal, B. Rindone and C. Zetsch Eds.), Erich Schmidt Verlag (**2001**), pag. 180-188.

M. Bruschi, P. Fantucci, L. De Gioia

DFT Investigation of Structural, Electronic, and Catalytic Properties of Diiron Complexes Related to the $[2Fe]_H$ Subcluster of Fe-Only Hydrogenases

Inorganic Chemistry **2002**, 41(6), 1421-1429.

F. Tordini, A. Bencini, M. Bruschi, L. De Gioia, G. Zampella, P. Fantucci

A Theoretical Study of Hydration of Cyanamide and Carbodiimide

Journal of Physical Chemistry A **2003**, 107(8), 1188-1196.

M. Bruschi, P. Fantucci, L. De Gioia

Density Functional Theory Investigation of the Active Site of $[Fe]$ -Hydrogenases: Effects of Redox State and Ligand Characteristics on Structural, Electronic, and Reactivity Properties of Complexes Related to the $[2Fe]_H$ Subcluster

Inorganic Chemistry **2003**, 42(15), 4773-4781.

M. Bruschi, P. Fantucci, L. De Gioia

Density Functional Theory Investigation of the Active Site of $[Fe]$ -Hydrogenases. Systematic Study of the Effects of Redox State and Ligands Hardness on Structural and Electronic Properties of Complexes Related to the $[2Fe]_H$ Subcluster

Inorganic Chemistry **2004**, 43(12), 3733-3741.

M. Bruschi, L. De Gioia, G. Zampella, M. Reiher, P. Fantucci, M. Stein

A Theoretical Study of Spin States in $Ni-S_4$ Complexes and Models of the $[NiFe]$ Hydrogenase Active Site

Journal of Biological Inorganic Chemistry **9**, **2004**, 873-884.

M. Pizzotti, E. Annoni, R. Ugo, S. Bruni, S. Quici, P. Fantucci, M. Bruschi, G. Zerbi, M. del Zoppo

A Multitechnique Investigation of the Second Order NLO Response of a 10,20-Diphenylporphyrinato Nickel(II) Complex Carrying a Phenylethynyl Based push-pull System in the 5- and 15-Positions

Journal of Porphyrins and Phtalocyanines **2004**, 8, 1311-1324.

G. Zampella, M. Bruschi, P. Fantucci, M. Razavet, C. J. Pickett, L. De Gioia

Dissecting the Intimate Mechanism of Cyanation of [Fe2S3] Complexes Related to the Active Site of All-Iron Hydrogenases by DFT Analysis of Energetics, Transition States, Intermediates and Products in the Carbonyl Substitution Pathway

Chemistry-a European Journal **2005**, 11(1), 509-520.

C. Tard, X. Liu, S. K. Ibrahim, M. Bruschi, L. De Gioia, S. Davies, X. Yang, L-S. Wang and C. J. Pickett

De novo Synthesis of the H-Cluster Framework of Iron-Only Hydrogenase

Nature **2005**, 433, 610-613.

M. Bruschi, G. Zampella, P. Fantucci, L. De Gioia

In-Silico Modelling of Hydrogenase Chemistry

Coordination Chemistry Review **2005**, 249(15-16), 1620-1640.

E. Annoni, M. Pizzotti, R. Ugo, S. Quici, T. Morotti, M. Bruschi, P. Mussini

Synthesis, Electronic Characterisation and Significant Second-Order Non-Linear Optical Responses of meso-Tetraphenylporphyrins and Their ZnII Complexes Carrying a Push or Pull Group in the β Pyrrolic Position

European Journal of Inorganic Chemistry, in press.

R. Della Pergola, M. Bruschi, F. Fabrizi de Biani, A. Fumagalli, L. Garlaschelli, F. Laschi, M. Manassero, M. Sansoni, P. Zanello

A new Multivalent Cluster: Synthesis, Electrochemistry, Solid State Structure and Computational Studies on the Iron-Nickel Mixed-metal Nitride Anions $[Fe_6Ni_6N_2(CO)_{24}]^{n-}$ ($n=2, 3, 4$)

Comptes Rendus Chimie **2005**, 8, 1850-1854.

G. Zampella, M. Bruschi, L. P. Fantucci, L. De Gioia

DFT Investigation of H_2 Activation by $[(MNHPnPr_3)(\text{'S3'})]$ ($M=Ni, Pd$). Insight Into Key factors Relevant to the Design of Functional Hydrogenase Models

Journal of American Chemical Society **2005**, 127(38), 13180-13189